



**This electronic thesis or dissertation has been
downloaded from Explore Bristol Research,
<http://research-information.bristol.ac.uk>**

Author:

Czajka, Adam

Title:

Surfactants at the Design Limit

General rights

Access to the thesis is subject to the Creative Commons Attribution - NonCommercial-No Derivatives 4.0 International Public License. A copy of this may be found at <https://creativecommons.org/licenses/by-nc-nd/4.0/legalcode>. This license sets out your rights and the restrictions that apply to your access to the thesis so it is important you read this before proceeding.

Take down policy

Some pages of this thesis may have been removed for copyright restrictions prior to having it been deposited in Explore Bristol Research. However, if you have discovered material within the thesis that you consider to be unlawful e.g. breaches of copyright (either yours or that of a third party) or any other law, including but not limited to those relating to patent, trademark, confidentiality, data protection, obscenity, defamation, libel, then please contact collections-metadata@bristol.ac.uk and include the following information in your message:

- Your contact details
- Bibliographic details for the item, including a URL
- An outline nature of the complaint

Your claim will be investigated and, where appropriate, the item in question will be removed from public view as soon as possible.

SURFACTANTS AT THE DESIGN LIMIT

by

ADAM CZAJKA



A dissertation submitted to the University of Bristol in accordance
with the requirements for award of the degree of Doctor
of Philosophy in the School of Chemistry,
Faculty of Science.

June 2018

Word count - fifty two thousand one hundred and thirty three

ABSTRACT

The adsorption and aggregation properties of twenty seven anionic hydrocarbon surfactants have been studied in aqueous systems. They are single-chain sulfonates with sodium or TAA counterions (where TAA = tetraalkylammonium, i.e. tetrapropylammonium), and di-chain sulfosuccinates with sodium counterions. The novel surfactants introduced possess branched tail structures which differ by the extent and position of branching. All

surfactants were synthesised and purified to investigate the relationships between surfactant structure and performance. The aim of this project is to fundamentally improve our understanding of controlling surface tension, and consequently use this to improve the performance of hydrocarbon surfactants to achieve low surface energies.

First, by evaluating the surface coverage of various effective surfactants, a new general property to account for low aqueous surface tension regardless of surfactant type is introduced. Where it is shown that all super-effective surfactants pack efficiently at air-water interfaces to generate dense surface coverages. With this general property in mind, the adsorption and aggregation properties of novel surfactants are studied through tensiometry and small-angle neutron scattering (SANS). By making small systematic variations in the surfactant structure, general structure-property relationships of effective hydrocarbon surfactants have been distinguished. The branching position, extent, and chain length are all shown to be both highly sensitive, and critical to generate low surface energies. The structural characteristics of effective hydrocarbon surfactants are encapsulated in a new index to assess potential surfactant performance, based on the molecular structure of the tail alone, H-Gamma.

Novel approaches to improve packing efficiency at the surface have been explored, leading to the lowest surface tensions for single-chain, di-chain and mixed hydrocarbon surfactant systems. For example, replacing carbon in the surfactant tail chain-tip with silicon leads to an increased molecular volume, greater packing efficiency and thus, lower surface tension. The ability to further improve packing efficiency by choice of surfactant counterion is demonstrated. By systematically changing the identity of the head group for various tail structures, the TPA (tetrapropylammonium) counterion is shown to be an effective alternative for all hydrocarbon surfactants. Furthermore, mixing linear and branched surfactants help to generate dense surface coverages, as spaces within the monolayer are effectively filled, generating lower surface energies than either constituent surfactant. The research presented here highlights structural characteristics of effective hydrocarbon surfactants, outlines design principles, developing our understanding and ability to control, surface tension.

ACKNOWLEDGMENTS

I would like to first and foremost thank my project supervisor Professor Julian Eastoe. An almighty force in the field of colloidal chemistry who has provided me much invaluable advice and support throughout my time at Bristol. His passion for science, assiduous approach to work and extensive ability to provide opportunities, coupled with being an all round great guy, have created a truly solid foundation for an aspiring colloidal chemist, cheers J.

I could also not have done it without the help of my family. Their continuous support, from start to finish, has helped me maintain an immensely enjoyable time in Bristol. They have got me through the thick, and kept me moving on up through the thin. I feel sincerely grateful to have such a remarkable set of parents who have truly helped me get to where I am today, thank you.

It would not have been such an enjoyable time in Bristol though were it not for characters such as The Illusionist, aka, Chris ~~Murphy~~ Hill. You made the daily job of a PhD thoroughly hilarious, provided my project much essential support throughout, and unlocked....The Architect. You're a top guy and I really couldn't have done it without you my man, peace....believe. Talking of top guys, I never thought I would have been so lucky to meet and form such an upstanding group of friends - *The Lost Stash*. Sammy, Bri, Michael and Gav, you've all been such a massive influence to my life in Bristol and thus, my PhD. A few sentences can't explain the appreciation and love I have for you guys. Our adventures are already known across the land and this is just the beginning! Also thank you Gav for generously giving your time and helping guide me as a colloidal chemist. To The Senate and the Leicester boys, two groups composed of exceptional people. Thank you for all the fun and support you have provided me over the last four years. You have all shaped me and my life, and I feel very fortuitous for having such a decent, diverse and benevolent group of friends.

I would also like to take this opportunity to thank various members of the Eastoe group. Joc, Jonny and Miguel, you guys made the House of Eastoe a distinct, energetic and fun group, and I have many great memories because of you, so thank you. Previous members for providing the foundation of this work, Shirin Alexander and Sandrine Nave. Finally, Sarah Rodgers for her continuous support on the front line, an invaluable member of the Eastoe team. Other non-Eastoe notables in no particular order: Speedy, Shooter, big doinks, Korton, squashies, Anna, DC's and topspin.

AUTHOR'S DECLARATION

I declare that the work in this dissertation was carried out in accordance with the requirements of the University's Regulations and Code of Practice for Research Degree Programmes and that it has not been submitted for any other academic award. Except where indicated by specific reference in the text, the work is the candidate's own work. Work done in collaboration with, or with the assistance of, others, is indicated as such. Any views expressed in the dissertation are those of the author.

.....

Adam Czajka

June 25th 2018

LIST OF PUBLICATIONS

Surfactants at the Design Limit

Czajka, A.; Hazell, G.; Eastoe, J.

Langmuir **2015**, *31*, 8205-8217.

Trimethylsilyl hedgehogs - a novel class of super-efficient hydrocarbon surfactants

Czajka, A.; Hill, C.; Peach, J.; Pegg, J. C.; Grillo, I.; Guittard, F.; Rogers, S. E.; Sagisaka, M.; Eastoe, J.

Physical Chemistry Chemical Physics **2017**, *19*, 23869-23877.

Designing a hydrocarbon surfactant from head to tail

Czajka, A.; Hill, C.; Eastoe, J.

Manuscript currently being prepared.

Super low surface energies with mixed hydrocarbon surfactant systems

Czajka, A.; Eastoe, J.

Manuscript currently being prepared.

If you wish to make an apple pie from scratch, you must first invent the universe.

CARL SAGAN

TABLE OF CONTENTS

Abstract	i
List of Tables	xi
List of Figures	xv
Nomenclature	xvi
Project Overview	xvii
1 Introduction	1
1.1 Surfactants in colloidal systems	1
1.2 Types of surfactants	3
1.3 Characteristic features of surfactants	5
1.3.1 Adsorption	5
1.3.2 Aggregation	6
1.4 Uses of surfactants	7
1.5 Environmental consequences of fluorosurfactants	8
1.6 Project aims	9
References	10
2 Structure-Property Relationships of Surfactants	12
2.1 Surface tension	12
2.1.1 Equilibrium and dynamic surface tension	14
2.2 Surface properties of surfactants	15
2.2.1 Surfactant efficiency and effectiveness	17
2.3 Influence of the hydrophobic tail on surface tension	18

2.4	Fluorosurfactants	19
2.5	Silicone surfactants	21
2.6	Hydrocarbon surfactants	23
2.7	General structure-property relationship of low aqueous surface tension	25
	References	29
3	Thermodynamics and Scattering Theory	32
3.1	Surfactant adsorption	32
3.2	Mixed surfactant systems	37
3.2.1	Mixing in binary surfactant mixtures	37
3.2.2	Regular Solution Theory	39
3.2.3	Adsorption at interfaces of binary surfactant mixtures	41
3.3	Small-angle neutron scattering	44
3.3.1	Neutrons	44
3.3.2	Neutron sources	46
3.3.3	SANS instruments	47
3.3.4	Scattering theory	49
3.3.5	Scattering by micellar aggregates	53
3.3.6	SANS approximations	58
	References	62
4	Experimental	64
4.1	Introduction	64
4.2	Materials	64
4.3	Synthesis of single-chain surfactants	73
4.3.1	Surfactant purification	75
4.4	Synthesis of di-chain surfactants	76
4.4.1	Surfactant purification	77
4.4.2	Synthesising surfactants from tertiary alcohols	79
4.5	Surfactant analysis	80
4.5.1	Nuclear Magnetic Resonance (NMR) spectroscopy	80
4.5.2	Elemental analysis	82
4.6	Techniques	97

4.6.1	Conductivity	97
4.6.2	Surface tension	97
4.6.3	Small-angle neutron scattering (SANS)	98
4.7	Conclusions	99
	References	100
5	Designing Optimised Surfactant Tails	101
5.1	The limit of γ for hydrocarbon surfactants	102
5.2	Determining accurate surface properties	104
5.2.1	Calculating activity coefficients	104
5.2.2	Determining the cmc by electrical conductivity	105
5.2.3	Determining the cmc by surface tension	109
5.2.4	The pre-factor m in the Gibbs equation	111
5.2.5	The optimum level of EDTA	113
5.2.6	Calculating A_{cmc} from γ -ln(a) plots	114
5.2.7	Considerations when determining the packing efficiency, Φ_{cmc} .	115
5.3	Importance of the CH ₃ to CH ₂ ratio	116
5.3.1	Steric hindrance of the head group	121
5.4	Trimethylsilyl (TMS) - Hedgehogs	123
5.4.1	Surface coverage	126
5.4.2	Small-angle neutron scattering (SANS)	128
5.5	Designing an effective surfactant tail	132
5.5.1	Generating low γ_{cmc} with short tails	132
5.5.2	Generating low γ_{cmc} with long tails	134
5.5.3	The effectiveness of a hydrocarbon surfactant - H_{γ}	135
5.5.4	Predicting potential super-effective hydrocarbon surfactants .	145
5.6	Conclusions	149
	References	150
6	Optimising Surfactant Performance with the Head Group	153
6.1	Introduction	154
6.1.1	Surfactants investigated	157
6.1.2	Determining surface properties of single-chain surfactants . . .	158

6.2	Surface properties	159
6.2.1	Critical micelle concentration	162
6.2.2	Surface tension	164
6.2.3	Area occupied at the air-water interface	166
6.3	Small-angle neutron scattering	168
6.4	The tetrapropylammonium head group	173
6.5	Conclusions	175
	References	176
7	Mixed Surfactant Systems	178
7.1	Introduction	178
7.1.1	Surfactants investigated	180
7.2	Determining cmc's of mixed systems	182
7.3	Analysis of cmc data using Regular Solution Theory	185
7.4	Linear-branched mixed systems	191
7.4.1	Surface tension results	191
7.4.2	Effect of chain length	194
7.4.3	Importance of the linear component	196
7.4.4	Packing efficiency at the surface	199
7.5	Branched-branched mixed systems	202
7.5.1	Surface tension results	203
7.6	Generating low surface energies	206
7.7	Conclusions	207
	References	208
	Project Conclusions	210
	Future Outlook	213
	Supporting Information	215

LIST OF TABLES

1 Introduction

1.1	Examples of synthetic and natural colloidal systems	2
1.2	Common surfactant classes encountered in colloidal systems	3
1.3	Common hydrophobic groups encountered in commercial surfactants	4

2 Structure-Property Relationships of Surfactants

2.1	Free energy of transfer of $-\text{CH}_2-$ and $-\text{CF}_2-$ from bulk to the surface	21
-----	---	----

3 Thermodynamics and Scattering Theory

3.1	Coherent scattering lengths for various atoms and molecules	50
-----	---	----

4 Experimental

4.1	Molecular structures and nomenclature of surfactants synthesised	67
4.2	Data from selected ^1H NMR spectra of single-chain surfactants	88
4.3	Data from selected ^1H NMR spectra of di-esters and di-chain surfactants	95
4.4	Elemental analysis results for single and di-chain surfactants	96

5 Designing Optimised Surfactant Tails

5.1	Surface tension for selected pure liquid alkanes and alcohols at 20 °C	102
5.2	Parameters derived from surface tension measurements of di-C7SS	114
5.3	Surface properties derived from γ -ln(a) plots for HS surfactant series	118
5.4	Surface coverage, tension and branching factor for the HS series	120
5.5	Surface tensions for synthesised surfactants and corresponding alcohols	122
5.6	Surface properties derived from γ -ln(a) plots for the TMS series	126

5.7	Surface coverage, tension and branching factor for TMS series	127
5.8	SANS Parameters fit to scattering models for TMS-hedgehog series	130
5.9	Surface properties for the most effective branched surfactants	136
5.10	Values of γ_{cmc} and H_γ for the most effective branched surfactants	145
6	Optimising Surfactant Performance with the Head Group	
6.1	Surface properties from γ -ln(a) plots for the single-chain surfactant series	162
6.2	Surface tension for select alcohols	165
6.3	SANS model fit parameters for the FO180 single-chain series	170
6.4	SANS model fit parameters for the FO180N single-chain series	171
6.5	SANS model fit parameters for the BC9 single-chain series	172
7	Mixed Surfactant Systems	
7.1	Properties derived from RST for the C6SS and C7SS mixed systems	188
7.2	Properties derived from RST for the C8SS mixed systems	189
7.3	Properties derived from RST for the AOT and HS3 mixed systems	190
7.4	Surface properties for the C6SS, C7SS and C8SS mixed systems	191
7.5	Surface properties of linear mixed systems at 0.01/0.99 mole fractions	196
7.6	Surface properties for the di-C8SS : AOTSiA/AOTSiB mixed systems	199
7.7	Surface properties for each branched mixed system	203

LIST OF FIGURES

1 Introduction

1.1	General structure of a surfactant molecule	2
1.2	Illustrated adsorption of surfactant molecules to the air-water interface	5
1.3	Cross section of a spherical micelle	6

2 Structure-Property Relationships of Surfactants

2.1	Forces acting on water molecules in the bulk and at the surface	13
2.2	Application of Gibbs adsorption equation to a typical γ -ln(C) plot	16
2.3	Comparison of surface properties for various linear surfactants	17
2.4	Surface character of hydrocarbon versus silicone surfactants	22
2.5	Molecular structure of the hedgehog surfactant Na-FO180	24
2.6	Representation of parameters used to calculate surface coverage, Φ_{cmc}	26
2.7	General structure-property relationship of low aqueous surface tension	27

3 Thermodynamics and Scattering Theory

3.1	Illustration of the ideal (air-water) interface in the Gibbs model	33
3.2	Neutron intensity for a steady state and pulsed neutron source	47
3.3	Schematic layout of D33 diffractometer (ILL)	48
3.4	Schematic setup of a small-angle scattering experiment	51
3.5	Vector relationship of the scattering vector Q	51
3.6	Illustration of the various Q domains in a scattering experiment	52
3.7	Representation of the particle form factor for a homogeneous sphere	54
3.8	Structure factor for attractive and repulsive homogeneous spheres	55
3.9	Combined particle form factor and structure factor for a sphere	56

3.10	Illustration of contrast variation for an example core-shell type particle	57
3.11	Representation of the particle form factor for a cylinder	59
3.12	Example Porod plot for near-monodisperse spheres	60
4	Experimental	
4.1	Single-chain synthetic routes followed	73
4.2	Di-chain synthetic route followed	76
4.3	¹ H NMR of Na-BC9 and corresponding starting alcohol	83
4.4	COSY NMR of Na-BC9	84
4.5	¹ H NMR of Na-BC9	85
4.6	¹ H NMR of TEA-BC9	86
4.7	¹ H NMR of TMA-FO180	87
4.8	¹ H NMR of AOTA di-ester	89
4.9	¹ H NMR of AOTSiB di-ester	90
4.10	¹³ C NMR of AOTSiC	91
4.11	¹ H NMR of AOTB	92
4.12	¹ H NMR of AOTSiB	93
4.13	¹ H NMR of di-C6SS	94
5	Designing Optimised Surfactant Tails	
5.1	Surface tension of di-C6SS and corresponding alkane/alcohol	103
5.2	Conductivity data for di-C7SS measured as a function of concentration	107
5.3	Determining the cmc from linear fits of conductivity data for di-C7SS	107
5.4	Determining the cmc from the double derivative of conductivity data	108
5.5	Variation in surface tension as a function of activity for di-C7SS	109
5.6	Illustration of how to highlight the cmc from surface tension data	110
5.7	Example of a metal-EDTA chelate	112
5.8	Effect of EDTA on the surface tension of di-C7SS	113
5.9	Surface tension behaviour of di-C7SS with and without EDTA at 25 °C	114
5.10	Representation of parameters used to calculate surface coverage, Φ_{cmc}	115
5.11	Molecular structures and γ_{cmc} values for AOT and di-C8SS	116
5.12	Molecular structures for the hydrocarbon surfactants HS1, HS2 & HS3	117

5.13	γ -ln(a) plots and corresponding adsorption isotherms for HS series	118
5.14	Equilibrium surface tension and surface coverage for the HS series	119
5.15	Surface tension of 2,2-Dimethyl-1-propanol at various temperatures	122
5.16	Surface packing of fluorocarbon and hydrocarbon surfactants	123
5.17	Molecular structures of TMS-hedgehog surfactant series	124
5.18	γ -ln(a) plots and corresponding adsorption isotherms for TMS series	125
5.19	SANS profiles for the TMS-hedgehog surfactant series	129
5.20	Structures and γ_{cmc} values for selected ‘short’ hedgehog surfactants	133
5.21	Structures and γ_{cmc} values for selected ‘long’ hedgehog surfactants	134
5.22	Molecular structures of surfactants that feature in Table 5.9	137
5.23	Example calculations of H_γ for ‘short’ hydrocarbon surfactants	139
5.24	Further example calculations of H_γ for ‘short’ hydrocarbon surfactants	140
5.25	Example calculation to determine H_γ for AOT3	141
5.26	Example calculation of H_γ for AOT5 and hypothetical equivalent AOTX	142
5.27	Illustrated calculation of H_γ where various branches are present	143
5.28	Illustrated calculations of H_γ for various different tail structures	144
5.29	Relationship between H_γ and γ_{cmc} for selected branched surfactants	146
5.30	Predicted super-effective hydrocarbon surfactants based on H_γ	148
6	Optimising Surfactant Performance with the Head Group	
6.1	Variation in γ_{cmc} for dodecylsulfate surfactants with various counterions	154
6.2	Variation in γ_{cmc} for AOT bearing various counterions	156
6.3	Molecular structures of surfactants investigated in this chapter	157
6.4	Procedure used to find the cmc from surface tension data	159
6.5	γ -ln(a) plots for the FO180 and FO180N surfactant series	160
6.6	γ -ln(a) plots for the BC9 and BC7 surfactant series	161
6.7	Variation in cmc for single-chain surfactant series with various counterions	163
6.8	Surface tension and area per molecule for each single-chain surfactant	167
6.9	SANS profiles for the FO180 single-chain series	170
6.10	SANS profiles for the FO180N single-chain series	171
6.11	SANS profiles for the BC9 single-chain series	172
6.12	γ_{cmc} data for five single-chain series with equivalent TAA ⁺ counterions	174

7 Mixed Surfactant Systems

7.1	Molecular structures of mixed surfactant systems studied	181
7.2	Conductivity data of di-C7SS:AOTB mixtures at various molar ratios	183
7.3	Variation of cmc with mole fraction of AOTB for each linear mixture	185
7.4	Visual representation of surface tension data for linear mixed systems	193
7.5	Variation in surface tension with increasing chain length	194
7.6	Surface tension at varying mole fractions of SDS mixed with AOTA	195
7.7	Surface tension at 0.01 mole fractions for each linear mixed system	197
7.8	Surface tension at 0.01/0.99 mole fractions for each linear mixed system	197
7.9	Visual representation of surface tension data for SiA/SiB mixed systems	200
7.10	An illustration of the volumes used to calculate Φ_{cmc}	201
7.11	Visual representation of surface tension data for branched systems	204

NOMENCLATURE

a_i	activity	β	interaction parameter
f_i	activity coefficient	τ	interfacial thickness (\AA)
A_{cmc}	area per molecule (\AA^2)	b_i	molality (mol kg^{-1})
N_a	Avogadro constant (mol^{-1})	α	mole fraction
ρ	bulk density (g cm^{-3})	V_{cal}	physical tail volume (cm^{-3})
μ_i	chemical potential (J mol^{-1})	h	Planck's constant (J s)
C^*	cmc of ideal mixture (mol dm^{-3})	R_{pol}	polar radius (\AA)
$b_{i,\text{coh}}$	coherent scattering length (cm)	P	pressure (Pa)
$\log\alpha_{\pm}$	Debye-Hückel limiting law	k_s	scattered wavevector (m^{-1})
H_{γ}	effectiveness index	Q	scattering vector (\AA^{-1})
H^{M}	enthalpy of mixing (J)	Φ_{cmc}	surface coverage
S	entropy (J K^{-1})	Γ	surface excess (mol m^{-2})
S^{M}	entropy of mixing (J K^{-1})	Γ_{cmc}	surface excess at cmc (mol m^{-2})
R_{eq}	equatorial radius (\AA)	γ	surface tension (N m^{-1})
V_{meas}	estimated tail volume (cm^{-3})	γ_{cmc}	surface tension at cmc (N m^{-1})
G^{M}	free energy of mixing (J mol^{-1})	T	temperature (K)
R	ideal gas constant ($\text{J K}^{-1} \text{mol}^{-1}$)	ϕ_i	volume fraction
k_i	incident wavevector (m^{-1})	λ	wavelength (m)

PROJECT OVERVIEW

The main objective of this research project is to improve the performance of hydrocarbon surfactants at air-water interfaces. Therefore fundamentally, an overall aim of this project is to improve our understanding of controlling surface tension. The structure of this thesis is outlined in the chapter descriptions below.

1. **Introduction** - A short introduction to surfactants in general, fluorosurfactants and their environmental constraints (which forms the justification for this research), finishing with a short description of the aims of this project.
2. **Structure-Property Relationships of Surfactants** - Covers surface tension and common surface properties to compare surfactant performance. The general structure-property relationship of low surface tension is introduced.
3. **Thermodynamics and Scattering Theory** - Provides a more thorough account of the background theory behind surfactant adsorption, aggregation and regular solution theory (mixed systems).
4. **Experimental** - Details the synthetic, purification and analytical characterisation procedures for surfactants introduced and discussed in this thesis
5. **Designing Optimised Surfactant Tails** - Outlines the key structural requirements of effective hydrocarbon surfactants, by comparing adsorption and aggregation results for various di-chain sulfosuccinate surfactants in water. The effectiveness index, H_γ , is introduced which provides a simple method to design strong performing hydrocarbon surfactants.
6. **Optimising Surfactant Performance with the Head Group** - Provides a new insight into improving the performance of hydrocarbon surfactants by controlling the identity of the head group. Surface and bulk properties are explored for many various single-chain anionic surfactants in aqueous systems.
7. **Mixed Surfactant Systems** - Mixed hydrocarbon surfactant systems are introduced which generate very low surface energies, below either constituent surfactant. The synergistic properties of these mixtures are attributed to enhanced molecular packing within the mixed monolayer.

Chapter 1

Introduction

This thesis is primarily concerned with the behaviour of surfactant molecules at air-water interfaces, and the various structure-property relationships required to generate low aqueous surface tensions. It is therefore important to first introduce surfactants, their characteristic features, diverse uses, and some colloidal systems of relevant interest.

1.1 Surfactants in colloidal systems

Surfactants are a powerful class of compounds which facilitate and improve many diverse processes, from breathing to extracting crude oil. The term *surfactant* is a contraction of the phrase, *surface active agent* which as implied, describes a molecule with a propensity for interfaces (an interface simply describes the boundary between two *phases*, i.e. the gas-liquid interface is commonly referred to as the surface). The reason surfactant molecules locate at an interface is due to their amphiphilic structure, meaning they are dual natured compounds composed of both hydrophilic and hydrophobic sections. A typical surfactant would possess a charged or highly polar moiety forming the hydrophilic section, commonly referred to as the *head group*, and a non-polar carbon chain referred to as the surfactant *tail*, example shown in Figure 1.1. It is because of their dual nature, possessing both strong polar and non-polar characteristics in a single molecule, that surfactants exhibit extraordinary properties and are found in an extensive and diverse range of colloidal systems.

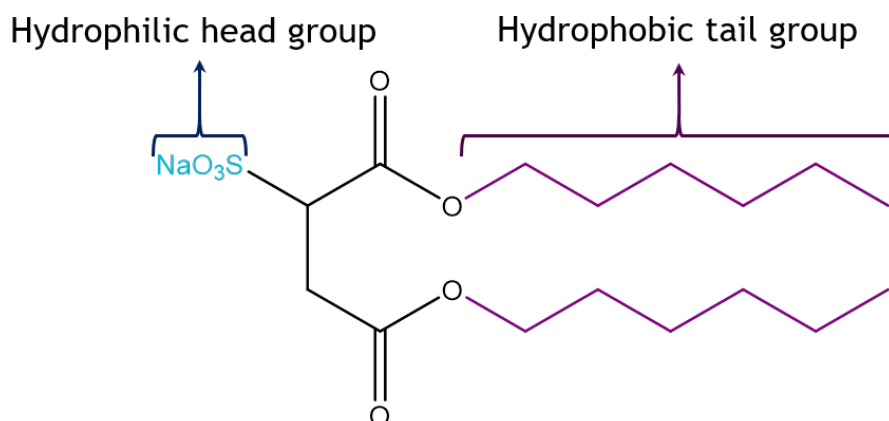


Figure 1.1: General structure of a surfactant molecule with the head and tail groups highlighted (surfactant shown is the linear dichain hydrocarbon surfactant di-C6SS).

Colloids are generally described as mixtures composed of one substance finely dispersed and suspended throughout another. However, the degree of subdivision within a colloid does not approach that found in simple molecular mixtures such as a solution, where solute and solvent constitute one phase. A colloidal system has a *dispersed phase*, the suspended particles with a size range approximately between 1 μm and 1 nm, distributed uniformly in a finely divided state throughout a *dispersion medium* (or continuous phase). Either phase can be a solid, liquid, or gas. Hence, combinations of various phases, together with the large surface areas associated with the characteristic size of colloidal particles, give rise to a large variety of systems and practical applications, see Table 1.1.

Dispersed Phase	Dispersed in Gas	Dispersed in Liquid	Dispersed in Solid
Gas	-	<i>Foams:</i> deodorant, fizzy drinks	<i>Solid foams:</i> styrofoam, marshmallow
Liquid	<i>Fogs:</i> mist, clouds, hairsprays	<i>Emulsions:</i> milk, shampoo, mayonnaise	<i>Gels:</i> butter, jelly, hair-gel
Solid	<i>Smokes:</i> dust, industrial smoke	<i>Sols:</i> paint, ink, cell fluids	<i>Solid sol:</i> pearl, paper, certain alloys

Table 1.1: Examples of some commonly encountered synthetic and naturally occurring colloidal systems.

1.2 Types of surfactants

Because of their propensity for interfaces surfactants can be used to control the properties of a colloidal system. This control is further enhanced by the variety of surfactants available, each possessing unique characteristics. Because the hydrophilic part of a surfactant molecule commonly achieves solubility by either ionic interactions or by hydrogen bonding, classification is based on surfactant head group type, with further subgroups based on the nature of the hydrophobic tail. Some common examples of different surfactant classes are shown below in Table 1.2.

The most commonly encountered surfactants are anionic, cationic, non-ionic and zwitterionic. Anionic surfactants dissociate in water into two oppositely charged species, a negative surfactant ion and a positive counterion. Functional groups acting as the head group include sulfate, sulfonate, phosphate and carboxylates. The opposite is true for cationic surfactants which dissociate into positive surfactant ions, featuring functional groups such as amines and quarternary ammonium salts.

Class	Example Structure	Name
Anionic		Alkylsulfates
Cationic		Alkylammonium halides
Non-ionic		Polyoxyethylene alcohols
Zwitterionic		Carboxy betaines
Gemini		Linked alkylammonium halides
Bolaform		Metal alkyldianoates

Table 1.2: Common surfactant classes encountered in colloidal systems.

Non-ionic surfactants possess no charge on the head group, but include a strong polar group such as a polyoxyethylene or polyoxypropylene chain to produce a structure of amphiphilic nature. Zwitterionic surfactants combine both a cationic and anionic group into a single molecule. This makes them amphoretic and able to respond to pH, with common head groups being betaines and sulfobetaines. Gemini and bolaform are less common surfactant classes which have been developed more recently. A gemini surfactant is simply two identical surfactants which is linked by a spacer group, either close to or at the head group. A bolaform surfactant can be considered the opposite of a gemini, being two identical surfactants but instead linked at the end of the tail group, giving two separate head groups.

All surfactant classes can be further divided into subgroups based on the nature of the hydrophobic tail. A variety of hydrocarbon chains are encountered, for example, natural fatty acids, olefins, alkylbenzenes and alkylphenols (SDS and di-PhC4SS - Table 1.3). Such surfactants are collectively referred to as hydrocarbon (HC) surfactants. The other two most commonly encountered groups are fluorocarbon (FC) surfactants comprising fluorocarbon chains (PFOS - Table 1.3), and silicone or siloxane surfactants bearing siloxane chains (L77 - Table 1.3).

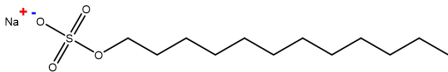
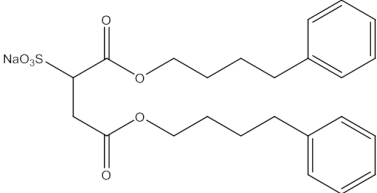
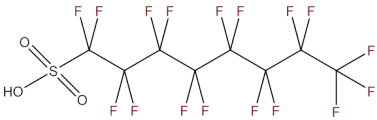
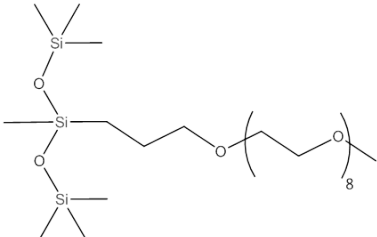
Group	Example Structure	Surfactant Name
Alkyl		SDS
Alkylphenol		di-PhC4SS
Fluorocarbon		PFOS
Silicone/Siloxane		L77

Table 1.3: Examples of common hydrophobic groups encountered in commercially available surfactants.

1.3 Characteristic features of surfactants

Although a great variety of different surfactant classes exist, they all possess amphiphilic structures. Therefore, when present in solution, there are characteristic features that all surfactant molecules display to accommodate for their dual nature.

1.3.1 Adsorption

When dissolved in aqueous solution, surfactant molecules will adsorb to the air-water interface (i.e. the surface) generating an orientated monolayer of surfactant tails. This happens because the free energy of a surfactant molecule located at the interface is lower than that of a molecule solubilised in either bulk phase. When present in bulk water, the hydrophobic tails will disrupt the hydrogen bonding network between water molecules, increasing the free energy of the system. On the other hand, the hydrophilic head group will decrease the free energy of the system by remaining solubilised in the water phase. Therefore, to satisfy these two conditions, surfactant molecules locate themselves at the air-water interface with the hydrophilic head group solvated in the water phase, and the hydrophobic tails orientated into the gas phase, see Figure 1.2. Air is by nature non-polar and by adsorbing to the surface, both moieties are solvated in their preferred bulk phase, generating a lower free energy of the system. Hence it takes less energy to bring a surfactant molecule to the surface than it does a water molecule. Therefore, adsorption of amphiphiles to an interface (liquid-liquid or gas-liquid) is a spontaneous process which alters the interfacial (surface) tension.

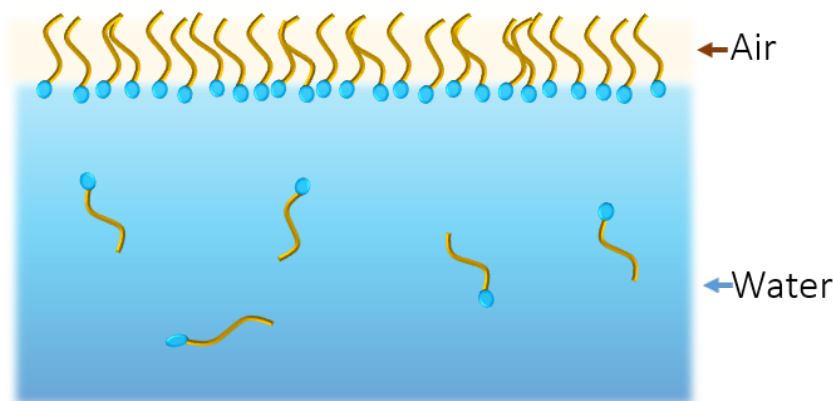


Figure 1.2: Surfactant molecules spontaneously adsorb to the air-water interface (surface) generating an orientated monolayer of surfactant tails.

1.3.2 Aggregation

As the concentration of surfactant in solution is increased, the surface coverage of surfactant molecules will also increase. At a well defined concentration, the surface is at (near) maximum coverage and surfactant molecules must adopt another configuration to minimise unfavourable, high energy interactions between the hydrophobic tails and water molecules. By undergoing self-aggregation, surfactant molecules can form structures where again both moieties are solvated in their preferred environment, generating a lower free energy. The hydrophobic tails orientate inwards, surrounding themselves by neighbouring tails whilst the hydrophilic head groups form a shell which can remain solvated in the bulk water, see Figure 1.3. By adopting this configuration, favourable interactions are formed between both the non-polar tails with each other and the polar head groups with water molecules, whilst also better conserving the hydrogen bonding between water molecules. These self-aggregated structures are called micelles, and the concentration at which they form is known as the critical micelle concentration (cmc). A variety of micellar shapes and sizes can be adopted with a typical micelle consisting of 50-200 surfactant molecules.

Above the cmc, the system has three states in equilibrium with each other - free surfactant molecules, an orientated monolayer, and micellised surfactant in the bulk. Below the cmc, the system is composed of an orientated monolayer and surfactant molecules which are perpetually arriving at, and leaving, the surface.

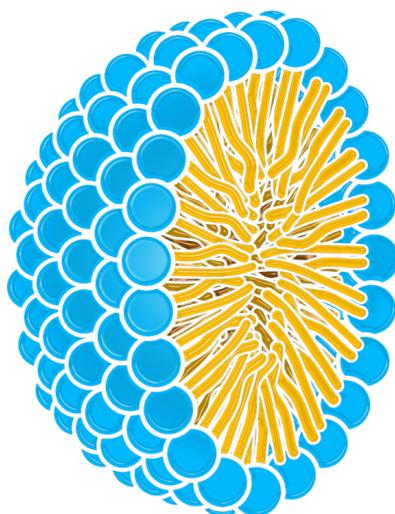


Figure 1.3: Cross section of a spherical micelle.

1.4 Uses of surfactants

Surfactants have an extremely widespread set of uses, being an integral group of chemicals in both nature and today's society. For example, pulmonary surfactants present in the lungs adsorb to the air-water interface of alveoli, reducing the surface tension to increase pulmonary compliance, prevent atelectasis (collapse of the lung) and reduce fluid accumulation.¹ The cell membrane is composed of a lipid bilayer, formed by amphiphilic phospholipids which undergo self-assembly. Surfactants have even shown to be crucial for effective anti-predator defence against invertebrates by offering a base level of protection.² However, although surfactants were clearly a crucial chemical for the evolution of biological species, they have also had a pivotal effect in the development of modern society.

Since the first synthetic detergents were developed in 1916 during World War I, synthetic surfactants have now become an essential component in many industrial formulations. Their broad applications include, but are not limited to: detergents, paints, inks, adhesives, agrochemicals, cosmetics, pharmaceuticals, firefighting, insecticides, printing and petroleum.³ The greatest demand for surfactants is in personal care products, being widely used in detergents, soaps, cosmetics etc. Out of the various classes of surfactants available, anionics account for the majority due to the ease and low cost of manufacture. Other classifications, although more expensive, still find specific uses for example, zwitterionics possess excellent dermatological properties, and because of their low skin and eye irritation are used in certain shampoos and cosmetics.

The most commonly used anionic surfactants possess a hydrocarbon tail, such as sodium stearate. However, certain applications (such as paints, polishes and coatings) require a more effective lowering of surface tension than typical HC surfactants. Fluorosurfactants, composed of a fluorocarbon tail, are more effective at reducing the surface tension than comparable HC surfactants and are therefore extensively used in many applications. Furthermore, FC surfactants are able to withstand harsher conditions than HC surfactants because of the stability of the carbon-fluorine bond (for more details see Section 2.4). Likewise, this also makes fluorosurfactants persistent organic pollutants, detectable in humans and wildlife.⁴

1.5 Environmental consequences of fluorosurfactants

Carboxylated and sulfonyl-based fluorochemicals have been produced and used for more than 50 years both industrially and commercially. These polyfluoroalkyl substances (PFSs) can degrade to persistent perfluorocarboxylates (PFCAs) and perfluoroalkyl sulfonates (PFSAAs).⁵ It is widely recognised that PFCAs and PFSAAs bioaccumulate in the environment, being measured in water, fish, birds, mammals and humans worldwide.⁶⁻⁸ Although some PFCAs possess a low bioaccumulation potential, the presence of detectable concentrations in higher trophic level biota (polar bears, minks and predatory birds) has generated concerns regarding the biomagnification potential in food webs.^{9,10} Toxic effects of PFCAs/PFSAAs vary depending on the species affected, as one example in mammals, PFCAs interact with nuclear receptor proteins which regulate the expression of genes, affecting enzymes and proteins involved in lipid metabolism.¹¹

Extensive studies determined that bioaccumulation was directly related to fluorinated carbon chain length, with the highest bioaccumulation potential noted for the longest perfluorinated acids.¹²⁻¹⁴ In 2009 PFSs with a carbon chain length of eight or more were listed as persistent organic pollutants under the Stockholm Convention.¹⁵ Short chain PFSs are the most common replacement, however, they are still environmentally persistent or have persistent degradation products. Hence, there is now a real need to develop environmentally friendly alternatives to FC surfactants. Hydrocarbon surfactants are considered more environmentally friendly and thus, could provide an alternative. However, conventionally HC surfactants are unable to reduce surface tension to the very low values achieved by FC surfactants, e.g. PFOS = 17.8 mN m^{-1} .¹⁶ Recent novel HC surfactants which have a highly branched surfactant tail have generated very low values of surface tension, comparable with certain FC surfactants.¹⁷ This result strongly promotes the possibility of using HC surfactants as an environmentally friendly alternative, pointing to new ways of designing 21st century surfactants and controlling surface energy.

1.6 Project aims

To establish a suitable and viable replacement for fluorosurfactants, the performance of hydrocarbon surfactants must be improved beyond what is currently achieved. To accomplish this, strong links between molecular structure and physio-chemical action must be determined. Previous attempts, most notably the work of Nave *et al.*, have created a solid foundation to help elucidate further structure-property relationships of hydrocarbon surfactants. However, the need to generate very low surface energies with hydrocarbon surfactants has remained insignificant until now. Therefore, the structural characteristics of exceptionally strong performing hydrocarbon surfactants is currently unknown. The main aim of this project is to understand how the performance of hydrocarbon surfactants can be significantly improved, by controlled design of the surfactant structure. Which in turn, will improve our fundamental understanding of controlling surface tension. This thesis therefore primarily focuses on structural effects of surfactant molecules at air-water interfaces, which are investigated through techniques such as tensiometry.

As briefly introduced towards the end of this chapter, hydrocarbon surfactants have been highlighted as a possible alternative to environmentally hazardous fluorosurfactants, due to the low surface energies generated by highly branched tail structures. Therefore, a primary objective of this work is to identify why highly branched hydrocarbon tails are effective. By synthesising, characterising and comparing surface properties for a large range of anionic hydrocarbon surfactants, important structure-property relationships required to generate low surface energies can be distinguished. Thus, it should be possible to identify *general* structure-property relationships of effective hydrocarbon surfactants, which can then be used to guide the design of new, high performance surfactants. A secondary objective is to achieve the lowest surface energies with all major forms of surfactants: single-chain, di-chain and mixed surfactant systems, providing alternatives for industrial formulations.

Overall, this work aims to use and consolidate research over the last twenty years to outline the general, necessary structural characteristics of effective hydrocarbon surfactants. It will therefore act as a guide, or manual, to design low surface energy hydrocarbon surfactants. Establishing a secure, viable, and strong future for designing environmentally acceptable replacements to fluorosurfactants.

References

- [1] Zasadzinski, J.; Ding, J.; Warriner, H.; Bringezu, F.; Waring, A. J. *Curr. Opin. Colloid Interface Sci.* **2001**, *6*, 506–513.
- [2] Rostás, M.; Blassmann, K. *Proc. R. Soc. Lond., B, Biol. Sci.* **2009**, *276*, 633–638.
- [3] Schramm, L. L.; Stasiuk, E. N.; Marangoni, D. G. *Annu. Rep. Prof. Chem., Sect. C: Phys. Chem.* **2003**, *99*, 3–48.
- [4] Giesy, J. P.; Kannan, K. *Environ. Sci. Technol.* **2002**, *36*, 146A–152A.
- [5] Houde, M.; Martin, J. W.; Letcher, R. J.; Solomon, K. R.; Muir, D. C. *Environ. Sci. Technol.* **2006**, *40*, 3463–3473.
- [6] Taniyasu, S.; Kannan, K.; Horii, Y.; Hanari, N.; Yamashita, N. *Environ. Sci. Technol.* **2003**, *37*, 2634–2639.
- [7] Kannan, K.; Corsolini, S.; Falandysz, J.; Fillmann, G.; Kumar, K. S.; Loganathan, B. G.; Mohd, M. A.; Olivero, J.; Wouwe, N. V.; Yang, J. H. *Environ. Sci. Technol.* **2004**, *38*, 4489–4495.
- [8] Martin, J. W.; Smithwick, M. M.; Braune, B. M.; Hoekstra, P. F.; Muir, D. C.; Mabury, S. A. *Environ. Sci. Technol.* **2004**, *38*, 373–380.
- [9] Muir, D. C.; Howard, P. H. *Environ. Sci. Technol.* **2006**, *40*, 7157–7166.
- [10] Martin, J. W.; Whittle, D. M.; Muir, D. C.; Mabury, S. A. *Environ. Sci. Technol.* **2004**, *38*, 5379–5385.
- [11] Chinje, E.; Kentish, P.; Jarnot, B.; George, M.; Gibson, G. *Toxicol. Lett.* **1994**, *71*, 69–75.

- [12] Conder, J. M.; Hoke, R. A.; Wolf, W. d.; Russell, M. H.; Buck, R. C. *Environ. Sci. Technol.* **2008**, *42*, 995–1003.
- [13] Martin, J. W.; Mabury, S. A.; Solomon, K. R.; Muir, D. C. *Environ. Toxicol. Chem.* **2003**, *22*, 196–204.
- [14] Van de Vijver, K. I.; Holsbeek, L.; Das, K.; Blust, R.; Joiris, C.; De Coen, W. *Environ. Sci. Technol.* **2007**, *41*, 315–320.
- [15] Blum, A.; Balan, S. A.; Scheringer, M.; Trier, X.; Goldenman, G.; Cousins, I. T.; Diamond, M.; Fletcher, T.; Higgins, C.; Lindeman, A. E. *Environ. Health Perspect.* **2015**, *123*, A107–11.
- [16] Gorodinsky, E.; Efrima, S. *Langmuir* **1994**, *10*, 2151–2158.
- [17] Alexander, S.; Smith, G. N.; James, C.; Rogers, S. E.; Guittard, F.; Sagisaka, M.; Eastoe, J. *Langmuir* **2014**, *30*, 3413–3421.

Chapter 2

Structure-Property Relationships of Surfactants

To generate lower surface tensions than previously achieved by hydrocarbon surfactants, our fundamental understanding of how we control surface tension must be developed. In this chapter, a more thorough explanation of surface tension is given, and common surface properties used to compare surfactant performance are introduced. Relationships between surface tension and surfactant structure are discussed for fluorocarbon, hydrocarbon, and silicone surfactants. By comparing the performance of these three classes of surfactant a new, general property that accounts for low aqueous surface tension is introduced. This general structure-property relationship of surfactants has not been highlighted before, and points to new ways of controlling surface tension. This chapter is adapted from a literature review published by the author of this thesis.¹

2.1 Surface tension

The area where two bulk phases meet is referred to as the interface. Because the molecular environment of each bulk phase is different at the interface, there is a corresponding interfacial free energy. When a gas meets a liquid, i.e. a surface, the interfacial free energy is referred to as the surface free energy, or surface tension - γ . Observed when pond skaters delicately move over water, γ is caused by an imbalance of attractive intermolecular interactions at a liquid surface. Molecules

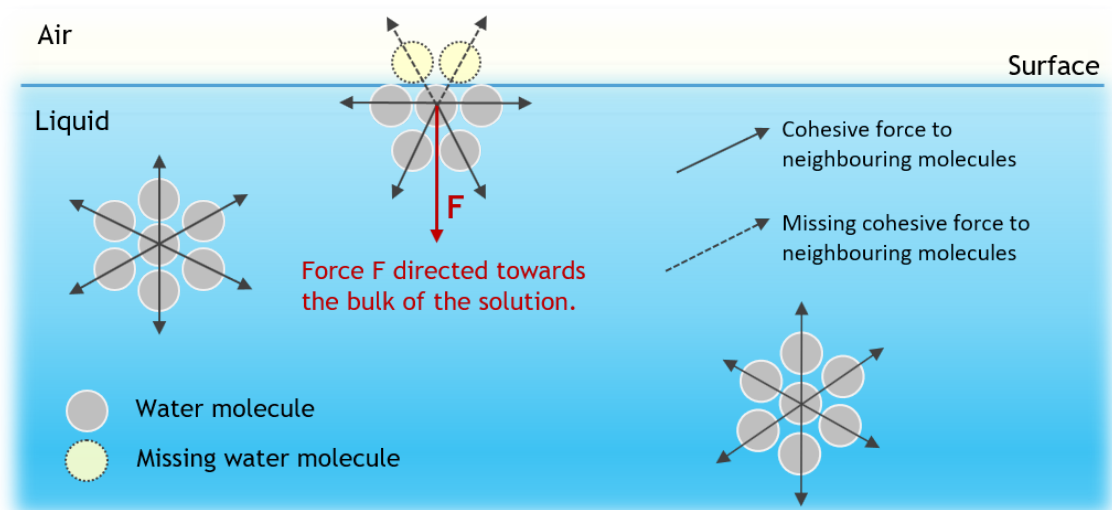


Figure 2.1: The forces acting on water molecules in the bulk and at the surface.

at the surface have no neighbours above, and are consequently pulled inwards by molecules in the bulk which causes the surface to contract, giving rise to surface tension. However, it is also possible to describe γ in terms of energy. Two molecules neighbouring each other will be in a lower energy state than if alone, due to mutual attractive interactions. Molecules on the surface have less neighbours compared to molecules in the bulk, and are therefore in a higher energy state, see Figure 2.1. This creates an excess energy on the surface, referred to as the surface free energy. To reduce this excess energy the surface will contract to reduce the exposed surface area (e.g. drops and bubbles are spherical because a sphere possesses the highest volume to surface area ratio). Hence, the surface free energy (units: J m^{-2}) and surface tension (units: N m^{-1}) of a liquid are equivalent, but a different definition of the same phenomenon.

Minimisation of the contact area with the gas phase is a spontaneous process and therefore, to create additional surface, a minimum amount of work (W_{min}) is required. This is simply a product of the surface tension γ and increase in interfacial area ΔA , so $W_{min} = \gamma \Delta A$. A surface-active agent (surfactant) is a substance that will adsorb to a surface, significantly alter the surface (interfacial) tension, thereby changing the amount of work required to expand the liquid surface. Surfactants reduce γ by forming an orientated monolayer of tails at the surface to accommodate for their dual-nature, as introduced in Section 1.3. The driving force for surfactant adsorption is unfavourable hydrophobic interactions within the bulk phase. There,

water molecules interact strongly with each other via hydrogen bonding and van der Waals interactions. The presence of a hydrophobic surfactant tail dissolved within the bulk disrupts the isotropically arranged hydrogen bonding network, causing an unfavourable increase in the free energy of the system. It therefore requires less work to bring a surfactant molecule to the surface than a water molecule hence, hydrophobic moieties will spontaneously be expelled from bulk water, an observed tendency known as *the hydrophobic effect*.² It should be noted that it is a loss of entropy rather than bond energy that leads to an unfavourable free energy change for the process.³ As surfactant molecules arrive at the surface, they form an *orientated monolayer* with the hydrophobic tails partitioned into the air (which is by nature non-polar) whilst the polar head groups remain solvated in water (Figure 1.2). The spontaneous formation of this orientated monolayer reduces the surface tension of pure water (72.5 mN m^{-1} at 298 K) because simply put, high energy polar water molecules are replaced by a layer of lower energy non-polar surfactant tails.

2.1.1 Equilibrium and dynamic surface tension

Equilibrium surface tension - Also referred to as the static or limiting surface tension, it represents the surface tension of a particular interface at its equilibrium state. Equilibrium is reached when sufficient time has passed allowing complete formation of the orientated surfactant monolayer. Dependent on conditions (i.e. temperature, etc.), there is only one value of static surface tension for a particular interface.

Dynamic surface tension - The equilibrium surface tension is not achieved instantaneously because surfactant molecules must first adsorb to the surface from the bulk, whilst also achieving the correct orientation. Eventually this dynamic surface tension will decay to the equilibrium value over a certain period of time which depends on the surfactant type and concentration, ranging from milliseconds to days. Measuring the surface tension over time (i.e. the dynamic surface tension) can provide information on the diffusion and adsorption rates. The efficiency of certain processes such as printing are highly dependent on these rates, attracting much attention to understand the processes governing transport of surfactant molecules from bulk to the interface.^{4,5} However, the primary concern of the research presented here is investigating the equilibrium surface tension, and will be the focus for the chapter.

2.2 Surface properties of surfactants

As surfactant is introduced into solution, the surface tension will begin to decrease due to adsorption of surfactant molecules to the surface. As the concentration of surfactant increases, the surface tension will continue to decrease until the surface becomes fully saturated and is at (near) maximum coverage. To further minimise the free energy of the system, surfactant molecules undergo self-aggregation (micellisation), forming structures in the bulk phase which continue to keep the surfactant head and tail solvated in their preferred environment. The well-defined concentration at which this happens is known as the cmc, or critical micelle concentration. Both the concentration of the cmc, and range at which adsorption takes place, depend on the molecular structure of the surfactant. A time-averaged value for the concentration of surfactant molecules at the surface can be determined directly, or indirectly, using thermodynamic equations. Both the thermodynamics of micellisation and adsorption, as well as details about micelle formation and structure will be more thoroughly described in Chapter 3.

The surface excess, Γ , provides a quantitative description of surfactant adsorption, and is defined as the concentration of surfactant molecules in a surface plane, relative to that at a similar plane in the bulk. The Gibbs equation (Eqn. 2.1) relates the change in surface tension with concentration, to the amount adsorbed at the surface:

$$\Gamma = \frac{-1}{mRT} \left(\frac{d\gamma}{d \ln C} \right) \quad (2.1)$$

where m is the number of adsorbing species, R is the ideal gas constant, T is the temperature, γ is the surface tension, and C is the surfactant concentration. Hence, by application of the Gibbs analysis, measurement of γ as a function of C allows a quantitative determination of the adsorbed amount $\Gamma(C)$. Figure 2.2 shows the typical behaviour of a surfactant in water (decreasing surface tension with increasing surfactant concentration), and how the Gibbs equation is applied to quantify adsorption at the surface. By determining the surface excess at the cmc, the area per molecule at the cmc A_{cmc} , that is, the average area one surfactant molecule occupies at the interface, can be estimated.

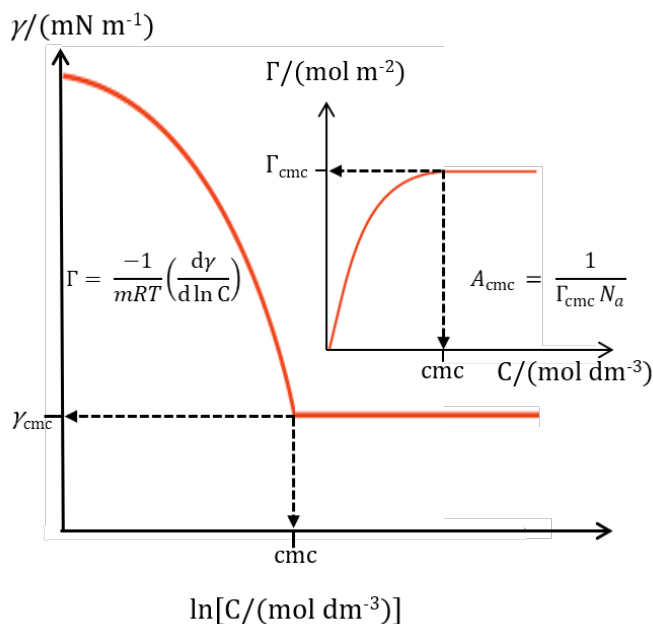


Figure 2.2: The surface tension (γ) is reduced as surfactant molecules adsorb to the air-water interface, simultaneously increasing the surface excess (Γ) until the cmc is reached, at which point there is generally a plateau. A_{cmc} corresponds to the area per surfactant molecule at the air-water interface at the cmc.

The surface tension remains constant after the cmc because the surface has become fully saturated hence, the surface tension at the cmc, γ_{cmc} , represents a useful reference value in surface tension for a particular surfactant. The critical micelle concentration (cmc), the limiting surface tension at the cmc (γ_{cmc}), the area per molecule at the cmc (A_{cmc}) and the dynamics of adsorption, are all influenced by the surfactant structure. For example, Figure 2.3 shows the aqueous limiting surface tension and molecular area for a common linear fluorocarbon (FC), silicone (SiC), and hydrocarbon (HC) surfactant. A large variation in γ_{cmc} is seen highlighting the importance of chemical structure. Note, the common linear HC surfactant SDS is a poor performer on this scale, suggesting such simple HC surfactants are inefficient. Hence, by comparing important physiochemical properties such as γ_{cmc} and A_{cmc} for a variety of different surfactant structures, relationships between surfactant structure and surface tension are highlighted. These structure-property relationships can then be used to help guide the design of novel surfactants for the application of interest, i.e. to generate low surface energies with HC surfactants.

The interfacial width (i.e. thickness) of a surfactant monolayer at the air-water interface can be determined by neutron reflectometry (NR).⁹ This will vary depend-

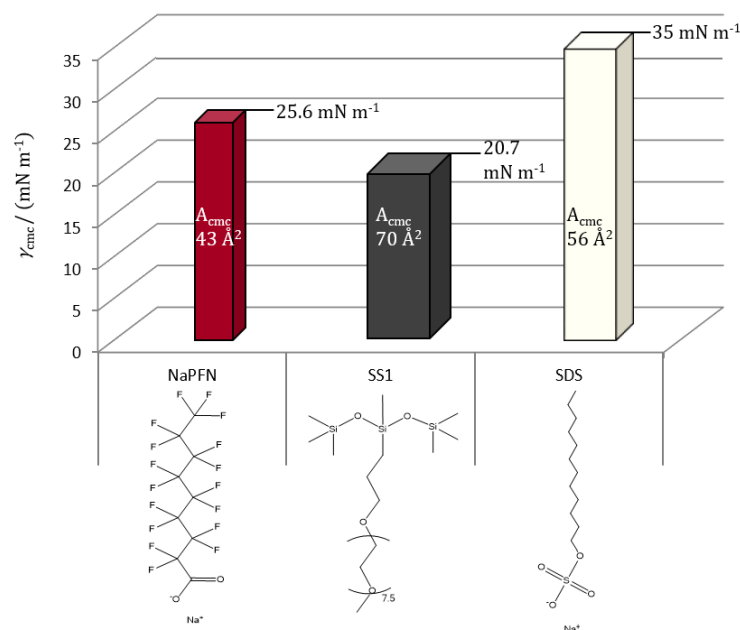


Figure 2.3: Aqueous limiting surface tension and corresponding interfacial molecular area for a typical linear fluorocarbon, silicone and hydrocarbon surfactant. The column height represents γ_{cmc} , and the column width is proportional to A_{cmc} . Data for NaPFN,⁶ SS1,⁷ and SDS.⁸

ing on the surfactant structure, but for hydrocarbon surfactants, the monolayer width generally falls in the range of 15 - 25 Å.¹⁰ However, surfactant structure does not solely define the interfacial width, and thermal fluctuations present at the surface will affect the observed monolayer thickness (i.e. capillary waves and surface roughness).¹¹ The Gibbs model does not account for these subtle surface effects as the interface is assumed to be infinitely thin (see Chapter 3). However, provided experiments are both constructed and conducted carefully, good agreement has been found for interfacial widths determined by surface tension and NR.¹²

2.2.1 Surfactant efficiency and effectiveness

To help compare the performance of surfactants, Rosen et al. provided specific definitions of the efficiency and effectiveness of surfactant molecules.¹³

Surfactant efficiency - “The bulk concentration of surfactant required to produce a 20 mN m⁻¹ reduction of surface tension.”

Surfactant effectiveness - “The maximum reduction of surface tension that a particular surfactant can generate, regardless of concentration.”

2.3 Influence of the hydrophobic tail on surface tension

The surface tension of a liquid is intimately related to intermolecular interactions.¹⁴ Fowkes suggested that by approximating intermolecular interactions as additive, surface tension γ may be represented by two dominant contributions, one due to dispersion interactions γ^d and one accounting for all other polar interactions γ^p (i.e. $\gamma = \gamma^d + \gamma^p$).¹⁵ This concept can be applied directly to the solid/liquid interface to obtain the two separate components of surface energy. By conducting contact angle studies Pitt et al. investigated the polar and dispersive components of sulfosuccinate and sulfotricarbalylate surfactants.¹⁶ Surface free energies were then compared with the limiting surface tensions of aqueous solutions. For both surfactant series, a strong correlation was seen between the dispersion component of surface free energy γ^d , but no correlation was seen for the polar component γ^p . For the first time Pitt highlighted clearly the strong relationship between surface tension and chemistry of the hydrophobic tails. By comparing surface properties of fluorocarbon and hydrocarbon surfactants, Pitt was able to identify some general structure-property relationships of surface tension (ref. [16]), namely:

- Increasing the number of tails (i.e. going from a single-chain to di-chain surfactant) caused a further reduction of surface tension.
- A variety of terminal chain groups were investigated and included fluoroalkyl, alkyl, and aryl groups, showing the following trend for γ_{cmc} : $CF_3-CF_2- < H(CF_2CF_2)- < \text{branched alkyl} < \text{single-tail alkyl} < \text{phenyl}$

The trend of a decreasing surface tension with increasing number of tails is a consequence of two effects: 1) an increase in the packing efficiency of the tail groups versus the electrostatic repulsion between neighbouring head groups and 2) a direct increase in the $-CH_3$ to $-CH_2-$ ratio per head group, based on the following order of increasing energy $CF_3 < CF_2 < CH_3 < CH_2$.¹⁷ The effects of various tail chemistries on limiting surface tension was extended to non-ionic surfactants. Despite being charge neutral, the pattern of behaviour and the effects of various tail chemistries were of the same order as seen with the anionic surfactants, further

reinforcing the strong relationship between surface activity and chemistry of the hydrophobic tails.

The most common surfactants are FC, SiC, and HC surfactants, based on hydrophobic tails composed of fluorocarbon, siloxane or hydrocarbon chains respectively. By comparing the structure-property relationships of three different classes of surfactant, it has been possible to identify a new general property of surfactants which accounts for a low aqueous surface tension. First though, a brief overview of the unique properties of each class.

2.4 Fluorosurfactants

In the 1950s, an unexpected discovery at 3M highlighted the potential of fluorochemical cleaning products and catalysed the development of fluorosurfactants. Fluorosurfactants now constitute an important class and appear in a diverse range of applications including biomedicine, firefighting applications, cosmetics, lubricants, paints, polishes, and adhesives, representing a multibillion dollar industry.¹⁸ Furthermore, the hydrophobic tails of fluorosurfactants display both oil and water repellency, and because of this, fluorosurfactants are used as low-surface-energy coatings, for example, on textiles or paper.¹⁹

In fluorinated surfactants, at least one hydrogen in the hydrophobic tail has been replaced by fluorine. Both the extent of fluorination and position of the fluorine atoms affect the characteristics of the surfactants. Fluorosurfactants can be described as perfluorinated, where all hydrogen in the hydrophobic tail has been replaced by fluorine, or as partially fluorinated. Fluorosurfactants display greater surface activities than their hydrocarbon counterparts and can lower surface tensions effectively at very low concentrations, typically lowering the surface tension of water from 72 to around 15-25 mN m⁻¹. The essential reasons fluorocarbon (FC) surfactants generate low γ_{cmc} are the following:

- (1) The lower polarisability of fluorine compared to hydrogen results in weaker attractive intermolecular forces.
- (2) The greater molecular volume of perfluoroalkyl moieties over hydrocarbon moieties makes fluoroalkyl chains more hydrophobic.

- (3) The larger cross section of fluorocarbon chains means the packing density per unit area is lower and hence so are the intermolecular forces.

The greater surface activity of fluorosurfactants over that of their hydrocarbon counterparts stems from the unique properties of fluorine. The cohesion of a liquid is due to the attractive forces between molecules. Although because of the high electronegativity of fluorine a C-F bond is polarised, a perfluorocarbon chain is overall nonpolar and has a zero dipole moment. In nonpolar liquids, only the induced-dipole/induced-dipole dispersion interactions are of relevance. The strength of this interaction is governed by the polarisability of the interacting atoms. Fluorine has a lower polarisability than hydrogen therefore, the total dispersion interaction is lower for the interaction between fluorine atoms. Hence, perfluoroalkane liquids are expected to have weaker attractive intermolecular forces than similar hydrocarbons.

The other principal reason for the lower surface tensions exhibited by perfluoroalkane liquids in comparison to those of analogous hydrocarbons is the larger volume of perfluoroalkyl moieties. The mean volumes of $-\text{CF}_2-$ and $-\text{CF}_3$ groups have been estimated to be 38 and 92 \AA^3 , whereas those of $-\text{CH}_2-$ and $-\text{CH}_3$ are around 27 and 54 \AA^3 respectively.²⁰ Linked to these steric reasons, the average limiting cross-sectional area for a fluorocarbon chain is 27-30 \AA^2 , which is larger than the range of 18-21 \AA^2 typically achieved for a hydrocarbon chain (ref. [20]). It is also instructive to examine the free energy of transfer of non-polar carbon moieties from water, ΔG , and hence quantify the hydrophobic effect. Table 2.1 compares the size and incremental changes in free energy of adsorption for the transfer of a mole of $-\text{CH}_2-$ or $-\text{CF}_2-$ groups from water to the air-water interface. It can be seen that a more favourable free energy of transfer is obtained for $-\text{CF}_2-$ groups and therefore, F chains are considerably more hydrophobic than H chains because of their relative larger size. Hence, because of the “bulk” of fluorocarbon surfactants, they will show an enhanced tendency to segregate, self-assemble, and collect at the air-water interface to alter the surface free energy.

The larger cross section of a fluorocarbon chain also means that the molecular packing density per unit area is lower than for hydrocarbon chains and therefore, so are the intermolecular interactions. Hence, because of the unique chemistry of fluorine over hydrogen, it can now be understood why fluorocarbon surfactants possess

Group	Cross-sectional area (\AA^2)	Group volume (\AA^3)	$-\Delta G$ (kJ mol^{-1})
$-\text{CH}_2-$	18-21	27	2.60
$-\text{CF}_2-$	27-30	38	5.10

Table 2.1: Comparison of the size and free energy of transfer from water to the air/water interface at 298.15 K for one mole of $-\text{CH}_2-$ and $-\text{CF}_2-$ groups. Data from ref. [20].

greater surface activities over hydrocarbon analogues and why longer fluoroalkyl chain lengths give the lowest reported surface energies. However, as described in Section 1.5, more recently it has been identified that fluorinated compounds with C8-C15 chain lengths are hazardous pollutants.²¹ Bioconcentration and bioaccumulation of perfluorinated acids are directly related to fluorination,²² and now there is a need to develop replacements for fluorosurfactants.

2.5 Silicone surfactants

Silicone surfactants, also commonly referred to as siloxane surfactants, are composed of permethylated siloxane hydrophobic groups coupled to one or more hydrophilic polar groups. There are three common molecular structures for silicone surfactants: rake-type copolymers (comb or graft copolymers),²³ ABA copolymers (where B represents the silicone portion),²⁴ and trisiloxane surfactants (Table 1.3).²⁵ Although the polar groups can be nonionic, anionic, cationic, or zwitterionic, nonionic groups based on polyoxyethylene (PEO) and polyoxypropylene (PPO) are the most common. Silicone surfactants can effectively reduce aqueous surface tensions, achieving γ_{cmc} in the range of 20-30 mN m^{-1} (compared to the value of $\sim 30 \text{ mN m}^{-1}$ for typical hydrocarbon surfactants) and can be surface-active in both aqueous and nonaqueous media.²⁶ The essential reasons silicone (SiC) surfactants generate low γ_{cmc} are the following:

- (1) the low intrinsic surface activity and lower surface energy of methyl groups.
- (2) the flexibility of the siloxane backbone which can adopt conformations to present available organic groups to their best advantage (i.e., a surface that is dominated by methyls).

The -O-Si-O-Si- backbone serves as a flexible framework on which to attach multiple methyl groups. The low intrinsic surface energy of methyl groups (ref. [17]) coupled with the unique flexibility of the siloxane backbone enables the surfactants to adopt a variety of configurations and to present surfaces that are dominated by methyl groups, compared to typical linear-chain HC surfactants, which promote films with a greater proportion of higher-surface-energy $-\text{CH}_2-$ groups (Figure 2.4).

These systems also display unique spreading properties; therefore, they are widely used in applications such as stabilisers for polyurethane foams, emulsifiers in cosmetics, agricultural adjuvants, textile conditioning, coating, and ink additives.²⁷ However, the Si-O-Si linkage is susceptible to hydrolysis in the presence of moisture, and the hydrolytic instability of trisiloxane surfactants is an inherent weakness which reduces their performance as well as requiring careful handling, synthesis and storage.²⁸

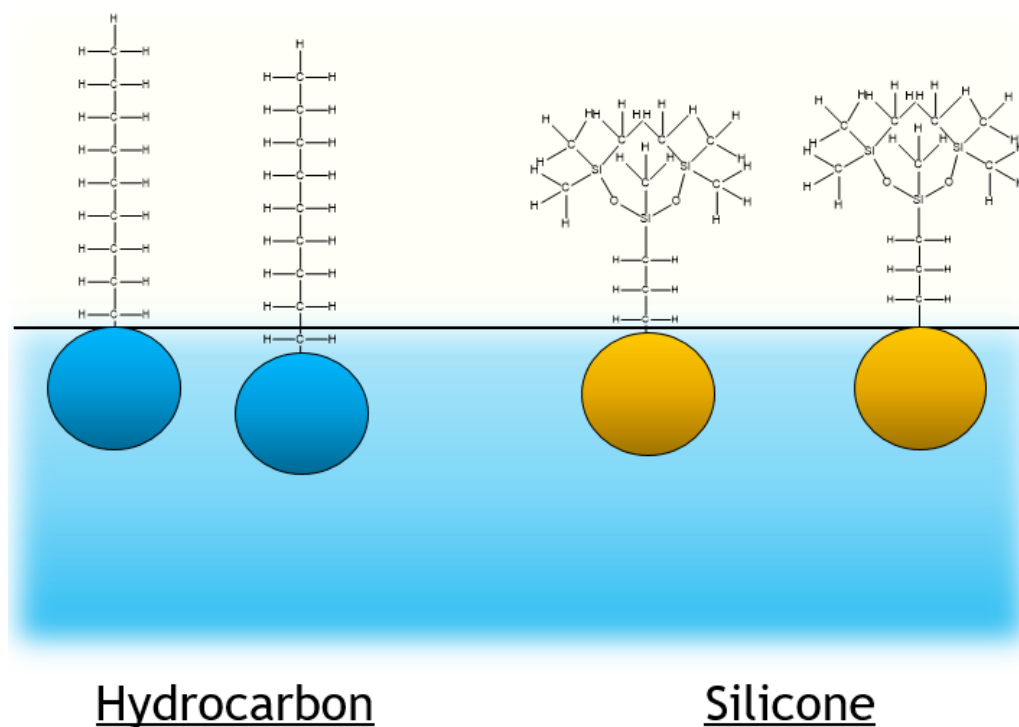


Figure 2.4: Schematic comparison of the surface character of hydrocarbon versus silicone surfactants.

2.6 Hydrocarbon surfactants

Because of the unique chemistry of fluorine compared to hydrogen, and the enhanced flexibility of a siloxane backbone, linear hydrocarbon surfactants are outperformed by common FC and SiC surfactants. Initially, it would appear that hydrocarbon surfactants are inferior. However, due to the environmentally hazardous nature of FC surfactants, and the hydrolytic instability of SiC surfactants, hydrocarbon surfactants offer an alternative which is both stable and environmentally safe. Recently, highly branched hydrocarbon surfactants have been synthesised which generate very low values of γ comparable with certain FC surfactants.²⁹ The essential reasons these HC surfactants generate low γ_{cmc} are:

- (1) the low intrinsic surface energy of methyl groups $-\text{CH}_3$ (ref. [17])
- (2) highly branched tails generate dense surface layers composed of $-\text{CH}_3$ groups with weaker tail-tail interactions compared to those of linear-chain HC tails.

Aerosol-OT (or AOT) is one of the most studied surfactants because of its high versatility, rich aqueous-phase behavior, and ability to form cosurfactant-free microemulsions. Investigations of the relationship between the surfactant molecular structure and phase behavior have previously been performed with 16 different aerosol-OT-related surfactants.³⁰ AOT with a limiting surface tension of $\gamma_{\text{cmc}} = 30.8 \text{ mN m}^{-1}$ and an effective area per molecule of $A_{\text{cmc}} = 75 \text{ \AA}^2$ was shown to behave in a very similar fashion to a range of related analogues. However, these studies revealed that the hydrocarbon backbone structure dictates the interfacial packing. The branched-chain compounds demonstrated a significant increase in A_{cmc} of between 10 and 20 \AA^2 over those found for equivalent carbon number linear-chain surfactants. Furthermore, slight variations in A_{cmc} were detected, reflecting changes in packing owing to differing extents of chain branching. It has been shown that the chain branching of hydrocarbon surfactants, especially an increasing level of chain tip methylation, can lead to γ_{cmc} values lower than those for linear chain analogues.³¹ This approach to packing the hydrocarbon chain termini with low surface-energy $-\text{CH}_3$ groups mirrors the architecture of the very effective siloxane surfactants mentioned in the previous section.

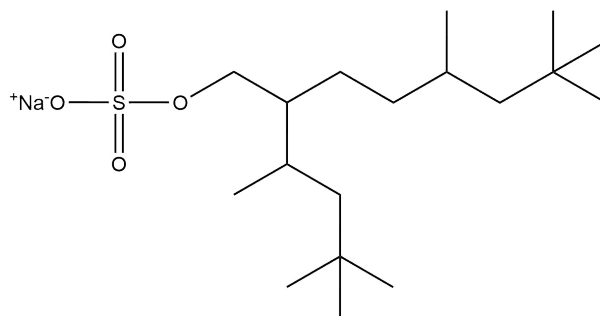


Figure 2.5: Molecular structure of the highly branched hydrocarbon surfactant Na-FO180.

In effect, the limiting γ that could be achieved with a HC surfactant would be that for the parent hydrocarbon. For example, the γ_{cmc} of SDS with linear nC12 chains is $\sim 35 \text{ mN m}^{-1}$, but $\gamma_{\text{air-liquid}}$ for pure n-dodecane is $\sim 26 \text{ mN m}^{-1}$.³² The reason for the difference is that the water-soluble head groups sterically hinder the surfactant tails from achieving a dense surface, and increase the dispersion contribution γ^{d} to the total tension by introducing dipolar interactions. Therefore, to obtain soluble and useful low-surface-energy HC surfactants, the van der Waals dispersion interactions must be maximised to promote dense surface packing of $-\text{CH}_3$ and $-\text{CH}_2-$ groups while at the same time minimising dipolar head group interactions, which are essential, and unavoidable, to promoting water solubility. Hence, the net limiting surface tension γ_{cmc} is a result of the balance between these two opposing effects.

One approach is to replace linear hydrocarbon chains with highly branched bulkier groups, also referred to as “*hedgehog*” surfactants owing to their unusual spiky brushlike structures. In these systems, branched alkyl moieties help to generate high densities of pure liquid alkanes at the air-water interface. The molecular structure of the effective hedgehog surfactant Na-FO180, achieving $\gamma_{\text{cmc}} = 25.4 \text{ mN m}^{-1}$, is shown in Figure 2.5. Compared to an appropriate pure alkane such as tetradecane, where $\gamma_{\text{tetradecane}} = 24.8 \text{ mN m}^{-1}$, it’s clear to see that γ_{cmc} has reached a natural limit of surface tension reduction. This remarkable reduction in γ is due to both the chain tip methylation which helps to generate a surface dominated by low surface-energy $-\text{CH}_3$ groups, and the chain branching which increases A_{cmc} . This increase in A_{cmc} reduces the number of surfactant molecules required to generate a dense surface coverage, and therefore, as a result, reduces the dispersion contribution to surface tension.

Hence, to develop HC surfactants with surface tensions as low as can be obtained for FC surfactants, dense surfactant films are needed. The optimal thickness of a surfactant layer (i.e., the optimal length of a surfactant tail) for attaining very low γ must be considered. If the tails are too long, then the surfactant will have poor solubility in water owing to the hydrophobic effect, and stronger tail-tail interactions will result in surfactants that are too hydrophobic, with low cmc's, tending towards insolubility. On the other hand, too short a tail is insufficiently hydrophobic demanding impractical quantities of surfactant to generate a sufficiently dense surface coverage.

The results presented above suggest that highly branched tail structures can indeed generate dense surface layers, which mimic the surfaces of pure alkane liquids. Hence, hydrocarbon surfactants could be developed to achieve equilibrium surface tensions which match those of fluorocarbon or silicone surfactants.

2.7 General structure-property relationship of low aqueous surface tension

Above, the effect of surfactant structure on aqueous γ_{cmc} has been reviewed for fluorocarbon, silicone, and hydrocarbon surfactants. It has been shown that each class of surfactant possesses chemical properties which are at the heart of notable performance. However, by comparing widely different classes of surfactants, is it possible to identify a general property, independent of the chemical type or structure, which explains low γ_{cmc} ? An index to assess the surface coverage at the cmc, Φ_{cmc} , is introduced (Eqn. 2.2):

$$\Phi_{\text{cmc}} = \frac{V_{\text{cal}}}{V_{\text{meas}}} \quad (2.2)$$

where V_{cal} is the total physical volume of surfactant molecular fragments (values taken from refs³³⁻³⁵) and V_{meas} is the total volume occupied by a molecule at the reference air-water interface, calculated using experimental values (Eqn. 2.3):

$$V_{\text{meas}} = A_{\text{cmc}} \times \tau \quad (2.3)$$

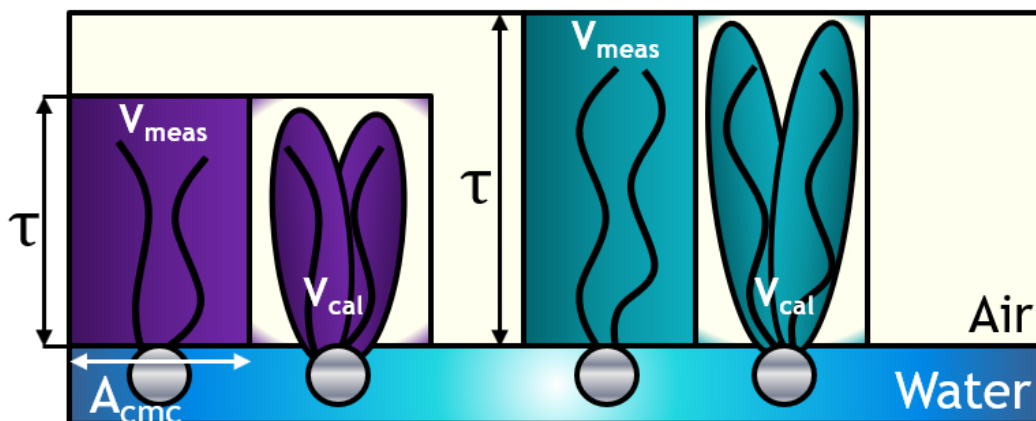


Figure 2.6: Visual representation of surfactants at the air-water interface, showing the different fragments and interfacial volumes used in the calculation of Φ_{cmc} . The measured surfactant molecular volume is V_{meas} , and the calculated volume based on summation of fragments is V_{cal} .

A_{cmc} corresponds to the surfactant head group area (which can be determined tensiometrically), and τ is an interfacial thickness which can be determined by neutron reflectivity, or the Tanford equation (Eqn. 2.4):

$$\tau = 1.5 + 1.256x \quad (2.4)$$

where x is the carbon number of the longest alkyl chain in the tail. An illustration of these volumes and dimensions is depicted in Figure 2.6. The part of the interfacial layer which is not occupied by molecular fragments is free space. Hence, assuming the layer is uniform, a high Φ_{cmc} indicates an efficiently packed surfactant monolayer with little free space. As an example, the common surfactant AOT with aqueous $\gamma_{\text{cmc}} = 30.8 \text{ mN m}^{-1}$ and $A_{\text{cmc}} = 75 \text{ \AA}^2$, has a corresponding $\Phi_{\text{cmc}} = 0.63$. In comparison, di-CF₂, a linear dichain fluorocarbon AOT-based analogue, has $\gamma_{\text{cmc}} = 22.4 \text{ mN m}^{-1}$ and $A_{\text{cmc}} = 65 \text{ \AA}^2$, giving a surface coverage value of $\Phi_{\text{cmc}} = 0.79$.³⁶

Figure 2.7 shows an illustration of aqueous limiting surface tensions, γ_{cmc} , corresponding areas per molecule at the surface, A_{cmc} , and film-packing volume fractions, Φ_{cmc} , for some of the most effective fluorocarbon, silicone, and hydrocarbon surfactants. The column height represents γ_{cmc} , and the column width represents A_{cmc} . Surface coverage Φ_{cmc} is also given in each column. From Figure 2.7, it can be seen that all classes of these superefficient surfactants generate high interfacial coverages (i.e. $\Phi_{\text{cmc}} \rightarrow 1$).

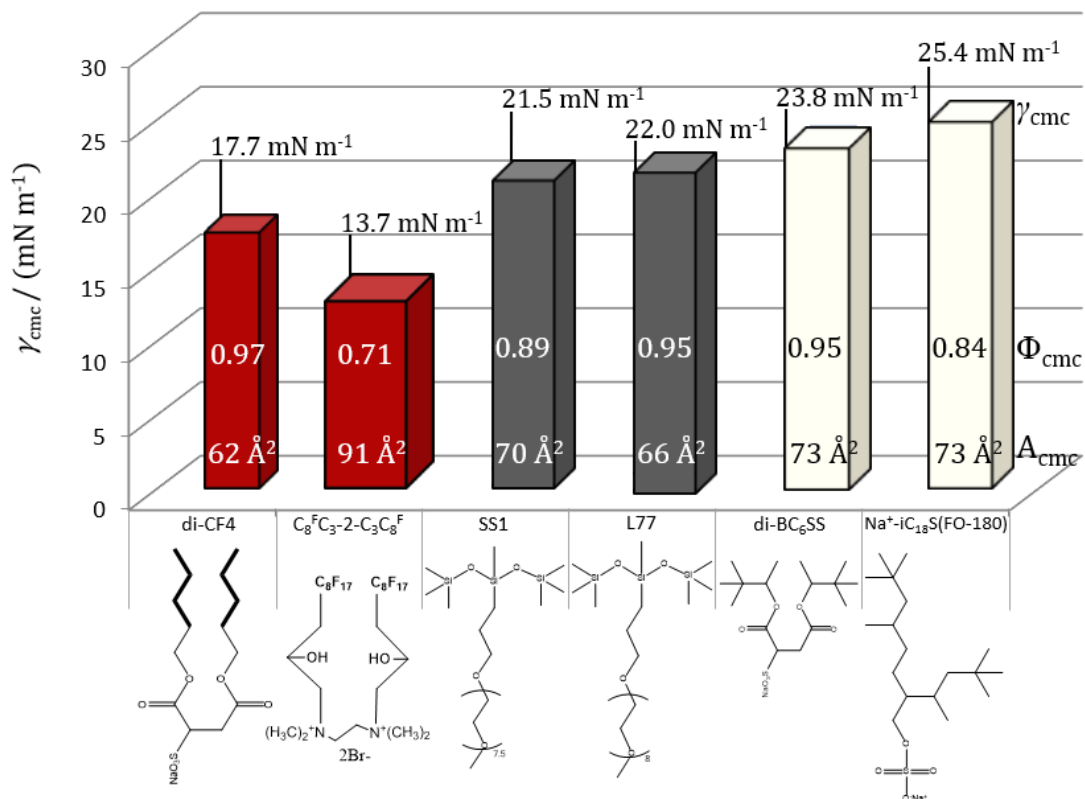


Figure 2.7: Comparison of the aqueous surface tension, area per molecule, and surface coverage at the cmc for some of the most effective fluorocarbon (red), silicone (grey), and hydrocarbon (cream) surfactants. The column height shows γ_{cmc} , and the column width represents A_{cmc} . Chains and end groups in bold represent perfluoroalkyl chains. Data from the literature: di-CF4,³⁷ $\text{C}_8\text{F}_{17}\text{C}_3-2-\text{C}_3\text{C}_8\text{F}$,³⁸ SS1 (ref. [7]), L77,³⁹ diBC₆SS,⁴⁰ and Na⁺-iC₁₈S(FO-180) (ref. [29]).

The values obtained for Φ_{cmc} are independent of both the surfactant geometry and chemistry of the surfactants. Therefore, by comparing Φ_{cmc} alongside γ_{cmc} and A_{cmc} for three main classes of low-surface-energy surfactants, it is possible to identify a general structure-property relationship of surfactants that accounts for low γ_{cmc} :

Low aqueous surface tensions are achieved through efficient surface packing and hence superior coverages at the air-water interface (ref. [1]).

That is, an efficiently packed surface monolayer is required for low γ_{cmc} , consistent with a high value of Φ_{cmc} . This has been identified by evaluating surface tension in terms of surface coverage at the cmc, Φ_{cmc} , where the most effective surfactants known all show high surface coverages. This general structure-property relationship of surfactants has not been highlighted before, and it points to new ways of controlling the surface energy through the design of superefficient, environmentally acceptable, and commercially viable surfactants.

References

- [1] Czajka, A.; Hazell, G.; Eastoe, J. *Langmuir* **2015**, *31*, 8205–8217.
- [2] Tanford, C. *The Hydrophobic Effect: Formation of Micelles and Biological Membranes*; John Wiley & Sons, 1980.
- [3] Frank, H. S.; Evans, M. W. *J. Chem. Phys.* **1945**, *13*, 507–532.
- [4] Eastoe, J.; Dalton, J. *Adv. Colloid Interface Sci.* **2000**, *85*, 103–144.
- [5] Lin, S. Y.; McKeigue, K.; Maldarelli, C. *Langmuir* **1991**, *7*, 1055–1066.
- [6] Downer, A.; Eastoe, J.; Pitt, A. R.; Simister, E. A.; Penfold, J. *Langmuir* **1999**, *15*, 7591–7599.
- [7] Ananthapadmanabhan, K.; Goddard, E.; Chandar, P. *Colloids Surf.* **1990**, *44*, 281–297.
- [8] Lu, J. R.; Marrocco, A.; Su, T. J.; Thomas, R. K.; Penfold, J. *J. Colloid Interface Sci.* **1993**, *158*, 303–316.
- [9] Penfold, J.; Thomas, R. *Journal of Physics: Condensed Matter* **1990**, *2*, 1369.
- [10] Lu, J.; Li, Z.; Smallwood, J.; Thomas, R.; Penfold, J. *The Journal of Physical Chemistry* **1995**, *99*, 8233–8243.
- [11] Lu, J.; Simister, E.; Thomas, R.; Penfold, J. *Journal of Physics: Condensed Matter* **1994**, *6*, A403.
- [12] Li, P. X.; Li, Z. X.; Shen, H.-H.; Thomas, R. K.; Penfold, J.; Lu, J. R. *Langmuir* **2013**, *29*, 9324–9334.
- [13] Rosen, M. J. *J. Am. Oil Chem. Soc.* **1972**, *49*, 293–297.

- [14] Fowkes, F. M. *Ind. Eng. Chem.* **1964**, *56*, 40–52.
- [15] Fowkes, F. M. *J. Phys. Chem.* **1963**, *67*, 2538–2541.
- [16] Pitt, A.; Morley, S.; Burbidge, N.; Quickenden, E. *Colloids Surf., A* **1996**, *114*, 321–335.
- [17] Zisman, W. A. *Adv. Chem. Ser.* **1964**, *43*, 1–51.
- [18] Kissa, E. *Fluorinated surfactants: synthesis, properties, applications*; Marcel Dekker, 1994; Vol. 50.
- [19] Rao, N. S.; Baker, B. E. *Textile finishes and fluorosurfactants*; Plenum: New York, 1994.
- [20] Krafft, M. P.; Riess, J. G. *Chem. Rev.* **2009**, *109*, 1714–1792.
- [21] Giesy, J. P.; Kannan, K. *Environ. Sci. Technol.* **2002**, *36*, 146A–152A.
- [22] Conder, J. M.; Hoke, R. A.; Wolf, W. d.; Russell, M. H.; Buck, R. C. *Environ. Sci. Technol.* **2008**, *42*, 995–1003.
- [23] Kim, D.-W.; Noh, S.-T.; Jo, B.-W. *Colloids Surf., A* **2006**, *287*, 106–116.
- [24] Owen, M.; Kendrick, T. *Macromol.* **1970**, *3*, 458–461.
- [25] Chengara, A.; Nikolov, A.; Wasan, D. *Colloids Surf., A* **2002**, *206*, 31–39.
- [26] Li, X.; Washenberger, R.; Scriven, L.; Davis, H.; Hill, R. M. *Langmuir* **1999**, *15*, 2278–2289.
- [27] Hill, R. *Silicone Surfactants*; Marcel Dekker: New York, 1999.
- [28] Knoche, M.; Tamura, H.; Bukovac, M. J. *J. Agric. Food. Chem.* **1991**, *39*, 202–206.
- [29] Alexander, S.; Smith, G. N.; James, C.; Rogers, S. E.; Guittard, F.; Sagisaka, M.; Eastoe, J. *Langmuir* **2014**, *30*, 3413–3421.
- [30] Nave, S.; Eastoe, J.; Penfold, J. *Langmuir* **2000**, *16*, 8733–8740.
- [31] Wormuth, K. R.; Zushma, S. *Langmuir* **1991**, *7*, 2048–2053.

- [32] Queimada, A.; Marrucho, I. M.; Coutinho, J. *Fluid Phase Equilib.* **2001**, *183*, 229–238.
- [33] Li, Z.; Lu, J.; Thomas, R.; Penfold, J. *J. Phys. Chem. B* **1997**, *101*, 1615–1620.
- [34] Berr, S. S.; Jones, R. R. *J. Phys. Chem.* **1989**, *93*, 2555–2558.
- [35] Tanford, C. *J. Phys. Chem.* **1972**, *76*, 3020–3024.
- [36] Mohamed, A.; Sagisaka, M.; Guittard, F.; Cummings, S.; Paul, A.; Rogers, S. E.; Heenan, R. K.; Dyer, R.; Eastoe, J. *Langmuir* **2011**, *27*, 10562–10569.
- [37] Eastoe, J.; Nave, S.; Downer, A.; Paul, A.; Rankin, A.; Tribe, K.; Penfold, J. *Langmuir* **2000**, *16*, 4511–4518.
- [38] Yoshimura, T.; Ohno, A.; Esumi, K. *Langmuir* **2006**, *22*, 4643–4648.
- [39] Rosen, M. J.; Wu, Y. *Langmuir* **2001**, *17*, 7296–7305.
- [40] Sagisaka, M.; Narumi, T.; Niwase, M.; Narita, S.; Ohata, A.; James, C.; Yoshizawa, A.; Taffin de Givenchy, E.; Guittard, F.; Alexander, S. *Langmuir* **2014**, *30*, 6057–6063.

Chapter 3

Thermodynamics and Scattering Theory

This section outlines the various thermodynamic models which are used to characterise surfactant properties which feature throughout this thesis, with particular emphasis on adsorption at the air-water interface and aggregation within the bulk.

3.1 Surfactant adsorption

To provide a quantitative description of surfactant adsorption the surface excess was introduced in Section 5.2, and defined as the concentration of surfactant molecules in a surface plane relative to that at a similar plane in the bulk. The Gibbs adsorption equation was also introduced, which is the most common thermodynamic model relating the change in surface tension with concentration, to the amount adsorbed at the surface.¹

The first approximation with the Gibbs model is the “exact” location of the air-water interface. Consider a surfactant aqueous phase α in equilibrium with a vapour phase β . The interface is a region of indeterminate thickness τ across which the properties of the system vary from values specific to phase α , to those characteristics of β . Since properties within this real interface cannot be well defined, a convenient assumption is to consider a mathematical plane σ , with zero thickness, so that the properties of α and β apply right up to that dividing plane positioned at some specific value X , Figure 3.1 illustrates this ideal system.

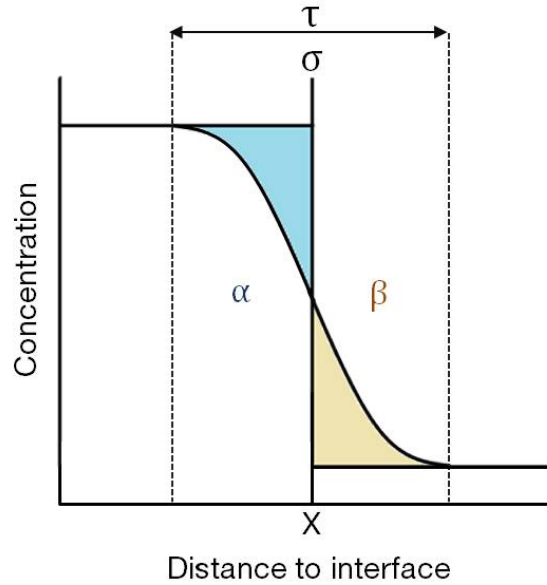


Figure 3.1: In the Gibbs approach to defining the surface excess concentration Γ , the two phases α and β are separated by an ideal interface which is infinitely thin. The chemical components of the α and β bulk phases remain unchanged except when approaching the dividing interface.

In the Gibbs model, the interface σ is ideally thin ($V^\sigma = 0$) and therefore the total volume is

$$V = V^\alpha + V^\beta \quad (3.1)$$

All other extensive quantities can be written as a sum of three components: one of the bulk phase α , one of the bulk phase β , and one of the interfacial region σ . For example, the internal energy U :

$$U = U^\alpha + U^\beta + U^\sigma \quad (3.2)$$

The internal energies of α and β are determined from the homogeneous bulk regions of the two phases. Taking u^α and u^β to be the internal energies per unit volume of the two phases, and considering the volume phases to the total energy of the system, the internal energy of the interface becomes

$$U^\sigma = U - u^\alpha V^\alpha - u^\beta V^\beta \quad (3.3)$$

The concentration of the chemical components α and β remain unchanged except when approaching the interface. The moles of the i^{th} component present at the interface is the total moles of i in the system, minus the moles of i in α and β respectively.

$$N_i^\sigma = N_i - N_i^\alpha - N_i^\beta \quad (3.4)$$

$$N_i^\sigma = N_i - c_i^\alpha V^\alpha - c_i^\beta V^\beta \quad (3.5)$$

In the definition of the Gibbs dividing surface, X is placed in the middle of the interfacial region so that the surface excess adsorption of the solvent is zero (it can be positive, negative or zero depending on the location of the interface X.). From Eqn. 3.5 it is possible to define a surface concentration, or interfacial excess:

$$\Gamma_i^\sigma = \frac{N_i^\sigma}{A} \quad (3.6)$$

where A is the interfacial area. Γ_i^σ given in units of mol m^{-2} , represents the excess of solute per unit area of the surface over what would be present if the bulk concentration prevailed all the way to the surface.

For a two-phase system consisting of α and β with a surface σ dividing the phases, the total internal energy U of the system can be written as shown in Eqn. 3.2, this can be expanded as follows:

$$\begin{aligned} U &= U^\alpha + U^\beta + U^\sigma \\ U^\alpha &= TS^\alpha - PV^\alpha + \sum \mu_i n_i^\alpha \\ U^\beta &= TS^\beta - PV^\beta + \sum \mu_i n_i^\beta \end{aligned} \quad (3.7)$$

where T is the temperature, S is the entropy, P is the pressure, V is the volume and μ_i represents the chemical potential of the i -th component. The corresponding expression for the thermodynamic energy of the interfacial region σ is

$$U^\sigma = TS^\sigma + \gamma A + \sum \mu_i n_i^\sigma \quad (3.8)$$

where γ represents the surface tension and A the interfacial area. For any infinitesimal change in T , S , A , μ , and n , differentiation of Eqn. 3.8 gives

$$dU^\sigma = \sum (T dS^\sigma + S^\sigma dT + \sum \mu_i dn_i^\sigma + \sum n_i^\sigma d\mu_i) + \gamma dA + A d\gamma \quad (3.9)$$

For a small, reversible change, the change in total internal energy of a bulk phase is

$$dU = T dS - P dV + \sum \mu_i dn_i \quad (3.10)$$

similarly for the interfacial region

$$dU^\sigma = T dS^\sigma + \gamma dA + \sum \mu_i dn_i^\sigma \quad (3.11)$$

subtracting Eqn. 3.11 from Eqn. 3.9 gives

$$S^\sigma dT + A d\gamma + \sum n_i^\sigma d\mu_i = 0 \quad (3.12)$$

Then at constant temperature, with the surface excess of component i , Γ_i^σ , as defined in Eqn. 3.6, Eqn 3.12 can be simplified to obtain the general form of the Gibbs equation

$$d\gamma = -\sum (\Gamma_i^\sigma d\mu_i) \quad (3.13)$$

For a simple system consisting of a solvent and a solute, denoted by the subscripts 1 and 2 respectively, Eqn. 3.13 reduces to

$$d\gamma = -\Gamma_1^\sigma d\mu_1 - \Gamma_2^\sigma d\mu_2 \quad (3.14)$$

Considering the choice of the Gibbs dividing surface position so that $\Gamma_1^\sigma = 0$, Eqn. 3.14 simplifies to

$$d\gamma = -\Gamma_2^\sigma d\mu_2 \quad (3.15)$$

where Γ_2^σ is the solute excess concentration, and μ_2 is the chemical potential of the i^{th} component which depends on the activity and is given by

$$\mu_i = \mu_i^o + RT \ln a_i \quad (3.16)$$

where μ_i^o is the chemical potential of the i -th component at a reference state (1 Atm, 298 K), R is the gas constant, T is the temperature, and a_i is the activity of the i -th component.

Differentiation of Eqn. 3.16 results in

$$d\mu_i = RT d \ln a_i \quad (3.17)$$

Applying to Eqn. 3.15 gives the form of the Gibbs equation for non-dissociated materials (e.g. non-ionic surfactants)

$$d\gamma = -\Gamma_2^\sigma RT d \ln a_2 \quad (3.18)$$

$$\Gamma_2^\sigma = -\frac{1}{RT} \frac{d\gamma}{d \ln a_2} \quad (3.19)$$

For dissociating solutes, such as ionic surfactants of the form R^-M^+ and assuming ideal behaviour below the cmc, Eqn. 3.18 becomes

$$d\gamma = -\Gamma_R^\sigma d\mu_R - \Gamma_M^\sigma d\mu_M \quad (3.20)$$

If no electrolyte is added, electroneutrality of the interface requires that $\Gamma_R^\sigma = \Gamma_M^\sigma$. Using the mean ionic activities so that $a_2 = (a_R a_M)^{\frac{1}{2}}$ and substituting in Eqn. 3.20 gives the Gibbs equation for 1:1 dissociating compounds

$$\Gamma_2^\sigma = -\frac{1}{2RT} \frac{d\gamma}{d \ln a_2} \quad (3.21)$$

where Γ_2^σ refers to the concentration of surfactant molecules, without considering the counter ion. If swamping electrolyte is introduced (such that electrostatic effects are unimportant) and the same gegenion M^+ as the surfactant is present, then the activity of M^+ and the pre-factor becomes unity, so that Eqn. 3.19 is valid.

The practical applicability of this relationship is that relative adsorption of a material at an interface, its surface activity, can be determined by measuring the interfacial tension as a function of solute concentration. By plotting the change in surface excess as a function of surfactant concentration (C), it is possible to calculate the area per molecule at the cmc, A_{cmc} . The area per molecule corresponds to the average area one surfactant molecule possesses at the air-water interface. This, along with other surface properties such as γ_{cmc} and Φ_{cmc} can be used to provide an insight into the relationship between surfactant structure and surface tension.

3.2 Mixed surfactant systems

Mixing different surfactants together can often lead to surprising properties which deviate greatly from the properties of the individual pure surfactants. Mixed systems constitute an area of great practical importance and in fact, mixed surfactant systems are encountered in nearly all practical applications of surfactants. In Chapter 7 mixtures of anionic hydrocarbon surfactants are introduced which are capable of generating surface tensions far lower than either of the constituent surfactants. It is therefore important to first briefly introduce mixed surfactant systems, and the models used to help characterise surfactant mixing. There is a great variety of different surfactant types and thus, an even greater variety of mixtures that can be formed. To address all is beyond the scope of this thesis and the reader is referred to relevant literature.^{2,3}

3.2.1 Mixing in binary surfactant mixtures

A wide range of surfactant types have been studied in mixed systems, including all combinations of anionic, cationic, non-ionic and zwitterionic.^{4,5} The general behaviour exhibited by a solution of pure surfactant molecules, i.e. adsorption to interfaces and micellisation above a certain critical concentration, are also exhibited by solutions of mixed surfactants. However, the properties of mixed surfactant solutions will depend differently on the concentration and conditions (e.g. pH, ionic strength, temperature etc) when compared with the pure surfactant. Therefore, by careful choice of ingredients the behaviour of a surfactant solution can be altered, leading to the enhancement or reduction of a desirable or undesirable property.

In an aqueous solution of an individual surfactant, the distribution between the monomeric state, micelles and monolayers at the air-liquid interface depends only on the solution conditions and surfactant concentration. However, for a mixture of two different surfactants this distribution also depends on the nature of the two surfactants. If two surfactants are mixed which possess very similar structures, then their free energies of micellisation will be similar. Therefore, the environment experienced by surfactant molecules within the mixed micelle will be similar to that experienced by molecules within the single component micelle. The micellar and

monomer composition, as well as the cmc of the mixture, could be expected to be a simple function of the bulk concentration, composition, and individual surfactant cmc's. Such mixing is termed "*ideal mixing*". For example, mixtures of homologous nonionic and ionic surfactants have been shown to behave like an ideal mixture.⁶

If however the two surfactants that are mixed have significant differences in their structure, the environment experienced by surfactant molecules in the mixed micelle will differ from that in the single component micelle. The surfactant with the lower free energy of micellisation will dominate the composition of the mixed micelle at the cmc of the mixture. And the monomer concentrations would therefore be biased towards the component with the higher free energy of micellisation. The distribution of components between the monomeric and micellar forms would not be a simple function of the free energies of micellisation of the single components, but also be influenced by the interactions between the two surfactants. This form of mixing is known as "*non-ideal mixing*".

When mixing anionic/cationic or non-ionic/ionic systems, mixed micelle formation is enhanced compared with the ideal case. This is because the inter-molecular electronic repulsion in the Stern layer is reduced in the mixed micelle which facilitates their formation. The mixed cmc would be lower than the value predicted by ideal solution theory and the system is said to exhibit negative deviations from ideality. In some cases, the mixed cmc can be lower than the cmc of either constituent surfactant.⁷ Binary mixtures of fluorocarbon and hydrocarbon surfactants often are found to have higher cmc's than what would be predicted from ideal solution theory, exhibiting positive deviations from ideality. This is because of the dissimilar nature of fluorocarbon and hydrocarbon chains which affects packing in the mixed micelle. Hence, the packing constraints of differently structured surfactants can cause non-ideality, even for mixtures of surfactants with like charge.

3.2.2 Regular Solution Theory

With the great practical importance of mixed surfactant systems, there has been much work in developing theories and models to predict and explain the behaviour of mixing in binary surfactant systems. In the 1970s Clint proposed a model to describe ideal mixing based on the thermodynamics of mixing in liquids.^{8,9} This is still used today to successfully predict cmc's, as well as monomer and micelle compositions for many mixed systems. An adaptation of Clint's ideal-mixing model proposed by Rubingh is the most commonly used thermodynamic approach to describe non-ideal mixing, and generally known as Regular Solution Theory (RST).¹⁰ Models to describe mixed surfactant systems use a simplified equilibrium thermodynamic approach which assumes that the mixed micelle or other mixed surfactant aggregates can be treated as separate phases. Use of this pseudophase separation approach greatly simplifies the modeling of properties in complex mixed systems.

By considering the chemical potentials of various surfactant species in solution, Clint derived the following formula to describe the cmc of an ideal binary mixture of surfactants, C^* , in terms of the cmc's of the pure surfactants, C_1 and C_2 , and the mole fractions of each component, α and $(1-\alpha)$ respectively.

$$\frac{1}{C^*} = \frac{\alpha}{C_1} + \frac{(1-\alpha)}{C_2} \quad (3.22)$$

In RST this equation is modified to include the activity coefficients of each surfactant, f_1 and f_2 .

$$\frac{1}{C^*} = \frac{\alpha}{f_1 C_1} + \frac{(1-\alpha)}{f_2 C_2} \quad (3.23)$$

Hence, for ideal mixing, the activity coefficients equal one by definition and the model can be easily solved for any number of surfactant components in the mixed system. For non-ideal systems, activity coefficients must first be determined. A general form for the activity coefficients in the micellar pseudophase can be developed by considering the thermodynamics of mixing.¹¹ In mixtures of liquids, the excess free energy of mixing, G^M , can be expressed as

$$G^M = RT(x_1 \ln f_1 + (1-x_1) \ln f_2) \quad (3.24)$$

where x_1 represents the mole fraction of surfactant one in the mixed micelle. The excess free energy of mixing itself is defined in terms of an excess enthalpy of mixing, H^M , and an excess entropy of mixing, S^M .

$$G^M = H^M - TS^M \quad (3.25)$$

In regular solution theory, the excess entropy of mixing, S^M , is assumed to be ideal and thus zero. This allows the substitution of H^M in place of G^M . For binary mixtures, this excess enthalpy of mixing can be represented by

$$H^M = \beta x_1(1 - x_1) RT \quad (3.26)$$

where β is a dimensionless parameter which times RT represents a net difference in interaction energy between the mixed and unmixed systems. Substituting H^M in place of G^M in Eqn. 3.24 leads to the activity coefficients of binary mixtures:

$$f_1 = e^{\beta(1-x_1)^2} \quad (3.27)$$

and

$$f_2 = e^{\beta x_1^2} \quad (3.28)$$

Unfortunately, since f_1 and f_2 are functions of β and x_1 which are both unknowns, Eqn. 3.23 cannot be used to give *a priori* predictions of mixed cmc's. However, with the knowledge of an experimentally obtained value for the cmc of a mixture, and cmc's of the pure surfactant components, both β and the micelle composition at the cmc can be obtained by iterative solutions of the following equations (obtained by combining equations 3.23, 3.27 and 3.28):

$$\beta = \frac{1}{(1 - x_1)^2} \ln \frac{C^* \alpha}{C_1 x_1} \quad (3.29)$$

and

$$\beta = \frac{1}{x_1^2} \ln \frac{C^*(1 - \alpha)}{C_2(1 - x_1)} \quad (3.30)$$

Iterative solutions of β can be calculated using appropriate software, for example a simple computer program in BASIC. Details of the code and procedure used for the

calculations in this thesis are included in the Supporting Information. For mixtures that show a synergistic departure from ideality β is negative, and if the mixing is antagonistic (i.e. a positive deviation from ideality) then β is positive. When β is zero, f_1 and f_2 are both unity and the above equations revert to those derived by Clint to describe ideal mixing (Eqn. 3.22).

The major assumption of regular solution theory is that molecules of different types have similar packing in the micelles, i.e. the entropy of mixing is ideal and thus zero. In this approximation, the parameter β can be formally interpreted as a parameter representing an excess heat of mixing. However, disagreement between calorimetric measurements of excess heats of micellar mixing, and β values determined independently from cmc measurements indicate that the regular solution approximation does not hold for many binary mixed systems.^{12,13} This has led to the suggestion that the β parameter be interpreted more generally as an excess free energy of mixing parameter, which only meets the formal criteria of the regular solution approximation when the excess entropy of mixing is zero. Furthermore, associated solution phase changes that accompany varying counterions or asymmetry in packing are beyond the scope of the model. There are many examples of non-ideal mixing which are not well described by RST, highlighting limitations in the models assumptions.^{14,15} However, despite this apparent limitation RST has been successful in predicting cmc's and providing information on monomer-micelle equilibria for a large number of mixed systems.^{16,17} Furthermore, small-angle neutron scattering (SANS) studies have provided direct measurements of mixed micelle compositions where good agreement was found with the predictions of RST.^{18,19}

3.2.3 Adsorption at interfaces of binary surfactant mixtures

Micellisation is a process that occurs due to the entropically favourable removal of hydrophobic surfactant tails from water. Adsorption of surfactant molecules at the air-liquid interface is mechanistically similar and therefore, likely to be affected by similar factors. However, there are fundamental differences between micellisation and adsorption. Firstly, adsorption occurs below the cmc. And secondly, the interface is of a finite size whereas micelle population can continue to increase as concentration is increased.

In the low concentration limit the air-liquid interface will have a low concentration of adsorbed species due to the low concentration of monomers present in the system. The composition of the adsorbed layer will simply reflect the surface activities of the two surfactants (regardless of ideal/non-ideal mixing), being dominated by the surfactant with the greater surface activity. As the overall concentration is increased, adsorption at the interface will also increase. In the case of ideal mixing, this increase would reflect the single surfactant adsorption isotherms with the surface excess increasing for both components. In the non-ideal case, compositional changes at the interface will reflect any synergy between the two surfactants.

At the cmc, the first micelles to form will be enriched in the component with the lower cmc and as a consequence, the monomer concentration becomes enriched in the component with the higher cmc. Hence the surface mole fraction of the less surface active (higher cmc) component might be expected to increase, reflecting the changes in monomer concentration of the two species. In understanding the surface composition at the high concentration limit, it is important to consider the finite size of the air-water interface. It cannot continuously “mop up” large amounts of surfactant in the way micelles can and therefore, the surface composition will not necessarily reflect the bulk composition, but instead the monomer concentrations in the high concentration limit.

Compared to a single surfactant system, the interfacial dynamics will also differ when the system is influenced by multiple surfactants. The dynamics of surfactant adsorption are defined by the time taken for surfactant molecules to adsorb from the bulk to the air-water interface, and then achieve correct orientation. Surfactant structure and the associated free energy change when removing non-polar moieties from water will largely dominate the dynamics of a single surfactant system. However, for a multiple surfactant system, variations in chain length will influence both adsorption and molecular packing at the air-water interface. For a binary surfactant system, the surfactant with the lower cmc is by nature more hydrophobic and will dominate the initial decrease in surface tension as surfactant molecules diffuse from bulk to the surface. The other surfactant species present in the system with a lower cmc will possess an associated smaller free energy change and hence, show a reduced relative tendency to adsorb from bulk to the surface. These surfactant

molecules will therefore arrive at a monolayer already partially saturated by the other surfactant (i.e. with the lower cmc). A delay time will exist as equilibrium is established between the two surfactants competing to pack at the surface and achieve the lowest free energy. If the two surfactants possess similar structures and hence cmc's, the time taken to achieve this equilibrium will be short as there will be minimal competition to achieve optimal packing. Hence the dynamic surface tension can provide insight into packing between different surfactant structures at the air water interface.²⁰ Revealing further information about the relationships between surfactant structure, surface packing and surface tension.

Molar areas can be determined by applying the Gibbs equation to the constant slope of surface tension versus logarithm of surfactant concentration. However, molar areas determined by tensiometry will not provide accurate estimates of surface compositions for mixed systems. Neutron reflectivity is a direct method of providing detailed structural information about mixed monolayers, including accurate measurements of the adsorbed amounts of individual surfactants. For example, Hines et al. used neutron reflection to study mixtures of SDS-C₁₂maltoside and test predictions made by the partial phase separation model in the case of non-ideal mixing.²¹ Using RST alongside tensiometric data can provide a greater insight into the adsorption and aggregation phenomena of mixed surfactant systems. In Chapter 7, RST is used to further characterise an array of unique systems, providing further information to help identify and explain the extraordinary properties observed.

3.3 Small-angle neutron scattering

To study relationships between molecular structure and physical properties within a colloidal system, the molecular organisation within the system must be determined. The most obvious method to determine the size, shape and structure of colloidal particles is scattering, as this provides a direct measure of the interactions between particles and incident radiation (i.e. light, X-ray, neutron). The colloidal size range is approximately $10 - 10^4 \text{ \AA}$ and hence, can be studied by scattering methods provided the incident wavelength falls within this range. Micelles or microemulsions on the order of 10^2 \AA in size are well characterised by X-ray ($\lambda = 0.5 - 2.3 \text{ \AA}$) and neutrons ($\lambda = 0.1 - 30 \text{ \AA}$). For larger aggregates, light scattering ($\lambda = 4000 - 8000 \text{ \AA}$) is most suitable. If we consider the Bragg equation that defines the angle of diffraction θ of radiation of wavelength λ for a separation of lattice planes d :

$$\lambda = 2d \sin\theta \quad (3.31)$$

It's clear to see that micelle/microemulsion droplet sized particles will scatter well at small angles using incident radiation in the neutron wavelength range. Hence, small-angle neutron scattering (SANS) is an excellent technique to study such systems. The following section will summarise SANS, neutron scattering theory, and how one would use such techniques to further characterise colloidal systems.

3.3.1 Neutrons

The neutron is a subatomic particle with no net electric charge, mass = $1.67 \times 10^{-27} \text{ kg}$ (slightly more than a proton), spin = $\frac{1}{2}$, and a magnetic moment = -1.913 nuclear magnetons. Neutrons along with protons constitute the nucleus of an atom and since they behave similarly within the nucleus, and share an atomic mass of approximately 1 amu, are collectively referred to as nucleons. They can be classified according to their wavelength: “epithermal” for short wavelengths ($\lambda \sim 0.1 \text{ \AA}$) and “thermal” or “cold” for long wavelengths ($\lambda \sim 10 \text{ \AA}$). The desired range of λ can be tuned by moderation during their production.

The universe is made from 12 particles of matter, and four forces of nature. Neutrons interact with matter via all four forces - strong, weak, electromagnetic and

gravitational. However, it is their interaction via the strong nuclear force and their magnetic moment, that make neutrons a unique probe for scattering experiments. The advantages of neutrons over other forms of radiation are summarised below:

- Neutrons are uncharged so they can penetrate to the bulk of a material, where they will interact with nuclei via the strong nuclear force.
- Because they are scattered from the nucleus of an atom, as opposed to the electron cloud, the scattering is proportional to atomic cross section (and not atomic number like X-ray scattering). Therefore, light atoms can be distinguished next to heavy atoms, such as hydrogen and deuterium, due to the relatively large difference in atomic cross section. Hence, isotopic labelling can be used to create contrast and selectively highlight different parts of a molecule, e.g. the surfactant tail in a micelle. Providing an unmatched insight into the bulk internal structure of a system.
- The wavelength of a particle can be related to its momentum via the de Broglie equation

$$\lambda = \frac{h}{mv} \quad (3.32)$$

where h is Planck's constant (6.63×10^{-34} J s) and v the particle velocity. The associated kinetic energy is then given by

$$E = \frac{1}{2}mv^2 \quad \text{or} \quad E = \frac{h^2}{2(m\lambda)^2} \quad (3.33)$$

Because the energy and wavelength of a particle depends on its velocity, it is possible to select a specific neutron wavelength by the time-of-flight technique. Therefore, the energy and wavelength of neutrons can be set to the appropriate energy and length scales required for condensed matter.

- The magnetic moment of a neutron couples to the spatial variation of magnetisation on the atomic scale, making them ideally suited to study the magnetic structures, fluctuations and excitations of spin systems.

- The non-destructive nature of neutrons mean they do not significantly perturb the system under investigation, which also makes them well suited for biological systems.

3.3.2 Neutron sources

Neutron beams for scattering experiments can be produced by two ways: by nuclear fission in a reactor-based neutron source (Institut Laue-Langevin, ILL, Grenoble), or by spallation in an accelerator-based neutron source (ISIS Facility at the Rutherford Appleton Laboratory in Didcot, UK). A brief description of these two methods, and the benefits of each is given below.

Reactor-based neutron source

Uranium-235 nuclei absorb thermal neutrons and split into fission fragments, producing a very high energy (MeV) constant neutron flux (hence why reactor-based sources are also referred to as a “continuous” source or “steady-state” source). The initial high kinetic energy of the neutron flux is reduced by repeated collision with the hydrogen nuclei of a hydrogenous moderator (termed thermalisation), producing a beam with a broad band of wavelengths. Wavelength selection is then achieved by Bragg scattering from a crystal monochromator, or by velocity selection through a mechanical chopper. The final result is a constant stream of high-flux neutrons with a narrow wavelength distribution.

Accelerator-based pulsed neutron source

H^- ions are accelerated in a linear accelerator (Linac) and then enter a synchrotron in ‘bunches’. As they enter the synchrotron, the H^- ions pass through very thin alumina foil which strips both electrons, producing a proton beam. This is then accelerated further and collided with a heavy metal target (e.g. W, Ta, U) under constant cooling to dissipate the heat from the proton beam. The collision causes neutrons to spall off the heavy metal target (termed spallation) in bursts, which are then guided to various instruments.

This process releases much less heat per useful neutron compared to fission, which means that pulsed sources can deliver a higher neutron intensity than even the most

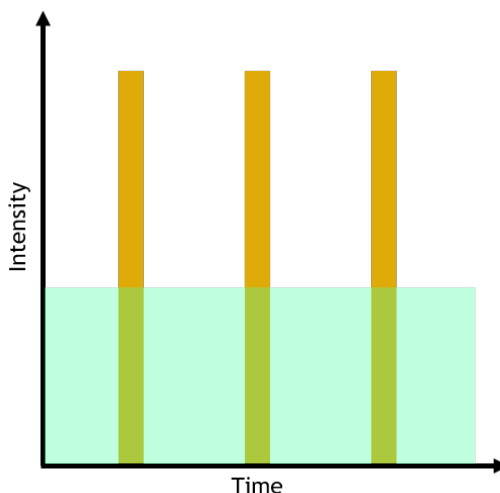


Figure 3.2: Neutron flux as a function of time at a steady state source (green), such as the ILL, and a pulsed source (orange), such as ISIS (not drawn to scale). Steady-state sources have high time-averaged fluxes, whereas pulsed sources are optimised for high brightness.

advanced steady-state source, see Figure 3.2. However, the time-averaged flux (in neutrons per second per unit area) of a pulsed source is low in comparison with a reactor source. Time-of-flight (TOF) techniques that exploit the high intensity in the pulse can compensate for this, and give a direct determination of the energy and wavelength of each neutron.

3.3.3 SANS instruments

In this work, SANS experiments were performed on the LOQ and SANS2D spectrometers at ISIS, and the D33 diffractometer at ILL. Due to the different characteristics of reactor and pulsed sources, neutron scattering experiments performed differ on these two instruments, to briefly summarise.

On D33 a single-wavelength (monochromatic) beam is normally used where a velocity selector and flexible system of inter-collimation apertures defines the neutron beam. To examine a wide range of particle sizes, at constant λ , the scattering intensity must be measured at various different angles. This is achieved by varying the sample-to-detector distance using a moveable detector. In contrast, at ISIS “white” neutron beams with a wide range of wavelengths are used and so multiple angles are not necessary. Energy analysis of the scattered beam is achieved by TOF (i.e. the time the neutron takes to travel from the source to the sample), hence the

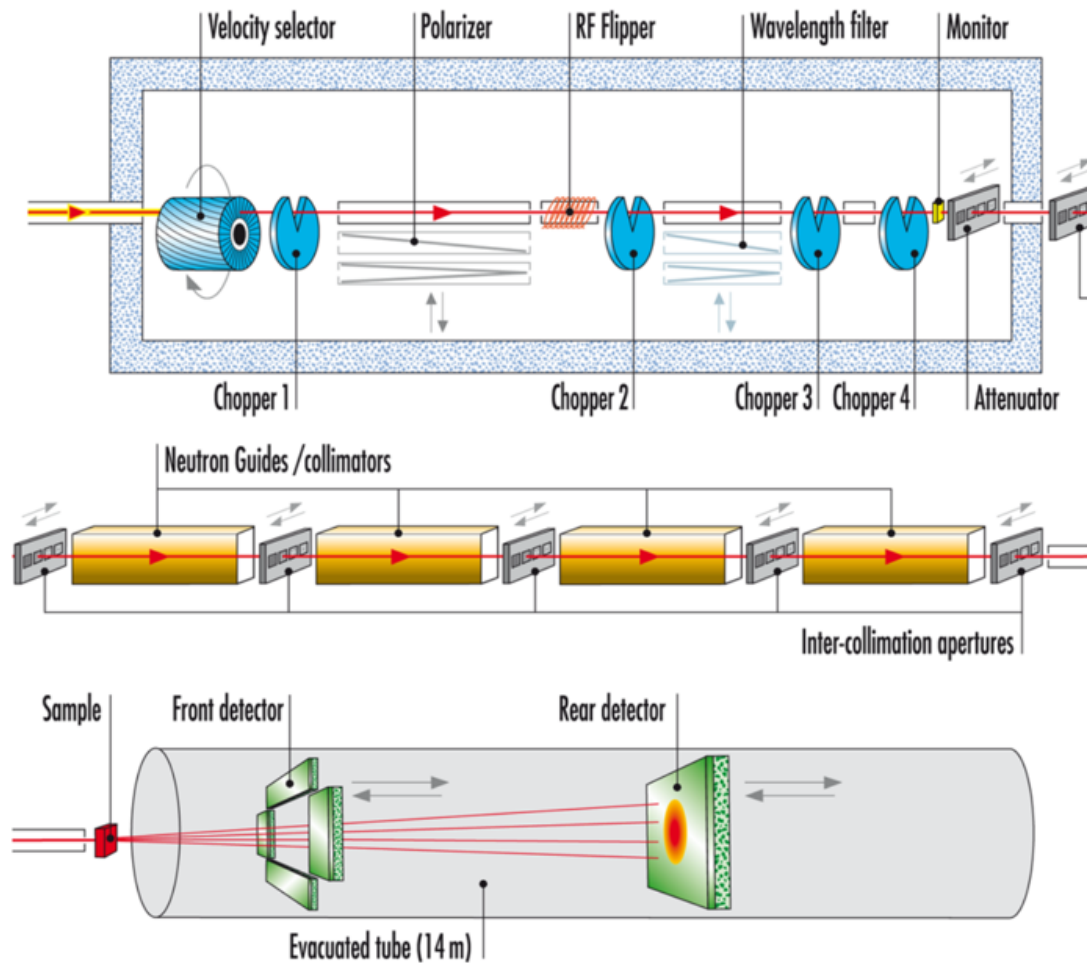


Figure 3.3: Layout of D33. The neutron enters the instrument casemate (top left) containing neutron optical elements, pass through the collimation (middle) to the sample area (bottom left). Neutrons are recorded on four front panels, and the rear detector of the instrument. Image taken from institute website.

detector for example on LOQ is fixed. SANS 2D offers two moveable detectors which extends the range of particle size that can be studied. D33 also offers a TOF flight mode which extends the particle size range that can be studied whilst providing flexible wavelength resolution. Figure 3.3 shows the schematic layout for D33. More technical details can be found at the institutions respective website.

3.3.4 Scattering theory

Regardless of the type of radiation, when it interacts with and is scattered by matter, patterns are produced which can provide information about the spatial arrangement and/or temporal changes within a sample. There are different forms of scattering that can be summarised as:

- *Elastic* - Where the kinetic energy of a particle is conserved, but its direction of propagation is modified.
- *Inelastic* - The kinetic energy of a particle, and its direction of propagation are modified. Hence, in this process the incident particle loses or gains energy.
- *Coherent* - When the phases of signals arising from different scattering centres are correlated.
- *Incoherent* - When the phases of signals arising from different scattering centres are uncorrelated, i.e. random.

Hence it is coherent scattering from ordered nuclei that produce constructive or destructive interference patterns, which can be used to obtain structural information. Whereas incoherent scattering is from unordered nuclei (perhaps due to random motion) and thus can provide dynamic information on the system.

To understand how neutrons are scattered by matter, it is helpful to first understand how a neutron is scattered by an individual fixed nucleus. Because neutrons are uncharged they interact via nuclear forces (as opposed to electrical forces) which are very short range, on the order of a few femtometres ($\sim 10^{-15}$ m). To a neutron, solid matter is not dense as a scattering centre (i.e. a nucleus) is approximately 100,000 times smaller than the distance between centres. The result is that the scattering centre essentially looks like a point scatterer, and if the neutron hits this area, it is scattered isotropically (with equal probability in any direction). This is because the range of the nuclear interaction between the neutron and nucleus is tiny in comparison with the wavelength of the neutron. Because the energy of the neutron is too small to change the internal state of the nucleus, scattering occurs without any change in the neutron energy and is thus elastic. When scattered by matter, each nucleus acts as a point scatterer to the incident neutron beam and the

scattering from each individual nucleus from the ensemble adds together. However, the scattering is not necessarily elastic as it is for a single fixed nucleus because the atoms in matter are free to move to some extent. Hence in SANS only *elastic coherent* scattering is considered, and the incoherent scattering which appears as background can be measured and subtracted from the total scattering.

The strength of the interaction between free neutrons and bound nuclei is quantified by the scattering length of the atom, $b_{i,\text{coh}}$, which is isotope dependent. From known scattering lengths, it is possible to define the mean coherent *scattering length density*, abbreviated as SLD, which is a measure of the scattering power of a material, i.e. a compound. The SLD can be calculated from the sum of scattering length contributions from all atoms, divided by the volume of the molecule:

$$\text{SLD} = \frac{1}{V_m} \sum_i b_{i,\text{coh}} = \frac{\rho N_a}{M_w} \sum_i b_{i,\text{coh}} \quad (3.34)$$

where $b_{i,\text{coh}}$ is the coherent scattering length of the i^{th} atom in the molecule, and V_m is the molecular volume which can be estimated from the known bulk density, ρ , and molecular weight M_w . Coherent scattering length values for selected atoms and molecules are given in Table 3.1. The significant difference in scattering length for hydrogen and deuterium can be exploited in the contrast-variation technique, allowing selective regions of a molecular structure to be highlighted. For example, a hydrocarbon surfactant dissolved in D_2O will highlight the whole micelle once the scattering from the D_2O background has been removed.

Table 3.1: Values of $b_{i,\text{coh}}$ and SLD's for selected atoms and molecules at 25 °C.²²

Nucleus	$b_{i,\text{coh}}$ (10^{-12} cm)
^1H	-0.3741
^2D	0.6671
^{12}C	0.6646
^{19}F	0.5605
Molecule	SLD (10^{-6} Å ⁻²)
H_2O	-0.560
D_2O	6.356
Heptane - C_7H_{16}	-0.548
d-heptane - C_7D_{16}	6.301

Scattering vector - Q

When a beam of neutrons are incident upon a sample, they are scattered at an angle θ onto a detector. This is illustrated in Figure 3.4 where the incident and scattered neutron beam have wavevectors k_i and k_s respectively. When a neutron is scattered by matter, as in all collisions, momentum and energy are conserved and the energy lost by the neutron is gained by the sample. Hence, $k_i - k_s$ corresponds to the *momentum transfer* that occurs during the collision. The quantity Q , where $Q = k_i - k_s$ is known as the *scattering vector*, and the vector relationship between all three is illustrated in Figure 3.5.

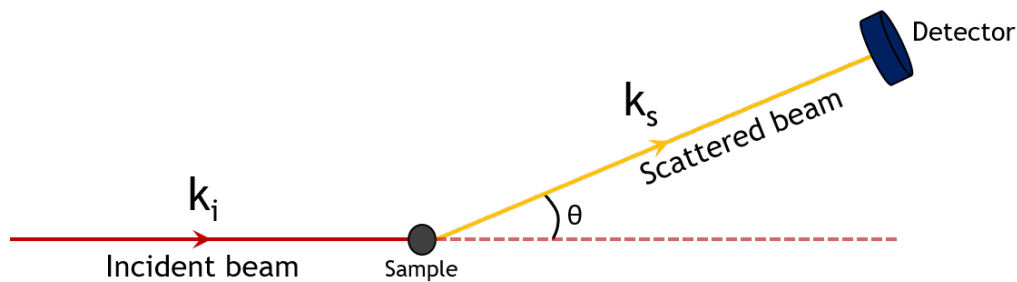


Figure 3.4: Schematic setup of a small-angle scattering experiment.

For coherent elastic scattering $|k_i| = |k_s|$, where the magnitude of the wavevector (i.e. the angular wavenumber) is defined as $2\pi/\lambda$. Therefore, $|Q|$ can be obtained by simple geometry as:

$$|Q| = Q = 2 |k_i| \sin \frac{\theta}{2} = \frac{4\pi}{\lambda} \sin \frac{\theta}{2} \quad (3.35)$$

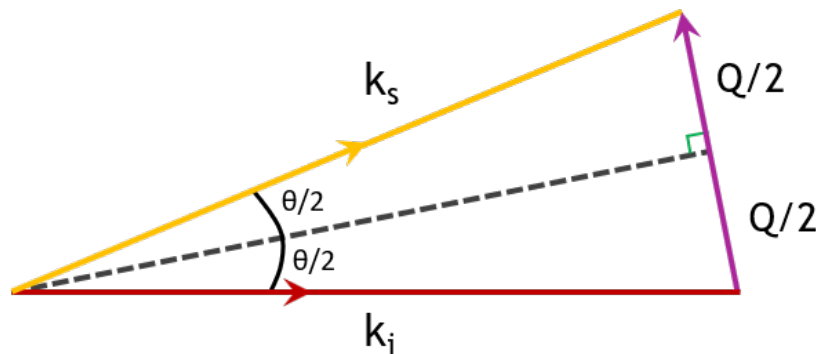


Figure 3.5: Vector relationship of the scattering vector $Q = k_i - k_s$. The amplitude of Q can be determined using trigonometry to obtain $Q = (4\pi/\lambda)\sin(\theta/2)$.

The magnitude of Q has dimensions of reciprocal length and units are commonly \AA^{-1} . It relates to the spatial sample properties, with large structures scattering at low Q (i.e. low angle) and small structures scattering at higher Q . In a small-angle scattering experiment the scattered intensity $I(Q)$ is measured across a q -range to provide structural information about the sample across a length scale. That is, the magnitude of Q could also be considered a window of observation, where at high- Q the window is very small and vice versa. This is illustrated in Figure 3.6.

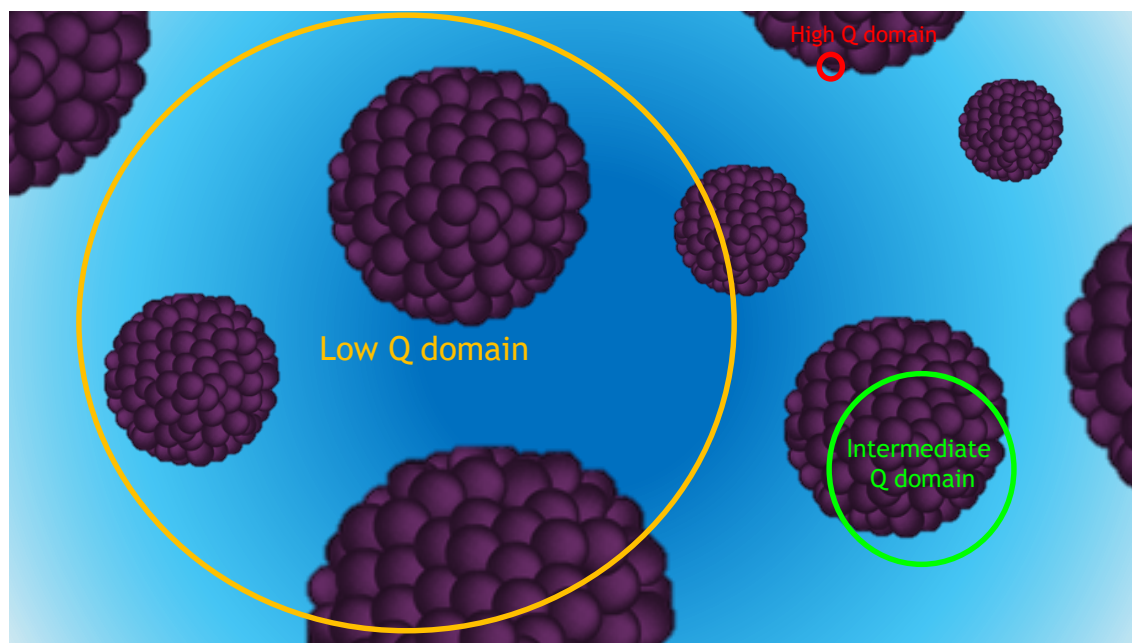


Figure 3.6: In a scattering experiment the intensity is measured across a q -range by varying the scattering angle. The q -range provides structural information at different length scales:

High Q domain - The window is very small, there is only contrast at the interface between the two media.

Intermediate Q domain - The window is on the order of the aggregate size. The size, shape and internal structure of one aggregate can be measured (i.e. the form factor $P(Q)$)

Low Q domain - The window is large and multiple aggregates are measured. The interactions within the system and structural order can be determined (i.e. the structure factor $S(Q)$)

3.3.5 Scattering by micellar aggregates

For monodisperse homogeneous spherical particles of radius R , volume V_p , number density n_p (cm^{-3}) and coherent scattering length density ρ_{SLD} , dispersed in a medium of density ρ_m , the normalised SANS intensity $I(Q)$ (cm^{-1}) may be written as:

$$I(Q) = n_p \Delta\rho^2 V_p^2 P(Q, R) S(Q) \quad (3.36)$$

where $\Delta\rho^2 = \rho_{\text{SLD}} - \rho_m$ (cm^{-2}). The first three terms in Eqn. 3.36 are independent of Q and account for the absolute intensity of scattering. This is referred to as the *scale factor*, S_F , which can be defined as:

$$S_F = n_p \Delta\rho^2 V_p^2 = \phi_p \Delta\rho^2 V_p \quad (3.37)$$

where ϕ_p is the volume fraction of the particles. The scale factor can be easily calculated for a system and hence provides a measure of the validity of a model when analysing SANS data, i.e. the S_F determined from the fit can be compared to the calculated value (Eqn. 3.37).

The other two terms in Eqn. 3.36 are Q -dependent functions. $P(Q, R)$ is the single particle *form factor* which arises from intra-particle scattering (see Figure 3.6). It provides information on the individual particle size and shape. $S(Q)$ is the *structure factor* which arises from inter-particle interactions. The following sections will briefly discuss both Q -dependent functions.

Single particle form factor $P(Q)$

The form factor $P(Q)$ tells you about the shape and size of the particles. There are various expressions of $P(Q)$ for a wide range of shapes such as spheres, cylinders, ellipsoids, discs and bilayers, all of which are commonly encountered in soft matter.²³ To discuss the form factor for each shape would be beyond the scope of this section, and the reader is referred to relevant literature for further details.²⁴ The form factor $P(Q)$ for a sphere of radius R and uniform density is represented as:

$$P(Q, R) = \left[\frac{3(\sin QR - QR \cos QR)}{(QR)^3} \right]^2 \quad (3.38)$$

An approximate representation of the form factor $P(Q,R)$ for spheres (Eqn. 3.38) is shown in Figure 3.7. In general, it shows a decay however, under high resolution maxima and minima would be expected at high Q values. For certain systems, aggregates of equal size are not formed and a polydispersity function must be introduced to account for the particle-size distribution. These probability functions differ for the type of aggregate under investigation, for example, for spherical droplets the polydispersity function may be represented by a Schultz distribution function $X(R_i)$.²⁵ Which itself is defined by an average radius R^{av} , over the width parameter Z to obtain the root mean square deviation $\sigma = \frac{R^{av}}{(Z+1)^{1/2}}$. $P(Q,R)$ may then be re-expressed as:

$$P(Q,R) = \left[\sum_i P(Q,R_i) X(R_i) \right] \quad (3.39)$$

If the particles in the system are non-interacting, than the form factor describes the scattering profile. However, often there are interactions between the particles (i.e. repulsion between charged head groups) and the scattering data cannot be modelled using the form factor alone and a structure factor $S(Q)$ is applied.

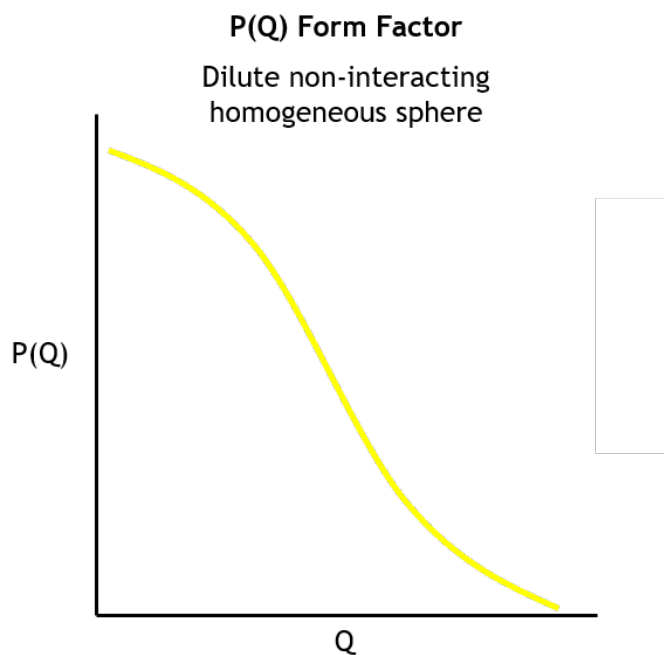


Figure 3.7: Schematic representation of the particle form factor $P(Q,R)$ for a homogeneous sphere of radius R .

Structure factor $S(Q)$

The structure factor $S(Q)$ describes the types of interactions in the system i.e. attractive, repulsive or excluded volume, and hence relates to inter-particle interactions. It is more important at low Q values where the ‘window of observation’ measures the scattering from multiple aggregates, see Figure 3.6. The structure factor for spherical particles with low attractive interactions can be approximated by a hard-sphere potential, $S_{\text{hs}}(Q)$, which is given by:

$$S_{\text{hs}}(Q) = \frac{1}{(1 - n_p) f(R_{\text{hs}} \phi_{\text{hs}})} \quad (3.40)$$

where R_{hs} is the hard-sphere radius and ϕ_{hs} is the hard-sphere volume fraction. Figure 3.8 shows a representation of the attractive (Eqn. 3.40) and repulsive $S(Q)$ for homogeneous spheres. The intensity of scattering can then be rewritten as:

$$I(Q) = \phi_p \Delta\rho^2 V_p \left[\sum_i P(Q, R_i) X(R_i) \right] S(Q, R_{\text{hs}}, \phi_{\text{hs}}) \quad (3.41)$$

Figure 3.9 shows a representation of the final scattering profile $I(Q)$ vs Q for a spherical form factor with an attractive or repulsive structure factor. For example, the orange line shows a peak which is characteristic of charged micelles. Effective ways of reducing this structure factor is diluting the system,²⁶ or adding salt.²⁷

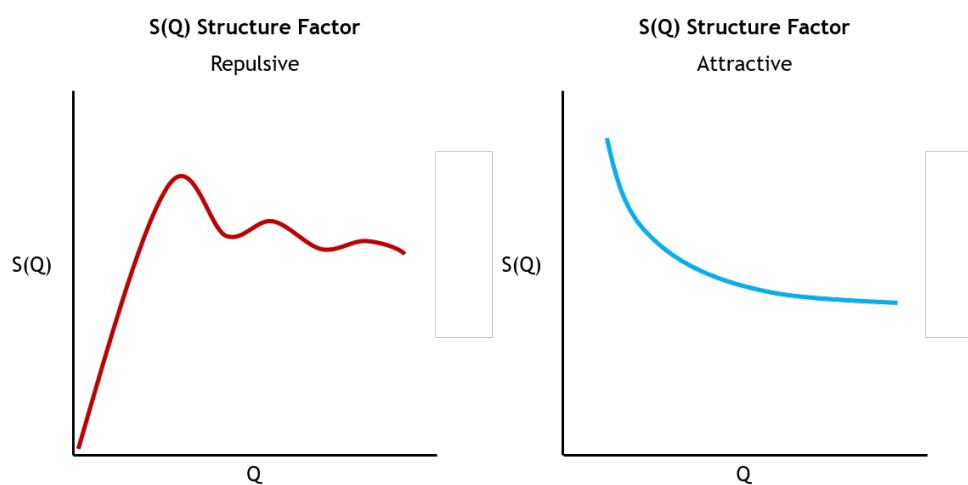


Figure 3.8: Schematic representation of the structure factor $S(Q)$ for attractive and repulsive homogeneous spheres.

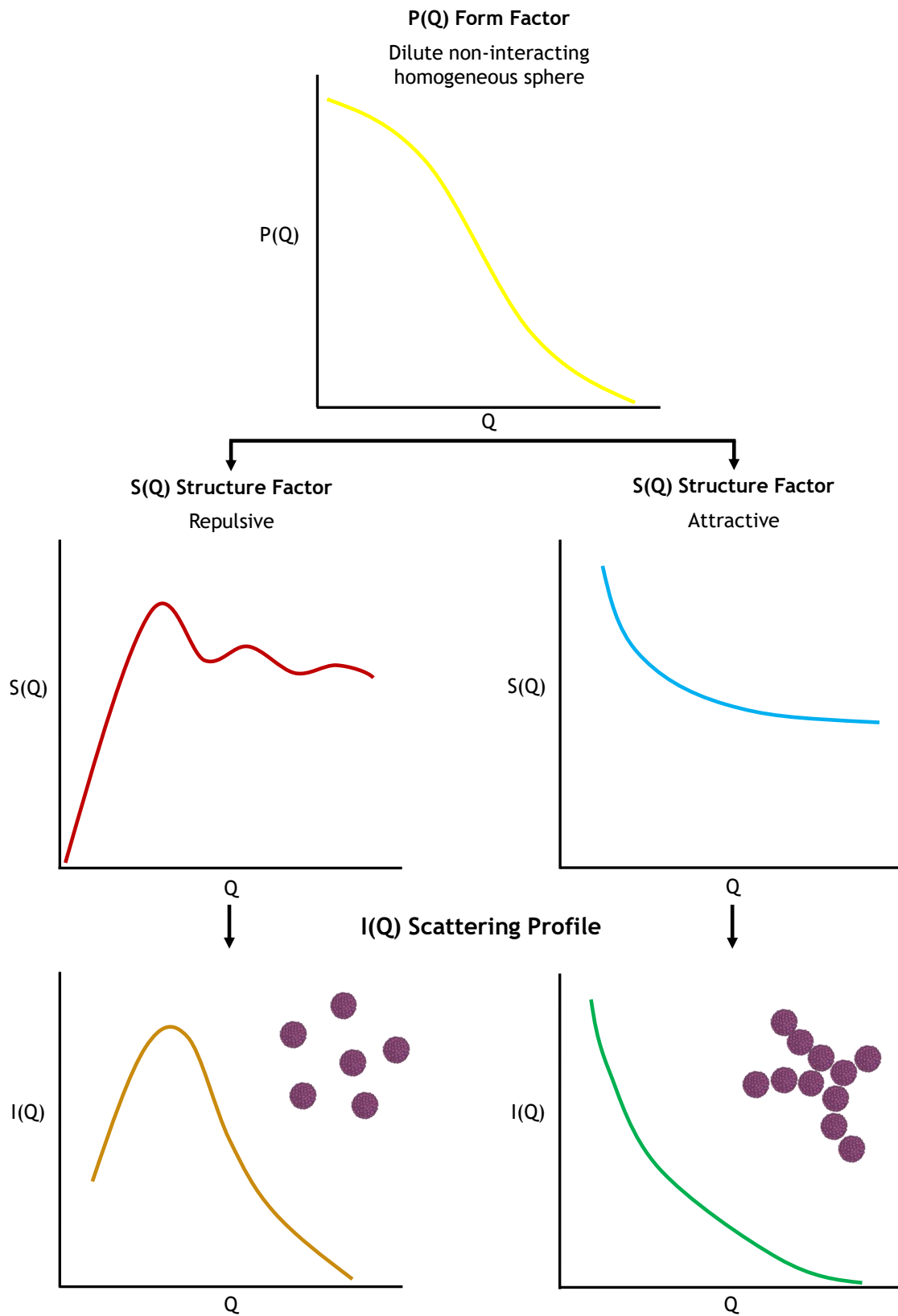


Figure 3.9: Schematic representation of the particle form factor $P(Q,R)$ and structure factor $S(Q)$ for a homogeneous sphere of radius R . The resultant scattering profiles when combined are also shown.

Neutron contrast variation

As previously mentioned, for neutrons the scattering power of any atom is dependent on its atomic cross section. Therefore, deuterium and hydrogen which relatively, have a very large difference in atomic cross section have very different scattering powers. This can be exploited in experiments by labeling different parts of a molecule with ^1H and ^2D to create contrast, allowing selective parts of a structure to be studied. This is routinely applied in microemulsion droplets, where different regions are highlighted by selectively varying the scattering length density of the surfactant, oil, or aqueous phase. Hence, three contrasts are commonly studied - the core, shell and drop - which can be fitted individually or simultaneously.²⁸ Figure 3.10 illustrates the three contrasts for an example core-shell type particle.

- **Natural contrast** - The whole aggregate is highlighted. For example, a deuterated surfactant dissolved in H_2O and d-oil.
- $\text{SLD}_{\text{solvent}} = \text{SLD}_{\text{core}}$ - The shell is highlighted. For example, a hydrogenated surfactant dissolved in D_2O and d-oil.
- $\text{SLD}_{\text{solvent}} = \text{SLD}_{\text{shell}}$ - The core is highlighted. For example, a deuterated surfactant dissolved in D_2O and h-oil.

Contrast variation is the single most powerful tool of neutron scattering which provides an unmatched insight into the internal structure of a system. Apart from a few subtle effects, such as hydrogen bonding, isotopic exchange usually does not affect the physiochemical properties of the system significantly.

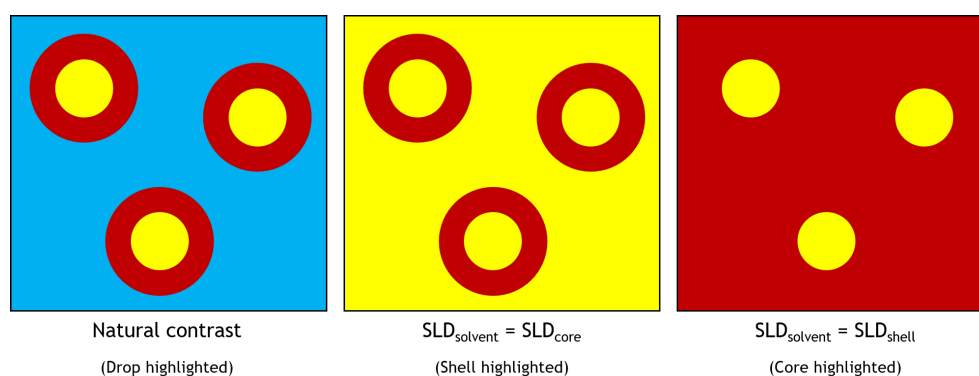


Figure 3.10: Example of a core-shell particle where the contrast is varied to selectively highlight different parts of the structure.

3.3.6 SANS approximations

The first step to understanding SANS data involves a set of standard plots that can be used right after data reduction, i.e. before modeling the data. These are linear plots which are obtained by plotting the scattered intensity $I(Q)$ against specific functions of scattering vector Q . This analysis is used to give an early indication about the particle shape and size.

Guinier approximation

The Guinier approximation analyses the low Q domain of the scattering profile to obtain a slope which is related to R_g , the radius of gyration.²⁹ Where R_g represents the effective size of the scattering particle, whether it is a polymer chain, micelle, part of protein etc. Furthermore, the radius of gyration obtained from the Guinier approximation is independent of the absolute intensity and of any model. At low- Q , the single particle form factor $P(Q,R)$ for dilute systems simplifies to:

$$P(Q,R) = 1 - \frac{Q^2 R_g^2}{3} \quad (3.42)$$

If it is assumed that the particles are non-interacting, so $S(Q) = 1$, then the equation for the scattering intensity (Eqn. 3.36) becomes:

$$I(Q) = \phi_p \Delta\rho^2 V_p \exp\left(-\frac{Q^2 R_g^2}{3}\right) \quad \text{i.e.} \quad \text{Ln}[I(Q)] = \text{Ln}[I_0] - \frac{Q^2 R_g^2}{3} \quad (3.43)$$

Hence a plot of $\text{Ln}[I(Q)]$ vs Q^2 yields an associated slope $-\frac{R_g^2}{3}$ which can then be solved to determine R_g for any isomeric particles. It is important that R_g is determined from the correct Q -range. For a Guinier plot, this range corresponds to $QR_g < \sqrt{3}$. This is obtained when the probed range ($2\pi/Q$) is larger than the particle size (i.e. low- Q domain on Figure 3.6). When analysing the scattering from elongated objects, the Guinier approximation is modified and uses scattering from the intermediate Q -domain, see Figure 3.11. For example, for a cylinder of length L and radius R , the intermediate- Q Guinier approximation is:

$$I(Q) = \frac{I_0}{Q} \exp\left(-\frac{Q^2 R_g^2}{2}\right) \quad (3.44)$$

The intermediate-Q Guinier plot of $\ln[Q I(Q)]$ vs Q^2 yields an associated slope $-\frac{R_g^2}{2}$. Hence the Guinier approximation can be used to determine different geometries by plotting specific functions against Q^2 . The various geometries, and associated dimension R that can be obtained by plotting different quantities against Q^2 are summarised below:

- $\ln[I(Q)]$ vs Q^2 Associated slope = $-\frac{R_g^2}{3}$ (*Low Q*)
- $\ln[I(Q) \cdot Q]$ vs Q^2 Associated slope = $-\frac{R_g^2}{2}$ (*Intermediate Q*)
- $\ln[I(Q) \cdot Q^2]$ vs Q^2 Associated slope = $-\frac{R_g^2}{1}$ (*Intermediate Q*)

R_g can then be related to the shape of the particles by:

- Spheres and cylinders $R_g = \left(\frac{3}{5}\right)^{\frac{1}{2}} R$
- Thin discs $R_g = \frac{R}{4^{\frac{1}{2}}}$
- Long rods $R_g = \frac{L}{12^{\frac{1}{2}}}$

The most probable particle shape can be predicted by comparing the three different $I(Q) \cdot Q^x$ vs Q^2 plots and finding the one that gives a linear decay.

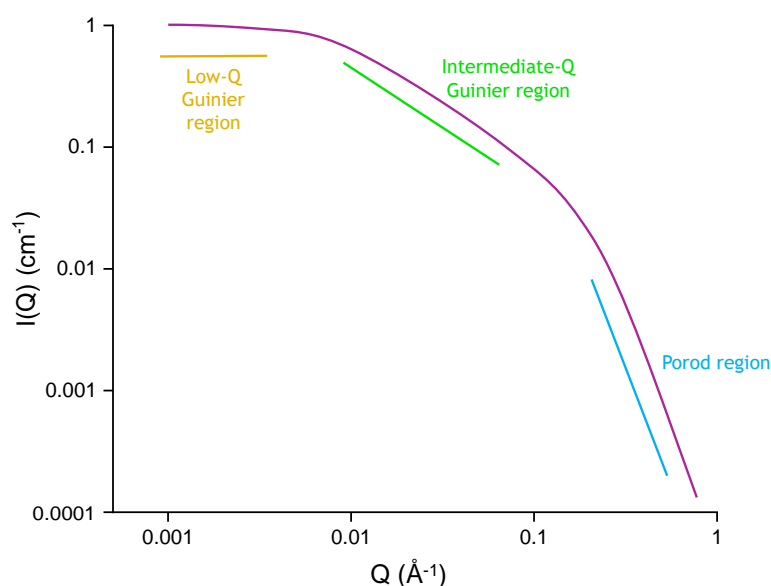


Figure 3.11: Example form factor for a cylinder showing the low-Q Guinier region, the intermediate-Q Guinier region and the high-Q porod region.

Porod Approximation

At the high- Q domain, the scattering intensity is from a region smaller than the scattering object so hence is probing the local interfacial structure. The Porod approximation is applied to the high- Q domain for a system of non-interacting particles to determine the fractal dimensions of the scattering object.³⁰ The Porod law is as follows:

$$I(Q) = 2\pi\Delta\rho^2\left(\frac{S}{V}\right)Q^{-4} \quad (3.45)$$

where S/V is the surface to volume ratio (cm^{-1}). The Porod law is only valid for smooth interfaces and above a Q range of $1/R$. If one assumes all surfactant molecules are located at the interface, the area per molecule, A , can be estimated from:

$$A = \left(\frac{S}{N_s}\right) \quad (3.46)$$

where N_s is the number density of surfactant molecules (i.e. surfactant concentration \times Avogadro's number). For example, for monodisperse spheres of radius R , a plot of $[I(Q).Q^4]$ vs Q yields a first maximum at $Q \sim 2.7/R$ and a minimum at $Q \sim 4.5/R$, see Figure 3.12, which can then be used to infer the spherical radius.

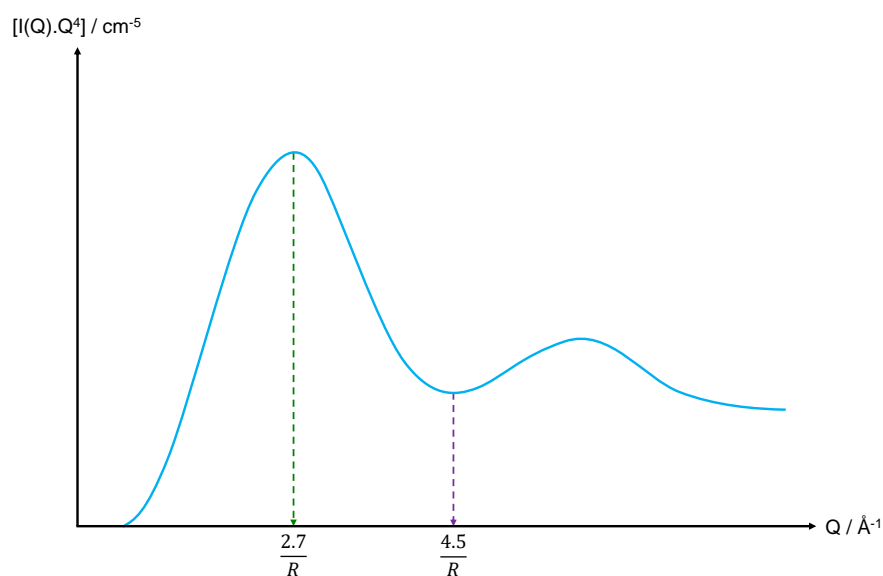


Figure 3.12: Schematic diagram of a Porod plot for near-monodisperse spheres

The Guinier and Porod approximations offer simple relations that allow first estimations of the size and shape of colloidal particles. However, they can only be applied to non-interacting (i.e. dilute) systems. This criteria can be met for other systems by adding salt to screen interactions between charged micelles, or additional dilution, which both would validate the assumption that $S(Q) = 1$ in the low- Q domain i.e. Guinier range. By applying these first approximations to scattering data, information can be obtained about the size and shape of aggregates to help guide the final fitting procedure which employ complex mathematical models.

References

- [1] Gibbs, J. W. *The Collected Works of J. Willard Gibbs-Volume 1: Thermodynamics*; Yale University Press, 1945.
- [2] Ogino, K.; Abe, M. *Mixed surfactant systems*; CRC Press, 1992.
- [3] Holland, P. M.; Rubingh, D. N. *Mixed surfactant systems: an overview*; ACS Publications, 1992.
- [4] Rosen, M. J.; Hua, X. Y. *J. Colloid Interface Sci.* **1982**, *86*, 164–172.
- [5] Rosen, M. J. *Langmuir* **1991**, *7*, 885–888.
- [6] Joshi, T.; Mata, J.; Bahadur, P. *Colloids Surf., A* **2005**, *260*, 209–215.
- [7] Parekh, P.; Varade, D.; Parikh, J.; Bahadur, P. *Colloids Surf., A* **2011**, *385*, 111–120.
- [8] Clint, J. H. *J. Chem. Soc., Faraday Trans* **1975**, *71*, 1327–1334.
- [9] Lange, v. H.; Beck, K.-H. *Kolloid-Z.u.Z.Polymere* **1973**, *251*, 424–431.
- [10] Rubingh, D. *Mixed micelle solutions*; Springer, 1979; pp 337–354.
- [11] Holland, P. M. *Adv. Colloid Interface Sci.* **1986**, *26*, 111–129.
- [12] Hey, M. J.; MacTaggart, J. W.; Rochester, C. H. *J. Chem. Soc., Faraday Trans* **1985**, *81*, 207–213.
- [13] Rathman, J. F.; Scamehorn, J. F. *Langmuir* **1988**, *4*, 474–481.
- [14] Penfold, J.; Thomas, R. K. *Phys. Chem. Chem. Phys.* **2013**, *15*, 7017–7027.
- [15] Hoffmann, H.; Pössnecker, G. *Langmuir* **1994**, *10*, 381–389.

- [16] Holland, P.; Rubingh, D. *J. Phys. Chem.* **1983**, *87*, 1984–1990.
- [17] Gu, B.; Rosen, M. J. *J. Colloid Interface Sci.* **1989**, *129*, 537–553.
- [18] Staples, E.; Thompson, L.; Tucker, I.; Penfold, J.; Thomas, R.; Lu, J. *Langmuir* **1993**, *9*, 1651–1656.
- [19] Penfold, J.; Staples, E.; Thompson, L.; Tucker, I.; Hines, J.; Thomas, R.; Lu, J. *Langmuir* **1995**, *11*, 2496–2503.
- [20] Jiang, Y.; Chen, H.; Mao, S.; Luo, P.; Du, Y.; Liu, M. *The Journal of Physical Chemistry B* **2011**, *115*, 1986–1990.
- [21] Hines, J.; Thomas, R.; Garrett, P. R.; Rennie, G.; Penfold, J. *J. Phys. Chem. B* **1997**, *101*, 9215–9223.
- [22] Sears, V. F. *Neutron news* **1992**, *3*, 26–37.
- [23] Zana, R. *Surfactant solutions new methods of investigations*; Marcel Dekker Inc., New York, NY, 1987; pp 57–139.
- [24] Hammouda, B. *The SANS toolbox*; NIST Center for Neutron Research, available at <http://tinyurl.com/SANStoolbox>, 2008.
- [25] Chen, S.-H. *Annu. Rev. Phys. Chem.* **1986**, *37*, 351–399.
- [26] Cebula, D. J.; Myers, D.; Ottewill, R. *Colloid. Polym. Sci.* **1982**, *260*, 96–107.
- [27] Beresford-Smith, B.; Chan, D. Y.; Mitchell, D. J. *J. Colloid Interface Sci.* **1985**, *105*, 216–234.
- [28] Heenan, R.; Eastoe, J. *J. Appl. Crystallogr.* **2000**, *33*, 749–752.
- [29] Guinier, A. *Ann Phys* **1939**, *12*, 161–237.
- [30] Porod, G. *Koll Z* **1951**, *124*, 83–114.

Chapter 4

Experimental

4.1 Introduction

This chapter describes the synthesis of the single- and di-chain anionic hydrocarbon surfactants examined in this thesis. They are single-chain sulfonates with sodium or TAA counterions (where TAA = tetraalkylammonium, i.e. tetrapropylammonium.), and di-chain sulfosuccinates with sodium counterions. Table 4.1 shows the molecular structures and nomenclature used. Where appropriate, information is provided on commonly encountered problems associated with synthesising surfactants, in an aim to aid future syntheses. Furthermore, the various common techniques used throughout this work and the associated experimental procedures are also outlined.

4.2 Materials

All solvents were used as purchased unless otherwise stated. Water was obtained from a 5 L Milli-Q (18.2 M Ω cm).

- Isostearyl alcohol FO180 (Nissan Chemical Industries; 90%)
- Isostearyl alcohol FO180N (Nissan Chemical Industries; 90%)
- 2,4-Dimethyl-3-pentanol (Aldrich; 99%)
- 2,6-Dimethyl-4-heptanol (Aldrich; 80%)
- 2,2-Dimethyl-1-propanol (Aldrich; 99%)

- 3,3-Dimethyl-1-butanol (Aldrich; 98%)
- (Trimethylsilyl)methanol (Aldrich; 98%)
- 2-(Trimethylsilyl)ethanol (Aldrich; 99%)
- 3-(Trimethylsilyl)-1-propanol (Aldrich; 97%)
- 3-Pentanol (Santa Cruz Biotechnology; 98%)
- 2-Methyl-3-pentanol (Aldrich; 99%)
- 1-Hexanol (Aldrich; 98%)
- 1-Heptanol (Aldrich; 98%)
- 1-Octanol (Aldrich; 98%)
- Glacial acetic acid (Fisher Chemical; 99%)
- Ethyl acetate (Aldrich; 99.8%+ anhydrous)
- Hydrochloric acid (Aldrich; 98%)
- Diethyl ether (VWR Chemicals; 95%)
- 1-Butanol (Aldrich; 99%)
- Methanol (Aldrich; 99.8%+ anhydrous)
- Ethanol (VWR Chemicals; 99.9%)
- Chloroform (VWR Chemicals; 99%)
- Tetrahydrofuran (Aldrich; 99%+ anhydrous)
- Hexanes (Aldrich; 98 %)
- CDCl_3 (Aldrich; 99.8%)
- D_2O (Aldrich; 99.9%)
- d_6 -DMSO (Aldrich; 99.9%)
- Tetramethylammonium (Aldrich; 40% H_2O)

- Tetraethylammonium (Aldrich; 40% H₂O)
- Tetrapropylammonium (Aldrich; 1.0 M H₂O)
- Chlorosulfonic acid (Aldrich; 99.9 %)
- Dimethylaniline (Aldrich; 99%)
- Fumaryl chloride (Aldrich; 95%)
- Anhydrous magnesium sulfate (VWR Chemicals; 65/70%)
- Anhydrous sodium carbonate (Fisher Scientific; 99.5%)
- Sodium hydrogen carbonate (Aldrich; 98%)
- Sodium metabisulfite (Aldrich; 98%)
- Sodium sulphite (Aldrich; 98%)
- Ethylenediaminetetraacetic acid tetrasodium salt hydrate (Aldrich; 98%)
- Amberlite IR 120 H⁺ ion-exchange resin
- Sodium dodecylsulfate (Aldrich; 99%)
- AOT (Diocetyl sulfosuccinate sodium, Aldrich; 98%)

Table 4.1: Molecular structures and nomenclature of surfactants synthesised

Molecular Structure	Nomenclature
	Na-FO180
	TMA-FO180
	TEA-FO180
	TPA-FO180
	Na-FO180N

Table 4.1 – continued from previous page

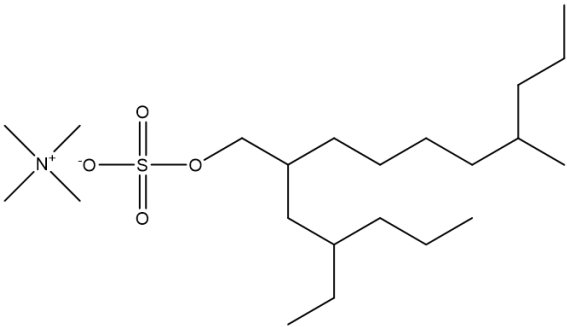
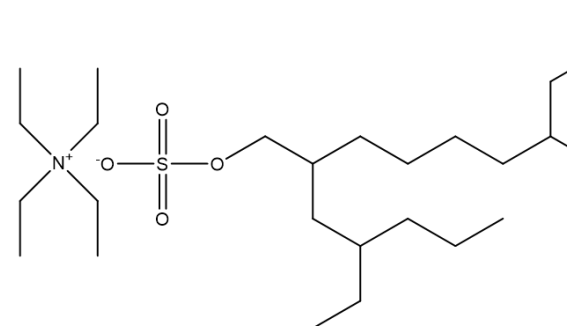
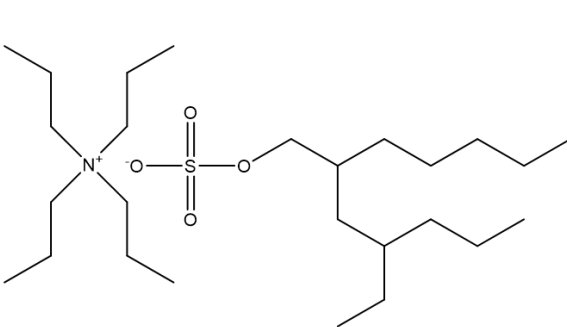
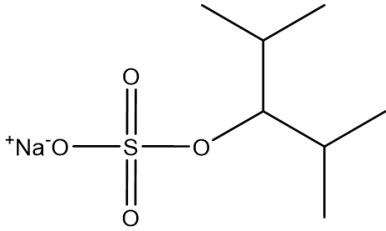
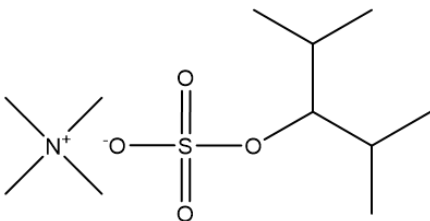
Molecular Structure	Nomenclature
	TMA-FO180N
	TEA-FO180N
	TPA-FO180N
	Na-BC7
	TMA-BC7

Table 4.1 – continued from previous page

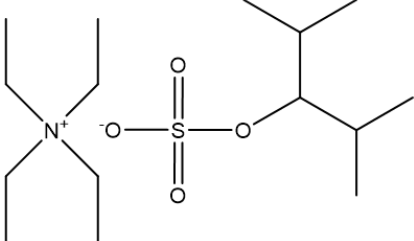
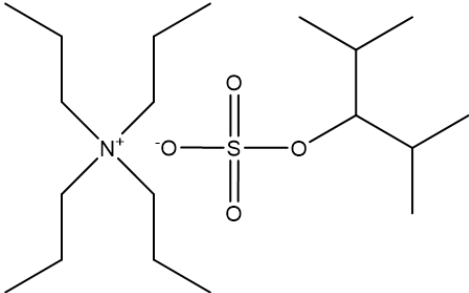
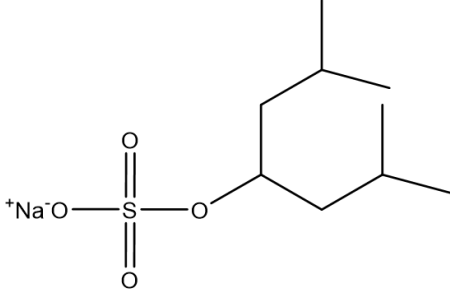
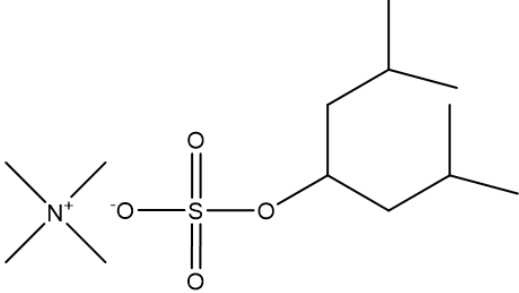
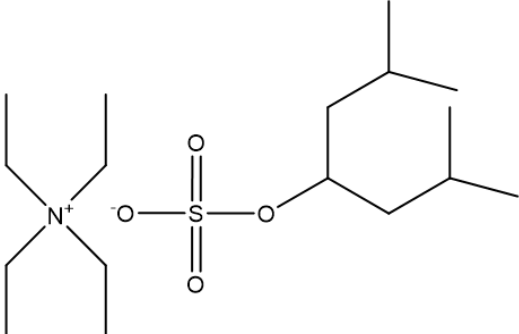
Molecular Structure	Nomenclature
	TEA-BC7
	TPA-BC7
	Na-BC9
	TMA-BC9
	TEA-BC9

Table 4.1 – continued from previous page

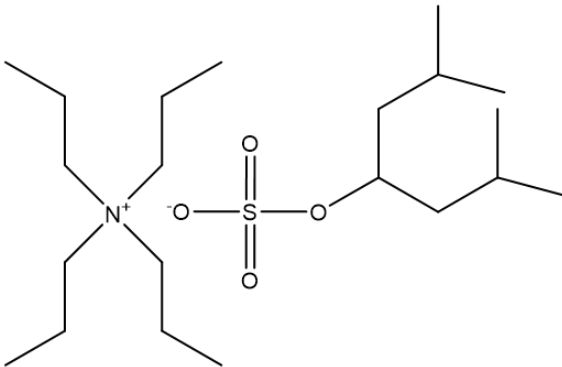
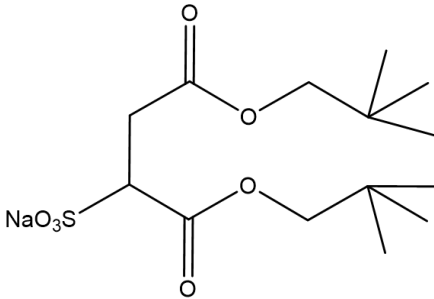
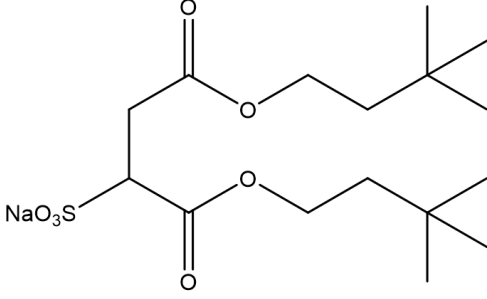
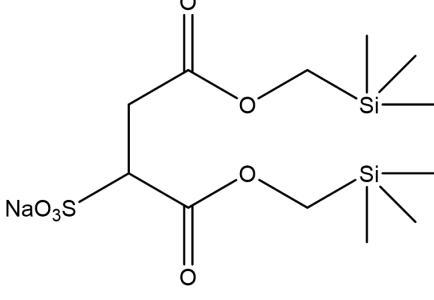
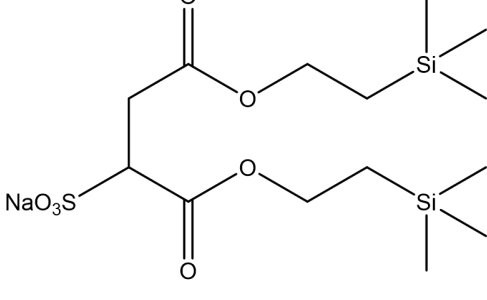
Molecular Structure	Nomenclature
	TPA-BC9
	AOTA
	AOTB
	AOTSiA
	AOTSiB

Table 4.1 – continued from previous page

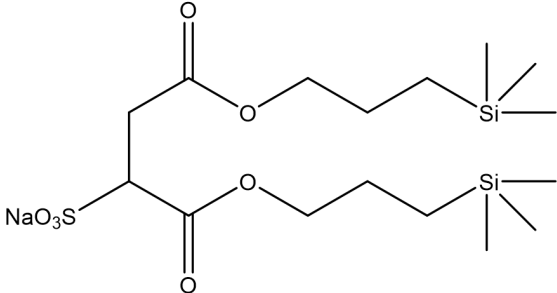
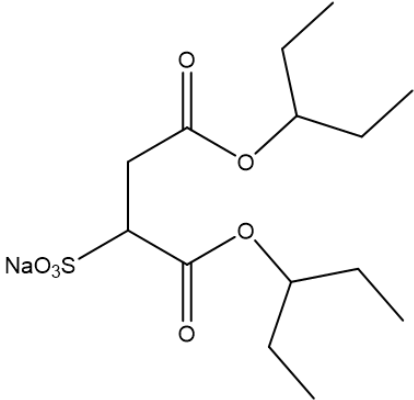
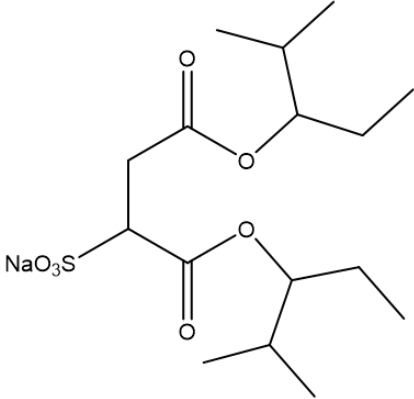
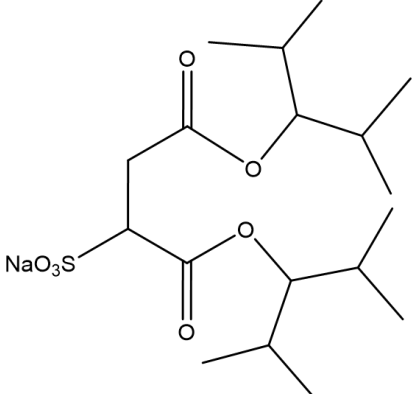
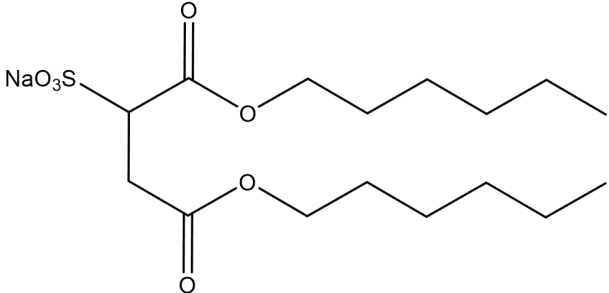
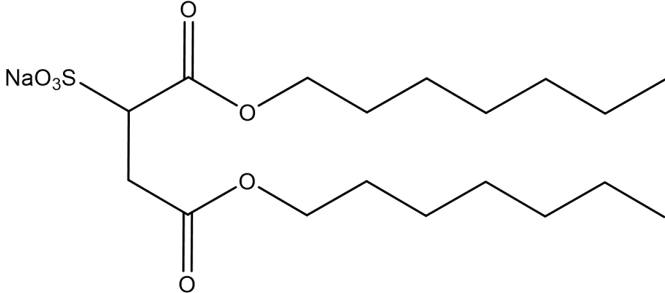
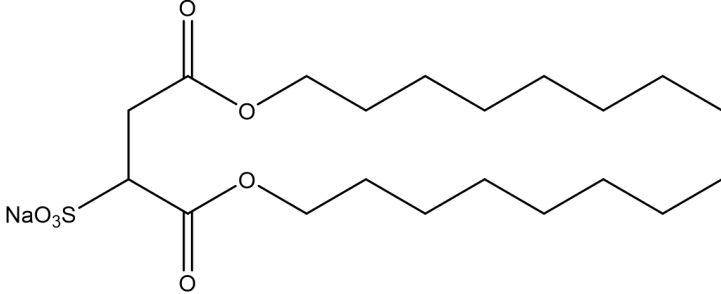
Molecular Structure	Nomenclature
	AOTSiC
	HS1
	HS2
	HS3

Table 4.1 – continued from previous page

Molecular Structure	Nomenclature
	di-C6SS
	di-C7SS
	di-C8SS

4.3 Synthesis of single-chain surfactants

Sulfonating alcohols with chlorosulfonic acid was established in Germany before World War II and is still considered the most suitable method for small-scale preparation. The reaction proceeds with the evolution of hydrogen chloride and can leave residual traces of sulfonyl chloride if not treated carefully, imparting a high apparent viscosity to the final product. General conditions are one molar equivalent of reagent at -5 to 25 °C. Higher temperatures cause chlorosulfonic acid to decompose producing appreciable amounts of hydrogen chloride.¹ With liquid alcohols no solvent is necessary, but when using solid alcohols, the reaction may be performed in suitable solvents such as chloroform. A mixture of chlorosulfonic acid with acetic acid has been used before to sulfonate alcohols with good yields and purity.² The chlorosulfonic acid-acetic acid complex is a milder reagent than free chlorosulfonic acid, attributed to the intermediate formation of acetyl sulfate. The procedure outlined below is highly suitable for long chain 1° or 2° alcohols which can be separated and removed easily from the reaction mixture, see reaction scheme Figure 4.1 (a). For smaller alcohols, further steps are required at the end to ensure a high purity. The TAA⁺ form of each single-chain surfactant was produced by counterion exchange of the sodium equivalent, Figure 4.1 (b). The same synthetic procedure was used for all single-chain surfactants shown in Table 4.1, as an example, the synthesis of Na-FO180 is outlined here.

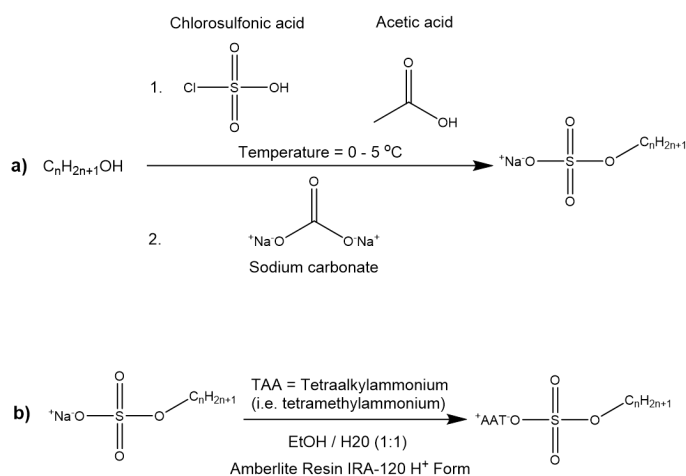


Figure 4.1: Single-chain synthetic routes: a) esterification of a 1° or 2° alcohol, b) counterion exchange to form TAA⁺ equivalent.

1) Preparation of chlorosulfonic acid/acetic acid solution

Glacial acetic acid (5.547 g, 2.5 eq.) was cooled in an ice bath for approximately ten minutes. Chlorosulfonic acid (4.036 g, 2.460 mL, 1 eq.) was then slowly added to the flask containing the acetic acid using a graduated pipette.

2) Reaction of chlorosulfonic acid with alcohol

Isostearyl alcohol FO180 (10 g, 1 eq.) was added dropwise to the chlorosulfonic acid/acetic acid mixture in the ice bath whilst also being stirred. Once all alcohol was added the reaction flask was removed from the ice bath and left to stir for a further 15 minutes. Ice-cold water (20 mL) was then added dropwise over a period of about 10 minutes.

3) Extraction and purification

1-Butanol (20 mL) was added and the mixture was left to stir for five minutes. After this time, anhydrous sodium carbonate (4.308 g, 1.2 eq.) was added portion wise to ensure a controlled neutralisation. The reaction mixture was then left to stir for the appropriate amount of time to ensure all sodium carbonate had dissolved (add small additional volumes of water here if necessary). The aqueous layer was then removed with a separating funnel and the organic layer retained. The aqueous layer was then extracted one further time with additional 1-Butanol. Organic fragments were recombined and rotary evaporated. The product was then dissolved in the minimum amount of methanol and centrifuged at 4000 rpm for 45 minutes. This stage was repeated (with careful decanting) until the reaction mixture was clear, showing the sign of no additional salts. The solvent was removed on a rotary evaporator and the product dried overnight in a vacuum oven (15 mbar, 40 °C) to yield the final product Na-FO180 as white solid (9.658 g, 97% yield).

Sodium bearing single-chain surfactants were then converted into the surfactants bearing different TAA⁺ counterions by an ion-exchange technique as follows:

3) Counterion exchange

A column (30 cm x 1 cm²) was filled with ion exchange resin Amberlite IR 120 H⁺. The column was rinsed with pure water until the water passing through was clear. Surfactant (sodium salt, 2-3 g) was dissolved in 30 mL of EtOH/H₂O (1:1 v/v) and

passed through the column. The free sulfonic acid formed was immediately neutralised with an aqueous solution of tetraalkylammonium hydroxide of the desired counterion. The solvent was then removed by evaporation. To remove excess TAA, the product was dissolved in chloroform and centrifuged at 4000 rpm for 45 minutes. Once the solvent was removed by rotary evaporation the product was dried in a vacuum oven overnight (25 mbar, 40 °C).

Once dried, the final products were stored in sealed vials in a desiccating cabinet over refreshed phosphorus pentoxide. All single-chain surfactants were investigated with ^1H NMR and EA analyses, which confirmed the desired products at >95% purity. Selected spectra are shown in Section 4.5 along with EA analysis, all other NMR spectra can be found in the Supporting Information.

4.3.1 Surfactant purification

The above procedures are very effective at producing high purity single-chain surfactants provided the starting alcohols are of sufficient size to allow effective extraction with 1-Butanol. Other solvents were tried for smaller chain alcohols however, the extracted yield was often low. Therefore, the following methods were used to achieve both high yield and purity of single-chain surfactants composed of small alcohols (<C8). Instead of extracting with 1-Butanol, once all anhydrous sodium carbonate had fully dissolved solvent was removed. Residual acetic acid would remain in the product which can be removed by the following processes:

1. The product was redissolved in pure water and rotary evaporated. This would be repeated several times until all acetic acid was removed (^1H NMR).
2. If the following step above was unsuccessful, the surfactant would be passed over ion exchange resin Amberlite IR 120 H^+ following the procedure above, but instead the free sulfonic acid formed was immediately neutralised with an aqueous sodium carbonate solution. The solution was then rotary evaporated.

For both steps, the final product would undergo the same centrifuge purification step as the other sodium single-chain surfactants and then be dried in a vacuum oven overnight (25 mbar, 40 °C).

4.4 Synthesis of di-chain surfactants

The ease and yield of synthesising di-chain surfactants is dependent on the structure of the starting alcohol. Provided the alcohol is 1° or 2°, reacting with fumaryl chloride as outlined below can successfully produce di-chain surfactants of high quality and yield. The common alternative is by reaction of maleic anhydride with the appropriate alcohol. The main advantages of the fumaryl chloride route is a) shorter reaction times and b) the greater reactivity of fumaryl chloride over maleic anhydride can lead to higher yields. The reaction scheme is shown in Figure 4.2. The same synthetic procedure was used for all di-chain surfactants shown in Table 4.1, as an example, the synthesis of AOTA is outlined here.

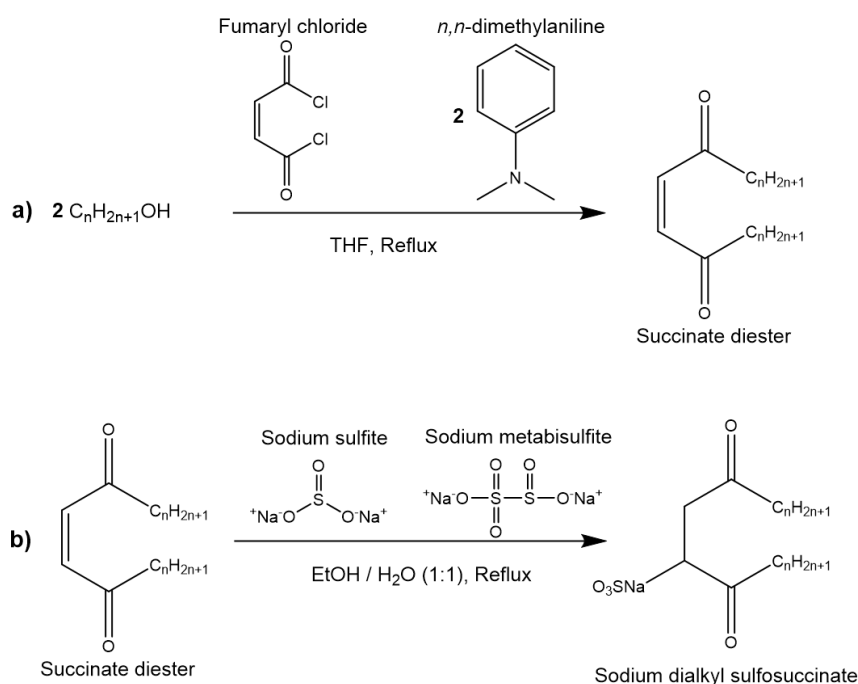


Figure 4.2: Di-chain synthetic routes: a) esterification of a 1° or 2° alcohol, b) sulfonation of the diester intermediate

1) Esterification

2,2-dimethylpropanol (8.055 g, 2.2 eq.) and dimethylaniline (10.069 g, 2.0 eq.) were dissolved in 150 mL dry tetrahydrofuran. The reaction vessel was flushed with N₂ and then fumaryl chloride (6.355 g, 1.0 eq.) was added dropwise. As the fumaryl chloride was added the internal temperature rose to approximately 65 °C. Once all the fumaryl chloride was added, the reaction mixture was refluxed and TLC plates

developed periodically (4:1 hexane:ethyl acetate eluent) to check for residual fumaryl chloride (baseline spot). After approximately 4 hours the reaction was complete and THF was removed by rotary evaporation. The product was dissolved in diethyl ether and the ethereal solution was washed sequentially with 10 % hydrochloric acid (100 cm³) and saturated aqueous sodium hydrogen carbonate solution (100 cm³) until the aqueous phase was clear. The washed ethereal solution was dried over anhydrous magnesium sulfate, filtered, and rotary evaporated to yield the crude diester as an oil. The crude diester was purified by column chromatography, with a petroleum spirit (40/60):diethyl ether eluent in a 80:20 ratio (for some diesters, a pet:ether 90:10 eluent gave better separation). Fragments were checked by TLC, recombined, and rotary evaporated to yield the pure diester bis(2,2-dimethylpropanol) fumarate as a white solid (7.250 g, 90% yield)

2) Sulfonation

Bis(2,2-dimethylpropanol) fumarate (7.250 g, 1.0 eq.) was dissolved in a 1:1 mixture of ethanol/water (250 mL) and refluxed. Sodium metabisulfite (9.229 g, 1.1 eq.) and sodium sulphite (4.464 g, 0.9 eq.) were added portion-wise during the first hour of reflux. The reaction was monitored by TLC (eluting with ethyl acetate). If some residual diester remained after 2 hours, additional disulfite and sulphite were added. Once complete, the reaction mixture was decanted off and rotary evaporated.

4.4.1 Surfactant purification

The properties of any interface will be affected by the presence of impurities and hence, to accurately study the effects of surfactant molecules at an interface, the system must be clean of surface active impurities. The most common impurities in these surfactants are residual salts left over from sulfonation, or unreacted starting materials. The following steps yield pure surfactants that give clean breaks in γ vs log (conc.) plots, showing the sign of no surface active impurities.

1) Soxhlet extraction

To remove residual inorganic material left over from the sulfonation step, Soxhlet extraction with ethyl acetate was performed for 24 hours. The ethyl acetate used

was purchased in a dried form, otherwise the solvent would be dried with MgSO_4 and distilled. After 24 hours the solvent was removed by rotary evaporation.

2) *Centrifuge*

Salts have a low solubility in certain solvents such as methanol or acetone. Therefore, centrifugation is a common and simple method to easily remove excess salts present in the system. The product from Soxhlet extraction was dissolved in the minimum amount of methanol and centrifuged at 4000 rpm for 45 minutes. The reaction mixture was decanted leaving any residual salt, and the process repeated until the solution became clear. The solvent was removed by rotary evaporation, and the product dried in a vacuum oven overnight (40 °C, 25 mbar).

3) *Recrystallisation*

A combination of Soxhlet extraction and centrifugation was appropriate to yield pure diesters in most cases. However, it was clear to see by ^1H NMR analysis that some residual impurities still remained on occasion. The product from centrifugation would then be then recrystallised from either methanol or ethyl acetate, followed by drying under vacuum for at least 24 hours (40 °C, 25 mbar) to yield the pure surfactant as a white solid or wax.

4) *Foam fractionation*

Foam fractionation is a very good technique for removing trace quantities of surface-active impurities.³ A solution is made up slightly below the cmc, and N_2 gas that has passed through several cleaning stages is bubbled through the solution, causing the more surface active impurities to be removed with the foam that is produced. However, surfactant molecules adsorbed to the surface are also removed with the foam produced and hence, foam fractionation also causes loss of product. Therefore, foam fractionation could not be used for the surfactants discussed in this work as they could often only be synthesised in small quantities due to the unique, and expensive starting material alcohols. It is worth mentioning the technique and setup used, for other studies that may benefit from foam fractionation.

Method: A solution of surfactant in ultra-pure water was made up to 0.85 x cmc. Nitrogen gas was passed through a calcium sulfate drying set-up and a carbon filter, and then bubbled through aqueous solutions of HCl and NaOH, followed by several flasks of pure water before finally reaching the surfactant solution. It was necessary to control the gas flow and vacuum suction rates to allow sufficient drainage time before the foam was removed. The pure surfactant was recovered by rotary evaporation and dried as before.

Once dried, the final products from purification were stored in sealed vials in a desiccating cabinet over refreshed phosphorus pentoxide. All purified surfactants were investigated with a range of analytical methods, ^1H , ^{13}C and EA (elemental analysis), which confirmed the desired products at >95% purity. Selected spectra are shown in Section 4.5 along with EA analysis, all other NMR spectra can be found in the supporting information.

4.4.2 Synthesising surfactants from tertiary alcohols

When designing novel di-chain hydrocarbon surfactants to achieve very low surface tensions, various synthetic procedures were attempted with tertiary (3°) alcohols. These however, proved to be unsuccessful and thus, this section is to provide guidance for future chemists that may themselves attempt to synthesise surfactants from tertiary alcohols. For all procedures described, the alcohol used was tert-Butyl alcohol.

The method already described for forming di-chain surfactants (fumaryl chloride with alcohol) is insufficient for (3°) alcohols, due to the low conversion to di-ester. Various alternative methods based on similar chemicals were attempted.⁴⁻⁷ A more aggressive method of reacting with silver cyanide in benzene was also attempted.⁸ Due to the difficulty of forming di-chain esters from tertiary alcohols a particularly strong reagent is possibly required. There is reported success with tert-Butyllithium and this would perhaps be the next appropriate step.⁹

4.5 Surfactant analysis

Nuclear magnetic resonance and elemental analysis were used to characterise the purity of each surfactant shown in Table 4.1.

4.5.1 Nuclear Magnetic Resonance (NMR) spectroscopy

Proton NMR were recorded on a JOEL Lambda 400 MHz machine (NMR service, School of Chemistry, University of Bristol). Processed spectra were further analysed using MestReNova software to provide peak positions and integration values for chemically equivalent protons. The method used for preparing samples was as follows: Approximately 50 mg of product was dissolved in 1 mL of deuterated solvent (d_6 -DMSO, D_2O or $CDCl_3$). The sample was thoroughly mixed by vortex and ran through a pipette with a cotton wool bung. Due to incomplete deuteration of the solvents, residual proton signals are present, giving a septet at 2.46 and a singlet at 3.51 ppm for d_6 -DMSO, singlet at 4.79 ppm for D_2O , and a singlet at 7.26 ppm for $CDCl_3$. Spectra were obtained for all final products. The following section shows selected spectra and analysis of surfactant purity is discussed.

NMR of single-chain surfactants

Following the procedure outlined in section 4.3, 1H NMR analysis shows that single-chain surfactants are synthesised to a high purity with the presence of no unexpected signals. Noticeable peaks which would shown the sign of impurities would be a signal between 1-5 ppm for the OH of unreacted alcohol, and a singlet at 8.5 ppm for chlorosulfonic acid not bearing a Na^+ or TAA^+ counterion. For example, Figure 4.3 shows the 1H NMR for Na-BC9 and the corresponding starting alcohol (2,6-dimethyl-4-heptanol). The 1H NMR of the final surfactant product is similar to the original alcohol and contains no unexpected signals, i.e showing a clean synthesis without the presence of unreacted alcohol or acid in the final product. The signal for the hydrogen environment closest to the sulfonate group (peak *e* on Figure 4.3) has shifted downfield compared to the pure alcohol spectrum. This is expected because sulfur is more electronegative than hydrogen, which consequently makes the oxygen bonded to carbon a stronger electron withdrawing group. Interestingly,

peaks *c* and *d* on Figure 4.3 are separate environments which would perhaps not be expected given the symmetric structure of 2,6-dimethyl-4-heptanol. To accurately assign these signals ^1H NMR is not sufficient alone. Homonuclear correlation spectroscopy, or COSY, is a two-dimensional NMR technique which identifies spins coupled to each other. Figure 4.4 shows that hydrogen environment *a* ~ 0.82 ppm (the four methyl groups) are only coupled to the proton signal downfield at ~ 1.73 ppm, which therefore must be the C-H bond bearing the methyl groups (labelled *b*). Finally, the hydrogen signal most downfield at ~ 4.48 ppm labelled *e* shows coupling to signals at ~ 1.66 and 1.38 ppm which must be the two CH_2 groups. Now the proton NMR of Na-BC9 can be accurately assigned and is shown in Figure 4.5. Selected members of the BC9 family and other single-chain surfactants are shown in Figures 4.5-4.7. COSY analysis was required for some but not all single-chain surfactants, these, along with ^1H NMR for all other single-chain surfactants can be found in the Supporting Information. Details of proton assignments and integration for the selected NMR spectra are given in Table 4.2.

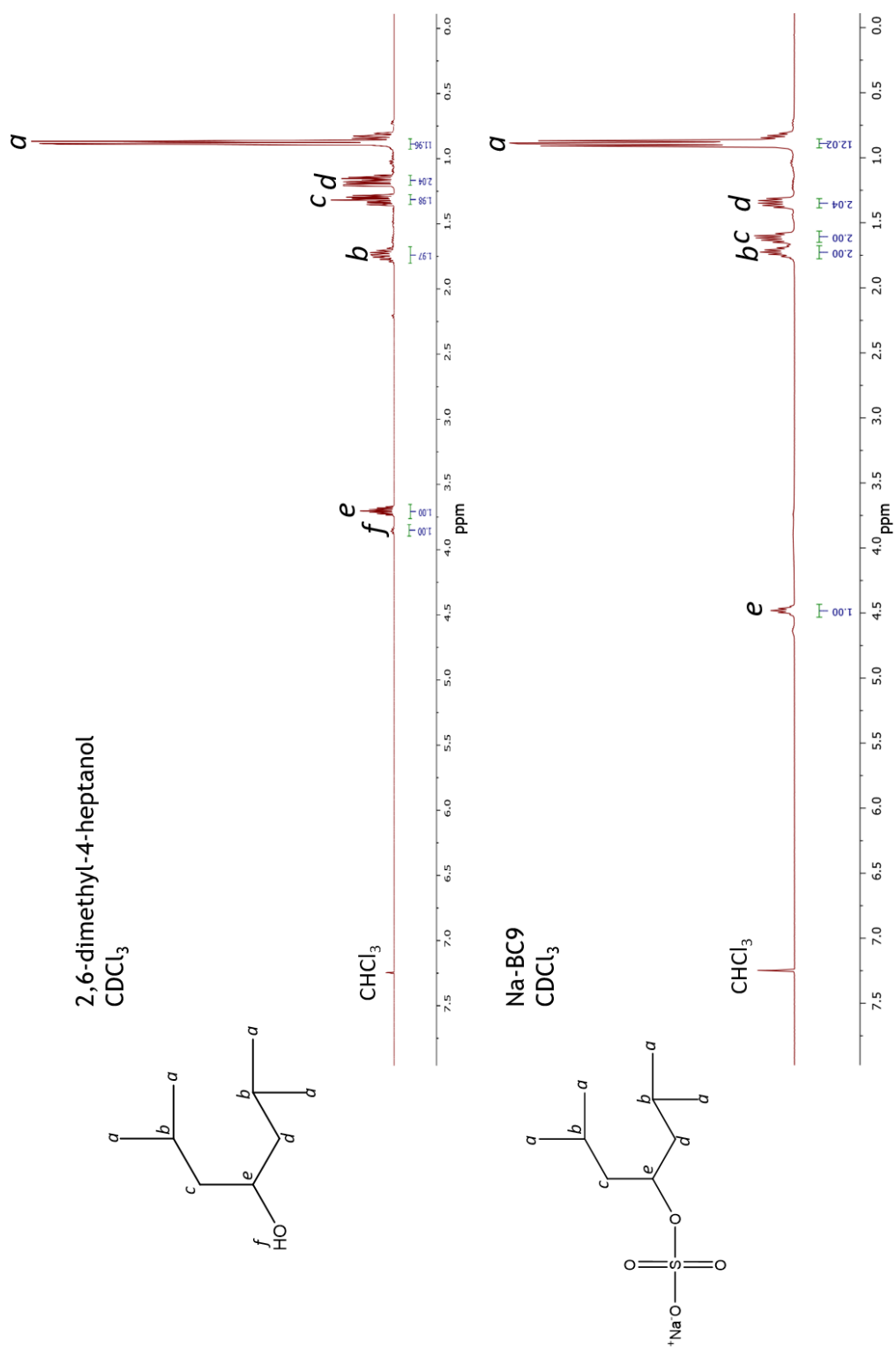
NMR of di-chain surfactants

Following the procedure outlined in Section 4.4, ^1H NMR analysis shows that di-chain surfactants are synthesised to a high purity. The di-ester that is formed as an intermediate product should be of a high purity to improve the purity of the final product, as the sulfonation step can introduce various unexpected species as seen by ^1H NMR. The purification step that was chosen for all di-ester intermediate products was column chromatography, the alternative being vacuum distillation. Figures 4.8 and 4.9 show the ^1H NMR for the di-esters of AOTA and AOTSiB. As can be seen from the figures, di-esters are synthesised to an excellent purity using the methods outlined in Section 4.4, with ^1H NMR showing exceptionally clean profiles. It should be noted that fumarate di-esters are of *trans* configuration and so only one singlet is obtained at ~ 7.0 ppm. Splitting patterns in the final products after sulfonation can be rather complex and unpredictable. This is due to asymmetry caused by the head group, which creates a slight difference in chemical environment at the two chain-ends. ^{13}C NMR can be used to highlight this, for example, Figure 4.10 shows the ^{13}C NMR for the chain ends of AOTSiC. Although slight, the peak position of

the same carbon environments are clearly shifted from each other. Sulfonated di-esters dissolved in d_6 -DMSO often gave clearer splitting patterns and thus was the solvent of choice for final products. For ^1H spectra noticeable peaks are the absence of any di-ester peak at ~ 7.0 ppm, which is replaced by the signature doublet of doublets (dd's) at ~ 3.5 ppm for the single hydrogen in the head group, and the two dd's at ~ 2.8 ppm for the CH_2 moiety in the head group. Other commonly encountered peaks are residual solvents from the various purification steps if the surfactant has not been dried at a sufficient temperature, or for sufficiently long enough. When dissolved in d_6 -DMSO, final products show two peaks for residual amounts of partially deuterated DMSO, or even undeuterated DMSO, that exists in the solvent. Selected ^1H NMR spectra for di-chain surfactants are shown in Figures 4.11-4.13 which show clean NMR profiles with integrations that match well with theoretical values. All other NMR spectra for final surfactant products can be found in the supporting information. Details of proton assignments and integration for the selected NMR spectra of di-esters and di-chain surfactants are given in Table 4.3.

4.5.2 Elemental analysis

Samples were submitted for elemental analysis of C, H, N and S where applicable (micro-analytical laboratory, School of Chemistry, University of Bristol / Elemental Microanalysis Ltd, Devon). From repeat measurements, the typical standard deviation for the percentage mass determined by elemental analysis was found to be approximately 0.3 to 0.8 %. As shown in Table 4.4, the agreement between theoretical and experimentally determined values is generally good and in most cases within the error. In particular, the good agreement between experimental and theoretical amounts of sulphur indicates that the extraction, washing and recrystallisation procedures effectively removed residual inorganic material.

Figure 4.3: ¹H NMR of Na-BC9 and corresponding starting alcohol with peak integrations also shown.

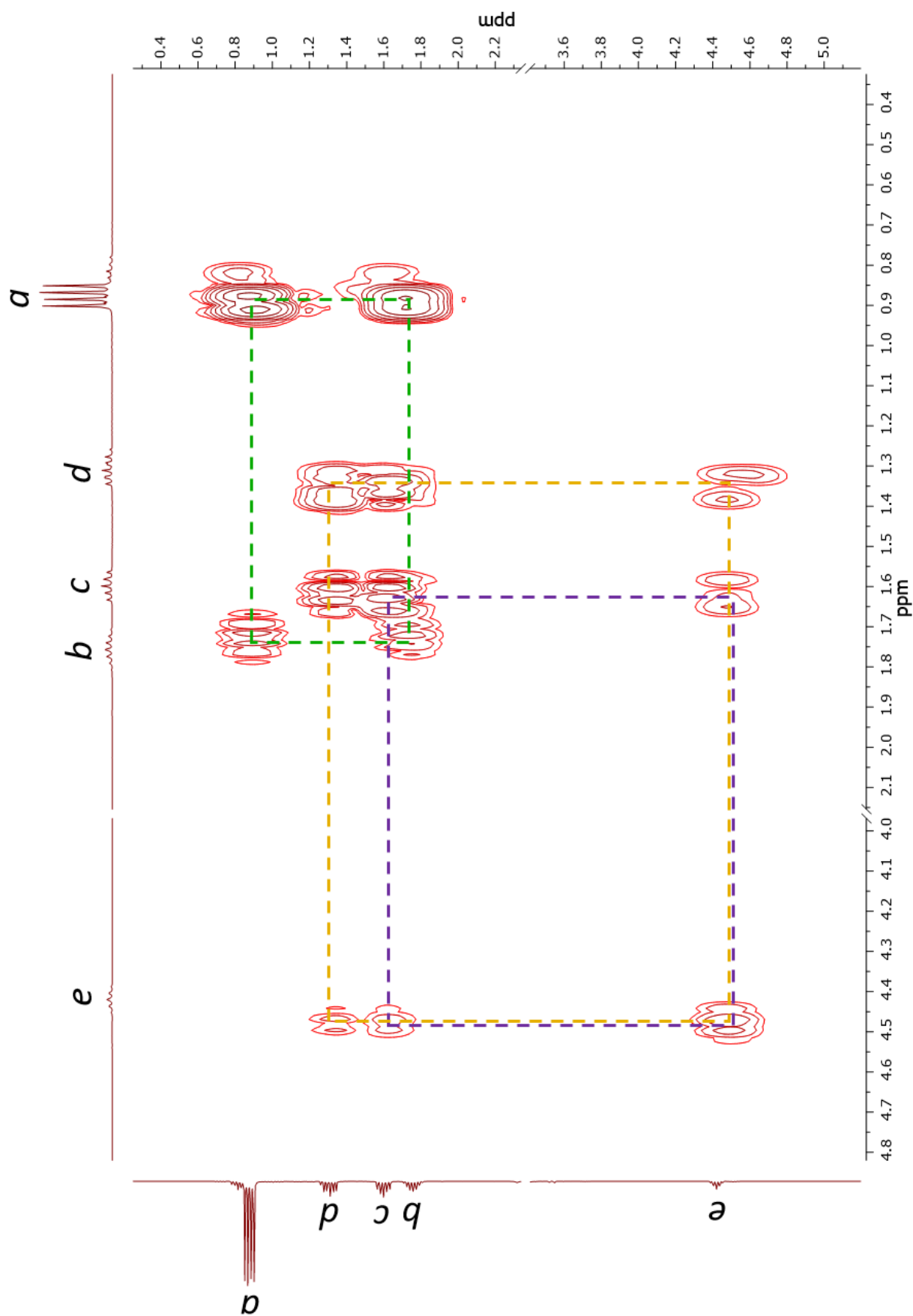
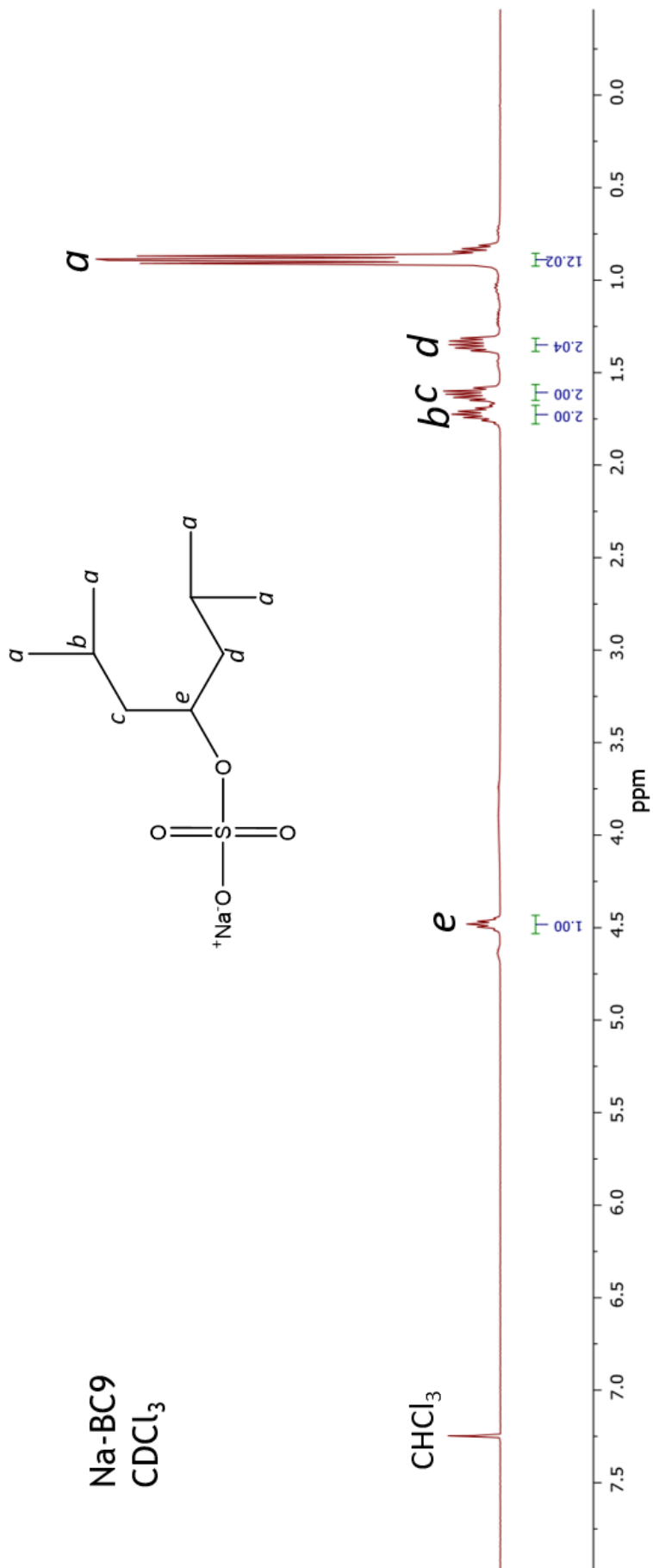
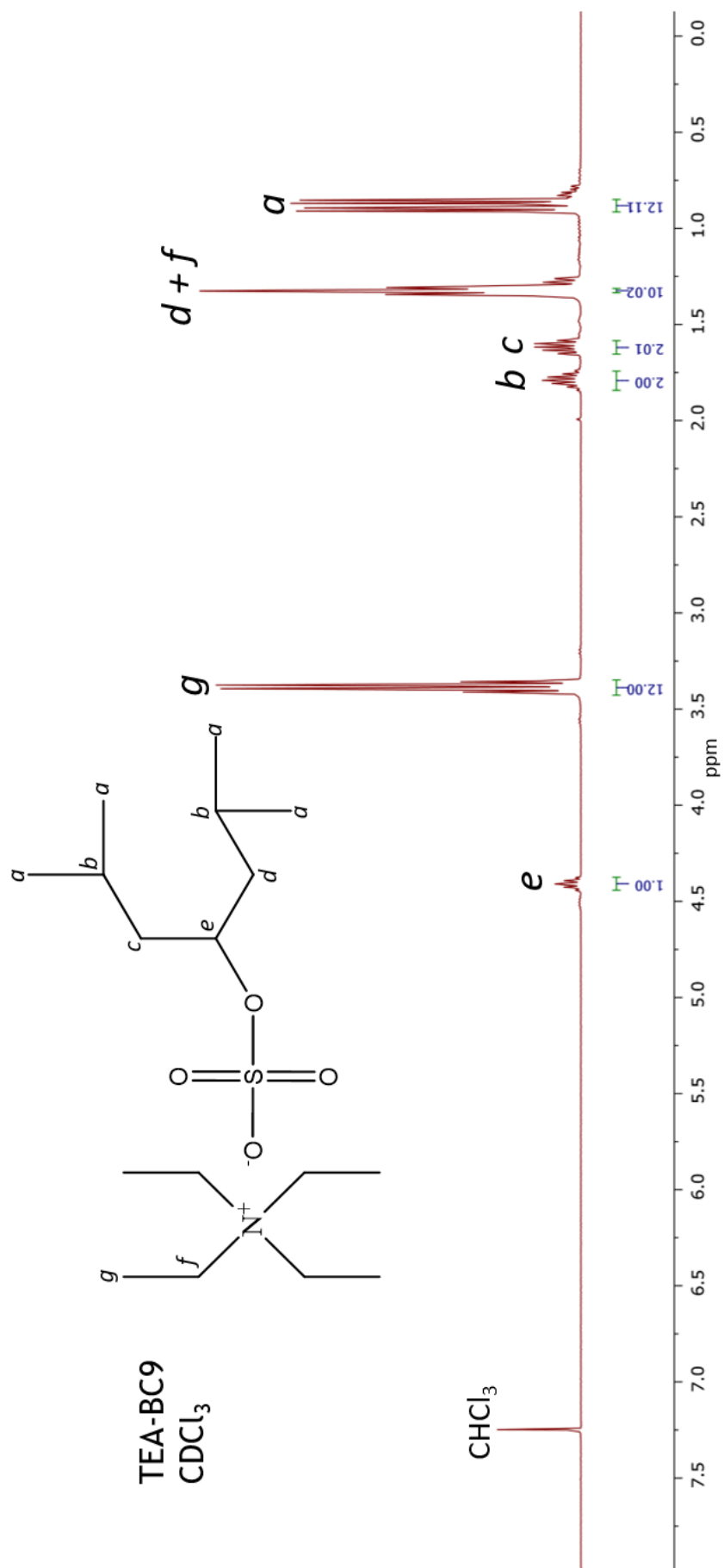


Figure 4.4: COSY NMR of Na-BC9 showing coupling between certain neighbouring hydrogen environments.

Figure 4.5: ¹H NMR of Na-BC9 with peak integrations also shown.

Figure 4.6: ¹H NMR of TEA-BC9 with peak integrations also shown.

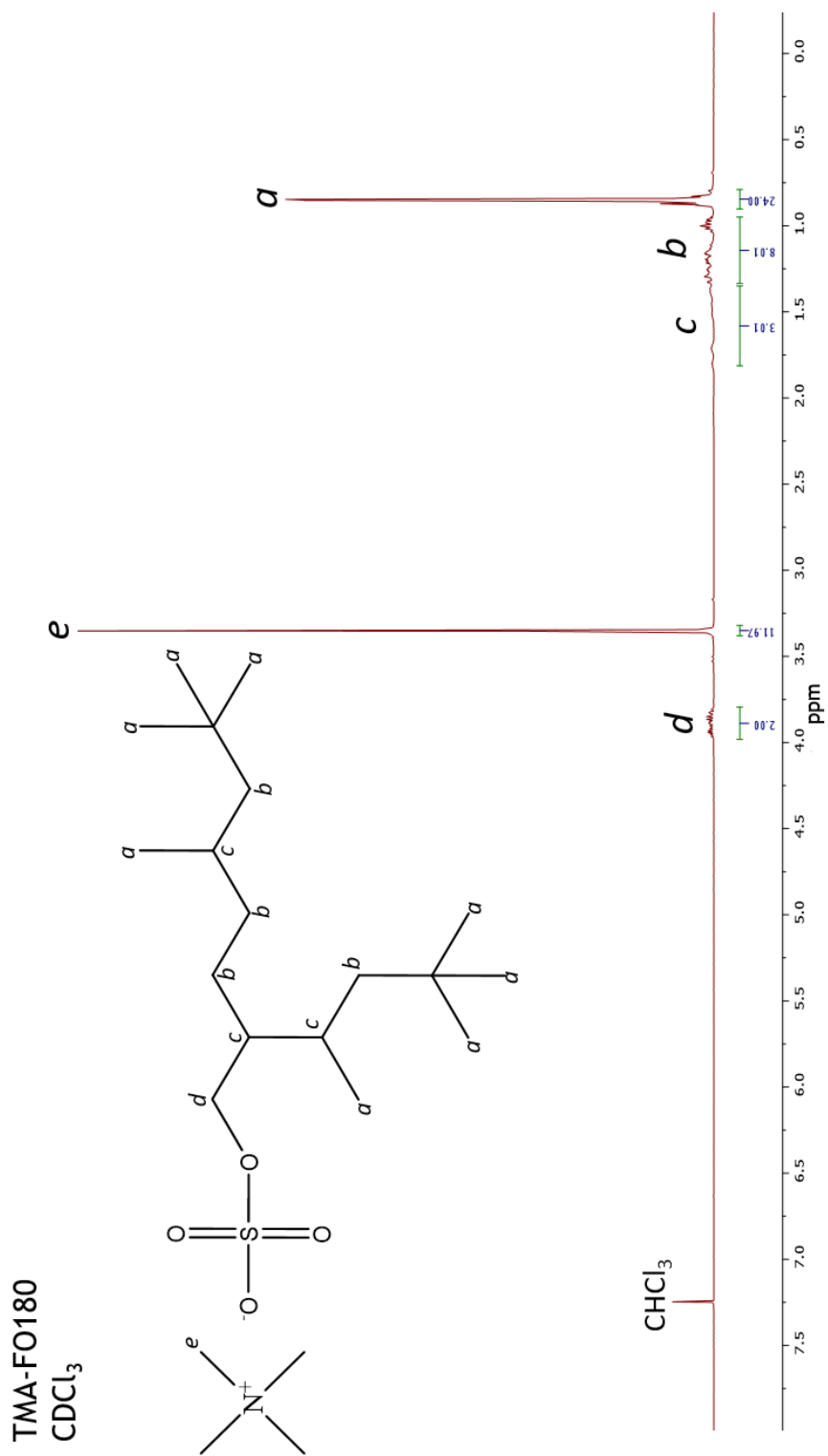
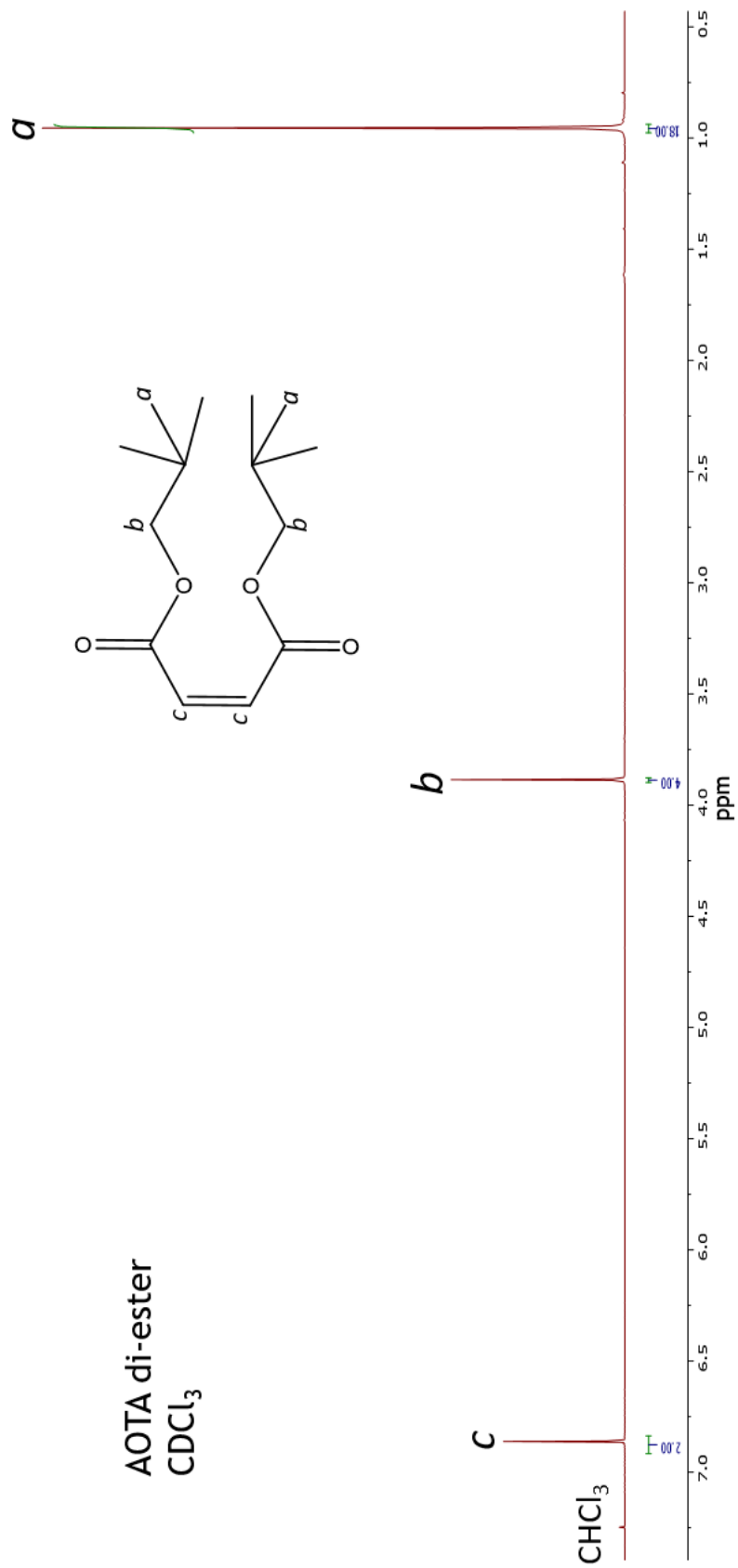
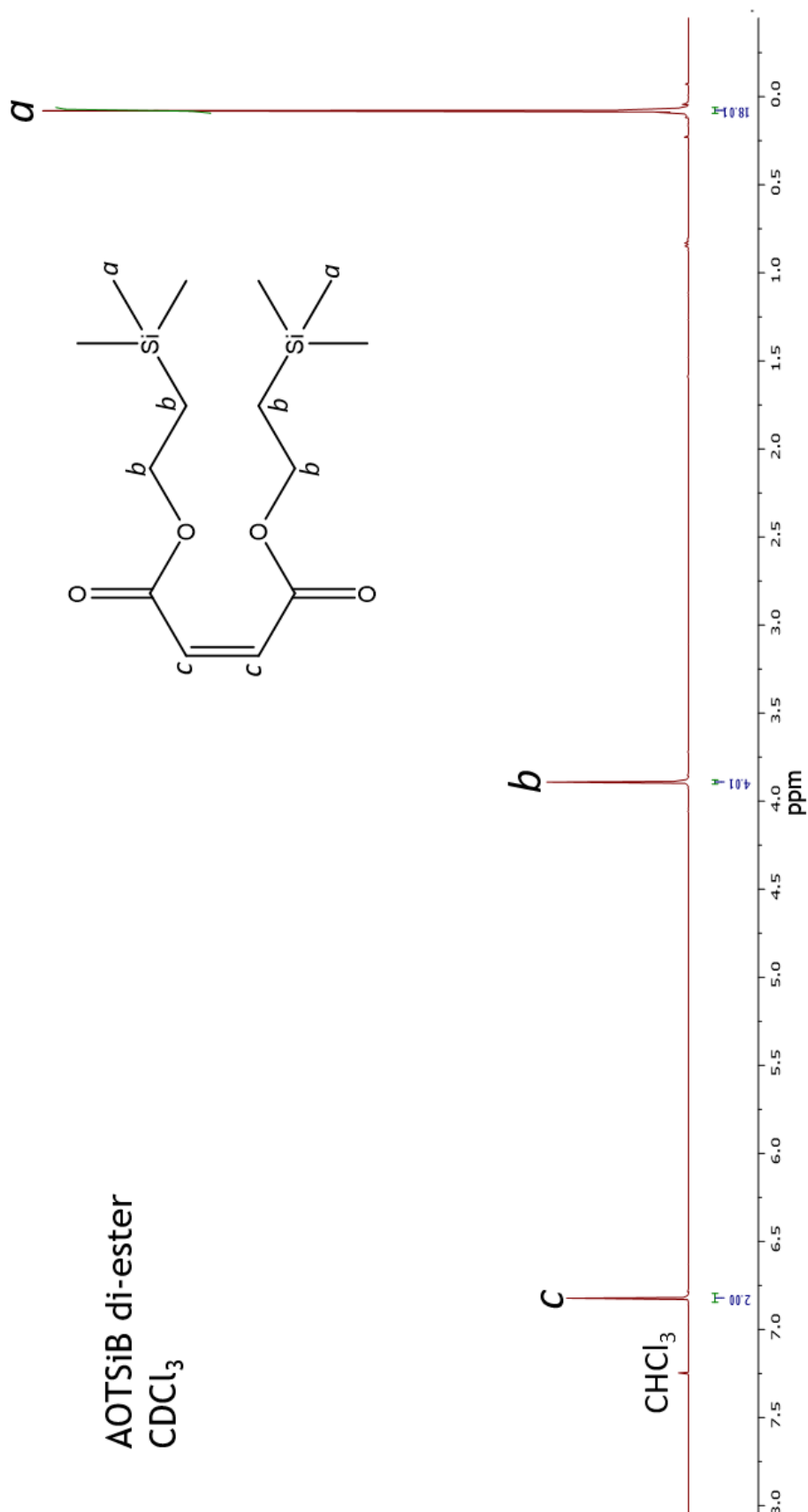
Figure 4.7: ¹H NMR of TMA-FO180 with peak integrations also shown.

Table 4.2: Data from selected ^1H NMR spectra of single-chain surfactants (Figures 4.3, 4.5 and 4.6).

Chemical Shift (ppm)	Molecular fragment	Integration	Identified proton
2,6-dimethyl-4-heptanol (BC9 alcohol)			
0.78 - 0.90	$-\text{CH}-(\text{CH}_3)_2$	11.96	a
1.11 - 1.23	$-\text{CH}-\text{CH}_2\text{CH}_2-$	2.04	d
1.25 - 1.34	$-\text{CH}-\text{CH}_2\text{CH}_2-$	1.98	c
1.69 - 1.79	$-\text{CH}-(\text{CH}_3)_2$	1.97	b
3.68 - 3.72	$-\text{CH}-(\text{CH}_2)_2-$	1.00	e
3.76 - 3.85	$\text{HO}-\text{CH}-$	1.00	f
Na-BC9			
0.83 - 0.94	$-\text{CH}-(\text{CH}_3)_2$	12.02	a
1.30 - 1.39	$-\text{CH}-\text{CH}_2\text{CH}_2-$	2.04	d
1.55 - 1.65	$-\text{CH}-\text{CH}_2\text{CH}_2-$	2.00	c
1.69 - 1.78	$-\text{CH}-(\text{CH}_3)_2$	2.00	b
4.45 - 4.53	$-\text{O}-\text{CH}-(\text{CH}_2)_2-$	1.00	e
TEA-BC9			
0.85 - 0.93	$-\text{CH}-(\text{CH}_3)_2$	12.11	a
1.30 - 1.35	$-\text{CH}-\text{CH}_2\text{CH}_2-$ $\text{N}-\text{CH}_2\text{CH}_3$	10.02	d + f
1.58 - 1.67	$-\text{CH}-\text{CH}_2\text{CH}_2-$	2.01	c
1.74 - 1.84	$-\text{CH}-(\text{CH}_3)_2$	2.00	b
3.35 - 3.43	$\text{N}-\text{CH}_2\text{CH}_3$	12.00	g
4.37 - 4.45	$-\text{O}-\text{CH}-(\text{CH}_2)_2-$	1.00	e
TMA-FO180			
0.79 - 0.90	$-\text{CH}_2-\text{C}(\text{CH}_3)_3$ $-\text{CH}-\text{CH}_3$	24.00	a
0.95 - 1.34	$-\text{CH}-\text{CH}_2-$	8.01	b
1.35 - 1.81	$-\text{CH}_3-\text{CH}-$	3.01	c
3.32 - 3.38	$\text{N}-\text{CH}_3$	11.97	e
3.79 - 3.98	$-\text{O}-\text{CH}_2-$	1.94	d

Figure 4.8: ^1H NMR of AOTA di-ester with peak integrations also shown.

Figure 4.9: ¹H NMR of AOTSiB di-ester with peak integrations also shown.

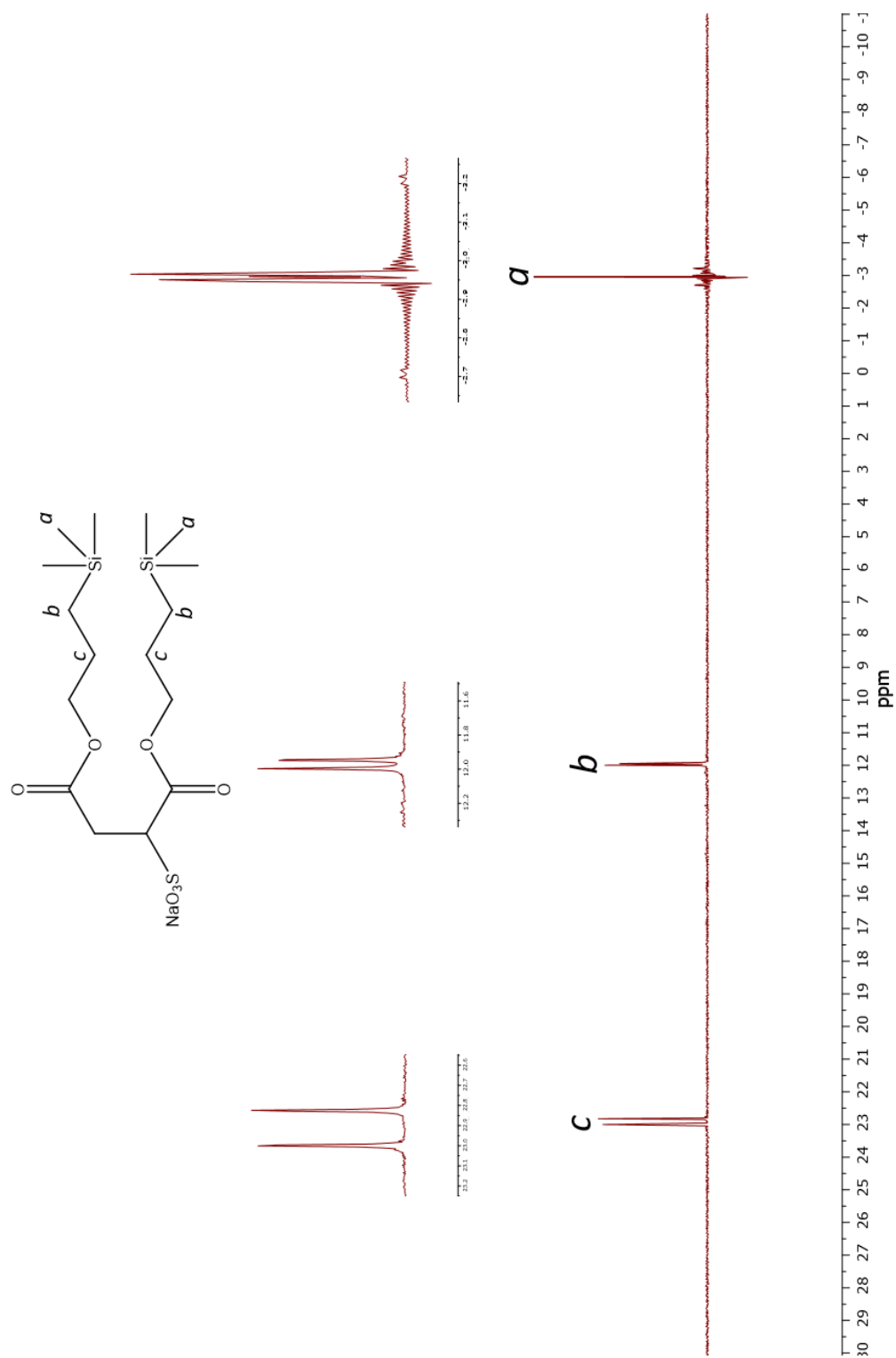
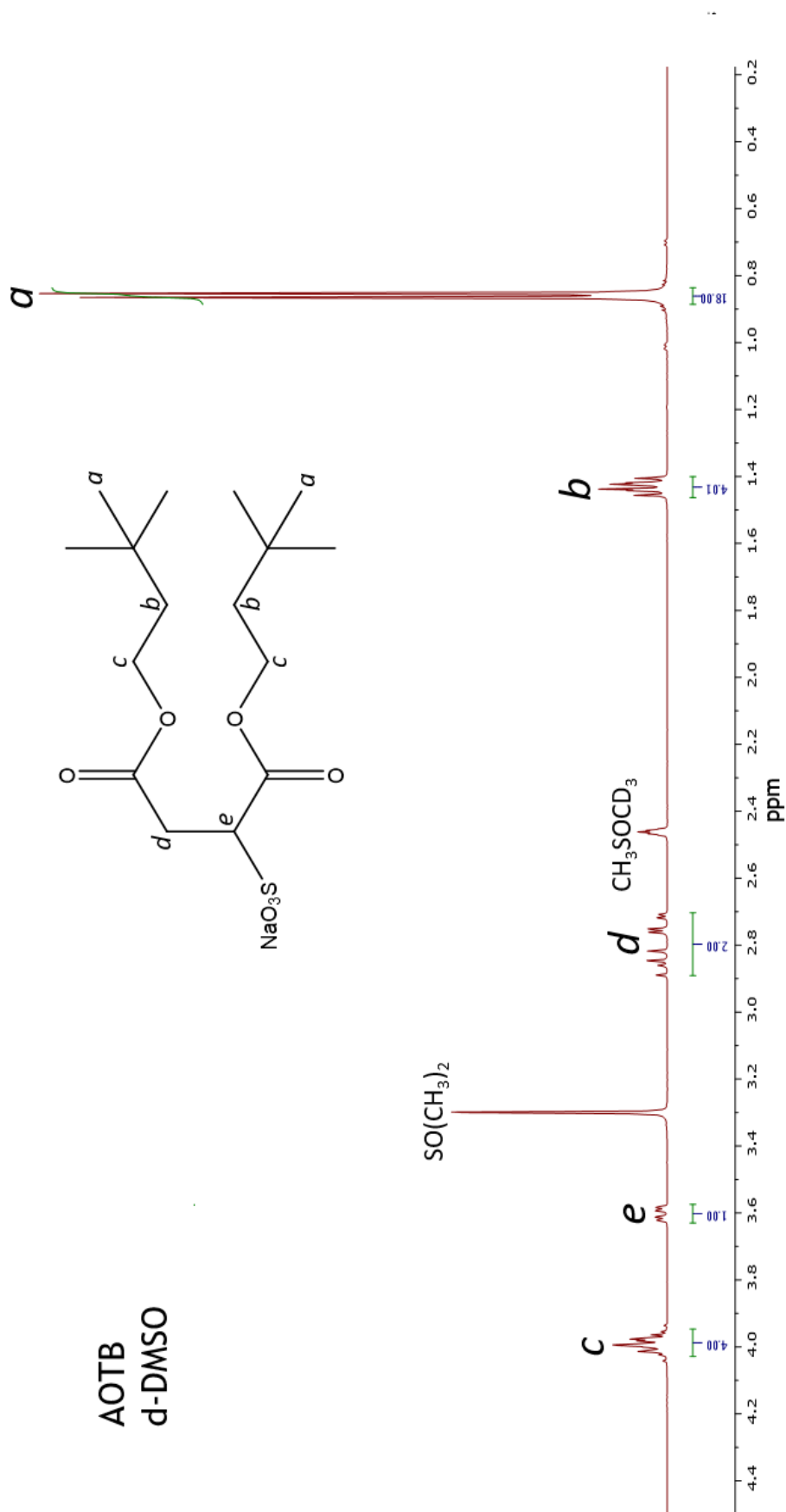
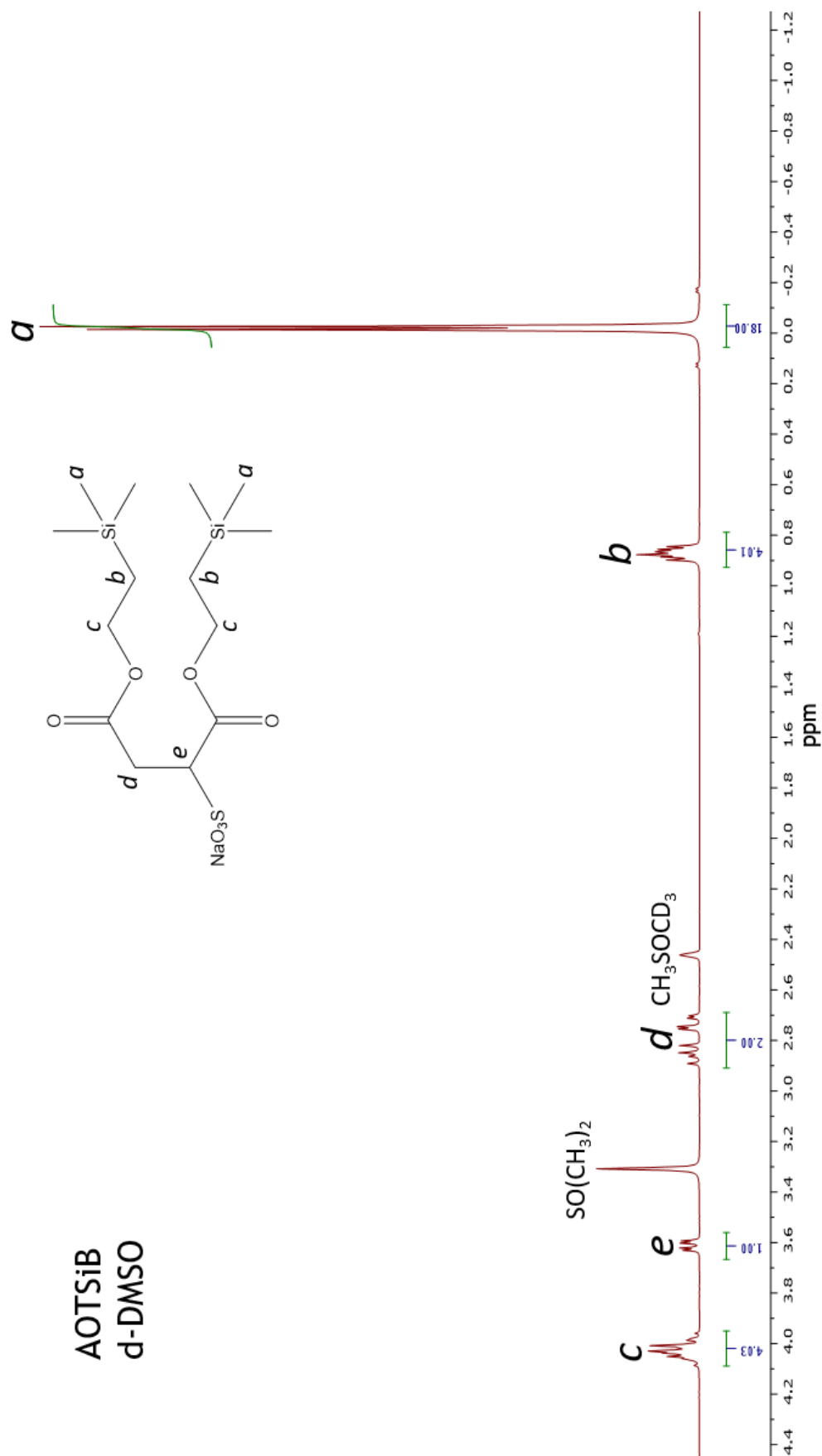


Figure 4.10: ^{13}C NMR of AOTSiC showing the difference in chemical environment of the two chains due to asymmetry in the head group

Figure 4.11: ¹H NMR of AOTB with peak integrations also shown.

Figure 4.12: ^1H NMR of AOTSiB with peak integrations also shown.

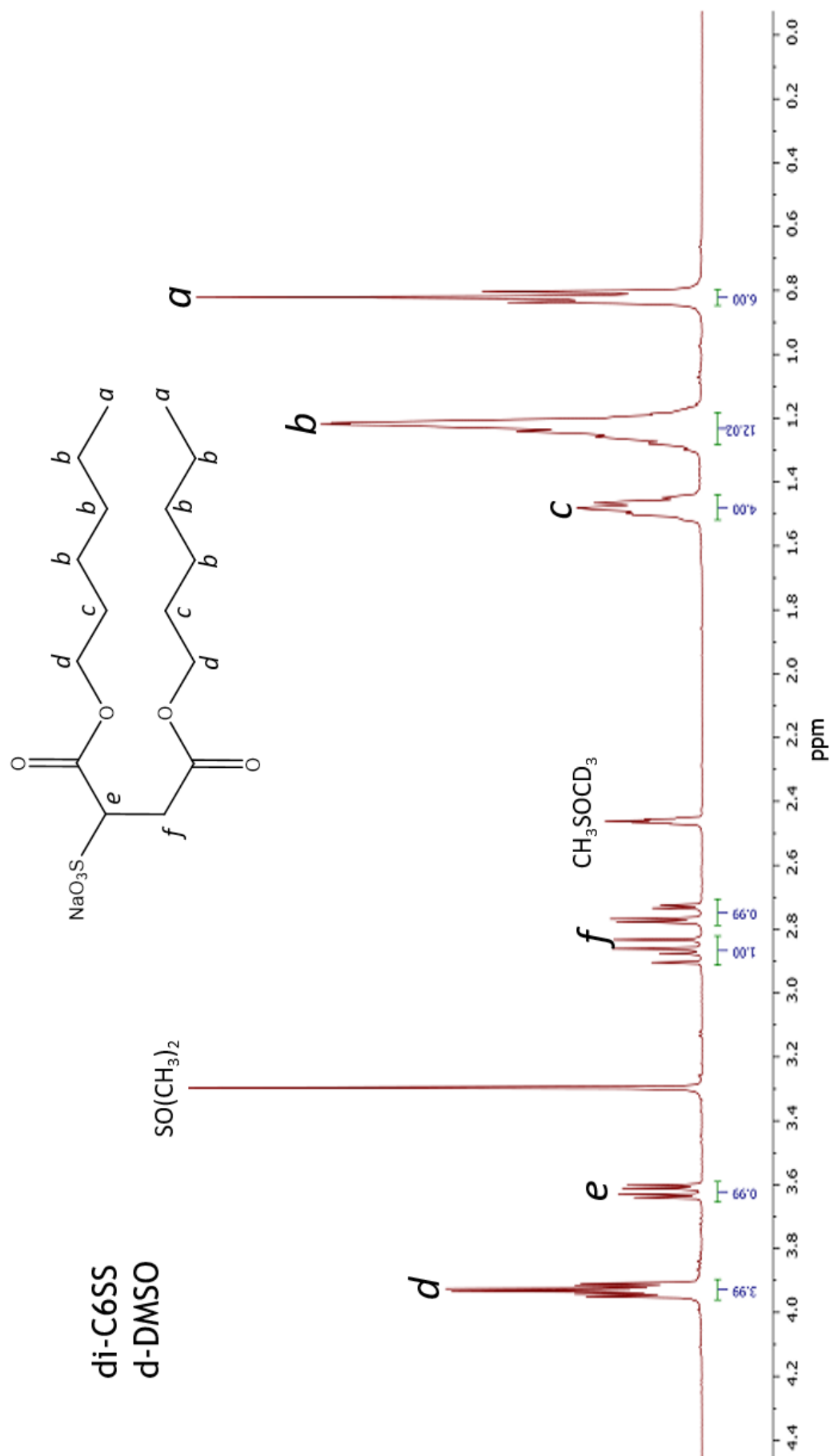


Figure 4.13: ^1H NMR of di-C6SS with peak integrations also shown.

Table 4.3: Data from selected ^1H NMR spectra of di-esters (Figures 4.8 and 4.9) and di-chain surfactants (Figures 4.11, 4.12 and 4.13).

Chemical Shift	Molecular fragment	Integration	Identified proton
AOTA - diester			
0.94 - 0.98	$-\text{CH}_2-\text{C}(\text{CH}_3)_3$	18.00	a
3.88 - 3.90	$-\text{O}-\text{CH}_2-$	4.00	b
6.84 - 6.92	$-\text{CO}-\text{CH}_2-\text{CO}-$	2.00	c
AOTSiB - diester			
0.061 - 0.094	$-\text{CH}_2-\text{Si}(\text{CH}_3)_3$	18.01	a
3.88 - 3.90	$-\text{O}-\text{C}_2\text{H}_4-$	4.01	b
6.80 - 6.85	$-\text{CO}-\text{CH}_2-\text{CO}-$	2.00	c
AOTB			
0.84 - 0.89	$-\text{CH}_2-\text{C}(\text{CH}_3)_3$	18.00	a
1.40 - 1.46	$-\text{CH}_2-\text{CH}_2-$	4.01	b
2.70 - 2.89	$-\text{CO}-\text{CH}_2-$	2.00	d
3.57 - 3.63	$\text{NaO}_3\text{S}-\text{CH}-$	1.00	e
3.95 - 4.03	$-\text{O}-\text{CH}_2-$	4.00	c
AOTSiB			
-0.11 - 0.057	$-\text{CH}_2-\text{Si}(\text{CH}_3)_3$	18.00	a
0.79 - 0.93	$-\text{CH}_2-\text{CH}_2-$	4.01	b
2.69 - 2.91	$-\text{CO}-\text{CH}_2-$	2.00	d
3.56 - 3.67	$\text{NaO}_3\text{S}-\text{CH}-$	1.00	e
3.95 - 4.09	$-\text{O}-\text{CH}_2-$	4.03	c
di-C6SS			
0.80 - 0.85	$-\text{CH}_2-\text{CH}_3$	6.00	a
1.18 - 1.28	$-\text{CH}_2-\text{C}_3\text{H}_6-$	4.01	b
1.44 - 1.52	$-\text{O}-\text{CH}_2-\text{CH}_2-$	4.00	c
2.71 - 2.79	$-\text{CO}-\text{CH}_2-$	1.99	f
2.82 - 2.91	$\text{NaO}_3\text{S}-\text{CH}-$	0.99	e
3.59 - 3.65	$-\text{O}-\text{CH}_2-$	3.99	d

Table 4.4: Elemental analysis results for single and di-chain surfactants.

Surfactant	Theoretical				Experimental			
	C	H	S	N	C	H	S	N
Single-chain surfactants								
Na-FO180	58.03	10.01	8.61	-	58.35	10.24	8.54	-
TMA-FO180	62.37	11.66	7.57	3.31	62.07	11.49	7.42	3.09
TEA-FO180	65.09	11.97	6.68	2.92	64.92	12.05	6.46	3.05
TPA-FO180	67.24	12.23	5.98	2.61	67.52	12.41	5.68	2.66
Na-FO180N	58.03	10.01	8.61	-	58.31	10.14	8.54	-
TMA-FO180N	62.37	11.66	7.57	3.31	62.31	11.89	7.21	3.08
TEA-FO180N	65.09	11.97	6.68	2.92	64.95	11.72	6.39	2.94
TPA-FO180N	67.24	12.23	5.98	2.61	67.22	12.36	6.69	2.36
Na-BC7	38.52	6.93	14.69	-	38.71	7.05	14.66	-
TMA-BC7	49.04	10.10	11.90	5.20	49.28	10.00	11.52	4.95
TEA-BC7	55.35	10.84	9.85	4.30	55.29	10.99	9.97	4.28
TPA-BC7	59.80	11.36	8.40	3.67	59.67	11.02	7.81	3.92
Na-BC9	43.89	7.78	13.02	-	43.74	7.82	12.75	-
TMA-BC9	52.49	10.51	10.78	4.71	52.36	10.66	10.24	4.98
TEA-BC9	57.75	11.12	9.07	3.96	57.69	11.26	9.33	4.24
TPA-BC9	61.57	11.56	7.83	3.42	61.41	11.62	8.09	3.15
SDS	54.31	9.50	12.08	-	52.28	9.69	11.56	-
Di-chain surfactants								
AOTA	46.66	6.99	8.90	-	46.76	7.19	8.78	-
AOTB	49.40	7.47	8.24	-	49.89	7.34	8.17	-
AOTSiA	36.72	6.42	8.17	-	36.98	6.48	8.01	-
AOTSiB	39.98	6.95	7.62	-	40.12	6.98	7.48	-
AOTSiC	42.83	7.41	7.15	-	42.88	7.48	7.07	-
HS1	46.66	6.99	8.90	-	46.74	7.00	8.47	-
HS2	49.47	7.53	8.25	-	49.24	7.59	8.17	-
HS3	51.91	7.99	7.70	-	51.41	7.81	7.55	-
di-C6SS	49.47	7.53	8.25	-	49.26	7.32	7.94	-
di-C7SS	51.91	7.99	7.70	-	51.72	7.82	7.68	-
di-C8SS	54.04	8.39	7.21	-	54.21	8.53	7.33	-

4.6 Techniques

4.6.1 Conductivity

To help guide surface tension experiments, novel surfactants would first have their cmc's determined by conductivity. Cmc's of mixed anionic surfactant systems were also determined using the same procedure. Measurements were made using a Jenway 4520 Conductivity Meter which was first calibrated with a 1 M KI solution following the supplier instructions. The probe was cleaned with ultra-pure water until a standing conductivity of $< 0.15 \mu\text{S cm}^{-1}$ was achieved. 20 mL of water was added to a sterile sample vial (or centrifuge tube) with a Gilson pipette. The probe was continuously submerged in the stirred sample throughout the experiment. Once a sufficient concentration range had been measured, and there was a noticeable drop in conductivity between concentrations, cmc's were determined using the procedure outlined in Section 5.2.2.

4.6.2 Surface tension

Surface measurements were made using a K100 tensiometer at the Krüss Surface Science centre at the University of Bristol, using the Wilhelmy plate method. Glassware used must be thoroughly cleaned to ensure no surface-active contaminants are introduced into an otherwise clean sample. This was achieved using a simple, but effective three stage washing process. A trough was cleaned with a dilute decon solution and then thoroughly rinsed with water. This process was repeated with methanol, and then finally ultra pure water (Millipore, $18.2 \text{ M}\Omega\text{cm}$) to remove any residual tap water. The cleanliness of the glassware can then be checked by conducting a surface tension measurement of ultra pure water, where a surface tension of $72.0 \text{ mN m}^{-1} \pm 0.2 \text{ mN m}^{-1}$ at $25 \text{ }^\circ\text{C}$ was considered satisfactory.

Equilibrium surface tension curves were obtained by preparing a 20 mL sample of surfactant at $4 \times \text{cmc}$. The solution was then diluted from here by replacing removed surfactant solution with pure water, which would allow greater control over the entire concentration regime. The Wilhelmy plate was cleaned between each repeat measurement. It is important to clean the probe between each repeat measurement and not just between different concentrations, because when working

with anionic surfactants, molecules remain on the plate. If not cleaned, a layer is formed on the plate which reduces the surface tension below the accurate value. This is also why the automatic dosing system is unsuitable for anionic surfactants. The Wilhelmy plate was cleaned by being rinsed with methanol, and then being placed under the blue flame of a bunsen burner. Initially it may seem appropriate to keep the plate under the blue flame for an extensive amount of time to ensure a clean surface. However, this can warp the plate which has a consequential effect on the surface tension values calculated. Therefore, the plate was removed from the blue flame as soon as the characteristic orange glow began to appear. Repeat measurements would be made at each concentration until the surface tension was constant within a range of $\pm 0.1 \text{ mN m}^{-1}$. Once the surface tension was constant, a final repeat measurement would be made with a longer time interval to ensure equilibrium surface tension had been achieved. All measurements were made at 25 °C using a Grant LTD6G circulating water bath.

4.6.3 Small-angle neutron scattering (SANS)

SANS measurements were performed on D33 at the Institute Laue-Langevin (ILL, Grenoble, France) and SANS 2D or LOQ at the ISIS facility (Rutherford Appleton Laboratory, Didcot, UK). The D33 instrument used neutrons with a wavelength of $\lambda = 6 \text{ \AA}$ and two sample-detector positions (2 and 7.5 m) providing an accessible Q range of 0.005-0.2 \AA^{-1} . On SANS 2D, a simultaneous Q range of 0.004-0.6 \AA^{-1} was achieved with a neutron wavelength range of $1.75 < \lambda < 15.5 \text{ \AA}$ and a source-sample-detector distance $L1=L2=4\text{m}$. On LOQ, a simultaneous Q range of 0.008-0.254 \AA^{-1} was achieved with a neutron wavelength range of $1.75 < \lambda < 15.5 \text{ \AA}$ and a source-sample-detector distance $L1=L2=8\text{m}$. Samples were made in D_2O , using 2 mm path length rectangular quartz cells at a temperature of either 25 °C or 60 °C as stated. Raw SANS data were reduced by subtracting the scattering of the empty cell and D_2O background and normalised to an appropriate standard using the instrument-specific software. SANS data were fit using SasView. Details of the models used can be found accompanying discussion of the data in the relevant results chapters.

4.7 Conclusions

Sixteen single-chain sulfonates and eleven sulfosuccinates have been successfully synthesised. NMR and elemental analyses show that all surfactants are of high chemical purity, and there is no significant residual inorganic material present. All surfactants are thus amenable to characterisation in aqueous systems.

References

- [1] Gilbert, E. E. *Sulfonation and related reactions*; Interscience Publishers, 1965.
- [2] Gilbert, E. E. *Chem. Rev.* **1962**, *62*, 549–589.
- [3] Eastoe, J.; Nave, S.; Downer, A.; Paul, A.; Rankin, A.; Tribe, K.; Penfold, J. *Langmuir* **2000**, *16*, 4511–4518.
- [4] Abramovitch, B.; Shivers, J.; Hudson, B.; Hauser, C. *J. Am. Chem. Soc.* **1943**, *65*, 986–986.
- [5] Puterbaugh, W. *J. Org. Chem* **1962**, *27*, 4010–4015.
- [6] Hassner, A.; Alexanian, V. *Tetrahedron Lett.* **1978**, *19*, 4475–4478.
- [7] Bagutski, V.; French, R. M.; Aggarwal, V. K. *Angew. Chem. Int. Ed* **2010**, *49*, 5142–5145.
- [8] Arora, P. S.; Van, Q. N.; Famulok, M.; Shaka, A.; Nowick, J. S. *Bioorganic Med. Chem* **1998**, *6*, 1421–1428.
- [9] Ritson, D. J.; Cox, R. J.; Berge, J. *Org. Biomol. Chem* **2004**, *2*, 1921–1933.

Chapter 5

Designing Optimised Surfactant Tails

The aim of this chapter is to provide a simple method for designing effective, highly branched anionic hydrocarbon surfactants. This has been achieved by comparing surface properties for a wide variety of hydrocarbon surfactants, allowing structure-property relationships of effective surfactants to be identified. First, the limit of achievable performance is outlined. This is followed by a detailed account of various considerations and procedures which are required to determine accurate surface properties. Two series of branched hydrocarbon surfactants are introduced, and their aggregation and adsorption behaviour in aqueous solutions discussed. By making small, systematic variations in the molecular structure of the surfactant tail, tensiometry and small-angle neutron scattering (SANS) are used to provide an insight into the relationship between structure and performance. Principal considerations for designing highly effective hydrocarbon surfactants are outlined, which are shown to be dependent on the alkyl chain length of the tail. By comparing surface properties for the most effective hydrocarbon surfactants a new index, H_γ , is introduced which can predict potential super-effective surfactants based on the molecular structure of the tail. By careful design of the surfactant tail, novel hydrocarbon surfactants are introduced which generate the lowest surface energies currently reported for hydrocarbon surfactants.

5.1 The limit of γ for hydrocarbon surfactants

When designing super-effective hydrocarbon surfactants, a fundamental question to ask is what is the lowest surface tension theoretically possible for a hydrocarbon (HC) surfactant? This can be identified by evaluating the surface tension of pure alkanes and alcohols. At room temperature, hydrocarbons only begin to exist as a liquid state above a chain length of 4 i.e. pentane onwards, as below this van der Waals interactions are insufficiently strong enough (butane boiling point = -1°C , 1 atm). As the chain length is increased, the total van der Waals interactions increase and hence so does the surface tension, see Table 5.1. Therefore for all hydrocarbons, pentane generates the lowest surface tension. Because alkanes are non-polar molecules, the only intermolecular interactions present between molecules at the surface and in the bulk are weak van der Waals interactions, hence why they generate such low surface energies. When comparing an alkane to the corresponding alcohol (i.e. heptane to heptanol), the inclusion of a $-\text{OH}$ group on the alcohol introduces polar interactions between molecules which are stronger than van der Waals interactions ($\rho_{\text{heptane}} = 0.684 \text{ g cm}^{-3}$ / $\rho_{\text{heptanol}} = 0.819 \text{ g cm}^{-3}$) and therefore raise the surface free energy, see Table 5.1.

Surfactant molecules possess a polar head group attached to a non-polar tail. Although there are only weak van der Waals interactions between tails, the polar head groups (which are necessary to ensure solubility) introduce strong polar interactions and sterically hinder efficient packing between tails, increasing the overall surface free energy. For example hexane, hexanol and di-C6SS all possess a six carbon linear alkyl chain and generate $\gamma = 18.4, 26.4$ and 29.1 mN m^{-1} respectively, see

Alkane	$\gamma \text{ (mN m}^{-1}\text{)}$ ± 0.1	Alcohol	$\gamma \text{ (mN m}^{-1}\text{)}$ ± 0.1
Pentane	16.1	Pentanol	25.8
Hexane	18.4	Hexanol	26.4
Heptane	20.1	Heptanol	26.9
Octane	21.6	Octanol	27.5
Nonane	22.9	Nonanol	28.3

Table 5.1: Surface tension for selected pure liquid alkanes and alcohols at 20°C .¹

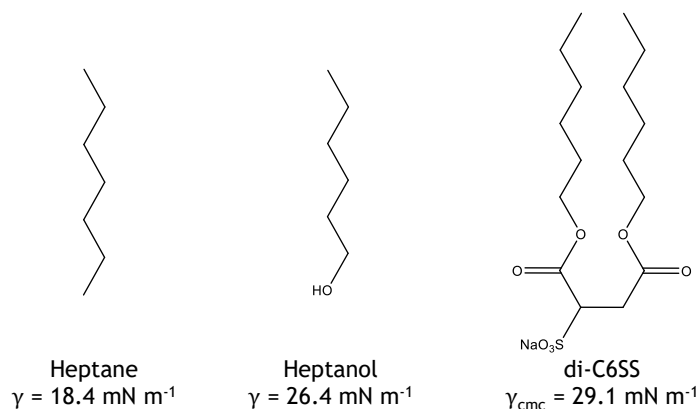


Figure 5.1: Molecular structures and surface tensions generated for the linear di-chain surfactant di-C6SS and corresponding alkane / alcohol.

Figure 5.1. The linear surfactant di-C6SS could never generate γ_{cmc} below that of hexane as polar interactions are now introduced into the surface monolayer. However, compared to hexanol where both molecules possess polar interactions, di-C6SS generates $\gamma_{\text{cmc}} \sim 3 \text{ mN m}^{-1}$ higher which highlights:

1. The adverse effect of the head group on generating low γ_{cmc} by sterically hindering efficient packing between surfactant tails.
2. Linear alkyl chains make inefficient HC surfactants.

Therefore to generate low surface energies with HC surfactants, the surfactant design must be developed to enhance packing at the interface. The first general structure-property relationship of surface tension highlighted that low γ_{cmc} can be achieved by an efficiently packed and hence, dense surface monolayer.² Branching the tail has lead to the lowest surface energies generated for HC surfactants.³⁻⁵ This is because surface densities are generated which have been shown to effectively mimic a pure alkane. So what is the lowest surface tension possible for a branched HC surfactant? For liquid hydrocarbons, when only van der Waals interactions are present, γ in the range of 16-20 mN m^{-1} can be achieved. Therefore, to generate a surface tension $< 20 \text{ mN m}^{-1}$ when polar interactions are also present is likely unachievable for hydrocarbon surfactants. By careful design of the surfactant tail structure, results are presented here for novel series of hedgehog surfactants which generate the lowest surface energies currently achieved by HC surfactants; close to the limit of achievable performance.

5.2 Determining accurate surface properties

To identify structure-property relationships of low surface energy hydrocarbon surfactants, the most effective approach is to compare surface properties for a variety of different molecular structures. However, it is imperative that the surface properties of the individual surfactants are determined accurately from a standard procedure that allows an impartial comparison to other literature. This section aims to outline important considerations when determining accurate surface properties for novel ionic surfactants.

5.2.1 Calculating activity coefficients

In nonelectrolyte solutions, intermolecular forces are dominated by weak van der Waals interactions and the solution can be considered to behave ideally. When studying the surface tension-concentration behaviour of ionic surfactants, activity should be used instead of concentration. This is because at higher concentrations (above 1 mM) Coulombic interactions increase, which causes departure from ideal behaviour. In a dilute solution below a concentration of 1 mM, activity coefficients can be regarded as unity and hence, unmodified concentration can be used. The deviation from ideal behaviour is described by the mean ionic activity coefficient of an electrolyte solution, α_{\pm} , which is calculated from Debye-Hückel theory. Only the relevant equations are provided here and detailed explanations of the theory can be found in the following texts.^{6,7}

At very low concentrations the activity coefficient can be calculated from the Debye-Hückel limiting law:

$$\log\alpha_{\pm} = -A|z_+z_-|I^{\frac{1}{2}} \quad (5.1)$$

where A is a constant which = 0.509 for ionic surfactants with a sodium counterion, z is the charge on the ion, and I is the dimensionless ionic strength of the solution:

$$I = \frac{1}{2} \sum_i z_i^2 (b_i/b^{\ominus}) \quad (5.2)$$

where z is the charge valency and b_i is the molality.

The Debye-Hückel limiting law (equation 5.1) is suitable for 1:1 electrolytes with concentrations below approximately 0.01 mol dm^{-3} . When the ionic strength of the solution is too high for the limiting law to be valid, the activity coefficient may be estimated from the extended Debye-Hückel law:

$$\log \alpha_{\pm} = \frac{A|z_+z_-|I^{\frac{1}{2}}}{1 + BaI^{\frac{1}{2}}} \quad (5.3)$$

where a is the mean effective ionic diameter which typically ranges from 3-9 Å, and B is a constant which can be interpreted as a measure of the closest approach of the ions. A value of $a = 6 \text{ Å}$ was assumed, which is approximately the diameter of a hydrated sodium ion.⁸ For aqueous solutions at 298 K, $B = 3.282 \times 10^9 \text{ m}^{-1} \text{ mol}^{-1/2} \text{ kg}^{1/2}$. Equation 6.1 is valid for concentrations of up to 0.1 mol dm^{-3} , at concentrations above 0.1 mol dm^{-3} the Gibbs-Duhem equation is used.

5.2.2 Determining the cmc by electrical conductivity

To accurately determine various surface properties including γ_{cmc} , A_{cmc} and Φ_{cmc} , the critical micelle concentration itself must be accurately known. There are various methods for determining the cmc of ionic surfactants, with two of the most common being electrical conductivity and fluorescence spectroscopy. All techniques exploit a noticeable change in the chosen measured property, which is observed when surfactant molecules begin to micellise and the system is no longer composed of only free surfactant molecules. Because the surfactants discussed in this thesis are all ionic, electrical conductivity is an appropriate technique to determine the critical micelle concentration. As the concentration of surfactant in solution is increased, the conductivity of the solution increases regularly because the number of charge carrying ions increases. The conductivity of the solution will continue to increase until the cmc is reached. At this point, further surfactant molecules aggregate into micelles and consequently the ability to carry charge through solution decreases. Hence, as the concentration is increased past the cmc the increase in conductivity becomes smaller. A plot of conductivity vs concentration, therefore ideally yields two straight lines where the inflexion point denotes the onset of micelle formation, i.e. the cmc.

When designing straight chain surfactants, the cmc can be estimated using relationships such as the Klevens equation.⁹

$$\log(\text{cmc}) = A - Bn_c \quad (5.4)$$

where A and B are constants which vary according to the charge, type of head group etc. However, the Klevens equation is only valid for linear alkyl chain surfactants. To predict the cmc of branched surfactants no simple equation currently exists as relationships between the molecular structure and cmc are not so straightforward. However, having prior knowledge of the cmc for a novel surfactant can allow one to plan surface tension profiles (γ vs $\log[\text{activity}]$ experiments) more effectively. For a novel ionic surfactant, once a suitable purity has been attained, determining the cmc by conductivity is an appropriate first experiment.

The linear di-chain surfactants di-C6SS, di-C7SS and di-C8SS have already been reported before.¹⁰ However, they feature in mixed surfactant systems that are discussed in Chapter 7 and were synthesised following the procedure outlined in Section 4.4. It is important to therefore check the purity of these linear surfactants by comparing experimentally determined surface properties, with those previously identified in the literature (ref. [10]). The conductivities of di-C6SS, di-C7SS and di-C8SS were individually measured in deionised water (18.2 M Ω cm) whilst the concentration of surfactant in solution was increased. The fitting procedure for di-C7SS is outlined here. The conductivity plots and data analysis for di-C6SS and di-C8SS are included in the Supporting Information.

Figure 5.2 shows the raw conductivity data which were collected for di-C7SS. From visually analysing the data at the high and low concentration domains, it is clear to see that the cmc has been reached across this concentration scale. The most common method of analysis to determine the break point is to apply two linear fits across the data and solve the simultaneous equation. Figure 5.3 shows the linear fits that were used. Following this method, the cmc of di-C7SS was determined to be 3.50 mM. This agrees well with previous literature, where a cmc = 3.55 mM was determined (ref. [10]). However, this method often leads to discrepancies as it is largely based on visually choosing the most appropriate linear fits. Therefore, accurate determination of the inflexion point was done using the following procedure.

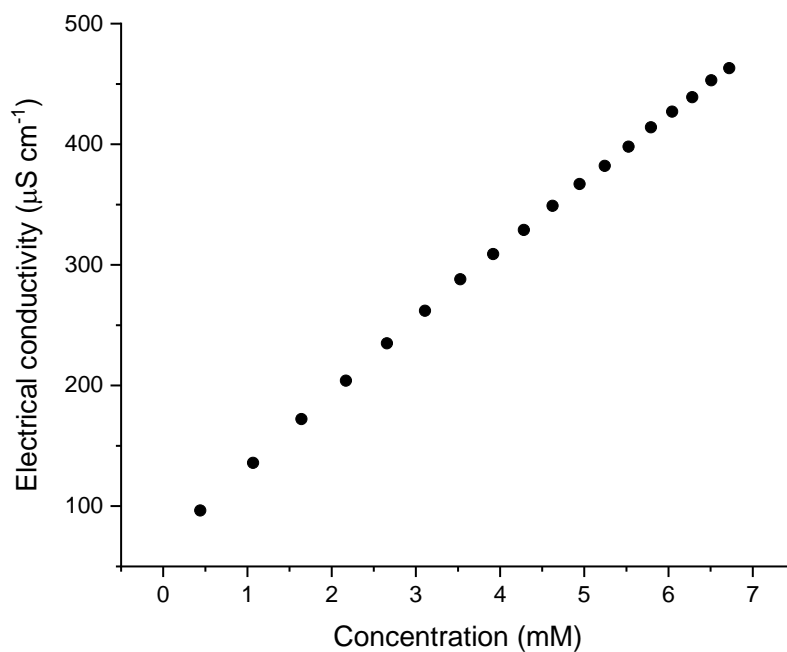


Figure 5.2: Conductivity data for the di-chain linear surfactant di-C7SS which was measured as a function of concentration.

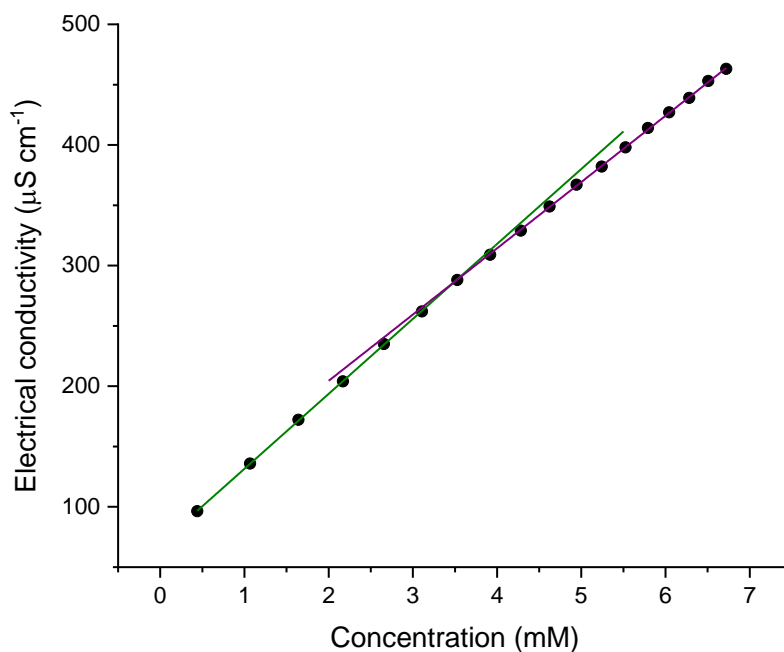


Figure 5.3: Linear fits applied to conductivity data where the simultaneous equation generated can be solved to estimate the inflexion point and hence, the cmc.

By taking the double derivative of conductivity with respect to concentration, points of inflexion are highlighted as peaks or troughs, see Figure 5.4. Because the gradient of the linear fit decreases past the cmc (i.e. the purple line on Figure 5.3), the point of inflexion must be identified as trough not a peak (which would signify an increase in gradient). From the analysis shown in Figure 5.3 the local minima, i.e. the cmc, is identified as 2.99 mM. This does not agree as well with the literature, however, as shown in the following section, when comparing cmc's determined by tensiometry and conductivity, the double derivative method provides far more robust values. For all cmc's which have been identified by conductivity throughout this thesis, the double derivative method was used because it provides a simple, reliable and accurate approach.

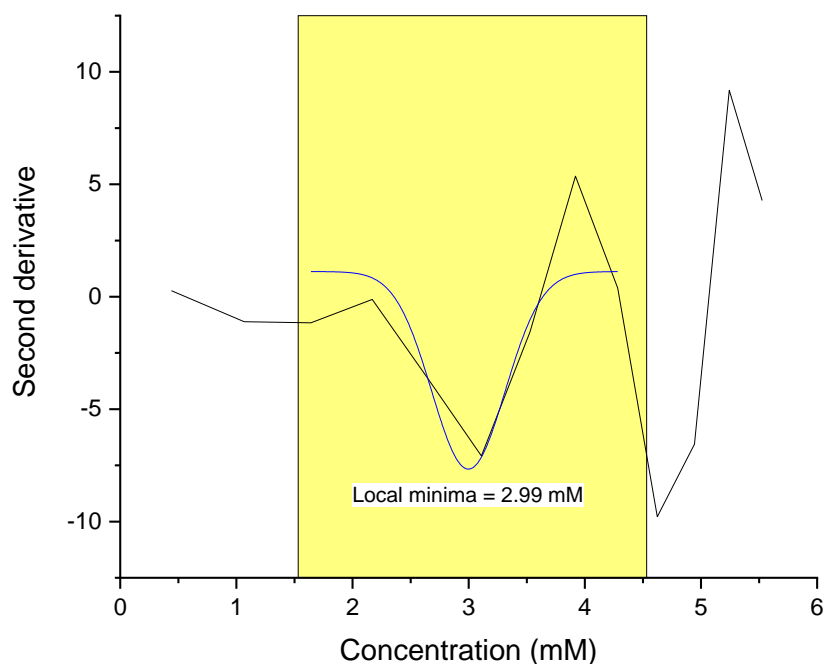


Figure 5.4: Double derivative of conductivity data with respect to concentration for di-C7SS where the point of inflexion is identified by applying a Gaussian distribution.

5.2.3 Determining the cmc by surface tension

Determining the cmc by electrical conductivity is a very effective method for ionic surfactants. However, if the increase in conductivity with increasing concentration is similar pre- and post-cmc, then identifying the inflexion point accurately can prove to be difficult. The most common method for determining the cmc of a surfactant, irregardless of surfactant class, is by tensiometry. The background theory of tensiometry is included in the Supporting Information and so this section will just discuss a suitable procedure for determining the cmc.

Figure 5.5 shows the variation in surface tension as a function of activity for the linear surfactant di-C7SS. The surface tension profile shows a nice clean break at the cmc, which shows the sign of no surface active impurities. A common method to determine the cmc from surface tension data is to apply linear fits to the pre- and post-cmc regions, and to then solve where the two lines meet. This method is suitable provided the surface tension profile behaves in an expected way (i.e. without any impurities) and that the most appropriate linear fits are selected. To provide a more robust and simple method for determining cmc's from surface tension data, a similar approach to determining cmc's from conductivity data was used.

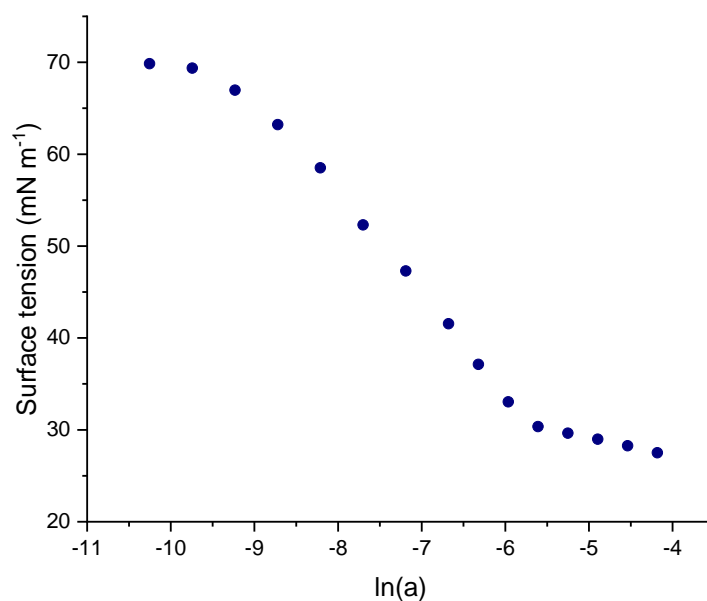


Figure 5.5: Variation in surface tension as a function of activity for the di-chain linear surfactant di-C7SS.

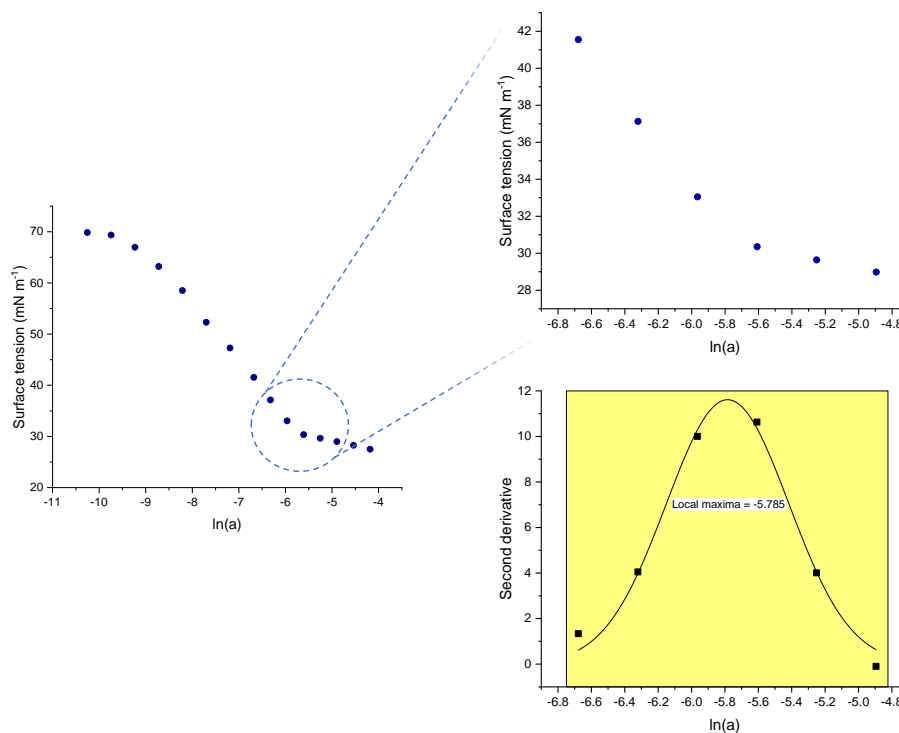


Figure 5.6: Procedure used to highlight the cmc from surface tension data. The double derivative of γ with respect to activity is taken around the cmc. A Gaussian distribution is then applied to accurately highlight the inflexion point, i.e. the cmc.

By taking the surface tension data around the cmc, and determining the double derivative with respect to activity, an accurate point of inflexion can be highlighted. Figure 5.6 shows an expansion of the surface tension data around the cmc for di-C7SS. The double derivative of these data was determined, plotted, and then a Gaussian distribution applied to highlight the maxima. The cmc can then be determined by taking the exponential of this number. From Figure 5.6 the cmc of di-C7SS was determined to be 3.07 mM. This agrees well with the value determined by conductivity when using the double derivative method (2.99 mM). The literature cmc value of di-C7SS (3.55 mM) is slightly higher however, given the variability in surfactant purity on a batch-by-batch basis coupled with variability in procedure used to determine the cmc, the disagreement in value is not beyond the order of unexpected. The procedure outlined in this section was used to determine the cmc's of all novel surfactants discussed in this thesis.

5.2.4 The pre-factor m in the Gibbs equation

The concentration of surfactant molecules in the surface monolayer can be described by analysing tensiometric data with the Gibbs equation, which has the general form:

$$\Gamma = \frac{-1}{mRT} \left(\frac{d\gamma}{d \ln a} \right) \quad (5.5)$$

where the terms have their usual meanings. For ionic surfactants, the pre-factor m is taken to be 2, meaning there is a 1:1 ratio of surfactant anion and counter cation present in the monolayer. However, there has been much debate over the value of 2 for ionic surfactants which is a fundamental issue in surfactant science.^{11,12}

By analysing the effect of electrolytes on surfactant adsorption, the pre-factor m is known to be theoretically dependent on surfactant type and structure, as well as the presence of any extra electrolyte in the aqueous phase.^{13,14} For non-ionic and zwitterionic surfactants, various experiments have confirmed the expected value of 1 for m .¹⁵⁻¹⁷ To verify the value of m in the Gibbs equation, a variety of complementary techniques for measuring Γ have been employed including radiotracer measurements using tritiated surfactants (replacing hydrogen with tritium),¹⁸ surface second-harmonic generation (SHG) spectroscopy (ref. [12]), and neutron reflection (NR).^{19,20} Because neutron reflectivity measures the surface excess, it is an ideal technique to complement tensiometry, which indirectly measures Γ through γ vs $\ln(a)$ plots.

By interpreting surface tension and neutron reflectivity data for several surfactants, some groups had previously identified a pre-factor less than 2 for the surfactant in the absence of electrolyte.²¹ By measuring the surface tension and neutron reflectivity of several perfluorooctanoic acid salts with monovalent metal cations, Penfold *et al* highlighted that this result was an artifact resulting from the presence of small amounts of divalent cation impurity (ref. [11]). Once the divalent ions were removed, complete consistency was found between neutron and surface tension results using a Gibbs pre-factor of 2 for ionic surfactants. Hence, it was concluded that anionic surfactants contaminated by divalent ions was the cause for discrepancy in determining m . Other groups have confirmed a pre-factor of 2 once the surface monolayer is free from polyvalent ion contaminants.²²

When synthesising anionic surfactants, polyvalent metal ions M^{n+} are generally the most prevalent surface impurity. For example, studies of AOT showed that even at ppm levels of M^{n+} , there can be a significant lowering of the surface tension in the pre-cmc region.²³ An effective way to remove trace levels of M^{n+} ions is to use the chelating agent ethylenediaminetetraacetic acid (EDTA), see Figure 5.7. In neutron reflection studies of Cs^+ , Na^+ and H^+ perfluorooctanoate (ref. [11]), as well as Na^+ AOT,²³ it was found that the pre-factor 2 agreed with NR data only in the presence of EDTA. Downer *et al.* performed detailed experiments on various perfluorononanoates to determine the optimum amount of EDTA (ref. [20]). The experiments highlighted that the level of EDTA must be determined for each surfactant separately, on a batch-by-batch basis. The following section provides the procedure used for determining the correct level of EDTA.

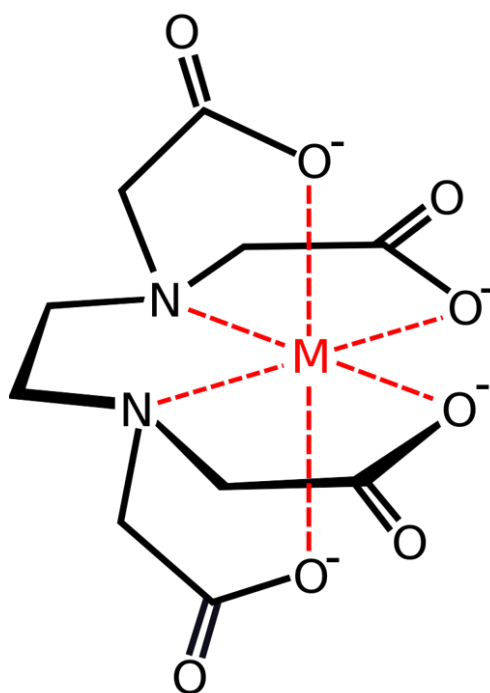


Figure 5.7: Example of a metal-EDTA chelate.

5.2.5 The optimum level of EDTA

As highlighted in the previous section, when studying the surface monolayer formed by ionic surfactants, the chelating agent EDTA must be used to ensure a clean surface free from inorganic impurities. Only when this criteria is met does the pre-factor $m = 2$ apply allowing the surface excess to be accurately determined. That is because polyvalent M^{n+} ions preferentially adsorb over the sodium ions, which can significantly lower the surface tension in the pre-cmc region. To determine the optimum level of EDTA (which must be determined for each surfactant on a batch-by-batch basis), the surface tension of di-C7SS was measured using the Wilhelmy plate method on a K100 tensiometer at a fixed concentration whilst varying the amount of EDTA. The amount of EDTA was varied in the range 10^{-9} to 10^{-1} mol dm^{-3} at surfactant concentrations of $1/20^{\text{th}}$ and $1/10^{\text{th}}$ the cmc, see Figure 5.8. For both concentrations, a plateau of constant γ is reached at an EDTA concentration of approximately 1×10^{-4} mol dm^{-3} . Hence it is at this concentration that presumably all polyvalent ion contaminants are complexed by EDTA. From the concentration of EDTA required at the concentrations studied, a surfactant:EDTA ratio of 200:1 was chosen. The same procedure was applied to all di-chain surfactants studied.

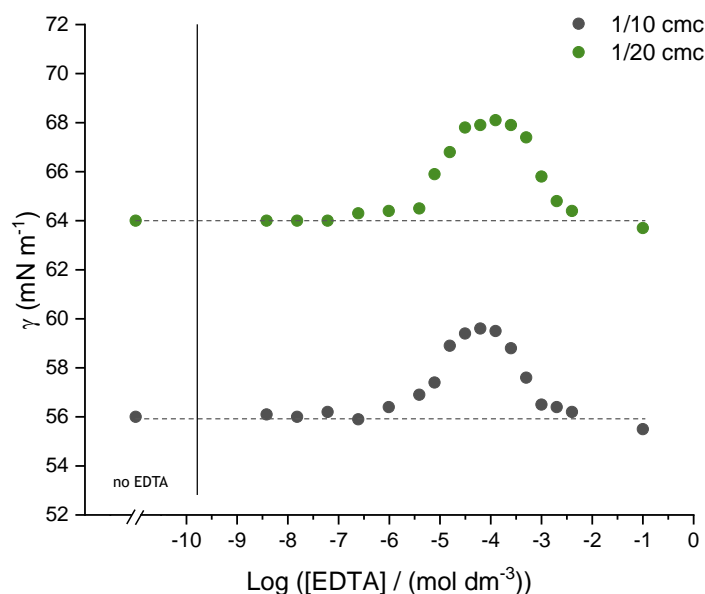


Figure 5.8: Effect of EDTA on surface tensions of di-C7SS solutions at various concentrations below the cmc.

5.2.6 Calculating A_{cmc} from γ - $\ln(a)$ plots

With the correct level of EDTA determined, γ - $\ln(a)$ plots were measured for di-C7SS both with and without EDTA at 25 °C, see Figure 5.9. The cmc was found to be the same within experimental error for both plots. However, the surface tension was lower without EDTA present which shows the presence of inorganic contaminants. With the cmc determined, a 4th order polynomial fit was applied to the pre-cmc data (lines on figure). The first derivative of the quartic function was calculated where $x =$ the cmc. This value of $\frac{dy}{dx}$ was then used in the Gibbs equation to calculate the surface excess, Γ , from which A_{cmc} can be determined. From analysing the data in Table 5.2, the presence of EDTA significantly alters the area per molecule. The values of A_{cmc} for di-C7SS with EDTA shown in Table 5.2 agree well with literature data (ref. [10]). The following methods outlined throughout these sections were used as the standard procedures, where appropriate, for all surfactants studied in this thesis.

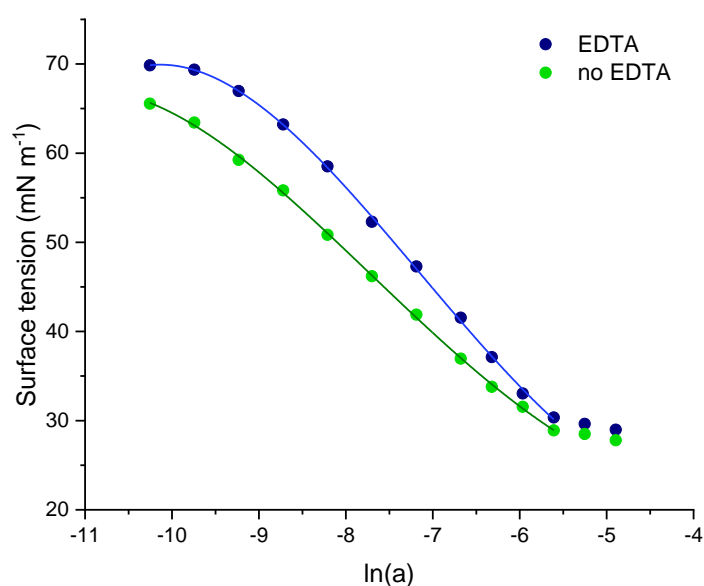


Figure 5.9: Surface tension behaviour of di-C7SS with and without EDTA at 25 °C. Lines represent polynomial fits used to calculate the surface excess and hence, A_{cmc} .

di-C7SS	cmc (mM) ± 0.1	γ_{cmc} (mN m ⁻¹) ± 0.1	A_{cmc} (Å ²) ± 2
no EDTA	3.09	28.9	72
EDTA	3.07	30.2	59

Table 5.2: Parameters derived from surface tension measurements of di-C7SS.

5.2.7 Considerations when determining the packing efficiency,

$$\Phi_{\text{cmc}}$$

Previously in Section 2.7 the packing efficiency of surfactant molecules at the air-water interface, Φ_{cmc} , was introduced:

$$\Phi_{\text{cmc}} = \frac{V_{\text{cal}}}{V_{\text{meas}}} \quad (5.6)$$

where V_{cal} is the total physical volume of surfactant molecular fragments and V_{meas} is the total volume occupied by a molecule at the reference air-water interface, see Figure 5.10. Determining V_{meas} requires knowledge of the head group area (A_{cmc}) and is thus determined experimentally either through tensiometry or neutron reflectivity. Calculating V_{cal} simply requires an estimate of the molecular volume of the surfactant tail which can be determined by summing individual fragments (i.e. $-\text{CH}_2- = 27 \text{ \AA}^3$). An alternative method which should also be used is to estimate the volume of the tail from the density of surfactant. If the density of the surfactant is unknown, the density of the alcohol precursor can be used to give an initial estimate.

To simplify matters, the packing efficiency, Φ_{cmc} , assumes that surfactant molecules occupy equal areas in a grid, i.e. A_{cmc} . Furthermore, the parameters involved (i.e. V_{cal}) are often inferred not directly measured, and overall this may not be representative of an efficiently packed monolayer. Therefore where possible, the area-per-molecule and tail volume should be determined experimentally by neutron reflectivity. Variations in calculated and experimentally measured scattering length densities of the surfactant monolayer will provide information on the relative tail densities, and hence volumes.

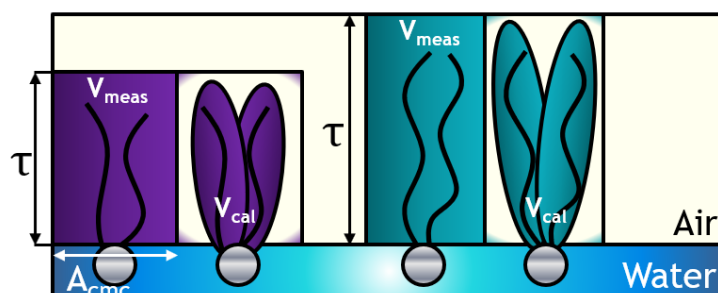


Figure 5.10: Visual representation of surfactants at the air-water interface, showing the different fragments and interfacial volumes used in the calculation of Φ_{cmc} .

5.3 Importance of the CH₃ to CH₂ ratio

In this section adsorption properties for a series of novel hydrocarbon (HC) surfactants are discussed, where the degree of branching is systematically increased. With a pre-factor of 2 for ionic surfactants validated in the previous section, tensiometry could be used with confidence to assess surface coverages and head group areas at the cmc. The purpose of this study is to identify principal considerations when designing hydrocarbon surfactants to achieve low surface energies.

Previous studies of effective HC surfactants have identified the relationship that increasing the degree of chain branching helps to generate low surface tensions (refs. [4, 5, 10]). This is because the surface becomes more populated by low surface energy methyl groups based on the following order of increasing surface energy:

$$\text{CF}_3 < \text{CF}_2 < \text{CH}_3 < \text{CH}_2.^{24}$$

However, this relationship does not always hold true. For example, AOT and di-C8SS both possess eight carbons in their respective tails, see Figure 5.11. AOT possesses more low surface energy CH₃ groups yet generates a higher surface tension. Although the difference is on the order of experimental uncertainty, it would be expected that AOT would generate the lower surface energy. This highlights that low surface energies are not generated by simply loading the surfactant tail with CH₃ groups, and that γ_{cmc} is both sensitively and intimately related to packing at the interface.

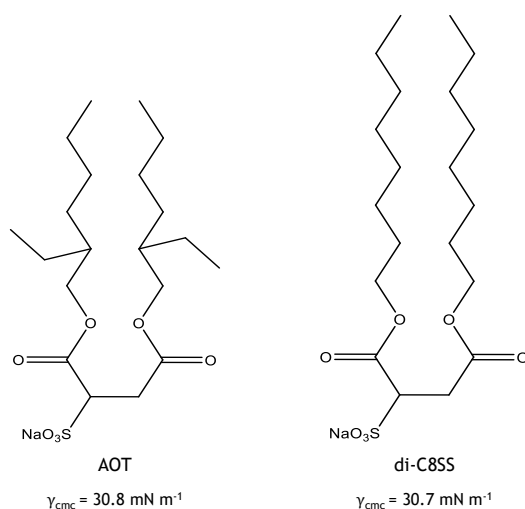


Figure 5.11: Molecular structures and γ_{cmc} values for AOT and di-C8SS (ref. [10]).

Although it is a long standing idea that increasing the CH₃:CH₂ ratio causes a decrease in surface tension, this idea has never been formally demonstrated. Therefore to consolidate this idea, a series of three hydrocarbon surfactants termed ‘HS1-3’ were synthesised following the procedure outlined in Section 4.4. Figure 5.12 shows the molecular structures, where the blue bond highlights the additional CH₃ group that is present on the tail. Hence, as we go across the series the CH₃:CH₂ ratio increases.

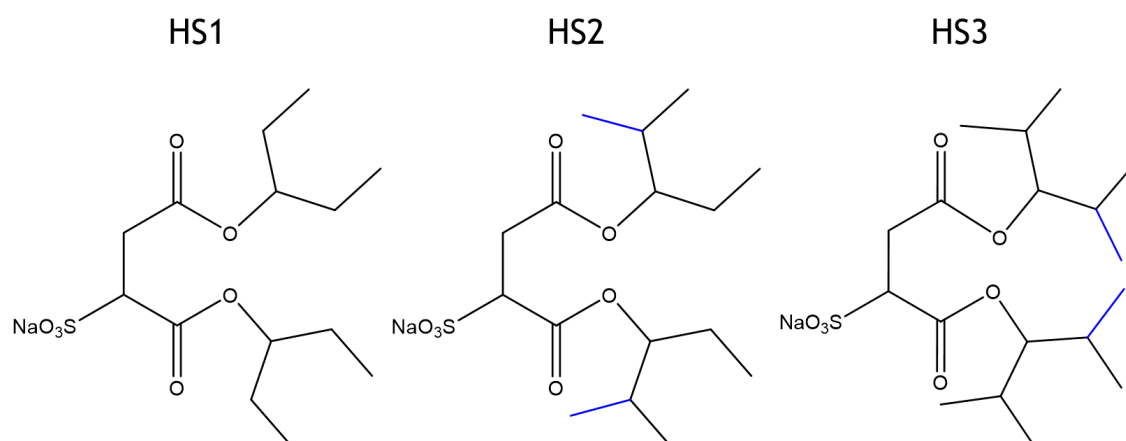


Figure 5.12: Molecular structures for the HC surfactants HS1, HS2 & HS3.

The critical micelle concentration, surface excess Γ , and equilibrium surface tension γ_{cmc} are characteristic of any given surfactant. Comparing these properties provides an insight into the adsorption behaviour of different surfactants, thus allowing structure-property relationships to be identified. Once a suitable purity was established, and EDTA:surfactant ratios determined, γ -ln(a) plots were obtained for HS1-3 at EDTA:surfactant ratios of 150:1, 200:1 and 150:1 respectively. Surface tension measurements were conducted on a K100 tensiometer following the experimental procedure outlined in Section 4.6.2. Figure 5.13 shows the change in surface tension as a function of activity for the three surfactants, where the lines represent the polynomial fits that were used to determine the area-per-molecule (A_{cmc}) at the cmc. All surface tension profiles produce nice clean breaks at the cmc which is consistent with an absence of surface-active impurities. Following the procedures outlined in Section 5.2 values for the cmc, γ_{cmc} , and A_{cmc} were determined for each surfactant and these data are shown in Table 5.3.

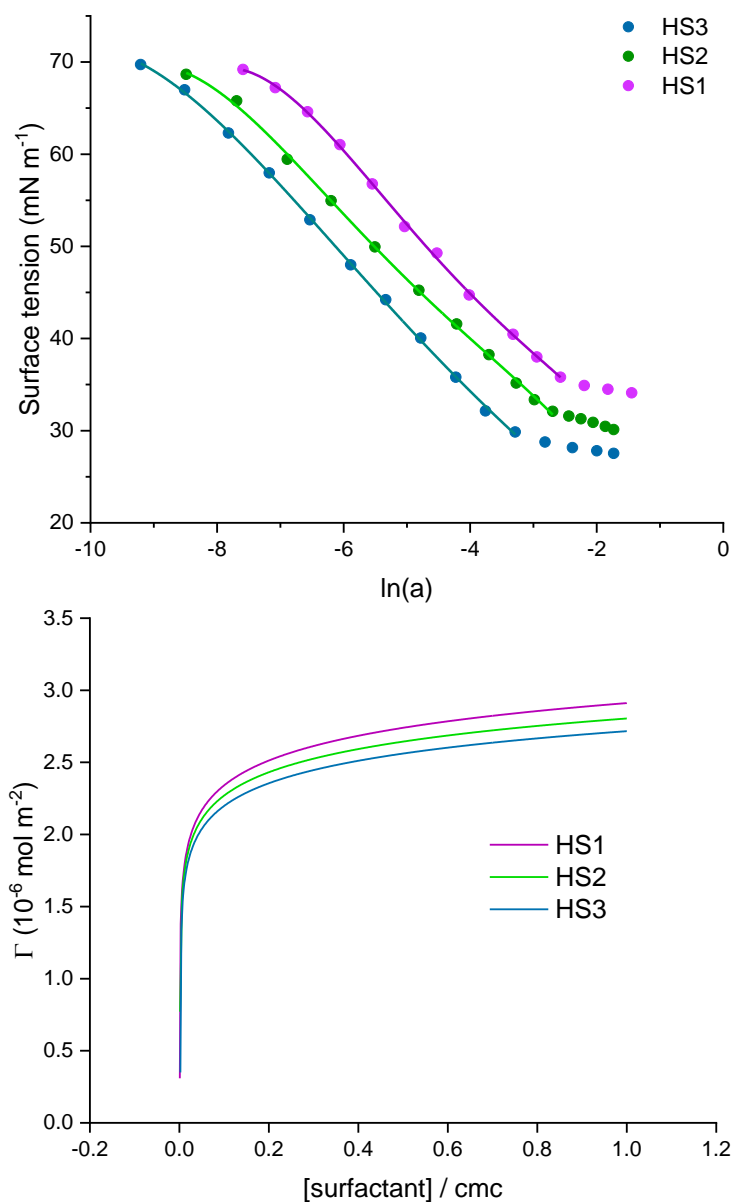


Figure 5.13: Change in surface tension as a function of activity for the branched hydrocarbon surfactants HS1, HS2 & HS3. Polynomial fits used to determine the surface excess and area-per-molecule at the cmc are included. Corresponding adsorption isotherms on a reduced concentration axes for fairer comparison (concentration/cmc) are also provided.

Surfactant	cmc (mM) ± 0.2	γ_{cmc} (mN m ⁻¹) ± 0.2	A_{cmc} (Å ²) ± 2
HS1	81.2	35.4	65
HS2	57.6	32.4	72
HS3	33.6	29.7	79

Table 5.3: Surface properties derived from γ -ln(a) plots for HS surfactant series.

From the surface properties shown in Table 5.3 there is a clear decrease in surface tension moving across the series as the branching is increased. The cmc decreases in an expected fashion, due to additional branching which further disrupts the hydrogen bonding network in water, creating a greater free energy of micellisation. Because the tail length is consistent across the series, as the branching is increased the bulkiness of the tail and hence volume of space occupied at the air-water interface increases. This is reflected in the area per molecule, with A_{cmc} being largest for the bulkiest surfactant HS3. An increase in the area per molecule going hand in hand with an increase in branching has been observed before (ref. [10]). From A_{cmc} it is possible to assess the surface coverage, Φ_{cmc} , introduced in Section 2.7 described as:

$$\Phi_{\text{cmc}} = \frac{V_{\text{cal}}}{V_{\text{meas}}} \quad (5.7)$$

where V_{cal} is the volume of the tail based on the summation of fragments and V_{meas} is the maximum volume the tail could occupy. The surface tension generated at the cmc, γ_{cmc} , as well as the corresponding packing efficiency, Φ_{cmc} , for each surfactant from the HS series is shown in Figure 5.14.

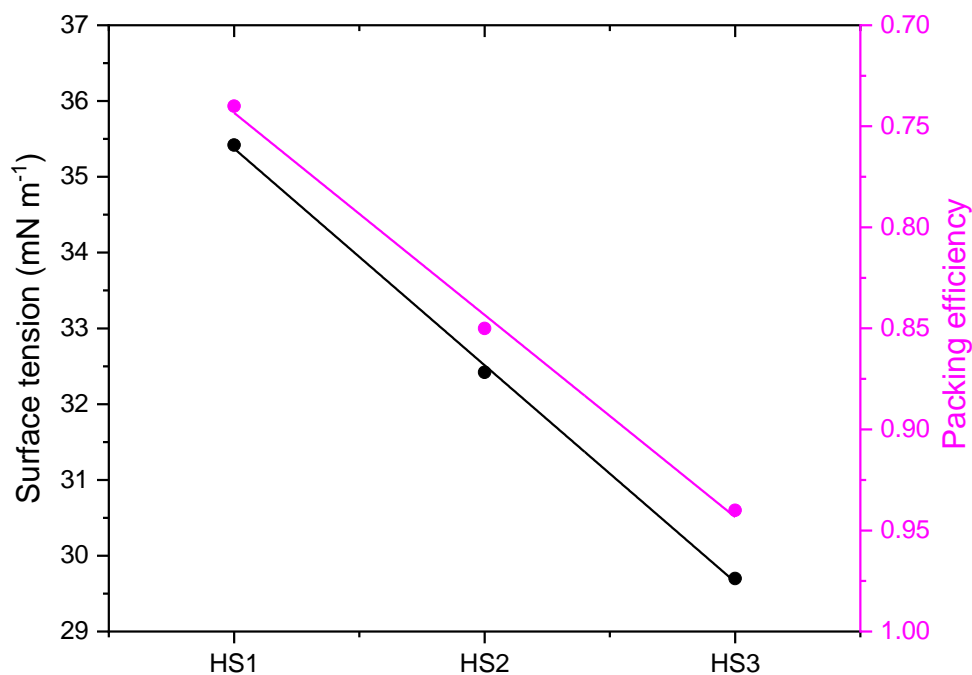


Figure 5.14: Surface tension generated at the cmc, γ_{cmc} , as well as the corresponding packing efficiency, Φ_{cmc} , for each surfactant from the HS series.

From Figure 5.14 there is a clear trend which shows a decreasing surface tension with an increase in the CH₃:CH₂ ratio, parallel to an increased packing efficiency. Hence this highlights that branching the tail is a suitable approach to generate lower surface energies with HC surfactants. This is thought to be due to several reasons:

- The surface becomes more populated by low surface energy $-\text{CH}_3$ groups which leads to weaker intermolecular interactions between tails (order of increasing surface energy: $\text{CF}_3 < \text{CF}_2 < \text{CH}_3 < \text{CH}_2$ - ref. [24]).
- The surface layer becomes more efficiently filled, i.e. a higher Φ_{cmc} , creating a surface monolayer which more effectively mimics a pure alkane.
- The area per molecule is increased which reduces the amount of intermolecular interactions between tails per unit area (it is important to point out that the increased A_{cmc} still maintains being filled effectively).

As highlighted at the start of this section, simply loading a surfactant tail with $-\text{CH}_3$ groups will not always generate low surface energies. The most effective surfactant from the series presented here, HS3, generates a very efficiently packed monolayer ($\Phi_{\text{cmc}} = 0.94$), has a high CH₃:CH₂ ratio, and yet only generates $\gamma_{\text{cmc}} = 29.7 \text{ mN m}^{-1}$, see Table 5.4. Given that HS3 meets the criteria of the general property of low aqueous surface tension, i.e. high Φ_{cmc} , and also possesses a high CH₃:CH₂ ratio, it would be expected that HS3 would generate very low γ_{cmc} ($< 25 \text{ mN m}^{-1}$). Therefore, given the small compact nature of HS3, this suggests that the length of the alkyl tail is also of importance to generate low γ_{cmc} .

Surfactant	Branching factor	Φ_{cmc}	γ_{cmc} (mN m^{-1}) ± 0.2
HS1	2.00	0.74	35.4
HS2	2.67	0.85	32.4
HS3	2.67	0.94	29.7

Table 5.4: Comparison of the packing efficiency, Φ_{cmc} , surface tension at the cmc, γ_{cmc} , and branching factor for HS1-3.

The empirical branching factor shown in Table 5.4 accounts for contributions from both the extent, and position, of a branch relative to the head group (ref. [10]). For example, the branching factor of HS2 was calculated as follows: 1 methyl branch in position 2 and 1 ethyl branch in position 3 on a C3 linear chain: $[(1*2)+(2*3)]/3 = 2.67$. The branching factor of HS2 and HS3 are equal, although HS3 possesses more branches. This is because the branching factor does not account for branched chains, and all groups are considered linear. Therefore a new method for empirically measuring the degree of branching is required, which more accurately accounts for all branches present on a surfactant tail.

From this study, a logical conclusion is that when designing low surface energy HC surfactants, the tail should possess *tert*-butyl groups as they have the highest CH₃ ratio of any single alkyl moiety. Furthermore, all of the current most effective hydrocarbon surfactants possess *tert*-butyl groups, for example AOT3 and AOT4 (ref. [10]).

5.3.1 Steric hindrance of the head group

There are various models used to predict the surface tension of a compound such as an organic liquid,^{25,26} however, for branched surfactants no such model has yet been established. One way to evaluate the final surface tension possible for a particular surfactant is to evaluate γ for the starting alcohol. Using a K100 tensiometer surface tension measurements were made at 25 °C for several alcohols used to synthesise surfactants which feature in this thesis, see Table 5.5. The melting point of 2,2-Dimethyl-1-propanol is 52.5 °C and therefore the value of γ at 25 °C shown in Table 5.5 was estimated, see Figure 5.15. From Table 5.5 the lowest surface tension is generated by *tert*-butanol. This further highlights the potential of the *tert*-butyl group to generate very low surface energies for HC surfactants as suggested previously in Section 5.3. Interestingly the three alcohols used to synthesise HS1-3 all generate $\gamma \sim 24.5 \text{ mN m}^{-1}$, whereas γ_{cmc} of the three di-chain surfactants decreases by $\sim 3 \text{ mN m}^{-1}$ across the series. This highlights the steric hindrance caused by the head group, and that the relationship between molecular structure and surface tension is clearly far more sensitive for surfactants. Therefore, to design super-effective HC surfactants, novel approaches to improve packing efficiency are required.

Alcohol	γ (mN m ⁻¹) ± 0.1	Surfactant	γ (mN m ⁻¹) ± 0.1
3-Pentanol	24.5	HS1	35.4
2-Methyl-3-pentanol	24.3	HS2	32.4
2,4-Dimethyl-3-pentanol	24.9	HS3	29.7
2,2-Dimethyl-1-propanol	20.5	AOTA	30.2
2,6-Dimethyl-4-heptanol	23.1	Na-BC9	30.8
<i>tert</i> -butanol	20.3	-	-
FO180	25.8	Na-FO180	27.2
FO180N	27.8	Na-FO180N	27.5

Table 5.5: Surface tension for selected alcohols which are precursors for surfactants synthesised in this thesis, except *tert*-butanol. All measurements made at 25 °C. The value for 2,2-Dimethyl-1-propanol was estimated, see Figure 5.15.

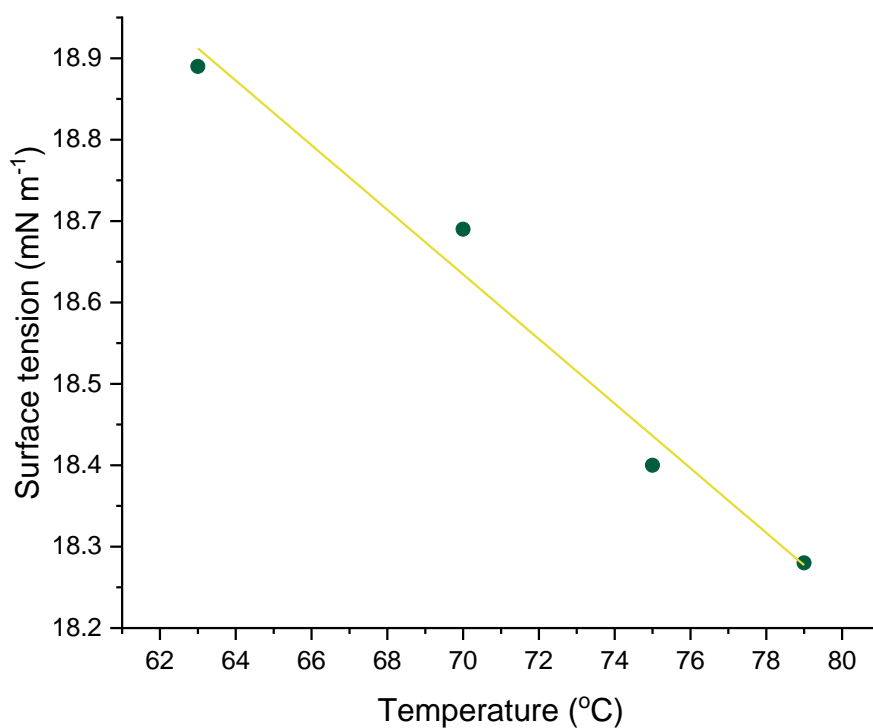


Figure 5.15: Surface tension of 2,2-Dimethyl-1-propanol at various temperatures. Data was extrapolated to estimate surface tension at 25 °C, shown in Table 5.5.

5.4 Trimethylsilyl (TMS) - Hedgehogs

In Section 2.4 the essential reasons fluorocarbon (FC) surfactants display greater surface activities over HC analogues were introduced, namely: 1) the lower polarisability of fluorine over hydrogen and 2) the larger atomic radius of fluorine. Because fluorine has a larger atomic radius compared to hydrogen, consequently a perfluoroalkyl moiety will have a larger molecular volume, e.g. $-\text{CF}_2-$ and $-\text{CH}_2-$ are estimated to be 38 and 27 Å³ respectively.²⁷ A perfluoroalkyl chain will therefore have a larger volume compared to a hydrocarbon analogue, and thus when packing at the air-water interface, less fluorocarbon surfactant molecules will be required to fill a ‘unit-area’, this is illustrated in Figure 5.16. Therefore there will be less intermolecular interactions between tails for FC surfactants, which reduces the dispersion contribution γ^{d} to the total surface tension ($\gamma = \gamma^{\text{d}} + \gamma^{\text{p}}$). Silicon has a larger atomic radius compared to carbon and therefore, a tail containing silicon should possess a larger molecular volume compared to a carbon analogue, producing a lower packing density per unit area and thus, lower γ . To test this idea, a novel series of hydrocarbon surfactants termed TMS-hedgehogs were synthesised where carbon in the *tert*-butyl group has been replaced by silicon, see Figure 5.17. The corresponding hydrocarbon equivalents have also been synthesised to provide a comparison and thus to investigate the effects of incorporating silicon into the chain-tip. AOTA has

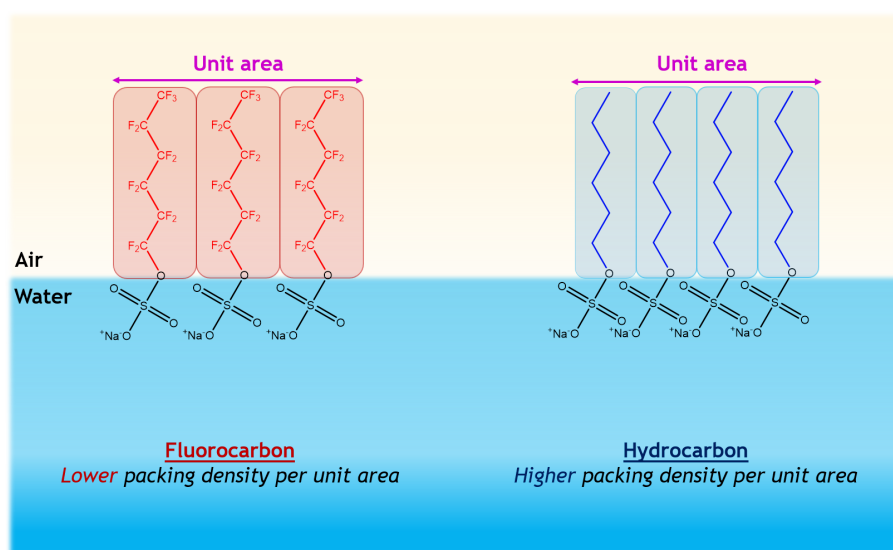


Figure 5.16: Schematic representation of fluorocarbon and hydrocarbon surfactants packing at the air-water interface. FC surfactant tails have a larger volume compared to a HC analogue and therefore produce a lower packing density per unit area.

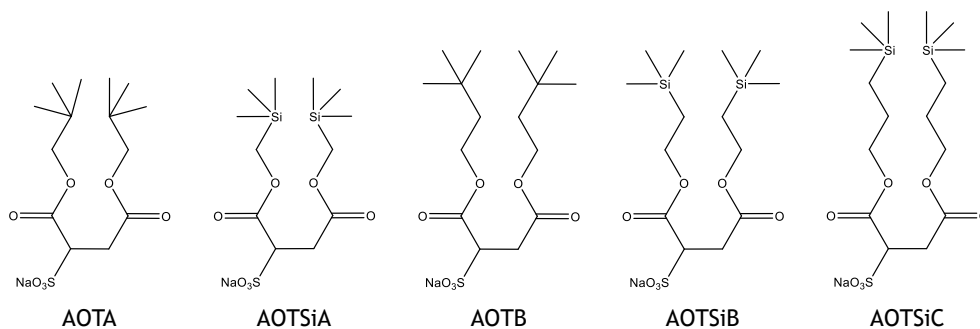


Figure 5.17: Molecular structures of TMS-hedgehog surfactants AOTSiA, AOTSiB and AOTSiC, where silicon has been incorporated into the *tert*-butyl group, as well as the corresponding hydrocarbon analogues AOTA and AOTB.

previously been referred to as AOT14,²⁸ and the HC equivalent of AOTSiC could not be synthesised in sufficient quantities due to expensive starting materials.

The performance of TMS-hedgehogs vs the hydrocarbon analogue can be compared through their effectiveness, i.e. γ_{cmc} . As discussed previously, to ensure a chemically pure surface free from polyvalent M^{n+} species that are inevitably introduced during synthesis, the appropriate surfactant:EDTA ratios must be determined separately for each surfactant on a batch-by-batch basis. Equilibrium γ vs $\ln(a)$ plots were obtained at EDTA ratios of - AOTA (275:1), AOTSiA (300:1), AOTB (425:1), AOTSiB (500:1) and AOTSiC (250:1). The surface tension profiles are shown in Figure 5.18. All curves show clean breaks at the cmc with no minima or shoulders which would indicate surface-active impurities. Cmc's were determined following the double differential method outlined in Section 5.2.3. The pre-cmc data were fit to quartic functions to estimate the limiting surface excess concentration at the cmc, and thus, the area per molecule. These results are given in Table 5.6.

Comparison of the cmc data presented in Table 5.6 shows a logarithmic decrease with increasing chain length (e.g. AOTA/AOTB), due to an increase in hydrophobicity. For AOTSiA, SiB and SiC, each tail possesses effectively 5, 6 and 7 carbons, with cmc's proportional to their linear analogues (ref. [10]). As expected, incorporating silicon into the chains (AOTA/AOTSiA) causes further decreases in cmc. There is also a clear decrease in γ_{cmc} when silicon is incorporated into the surfactant tail. This suggests a lower packing density per unit area. From the data presented in Table 5.6 AOTSiC is the strongest performer achieving $\gamma_{\text{cmc}} = 22.8 \text{ mN m}^{-1}$,

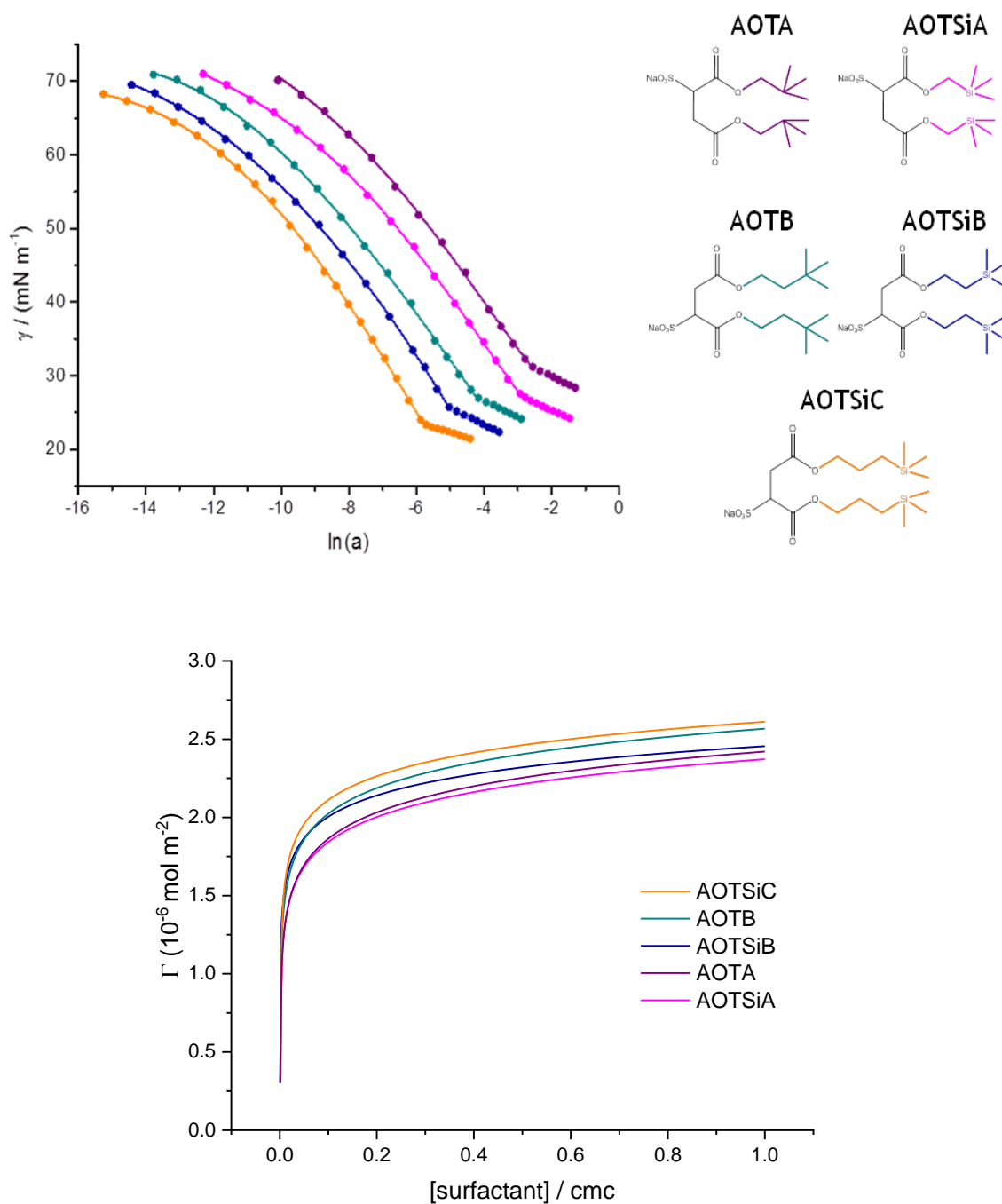


Figure 5.18: Equilibrium surface tension data from right to left for AOTA, AOTSiA, AOTB, AOTSiB and AOTSiC at 25 °C in water at EDTA:surfactant ratios as noted on the previous page. Polynomial lines fit to pre-cmc data are shown. Surfactant molecular structures are also included, the colour of the tail corresponds to the appropriate curve. Curves slightly off-set to improve clarity between surfactants with similar cmc's. Corresponding adsorption isotherms on a reduced concentration axes for fairer comparison (concentration/cmc) are also provided.

Surfactant	cmc (mM) ± 0.2	γ_{cmc} (mN m ⁻¹) ± 0.1	A_{cmc} (Å ²) ± 2
AOTA	89.6	30.2	79
AOTSiA	68.1	27.0	82
AOTB	25.9	26.7	75
AOTSiB	15.9	24.3	78
AOTSiC	3.0	22.8	74

Table 5.6: Surface properties derived from γ -ln(a) plots for the TMS series.

the lowest currently reported for a HC surfactant. Interestingly, the surface tension decreases as the tail length increases, which is perhaps counterintuitive as the CH₃ to CH₂ ratio decreases. The γ_{cmc} values of the HS series presented previously highlighted that highly branched but short tails are ineffective at generating low γ_{cmc} , this is further validated here. The A_{cmc} values presented in Table 5.6 decrease as the tail length increases which suggests more tightly packed molecules, given the increase in molecular volume. Similar trends have been found previously due to a decrease in chain rigidity, and changes in the head group hydration structure.²⁹

5.4.1 Surface coverage

The surface coverage at the cmc, Φ_{cmc} , is dependent on the area-per-molecule and the longest alkyl chain length (see Section 2.7). Therefore values obtained for Φ_{cmc} are an intrinsic property and independent of both surfactant geometry and chemistry of the surfactants. Assuming the layer is uniform, a high Φ_{cmc} indicates an efficiently packed monolayer with little free space. Values of γ_{cmc} for the TMS-series, as well as calculated values of Φ_{cmc} and branching factor are shown in Table 5.7.

The first general-structure property relationship of surface tension suggests that low surface tensions are generated by efficient monolayer packing, regardless of surfactant type (ref. [2]). From the data presented in Table 5.7, the TMS-hedgehog series all pack efficiently at the surface, producing high Φ_{cmc} values which are comparable with the super-efficient FC surfactant di-CF₄ ($\gamma_{\text{cmc}} = 17.7 \text{ mN m}^{-1}$ $\Phi_{\text{cmc}} = 0.97$).³⁰ Furthermore, if the TMS-hedgehog is compared to the purely HC analogue, for example AOTA versus AOTSiA, from the A_{cmc} data shown in Table 1, one might expect AOTSiA to produce a lower Φ_{cmc} given the larger A_{cmc} and hence

Surfactant	Branching factor	Φ_{cmc}	γ_{cmc} (mN m ⁻¹) \pm 0.1
AOTA	1.33	0.87	30.2
AOTSiA	1.33	0.96	27.0
AOTB	1.00	0.82	26.7
AOTSiB	1.00	0.93	24.3
AOTSiC	0.80	0.92	22.8

Table 5.7: Comparison of the packing efficiency, Φ_{cmc} , surface tension at the cmc, γ_{cmc} , and branching factor for TMS-hedgehogs and pure hydrocarbon analogues.

V_{meas} . However, it is clear that the presence of silicon in the chain in place of carbon improves packing efficiency and surface coverage (i.e. $\Phi_{\text{cmc}} \rightarrow 1$). Thus, the lower γ_{cmc} and higher Φ_{cmc} generated by AOTSiA over AOTA, can be attributed to the larger size of silicon ($r_{\text{Si}} = 1.1 \text{ \AA}$) compared to carbon ($r_{\text{C}} = 0.7 \text{ \AA}$) which helps fill the space between surfactant tails, due to the increased molecular volume of the chain tips. As the tail length increases, the branching factor decreases, due to a consistent chain-tip. The surface tension decreases as the branching factor decreases, where the opposite was true for the HS series. This highlights that the branching factor which is based on the molecular structure of the tail, is poorly equipped to predict the effectiveness of a HC surfactant.

By comparing the surface tension data, there is no evidence to suggest silicon induces strong dipoles in the chain tips, due the lower surface energies achieved by the trimethylsilyl analogues. Therefore, the low surface energies achieved by these TMS-hedgehogs can be attributed to an increased molecular volume which improves packing efficiency between surfactant tails in the surface monolayers leading to a higher surface coverage. Furthermore, these are not conventional hydrocarbon surfactants as they contain silicon (not to be confused with silicone surfactants, which are a distinctively different class). A characteristic of silicone surfactants is a highly flexible $-\text{O}-\text{Si}-\text{O}-\text{Si}-$ backbone. However, the $\text{Si}-\text{O}-\text{Si}$ linkage is susceptible to hydrolysis in the presence of moisture,³¹ and the hydrolytic instability of silicone surfactants is an inherent weakness. Therefore, the TMS-hedgehogs introduced here have been designed to circumvent both the hydrolytic instability of silicone surfactants, as well as the environmentally hazardous nature of fluorosurfactants, whilst generating the lowest surface energies currently achieved by HC surfactants.

5.4.2 Small-angle neutron scattering (SANS)

It is of interest to see if the subtle changes in molecular structure affect surfactant aggregation and preferred micellar shape, hence, small-angle neutron scattering (SANS) data were collected as a function of concentration. Measurements were made at 60 °C for all surfactants to ensure complete solubility in D₂O. Concentrations were kept consistent at multiples above the cmc (i.e. 40x, 20x etc). Scattering profiles with corresponding fits are shown in Figure 5.19. For AOTA/AOTSiA, the most dilute concentration did not scatter strongly enough and these data are not included.

The scattering profiles for AOTB, AOTSiA and AOTSiB are well described as oblate ellipsoid form factors with charged structure factors to account for repulsion. The parameters used to model the charged oblate ellipsoids - equatorial radius [$R_{\text{eq}} / \text{Å}$], polar radius [$R_{\text{pol}} / \text{Å}$], aspect ratio [$X = R_{\text{eq}} / R_{\text{pol}}$] and effective micellar charge (Z). For AOTA and AOTSiC the shape of the aggregates change with varying concentration. Oblate charged ellipsoids are still formed, but at low concentrations, a more spherical shape is observed and interestingly, for AOTSiC at the highest concentration, a lamella structure is formed. To model the lower concentrations of AOTA and AOTSiC a spherical model was used for the radius - [$R_{\text{sphere}} / \text{Å}$], and to model the the lamellar structures present at the highest concentration of AOTSiC, a paracrystal lamellar model was used,³² with the following parameters - bilayer thickness [$D - \text{Å}$], average distance between two adjacent layers [$L - \text{Å}$], distribution of layer distance [P], and number of layers [N_{layers}]. These data are shown in Table 5.8.

From Figure 5.19 all surfactants show an intermediate-Q peak which is characteristic of charged micelles. As the concentration increases this intermediate peak becomes more pronounced and moves to higher Q. For each surfactant, the sizes of the ellipsoids determined from the fits follows the expected trend, with the smallest surfactants forming the smallest micelles (e.g. AOTA $\approx 10 \text{ Å}$). The charge is also seen to decrease in accordance with decreasing micelle size. AOTSiA, AOTB and AOTSiB only form oblate ellipsoids which display common behaviour for charged anisotropic micelles when concentration is varied. Similar trends have been reported before for other surfactant systems including the common linear HC surfac-

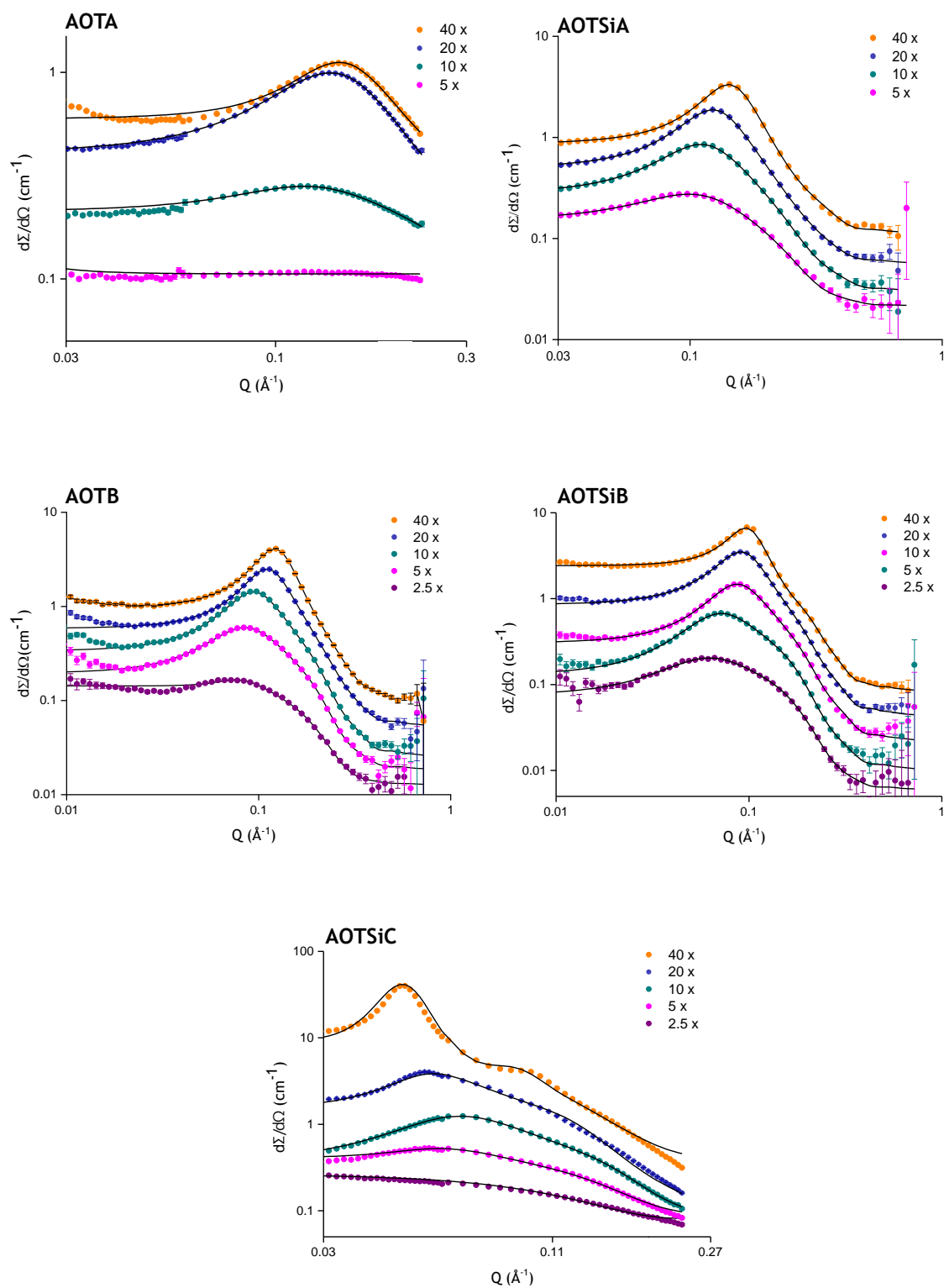


Figure 5.19: SANS profiles for AOTA, AOTSiA, AOTB, AOTSiB and AOTSiC in D_2O over a range of concentrations which are consistent multiples of the cmc. Measurements were made at $60^\circ C$ to ensure a mono-phasic system for all concentrations. Data for AOTSiA, B and SiB are from SANS 2D. Data for AOTA and AOTSiC are from D33, ILL. The lines are fitted functions for scattering laws as described in the text.

tant SDS.³³⁻³⁶ For AOTA and AOTSiC, charged oblate ellipsoids are formed in the intermediate concentration regime which follow the expected trend.

The sizes and shapes of micelles depend on a balance of interactions between molecular structure of the surfactant tail, and repulsion between head groups. At low concentrations of AOTA, the intermediate-Q peak is lost, due to weaker repulsion between neighbouring micelles. From the aspect ratio values in Table 5.8, there is a shape transition from ellipsoidal to spherical as concentration decreases. The same is true for AOTSiC in the low concentration regime, forming spherical micelles with radii ≈ 19 Å. This transition in shape is possibly due to the weaker charge on the micelles, reducing repulsion between neighbouring head groups.

For AOTSiC the intermediate-Q peak moves to lower Q as concentration is increased, showing the presence of larger aggregates. At the highest concentration (40 x cmc) a clear Bragg peak can be seen which is characteristic of d-spacing between lamellae. The average number of layers is around 11, indicating a large structure formed from many stacks of lamellar sheets with an average bilayer thickness of 22.1 Å. The average distance between layers obtained by the model agrees well with the estimated distance from the Q-value of the highest peak. Previous SANS studies of large, bulky hedgehog surfactants reported the formation of lamellar structures (ref. [4]). The transition to lamellar structures at high concentration has been reported before,³⁷ and is due to significant interactions between micelles that become over packed above a certain concentration.

Overall the subtle differences in molecular architecture of the surfactants discussed here do not seem to greatly affect the shapes of the micellar aggregates formed. The effect of concentration and micellar charge play bigger roles. Incorporating silicon into the chain tip only causes a slight increase in the micelle size. Highlighting that when nearing the limit of performance achievable with hydrocarbon surfactants, the relationship between molecular structure and packing is extremely sensitive in the surface monolayer, compared to micellar packing in solution.

5.5 Designing an effective surfactant tail

As outlined at the start in Section 5.1, the lowest surface tension possible for a hydrocarbon surfactant is suggested to be $\sim 20 \text{ mN m}^{-1}$. With the HC surfactants introduced in this chapter, surface tensions as low as 22.8 mN m^{-1} (AOTSiC) have been achieved, which is very near the limit of achievable performance. Compared to simple linear surfactants such as SDS or di-C7SS ($\gamma_{\text{cmc}} = 31.2$ and 29.8 mN m^{-1} respectively) branching the surfactant tail clearly generates a much more effective reduction of aqueous γ . As highlighted in Section 5.3, an imperative structure-property relationship shared by all effective HC surfactants is a high $\text{CH}_3:\text{CH}_2$ ratio in the chain-tip, i.e. a *tert*-butyl group. By comparing structure-property relationships of low surface energy HC surfactants, is it possible to predict the effectiveness of a HC surfactant based on the molecular architecture of the alkyl tail alone? In this section a new index, H_γ , is introduced which determines whether the molecular structure of a hydrocarbon tail is likely to generate $\gamma_{\text{cmc}} < 25 \text{ mN m}^{-1}$, i.e. it could be considered an identifier of super-effective HC surfactants. First though, the main principles of highly effective HC surfactants must be outlined, where it becomes clear that the rules are dependent on the alkyl chain length.

5.5.1 Generating low γ_{cmc} with short tails

There are very few studies which report surface properties for short HC surfactants. In the context of H_γ , short is defined as a surfactant tail where the longest alkyl chain length ≤ 3 . In this chapter, several short hedgehog surfactants have been introduced, all of which generate high $\gamma_{\text{cmc}} \sim 30 \text{ mN m}^{-1}$. At first short hedgehog surfactants would appear poorly equipped to generate low aqueous surface tensions. However, Sagisaka et al. conducted experiments relating the surfactant-tail layer density to surface tension for several novel hedgehog surfactants (ref. [5]). The short, highly branched hedgehog surfactant di-BC₆SS was introduced which generates $\gamma_{\text{cmc}} = 23.8 \text{ mN m}^{-1}$ (at 35°C). This is substantially lower than γ_{cmc} achieved by other short HC surfactants discussed in this chapter. Molecular structures and values of γ_{cmc} generated for di-BC₆SS and a few other select short hedgehog surfactants are shown in Figure 5.20. All structures are highly branched and yet only di-BC₆SS generates

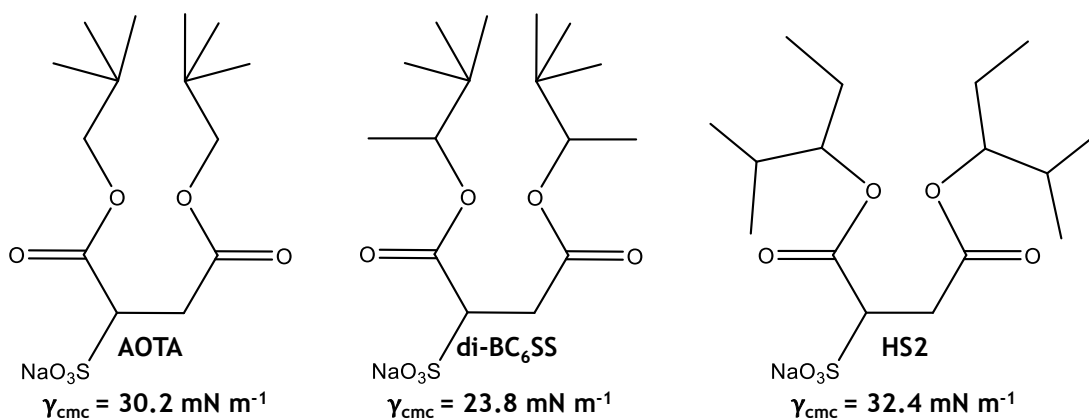


Figure 5.20: Molecular structures and respective γ_{cmc} values for the short hedgehog surfactants AOTA, di-BC₆SS (ref. [5]) and HS2. They are considered ‘short’ surfactants because the longest alkyl chain length is ≤ 3 .

low γ_{cmc} . Furthermore, the tail structures of AOTA and di-BC₆SS are extremely similar (one methyl group on each tail being the difference) yet di-BC₆SS generates $\gamma_{\text{cmc}} \sim 6 \text{ mN m}^{-1}$ lower than AOTA. Such a large difference in surface tension for such a small difference in molecular structure is remarkable. This result alone highlights that short highly branched hydrocarbon surfactants can be designed to be super-effective, generating very low values of γ_{cmc} . However, by comparing γ_{cmc} for AOTA and di-BC₆SS, the relationship between tail structure and low surface tension is clearly extremely sensitive for small highly branched surfactants. As highlighted in Section 5.4, for the TMS-hedgehogs, when the tail structure was kept constant and only the alkyl chain length was increased, a greater reduction of aqueous surface tension was achieved. This was suggested to be because of the increased flexibility of the tail, accompanied by a greater distance between the polar head group and low surface energy *tert*-butyl chain tip. By nature short hydrocarbon surfactants cannot generate low γ_{cmc} due to the benefits of an increased alkyl chain length. Therefore, for hydrocarbon surfactants with small alkyl chain lengths (≤ 3), these results suggest the approach to generate low γ_{cmc} is to use a tail that is nearly fully saturated (i.e. maximum number of CH₃ groups). And to design a short-tail super-effective HC surfactant which achieves $\gamma_{\text{cmc}} < 25 \text{ mN m}^{-1}$, a certain number of CH₃ groups are required, relative to the longest alkyl chain length.

5.5.2 Generating low γ_{cmc} with long tails

With regards to H_γ , a long tail is defined as a surfactant tail where the longest alkyl chain length ≥ 4 . The most effective HC surfactant is currently AOTSiC generating $\gamma_{\text{cmc}} = 22.8 \text{ mN m}^{-1}$ with a chain length 5 carbons long. In Section 5.4 where the TMS surfactant series was first introduced, a longer chain length was shown to be more effective at generating lower γ_{cmc} . However, it is possible to find examples where this structure-property relationship is not obeyed. Figure 5.21 shows the molecular structures and respective γ_{cmc} values for the branched di-chain surfactants AOTSiC, AOT1, 3 and 4, as well as the di-chain linear surfactant di-C6SS (ref. [10]). AOT4 has an identical tail structure to AOT3 except for a single additional CH_2 group, i.e. it is one carbon longer. However, AOT4 with the longer alkyl chain length generates a higher surface tension. This highlights the structure-property relationship of a lower surface tension generated by a longer alkyl chain length is sensitive to branching away from the chain tip. AOT3 could be considered the purely hydrocarbon equivalent of AOTSiC, with an additional CH_3 group present along the tail. When comparing γ_{cmc} for AOTSiC and AOT3, a substantially higher surface tension is generated for AOT3. Although AOT3 is a pure hydrocarbon and AOTSiC a TMS-hedgehog and therefore not directly comparable, the purely HC equivalent surfactant AOTB with a smaller alkyl chain length (hence less effective) still generates γ_{cmc} lower than AOT3 (26.7 mN m^{-1}). Therefore, clearly the presence of this additional CH_3 group on AOT3 has adverse effects on packing between tails, generating a higher surface tension. This is perhaps not as would be expected, given

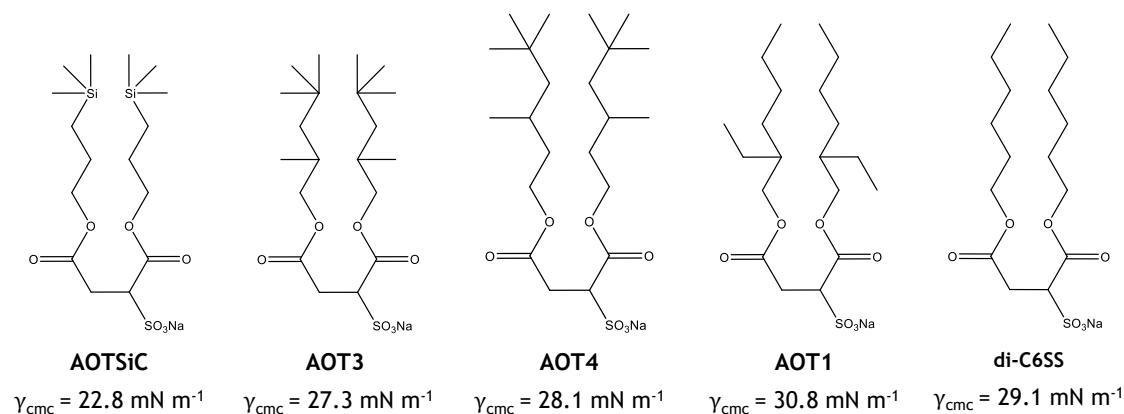


Figure 5.21: Molecular structures and respective γ_{cmc} values for the long hedgehog surfactants AOTSiC, AOT3 and AOT4 (ref. [10]).

that the number of low surface energy methyl groups is increased. Furthermore, this does not agree with the structure-property relationship identified for small effective hedgehog surfactants, where a higher $\text{CH}_3:\text{CH}_2$ ratio generates lower γ_{cmc} . A similar effect is seen for AOT1 and di-C6SS (see Figure 5.21) which both possess a 6 carbon alkyl chain. AOT1 is branched near the head group and therefore possesses more low surface energy CH_3 groups, but generates $\gamma_{\text{cmc}} \sim 2 \text{ mN m}^{-1}$ higher than di-C6SS. This suggests that for longer alkyl chain lengths (i.e. ≥ 4), branching away from the chain-tip hinders efficient surface packing and hence reduces the effectiveness of the surfactant. Therefore, to promote efficient packing between surfactant molecules, the branching should be localised to (or near) the chain-tip.

5.5.3 The effectiveness of a hydrocarbon surfactant - H_γ

By comparing the surface properties of various hydrocarbon surfactants in the previous section, structure-property relationships of effective surfactants have been identified. The relationships are not general to all hydrocarbon surfactants, but dependent on the alkyl chain length. These are summarised below:

1. Short tail hydrocarbon surfactants - Longest alkyl chain length ≤ 3

- The tail should be at near maximum saturation (i.e. maximum number of CH_3 groups).

2. Long tail hydrocarbon surfactants - Longest alkyl chain length ≥ 4

- The branching should be localised to (or near) the chain-tip.
- Branching near the head group reduces efficient packing.
- A longer alkyl chain length helps to generate lower γ_{cmc} provided the branching is localised only at the chain-tip.

Table 5.9 shows surface properties for several HC surfactants arranged in order of decreasing surface tension. Where all super-effective surfactants ($\gamma_{\text{cmc}} = < 25 \text{ mN m}^{-1}$) obey the structure-property relationships outlined above. Surface properties are also given for the common linear surfactants SDS and di-C7SS to provide comparison. Molecular structures for all surfactants are provided in Figure 5.22.

Surfactant	γ_{cmc} (mN m ⁻¹) ± 0.2	A_{cmc} (Å ²) ± 2	Φ_{cmc}	Branching Factor
Tail length ≤ 3				
HS1	35.4	65	0.74	2.00
HS2	32.4	72	0.85	2.67
AOTA	30.2	79	0.87	1.33
HS3	29.7	79	0.94	3.67
AOTSiA	27.0	82	0.96	1.33
di-BC ₆ SS	23.8	73	0.97	2.33
Tail length ≥ 4				
SDS	31.2	47	0.59	0
AOT1	30.8	75	0.66	1.67
AOT5	30.3	80	0.94	2.80
di-C7SS	29.8	59	0.71	0
AOT2	29.7	77	0.85	2.40
AOT6	29.1	70	0.92	1.33
AOT4	28.1	70	0.94	1.33
Na-FO180N	27.5	69	0.60	6.70
AOT3	27.3	73	0.95	1.60
Na-FO180	27.2	86	0.64	7.10
AOTB	26.7	75	0.82	1.00
di-BC ₁₂ SS	26.3	171	0.58	5.00
di-BC ₉ SS	24.5	120	0.87	4.50
AOTSiB	24.3	78	0.93	1.00
AOTSiC	22.8	74	0.92	0.80

Table 5.9: Surface properties for the most effective branched surfactants, and two linear surfactants (SDS & di-C7SS) to provide comparison. Properties obtained from surfactants already introduced in this thesis or from literature: di-BC₆SS / di-BC₉SS / di-BC₁₂SS (ref. [5]), SDS,³⁸ AOT 1-6 (ref. [10]), di-C7SS (ref. [10]), Na-FO180 & Na-FO180N from Chapter 6

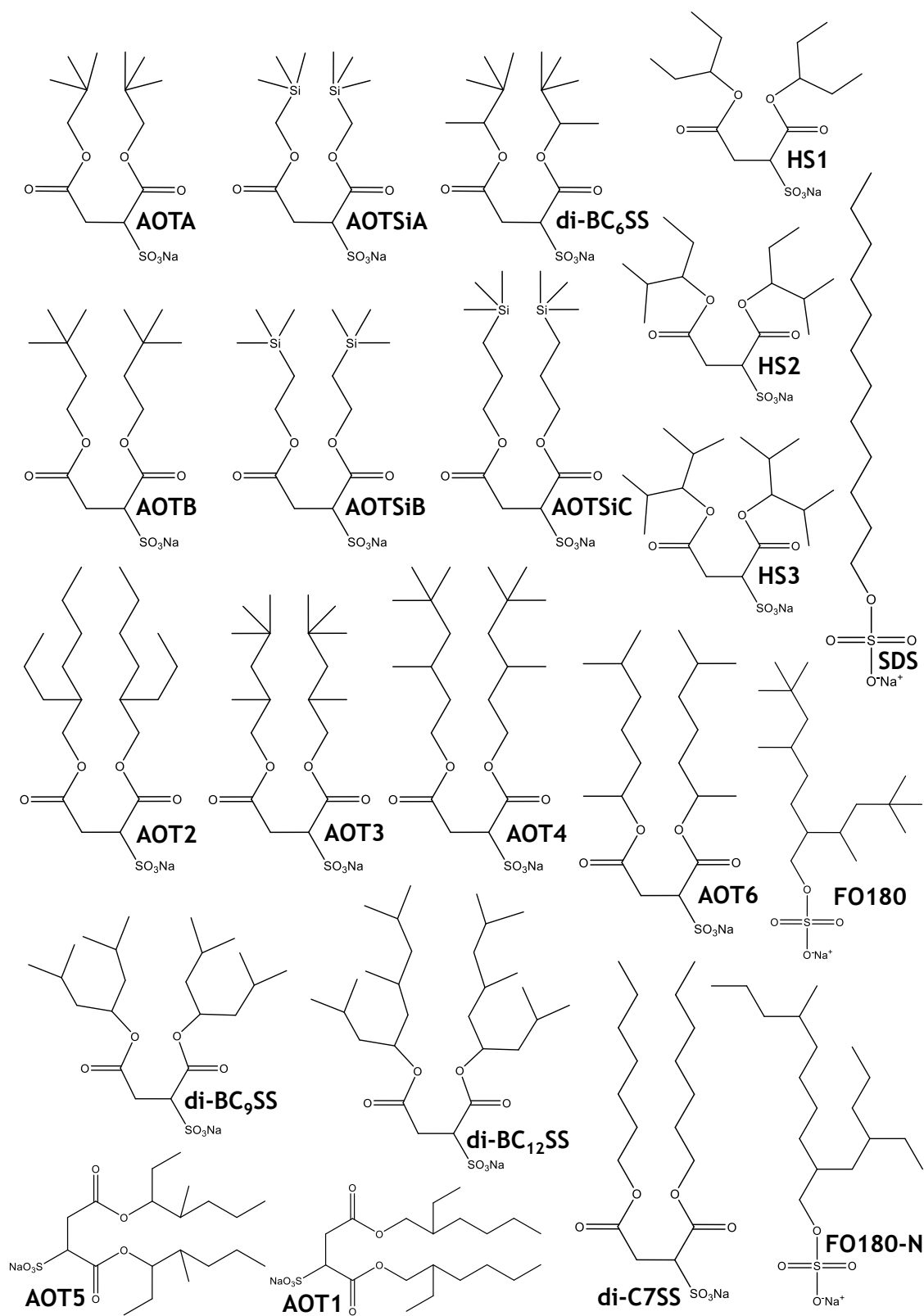


Figure 5.22: Molecular structures of hydrocarbon surfactants that feature in Table 5.9

In Table 5.9, the equilibrium surface tension (γ_{cmc}), area-per-molecule at the cmc (A_{cmc}), surface coverage at the cmc (Φ_{cmc}), and branching factor are shown for each surfactant. The area-per-molecule and surface coverage are two of the most common surface properties used to evaluate the structure-property relationships of effective HC surfactants. However, as we look down Table 5.9 there is no general trend that identifies effective HC surfactants from the area-per-molecule alone. Furthermore, the same can be said about the surface coverage values shown in Table 5.9. Although the first general structure-property relationship of low aqueous surface tension highlighted that effective surfactants are ones that pack efficiently to generate a high surface coverage. This is certainly true for the most effective surfactants shown in Table 5.9, but equally, there are less effective surfactants which also generate high Φ_{cmc} (i.e. AOT6 $\gamma_{\text{cmc}} = 29.1 \text{ mN m}^{-1}$ $\Phi_{\text{cmc}} = 0.92$, AOTSiC $\gamma_{\text{cmc}} = 22.8 \text{ mN m}^{-1}$ $\Phi_{\text{cmc}} = 0.92$). Furthermore, Φ_{cmc} requires knowledge of an experimentally determined A_{cmc} therefore, it can not be used to predict whether a particular tail structure could generate a super-effective HC surfactant. A simple method to evaluate the branching present for a particular tail is the branching factor. However, as shown in Table 5.9 again there is no clear trend that relates low γ_{cmc} to the branching factor.

Therefore, to evaluate the potential effectiveness of a hydrocarbon surfactant and thus guide the design of super-effective HC surfactants, a new index is required. One that is independent of surface properties and simply assesses the molecular structure of the tail. This takes a similar approach to the branching factor, except it must take into account the structure-property relationships of effective HC surfactants. The index, H_γ , is introduced which determines whether the molecular structure of a hydrocarbon tail is likely to generate $\gamma_{\text{cmc}} < 25 \text{ mN m}^{-1}$, i.e. an identifier of potential super-effective HC surfactants. As highlighted in Sections 5.5.1 and 5.5.2, the structure-property relationships of effective hydrocarbon surfactants differ depending on the longest alkyl chain length of the surfactant tail. Therefore, the index H_γ must also differ depending on the alkyl chain length, and can be split into two calculations one for short, and one for long tails. To begin with, H_γ is introduced for hydrocarbon surfactants with a short alkyl tail.

H_γ - Short tails

To clarify, here a short tail is defined as one where the longest alkyl chain length is ≤ 3 . The surfactants meeting this criterion are summarised at the top of Table 5.9. As identified in Section 5.5.1, short tail HC surfactants are effective if the tail is at near maximum saturation. By comparing γ_{cmc} for AOTA and di-BC₆SS, this relationship was shown to be extremely sensitive. From these results, H_γ can be defined for short tail HC surfactants as:

$$H_\gamma = \frac{\text{Total number of CH}_3 \text{ branches along the longest alkyl chain}}{\text{Longest alkyl chain length}} \quad (5.8)$$

where for super-effective HC surfactants, $H_\gamma \geq 0.70$. The longest alkyl chain length should be measured from the carbon nearest to the head group, and in one direction. Methyl groups are then counted along this chain. This is illustrated in the example calculations which are shown in Figure 5.23.

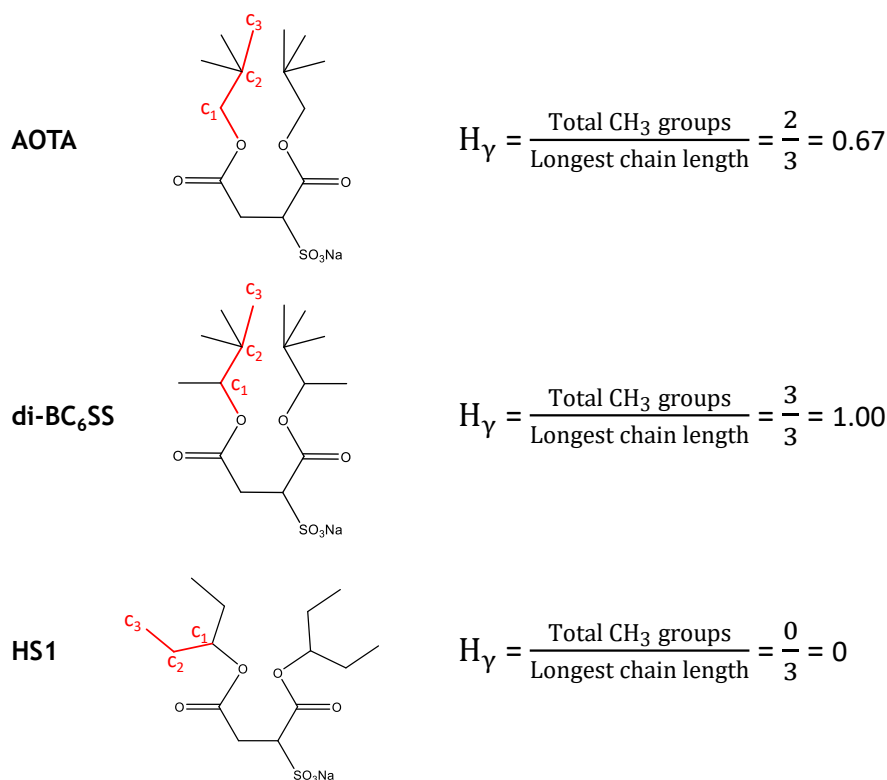


Figure 5.23: Example calculations of H_γ for short hydrocarbon surfactants. The longest alkyl chain length is highlighted in red.

For surfactants such as AOTA and di-BC₆SS, calculating H_γ is straightforward as the longest alkyl chain length is easy to identify. For HS1, the longest alkyl chain length could be misinterpreted as 5. Therefore, it is important to count from the head group, and in one direction. Because of the symmetrical tail structure of HS1, the degree of branching could also be misinterpreted when calculating H_γ . To clarify, *only* methyl groups attached to the alkyl chain are considered. For a tail structure such as HS1, H_γ should be determined separately for each tail, and then the summed total divided by two (irregardless of the number of chains considered). This is clarified in the illustrated calculations shown in Figure 5.24.

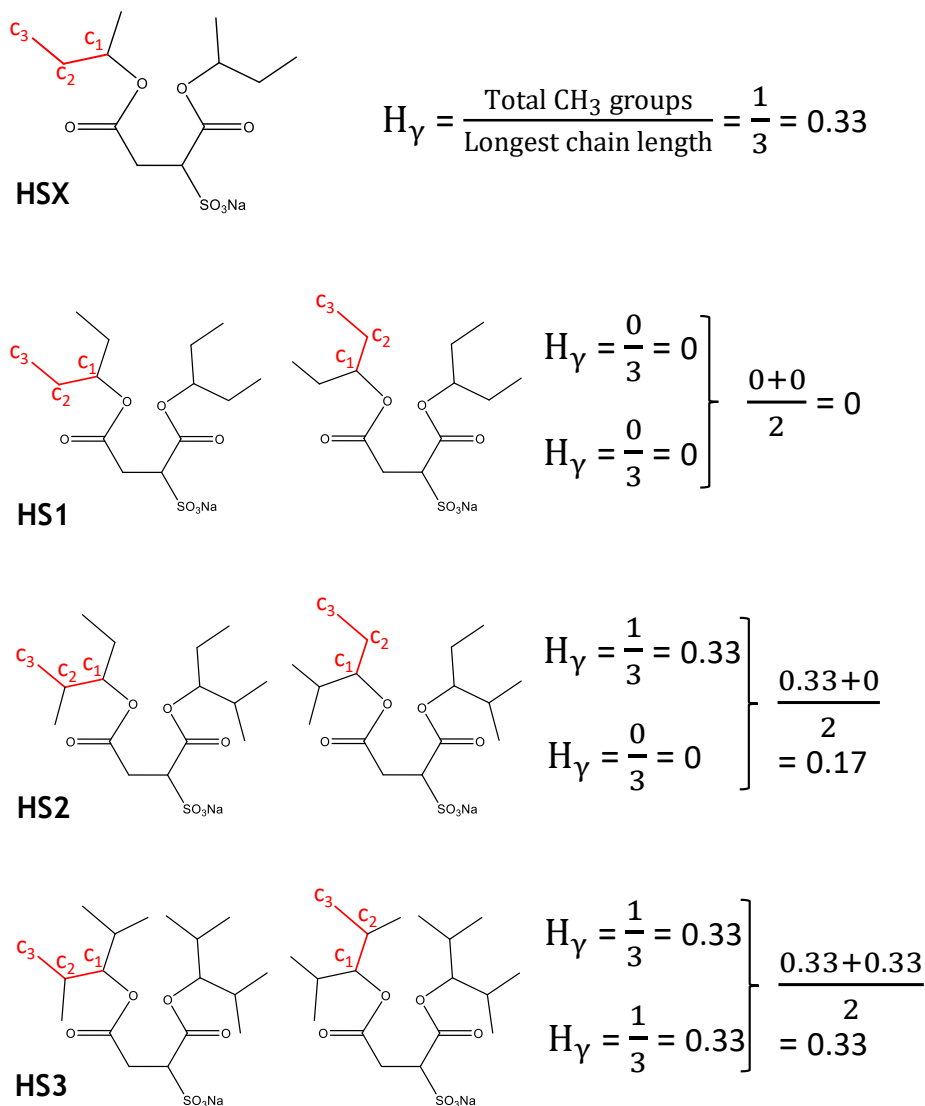


Figure 5.24: Example calculations of H_γ for short hydrocarbon surfactants. The longest alkyl chain length is highlighted in red.

H_γ - Long tails

For long alkyl tails, where the longest chain length is ≥ 4 , all super-effective surfactants shown in Table 5.9 share the following structural properties: a) a highly branched chain-tip, b) reduced branching away from the chain-tip, c) a longer alkyl chain length (provided (a) and (b) are met). To encapsulate the structure-property relationships of super-effective HC surfactants, for long tails H_γ is defined as:

$$H_{\gamma} = \frac{\frac{\beta}{3}(x - \alpha)}{\text{Total carbon number of tail}} \quad (5.9)$$

where β is the number of CH₃ groups in the chain tip, x is the longest alkyl chain length, and α corresponds to branching away from the chain tip. The various parameters are illustrated in the example calculation shown below in Figure 5.25.

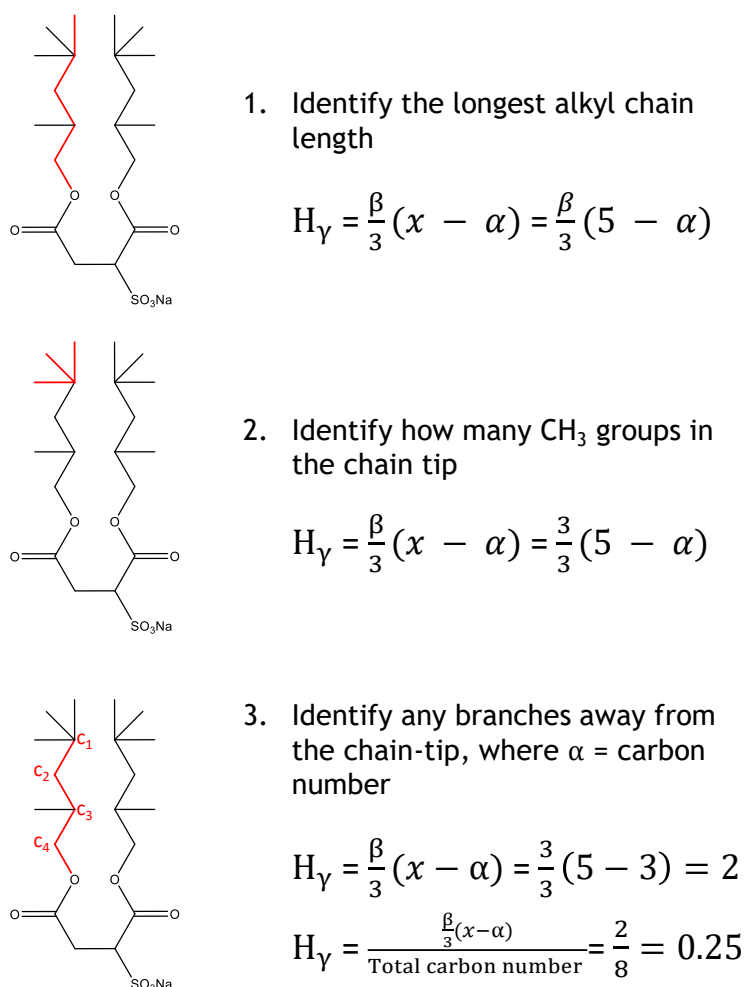


Figure 5.25: An example of each stage of the calculation used to determine H_γ for AOT3.

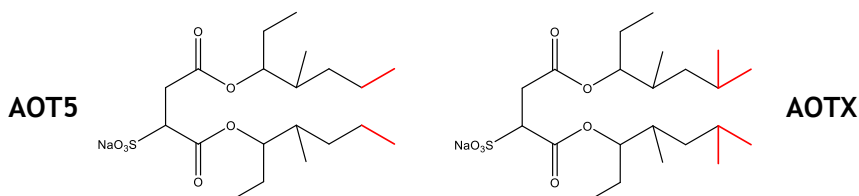
For super-effective HC surfactants that are predicted to generate $\gamma_{\text{cmc}} = < 25$ mN m^{-1} , H_γ should be ≥ 0.70 . As shown in Figure 5.25, for AOT3 $H_\gamma = 0.25$ and therefore is predicted not to be super-effective which agrees with the surface activity observed, AOT3 $\gamma_{\text{cmc}} = 27.3$ mN m^{-1} . Because of the wide variety of structures possible for an alkyl chain length ≥ 4 , the following pages provide several illustrated calculations to ensure clarity on each parameter when determining H_γ . Figure 5.26 highlights how to accurately identify β , as well as calculating α for a variety of different linear branch lengths present on one tail. The important consideration when calculating α is that the length of the linear chain is not considered, but instead how far away from the chain-end it is. Carbon one (C_1) is denoted by bearing the chain-tip, and branching at C_1 is not included in α , see Figure 5.26.

1. Identify the longest alkyl chain length - x

Starting from the carbon nearest the headgroup and in one direction.

2. Identify how many CH_3 groups in the chain tip - β

Where β is taken to be the number of CH_3 groups attached to the penultimate carbon on the longest alkyl chain. **AOT5, $\beta = 1$**
AOTX, $\beta = 2$



3. Identify any branching away from the chain-tip - α

For linear branches regardless of length $\alpha = \frac{(1 \times C_x) + (1 \times C_x) \text{ etc.}}{\text{Total number of branches}}$, where C_x corresponds to the carbon number, with carbon 1 (C_1) bearing the chain-tip.

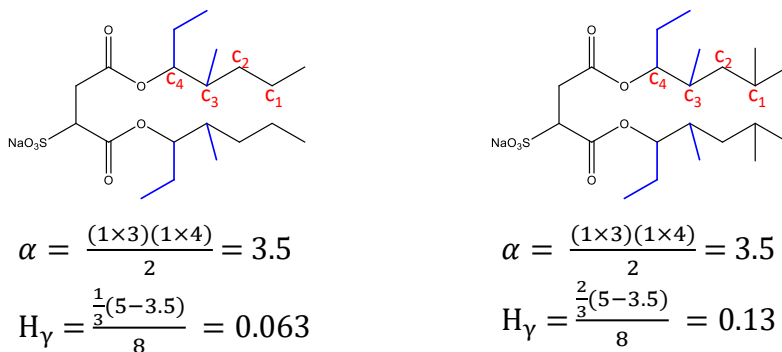
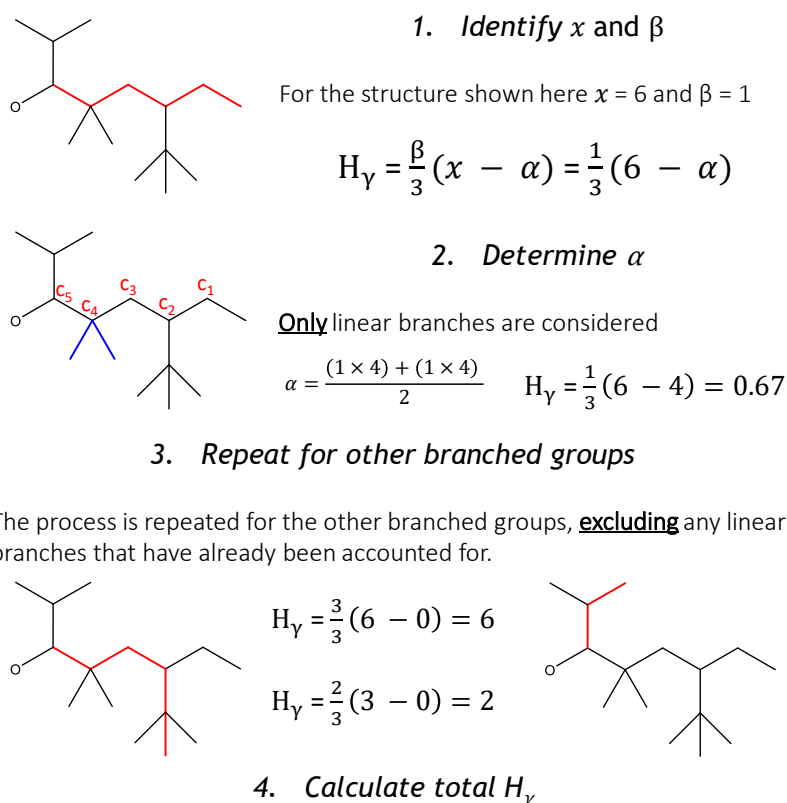


Figure 5.26: An illustrated calculation of H_γ for AOT5 and a hypothetical equivalent AOTX, highlighting how α is determined.

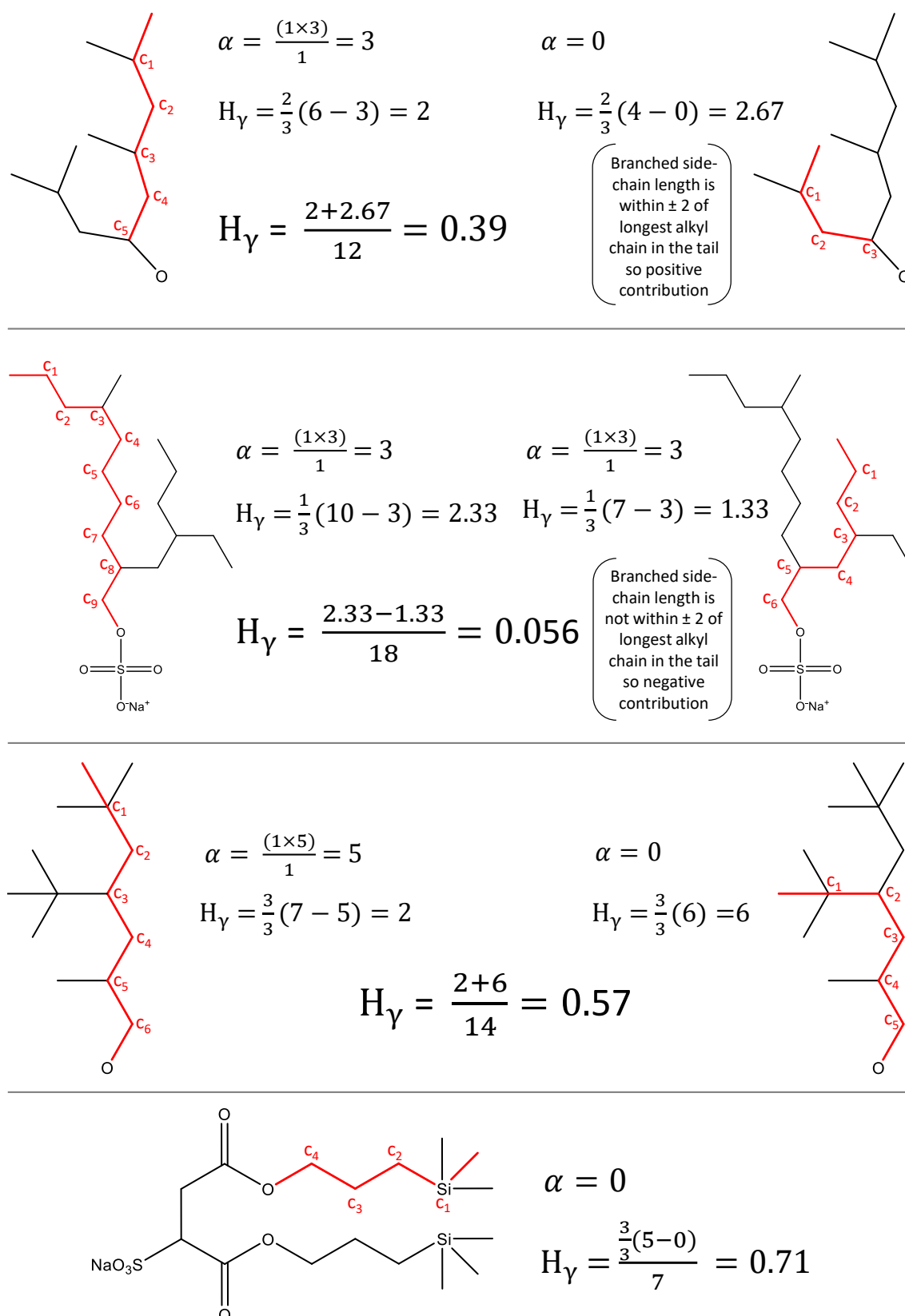
Figure 5.27 illustrates H_γ calculations for more complicated tail structures, where multiple highly branched groups may be present on a single tail. In this situation, H_γ is calculated for the longest alkyl tail, and linear branches along the chain are taken into account to calculate α , as shown previously in Figure 5.26. Branched chains are excluded from α , and instead H_γ is calculated for each branch separately, ignoring any linear branches already accounted for, see Figure 5.27. The values of H_γ for the branches are positive or negative depending on the chain length of the branch, relative to the longest chain length of the whole tail. The final value of H_γ is then calculated by summing all individual values, and dividing this summed total by the total carbon number of the whole tail. If an individual tail is symmetrical, such as di-BC₉SS, the individual combinations of H_γ are multiplied, not summed. Further examples for various structures shown in Figure 5.28.



If the chain length of the branched group is ± 2 the longest chain length of the tail, then the contribution of H_γ is additive, otherwise deductive.

$$H_\gamma = \frac{\text{Combined } H_\gamma}{\text{Total tail carbon number}} = \frac{0.67 + 6 - 2}{15} = 0.31$$

Figure 5.27: Illustrated calculation of H_γ for an example tail where multiple linear and non-linear branches are present.

Figure 5.28: Illustrated calculations of H_Y for various different tail structures.

5.5.4 Predicting potential super-effective hydrocarbon surfactants

From the tail structures H_γ was calculated for all surfactants shown in Table 5.9. These data, along with corresponding γ_{cmc} are shown in Table 5.10. From the values shown in Table 5.10, super-effective hydrocarbon surfactants are generated when:

$$- \textit{Short tail surfactants} = H_\gamma \geq 0.70$$

$$- \textit{Long tail surfactants} = H_\gamma \geq 0.70$$

Surfactant	γ_{cmc} (mN m ⁻¹)	H_γ
Tail length ≤ 3		
HS1	35.4	0
HS2	32.4	0.17
AOTA	30.2	0.67
HS3	29.7	0.33
AOTSiA	27.0	0.67
di-BC ₆ SS	23.8	1.00
Tail length ≥ 4		
SDS	31.2	0.33
AOT1	30.8	0.083
AOT5	30.3	0.063
di-C7SS	29.8	0.33
AOT2	29.7	0.074
AOT6	29.1	0.083
AOT4	28.1	0.33
Na-FO180N	27.5	0.056
AOT3	27.3	0.25
Na-FO180	27.2	0.44
AOTB	26.7	0.67
di-BC ₁₂ SS	26.3	0.39
di-BC ₉ SS	24.5	0.79
AOTSiB	24.3	0.67
AOTSiC	22.8	0.71

Table 5.10: Values of γ_{cmc} and H_γ for the most effective branched surfactants, and two linear surfactants for comparison (SDS & di-C7SS).

Figure 5.29 shows the relationship between H_γ and γ_{cmc} for all surfactants from Table 5.10. A clear trend is illustrated, low γ_{cmc} is achieved by tail structures that generate high H_γ . However, it is important to remember that H_γ does not compare the performance of hydrocarbon surfactants, but instead predicts whether a particular tail structure is likely to produce a super-effective hydrocarbon surfactant which could generate $\gamma_{\text{cmc}} < 25 \text{ mN m}^{-1}$. From all of the surfactants shown in Table 5.10 very few are super-effective, generating $\gamma_{\text{cmc}} < 25 \text{ mN m}^{-1}$. However, the ones that are super-effective share the same structure-property relationships. For example, for long alkyl tails this corresponds to a highly branched chain tip, attached to a long flexible tail with no branching down the chain (which reduces efficient packing). Figure 5.30 shows suggested structures that could generate very low values of γ_{cmc} based on predictions made by H_γ . Several of the structures predicted in Figure 5.30 would be synthesised from tertiary (3°) alcohols. As highlighted in Section 4.4.2, to synthesise surfactants from tertiary alcohols alternatives to the standard procedures are required. And thus, to push the limit of performance achieved by HC surfactants further, for these examples, extensive practical skills are required. Another alternative is to synthesise tri-chain surfactants from predicted effective 2°

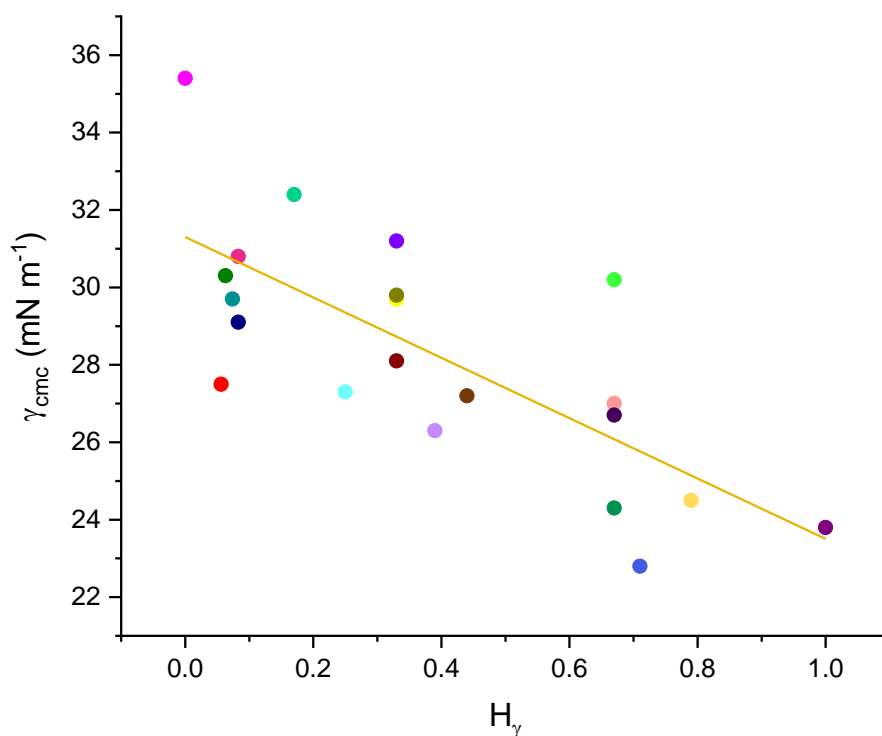


Figure 5.29: Relationship between H_γ and γ_{cmc} for selected branched surfactants.

and 1°alcohols. However, synthesising tri-chain surfactants is both time consuming and expensive. Synthesising single-chain surfactants is an option, but often display high cmc's requiring impractical amounts to generate γ_{cmc} . H_γ has been mainly devised from data for di-chain surfactants, however, because it evaluates only the tail structure is equally equipped for single and tri-chain surfactants. Furthermore, H_γ has been constructed from data for anionic HC surfactants and therefore is most suitable for predicting super-effective anionic surfactants. However, anionic surfactants dominate colloidal chemistry and also produce the lowest surface energies for HC surfactants, and thus are the most suitable class for H_γ to predict.

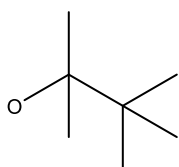
A level of care and intuition should be applied when evaluating predictions made by H_γ . For example, AOTB and AOTSiB both produce $H_\gamma = 0.67$. However, AOTSiB is a super-effective surfactant generating $\gamma_{\text{cmc}} = 24.3 \text{ mN m}^{-1}$. Given the increased volume of the chain-tip for AOTSiB over AOTB, it would be expected that AOTSiB would produce a slightly higher value of H_γ . The equation is not equipped to include this increased volume of the chain tip, however, it would be similar to $\beta/3$ being slightly larger than 1, producing a value of H_γ over the 0.70 requirement of super-effective HC surfactants.

By comparing surface properties for the most effective hydrocarbon surfactants, for the first time it has been possible to identify general structure property relationships shared by all effective HC surfactants. H_γ is a simple, empirical measure which encapsulates these structure-property relationships, allowing an initial assessment of surfactant structure and potential performance. This will provide a useful tool to help guide the design of novel, low surface energy hydrocarbon surfactants. In this chapter, the potential of hydrocarbon surfactants to rival and replace conventional fluorocarbon surfactants has been established. Now with the introduction of H_γ , a secured future lies ahead for generating low surface tensions in an environmentally friendly, 21st century manner.

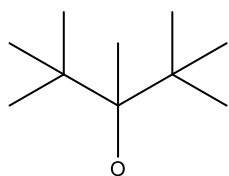
Short tails - Longest chain length ≤ 3

Single alkyl chain

$$H_{\gamma} = \frac{\text{Total CH}_3 \text{ groups}}{\text{Longest chain length}}$$



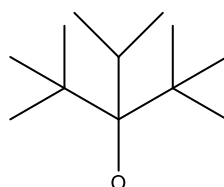
$$H_{\gamma} = 1.33$$



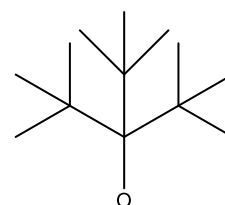
$$H_{\gamma} = 1.00$$

Multiple alkyl chains

$$H_{\gamma} = \frac{\text{Total } H_{\gamma} \text{ for each alkyl chain}}{2}$$



$$H_{\gamma} = 0.83$$



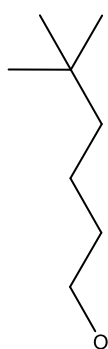
$$H_{\gamma} = 1.00$$

Long tails - Longest chain length ≥ 4

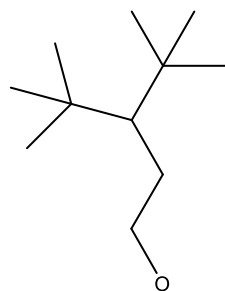
$$H_{\gamma} = \frac{\frac{\beta}{3}(x - \alpha)}{\text{Total tail carbon number}}$$

$$\alpha = \frac{(1 \times C_x) + (1 \times C_x) \text{ etc.}}{\text{Total number of branches}}$$

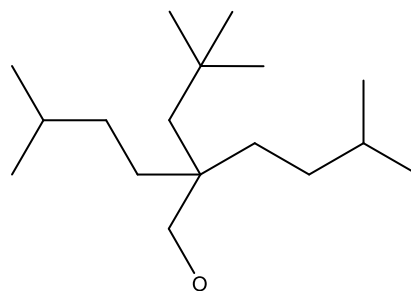
If multiple branches present on one tail, the contribution to H_{γ} is additive if the branched group is ± 2 the chain length of the tail, otherwise deductive. If symmetrical, the individual values of H_{γ} are multiplied, not summed.



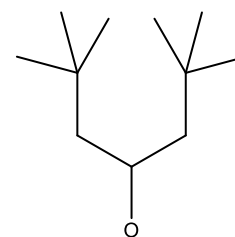
$$H_{\gamma} = 0.75$$



$$H_{\gamma} = 0.91$$



$$H_{\gamma} = 0.81$$



$$H_{\gamma} = 1.45$$

Figure 5.30: Predicted tail structures that could generate $\gamma_{cmc} < 25 \text{ mN m}^{-1}$ based on H_{γ} for long and short alkyl tails.

5.6 Conclusions

In this chapter the structure-property relationships of effective hydrocarbon surfactants have been outlined. Two novel series of hydrocarbon surfactants have been introduced, generating the lowest surface energies currently reported for hydrocarbon surfactants (AOTSiC $\gamma_{\text{cmc}} = 22.8 \text{ mN m}^{-1}$). These surface energies outperform certain fluorocarbon surfactants (di-HCF6 $\gamma_{\text{cmc}} = 24.1 \text{ mN m}^{-1}$),³⁹ and are approaching the surface tensions of pure liquid alkanes ($\gamma_{\text{octane}} = 21.6 \text{ mN m}^{-1}$, $\gamma_{\text{nonane}} = 22.9 \text{ mN m}^{-1}$). This has been achieved by identifying structure-property relationships of effective surfactants by making small systematic variations in the molecular structure of the tail, whilst studying adsorption and aggregation phenomena by tensiometry and small-angle neutron scattering (SANS). Previous investigations have identified structure-property relationships by studying an assorted variety of structures, as opposed to a systematic collection (refs. [4, 5, 10]). By adopting the systematic approach, the subtle relationships between structure and performance are revealed, allowing general structure-property relationships to be identified for HC surfactants. All super-effective hydrocarbon surfactants which generate surface tensions $< 25 \text{ mN m}^{-1}$ have been shown to share structural characteristics in the surfactant tail. These can be summarised as: a) a highly branched chain-tip, b) reduced branching away from the chain-tip, c) a long alkyl chain length (provided (a) and (b) are met). By comparing the most common surface properties for over 20 effective hydrocarbon surfactants, no trend was found which could relate low γ_{cmc} to the molecular structure of the surfactant tail. Based on the structure-property relationships of highly effective hydrocarbon surfactants, a new index to assess surfactant effectiveness, H_γ , is introduced. This predicts whether a particular tail structure is likely to generate a super-effective hydrocarbon surfactant ($\gamma_{\text{cmc}} < 25 \text{ mN m}^{-1}$) based on simply the structure of the tail, where super-effective surfactants generate $H_\gamma \geq 0.70$. Using the effectiveness index H_γ , predicted tail structures that could generate $\gamma_{\text{cmc}} < 25 \text{ mN m}^{-1}$ are highlighted. Thus, a method to guide the design of super-effective hydrocarbon surfactants has been established. This provides a new outlook on how to generate the lowest surface energies with novel, highly branched, hydrocarbon surfactants. Defining a strong future for hydrocarbon surfactants to rival and replace effective, but environmentally hazardous fluorocarbon surfactants.

References

- [1] Jasper, J. J.; Kring, E. V. *J. Phys. Chem.* **1955**, *59*, 1019–1021.
- [2] Czajka, A.; Hazell, G.; Eastoe, J. *Langmuir* **2015**, *31*, 8205–8217.
- [3] Czajka, A.; Hill, C.; Peach, J.; Pegg, J. C.; Grillo, I.; Guittard, F.; Rogers, S. E.; Sagisaka, M.; Eastoe, J. *Phys. Chem. Chem. Phys.* **2017**, *19*, 23869–23877.
- [4] Alexander, S.; Smith, G. N.; James, C.; Rogers, S. E.; Guittard, F.; Sagisaka, M.; Eastoe, J. *Langmuir* **2014**, *30*, 3413–3421.
- [5] Sagisaka, M.; Narumi, T.; Niwase, M.; Narita, S.; Ohata, A.; James, C.; Yoshizawa, A.; Taffin de Givenchy, E.; Guittard, F.; Alexander, S. *Langmuir* **2014**, *30*, 6057–6063.
- [6] Robbins, J. *Ions in solution: an introduction to electrochemistry*; CUP Archive, 1972; Vol. 2.
- [7] Atkins, P.; De Paula, J. *Atkins' physical chemistry*; OUP Oxford, 2006; Vol. 8.
- [8] Moore, W. J. *Physical Chemistry*; Longman, 1972; Vol. 1.
- [9] Klevens, H. *J. Am. Oil Chem. Soc.* **1953**, *30*, 74–80.
- [10] Nave, S.; Eastoe, J.; Penfold, J. *Langmuir* **2000**, *16*, 8733–8740.
- [11] An, S.; Lu, J.; Thomas, R.; Penfold, J. *Langmuir* **1996**, *12*, 2446–2453.
- [12] Bae, S.; Haage, K.; Wantke, K.; Motschmann, H. *J. Phys. Chem. B* **1999**, *103*, 1045–1050.
- [13] Hall, D. G. *Colloids Surf., A* **1994**, *90*, 285–288.

- [14] Hall, D. G.; Pethica, B. A.; Shinoda, K. *Bull. Chem. Soc. Jpn.* **1975**, *48*, 324–326.
- [15] Lu, J.; Lee, E.; Thomas, R.; Penfold, J.; Flitsch, S. *Langmuir* **1993**, *9*, 1352–1360.
- [16] Hines, J.; Garrett, P.; Rennie, G.; Thomas, R.; Penfold, J. *J. Phys. Chem. B* **1997**, *101*, 7121–7126.
- [17] Hines, J.; Thomas, R.; Garrett, P. R.; Rennie, G.; Penfold, J. *J. Phys. Chem. B* **1997**, *101*, 9215–9223.
- [18] Tajima, K.; Muramatsu, M.; Sasaki, T. *Bull. Chem. Soc. Jpn.* **1970**, *43*, 1991–1998.
- [19] Li, Z.; Dong, C.; Thomas, R. *Langmuir* **1999**, *15*, 4392–4396.
- [20] Downer, A.; Eastoe, J.; Pitt, A. R.; Penfold, J.; Heenan, R. K. *Colloids Surf., A* **1999**, *156*, 33–48.
- [21] Shinoda, K.; Nakayama, H. *J. Colloid Interface Sci.* **1963**, *18*, 705–712.
- [22] Eastoe, J.; Nave, S.; Downer, A.; Paul, A.; Rankin, A.; Tribe, K.; Penfold, J. *Langmuir* **2000**, *16*, 4511–4518.
- [23] Li, Z.; Lu, J.; Thomas, R.; Penfold, J. *J. Phys. Chem. B* **1997**, *101*, 1615–1620.
- [24] Zisman, W. A. *Adv. Chem. Ser.* **1964**, *43*, 1–51.
- [25] Sastri, S.; Rao, K. *Biochem. Eng. J.* **1995**, *59*, 181–186.
- [26] Leroy, P.; Lassin, A.; Azaroual, M.; André, L. *Geochim. Cosmochim. Acta* **2010**, *74*, 5427–5442.
- [27] Krafft, M. P.; Riess, J. G. *Chem. Rev.* **2009**, *109*, 1714–1792.
- [28] Gold, S.; Eastoe, J.; Grilli, R.; Steytler, D. C. *Colloid. Polym. Sci.* **2006**, *284*, 1333–1337.
- [29] Lunkenheimer, K.; Haage, K.; Hirte, R. *Langmuir* **1999**, *15*, 1052–1058.

- [30] Eastoe, J.; Downer, A.; Paul, A.; Steytler, D. C.; Rumsey, E.; Penfold, J.; Heenan, R. K. *Phys. Chem. Chem. Phys.* **2000**, *2*, 5235–5242.
- [31] Knoche, M.; Tamura, H.; Bukovac, M. J. *J. Agric. Food. Chem.* **1991**, *39*, 202–206.
- [32] Bergström, M.; Pedersen, J. S.; Schurtenberger, P.; Egelhaaf, S. U. *J. Phys. Chem. B* **1999**, *103*, 9888–9897.
- [33] Putra, E. G. R.; Ikram, A. *Indones. J. Chem.* **2010**, *6*, 117–120.
- [34] Hammouda, B. *J. Res. Natl. Inst. Stand. Technol.* **2013**, *118*, 151.
- [35] Brasher, L. L.; Kaler, E. W. *Langmuir* **1996**, *12*, 6270–6276.
- [36] Aswal, V.; Goyal, P. *Chem. Phys. Lett.* **2003**, *368*, 59–65.
- [37] Kekicheff, P.; Grabielle-Madelmont, C.; Ollivon, M. *J. Colloid Interface Sci.* **1989**, *131*, 112–132.
- [38] Lu, J. R.; Marrocco, A.; Su, T. J.; Thomas, R. K.; Penfold, J. *J. Colloid Interface Sci.* **1993**, *158*, 303–316.
- [39] Eastoe, J.; Paul, A.; Downer, A.; Steytler, D. C.; Rumsey, E. *Langmuir* **2002**, *18*, 3014–3017.

Chapter 6

Optimising Surfactant

Performance with the Head Group

This chapter aims to improve the performance of hydrocarbon surfactants by varying the head group. The vast majority of studies which relate surface tension to surfactant structure are predominantly concerned with surfactant tails. Methods for designing super-effective hydrocarbon surfactant tails which generate very low surface energies have been outlined in the previous chapter. Here, the study aims to provide insight into fine tuning the properties of hydrocarbon surfactants to generate surface densities to more effectively mimic a pure alkane, which is achieved by varying the head group, not the tail. Surface and bulk properties are explored through tensiometry and small-angle neutron scattering (SANS) for a variety of single-chain anionic surfactants. The tail structure is kept constant, whilst a variety of different counterions (sodium and tetraalkylammonium (TAA) ions) are studied. This highlights structure-property relationships for surface tension which are dependent on the head group. By making small, systematic variations in the head group structure, with a wide variety of different tail structures, the potential to improve surface effectiveness with TAA counterions is demonstrated. This potential has remained unnoticed until now, and provides a useful insight to design a new generation of super-effective hydrocarbon surfactants.

6.1 Introduction

It is commonly understood that the surface tension generated by surfactant molecules is strongly influenced by interfacial packing between the tails. As highlighted previously in Chapter 5, for hydrocarbon (HC) surfactants low surface energies can be achieved by careful design of the surfactant tail to generate dense surface coverages. However, a surfactant molecule is composed of both a head group (counterion) and a tail. Therefore by varying the counterion, is it possible to further improve the performance of an effective hydrocarbon surfactant?

By varying the counterion the degree of binding between surfactant and counterion will be altered, which will consequently affect the bulk and surface structure formed in aqueous systems. The effect of counterion binding on anionic surfactants has been largely focused on micellisation,¹⁻³ and aggregation in bulk.^{4,5} Only a few studies have investigated the structure of the surfactant monolayer adsorbed at the air-water interface and hence, the change in surface tension.^{6,7} Penfold et al. studied the adsorption of dodecylsulfate surfactants (DS) with various monovalent counterions, by tensiometry. Interestingly, a notable difference in γ_{cmc} was observed with changing counterion, summarised in Figure 6.1. The surface tension increases by 3 mN m^{-1} when Li^+ is replaced by Na^+ , and a further 5 mN m^{-1} when replaced by Cs^+ . Even combined with neutron reflection experiments for these aqueous sys-

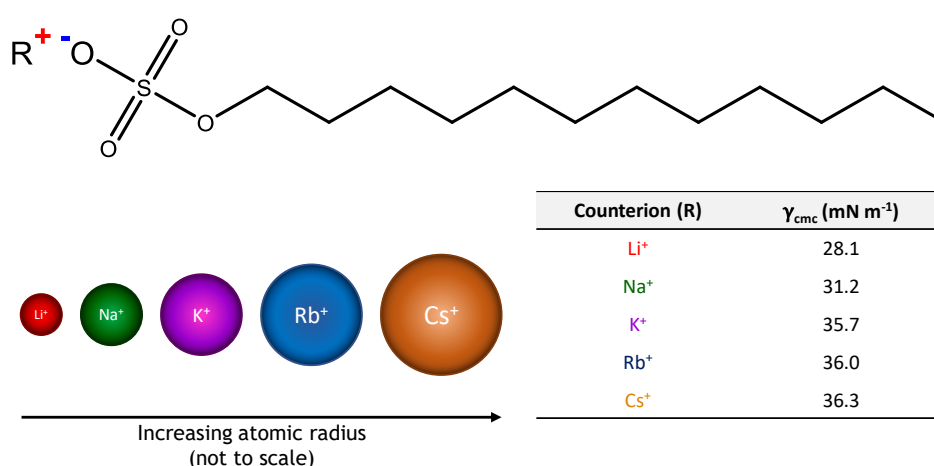


Figure 6.1: Variation in the equilibrium surface tension (γ_{cmc}) for dodecylsulfate (DS) surfactants bearing various monovalent metal counterions (R). Measurements made at 25 °C, data from ref. [7].

tems, Penfold et al. could not confidently rationalise the variation in surface tension. However from these results it is clear that the performance of surfactants is affected, and thus can be improved by varying the identity of the head group.

Surfactant counterions are commonly simple inorganic species such as sodium or potassium. Alternatives that are encountered are organic ions such as ethylsulfonate or tetramethylammonium. These are typically larger than inorganic metal ions and lower the cmc and solubility of ionic surfactants.⁸ Bonilha et al. determined that tetraalkylammonium (TAA^+) counterions bind more strongly than sodium to dodecylsulfate micelles.⁹ Brown et al. showed that TAA^+ ions can induce different aggregation structures, as well as controlling the phase behaviour for a variety of HC surfactants, as well as surfactant ionic liquids SAILS (i.e. ionic liquids which also show aggregation in aqueous solution).^{10,11} SAILS are an alternative ionic liquid (IL) which help to address the practical and environmental implications of common imidazolium based ILs. Although they have become more common in recent times, hydrophobic counterions (i.e. TAA^+) are encountered less in the literature than inorganic ions. As highlighted previously in Figure 6.1, changing the counterion could provide a useful approach to tune the properties of a particular surfactant, and TAA^+ ions offer properties that can outcompete certain simple metal ions.

Tetraalkylammonium counterions have been explored with a wide variety of surfactants which includes fluorocarbon,¹² hydrocarbon,¹³ and silicone surfactants.¹⁴ Aggregation within the bulk and the critical micelle concentration are the most commonly measured properties. Surface tension has been used to characterise surfactants with TAA^+ counterions,¹⁵ but is often only a secondary feature in the investigation. To date there are very few studies that investigate and compare the change in surface tension for anionic hydrocarbon surfactants with TAA^+ counterions. Brown et al. introduced a new series of SAILS which were based on common organic surfactant anions with substituted TAA^+ cations (ref. [6]). Figure 6.2 shows an overview of the surface tension data from this investigation collected for AOT-based surfactants. The equilibrium surface tension γ_{cmc} decreases by $\sim 4 \text{ mN m}^{-1}$ when Na^+ is replaced by TPA^+ , achieving $\gamma_{\text{cmc}} = 26.1 \text{ mN m}^{-1}$ which is approaching the super-effective surfactant domain ($\gamma_{\text{cmc}} < 25 \text{ mN m}^{-1}$). This was suggested to be because the packing efficiency between tails was balanced against electrostatic

head group repulsions, as well as an increase in the number of low surface energy methyl groups.

Organic counterions add additional complexity to surfactant-counterion interactions, with purely electrostatic interactions of simple metal ions being replaced by a thermodynamically complex balance between electrostatic and hydrophobic forces.¹⁶ From the data shown in Figure 6.2, this additional complexity can clearly act in a synergistic manner, further reducing γ_{cmc} for a particular surfactant. However, the reasons as to why this is remain unclear. The molecular volume of a TAA⁺ counterion is intrinsically larger than common simple inorganic metal ions. Perhaps this additional volume helps to generate a surfactant which can pack more efficiently at the surface, i.e simply put - the head group is a better ‘fit’ for the tail which allows a greater packing efficiency. To explore this idea, 16 single-chain anionic surfactants have been synthesised with a variety of TAA⁺ counterions to generate a systematic logical nature of surfactant structures. Surface tension and small-angle neutron scattering (SANS) data were collected, allowing structure-property relationships to be observed in the bulk, and at the surface. By keeping the tail constant whilst varying the head group, any improvements in surfactant effectiveness will be directly related to the head group. This is the approach that has been adopted in this study, where the tetrapropylammonium (TPA) counterion is highlighted as a suitable alternative for HC surfactants, able to reduce the surface tension below that of the alcohol precursor.

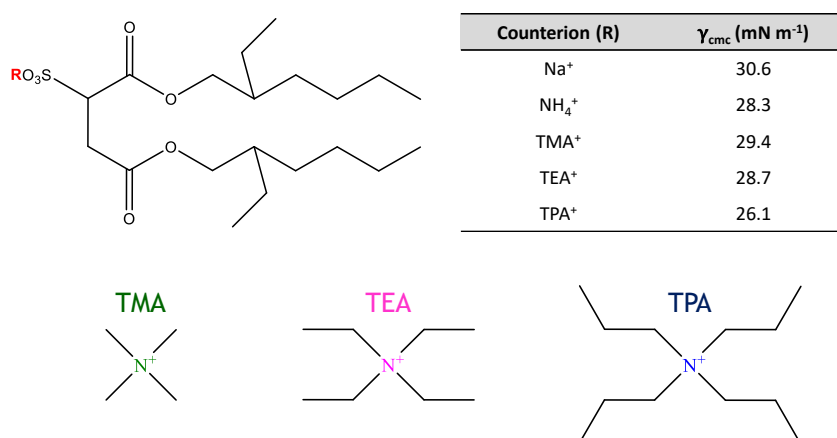


Figure 6.2: Variation in the equilibrium surface tension (γ_{cmc}) for AOT bearing various counterions (R). Measurements made at 25 °C, data from ref. [6].

6.1.1 Surfactants investigated

Sixteen single-chain anionic hydrocarbon surfactants were synthesised following the experimental procedure outlined in Section 4.3, molecular structures are shown in Figure 6.3. Each surfactant tail was synthesised with each of the four head groups (hence 16 surfactants total). The tails were selected to investigate the structure-property relationships of both large and small tails, allowing further comparison. FO180 and FO180N are both C18 tails and therefore only differ by their degree of branching. BC9 and BC7 have identical tails except BC9 possesses two extra CH_2 groups and thus is essentially a slightly elongated version of BC7 (BC7 is the single-chain version of HS3 introduced in the previous chapter). The TAA^+ head groups selected allow small, systematic variations in the structure to be examined. Furthermore, the Na^+ counterion provides a reference structure which allows the effects of incorporating TAA^+ counterions to be investigated. The analytical techniques NMR and EA show high purity for all surfactants, included in the Supporting Information.

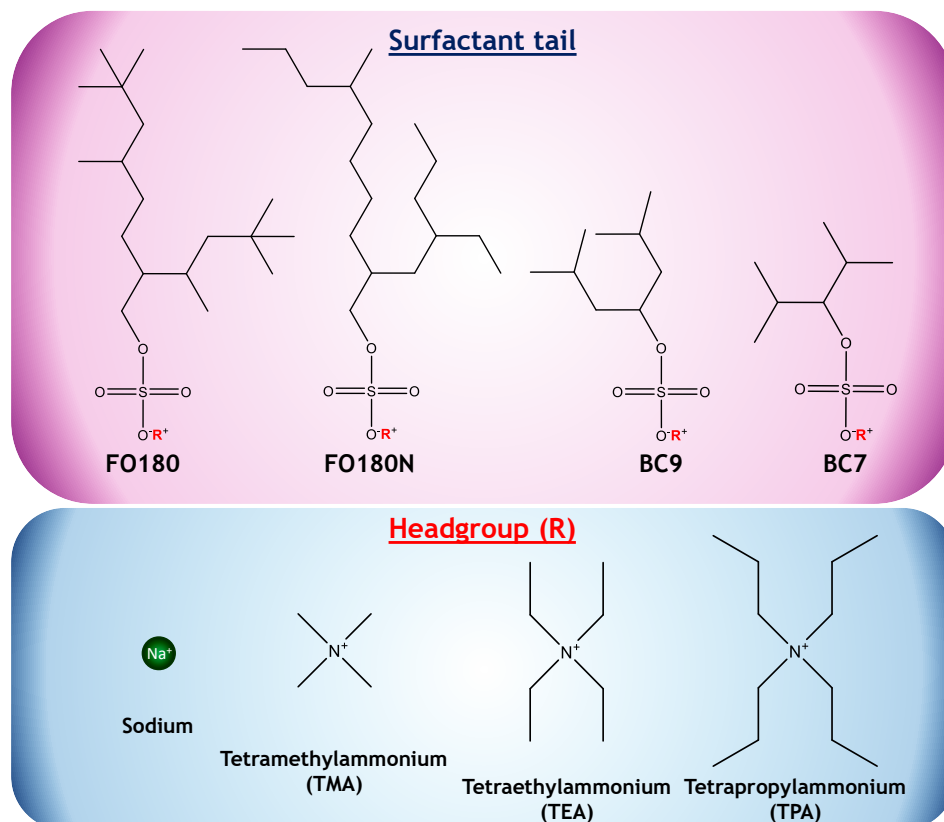


Figure 6.3: Molecular structures of surfactants investigated in this chapter. Each surfactant tail is synthesised with each of the four head groups

6.1.2 Determining surface properties of single-chain surfactants

To identify structure-property relationships of surfactants, an effective method is to compare physiochemical properties for a variety of different molecular structures. When trying to identify how the packing efficiency (and hence surface tension) is affected by varying the head group, suitable properties to compare are the cmc, γ_{cmc} , and A_{cmc} . These are fundamental properties for surfactants which can provide an insight into structural effects at the air-water interface. An overview of suitable methods and procedures for determining accurate surface properties has already been outlined in Section 5.2. The same methods, where appropriate, were applied to the single-chain surfactants discussed in this chapter. Because many of these surfactants do not possess simple inorganic metal counterions, minor variations are required to accurately account for the TAA⁺ counterions.

As highlighted in Section 5.2.1, with ionic surfactant solutions, activity should be used in place of concentration to account for the deviation from ideality. The mean activity coefficient can be estimated from the extended Debye-Hückel law:

$$\log \alpha_{\pm} = \frac{A|z_+z_-|I^{\frac{1}{2}}}{1 + BaI^{\frac{1}{2}}} \quad (6.1)$$

where A and B are constants, a is the mean effective ionic diameter, z is the ion charge and I is ionic strength. For surfactants with a Na counterion, a can be taken to equal 6 Å.¹⁷ For the TAA⁺ counterions that feature in this chapter, a was estimated as TMA = 6 Å, TEA = 4.5 Å, and TPA = 3 Å.¹⁸ To accurately determine both γ_{cmc} and A_{cmc} , it is important that the surface is free from any polyvalent Mⁿ⁺ ions. This can be achieved using the chelating agent EDTA (see Section 5.2.5). The surfactants discussed here were originally sulfonated, and then the corresponding TAA⁺ analogues formed by ion-exchange. Following the procedure outlined in Section 5.2.5, EDTA experiments performed on the TAA⁺ analogues observed no dramatic effect on the surface tension. This suggests that the ion-exchange process adequately removes polyvalent Mⁿ⁺ ions and hence, EDTA experiments do not need to be performed on these surfactants. However, it is important to still determine the optimum level of EDTA for all single-chain surfactants bearing a sodium counterion.

6.2 Surface properties

Using a K100 tensiometer, the surface tension as a function of activity was measured for each single-chain surfactant. The optimum EDTA:surfactant ratio was determined as 450:1, 250:1, 250:1 and 100:1 for Na-FO180, Na-FO180N, Na-BC9 and Na-BC7 respectively. Using the procedure described previously in Section 5.2.3, the cmc of each surfactant was determined from a Gaussian distribution applied over the double derivative of the surface tension data at the visual break point, an example for TMA-FO180 is shown in Figure 6.4. With the critical micelle concentration determined, both γ_{cmc} and A_{cmc} can be estimated following the procedures outlined in Section 5.2. The area per molecule is estimated from the surface excess Γ , determined from the Gibbs equation:

$$\Gamma = \frac{-1}{mRT} \left(\frac{d\gamma}{d \ln C} \right) \quad (6.2)$$

where m is the number of adsorbing species, R is the ideal gas constant, T is the temperature, γ is the surface tension, and C is the surfactant concentration. The γ - $\ln(a)$ plots for each single-chain surfactant are shown in Figures 6.5 and 6.6. Corresponding adsorption isotherms on a reduced concentration axes for fairer comparison (concentration/cmc) are also provided. Surface properties derived from the γ - $\ln(a)$ plots are shown in Table 6.1.

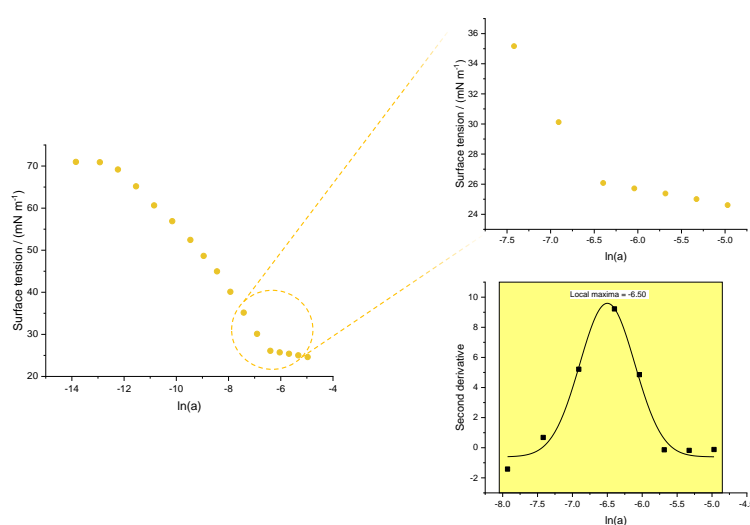


Figure 6.4: Procedure used to find the cmc from surface tension data. The double derivative of γ with respect to activity is taken around the cmc. A Gaussian distribution is then applied to accurately highlight the inflexion point, i.e. the cmc.

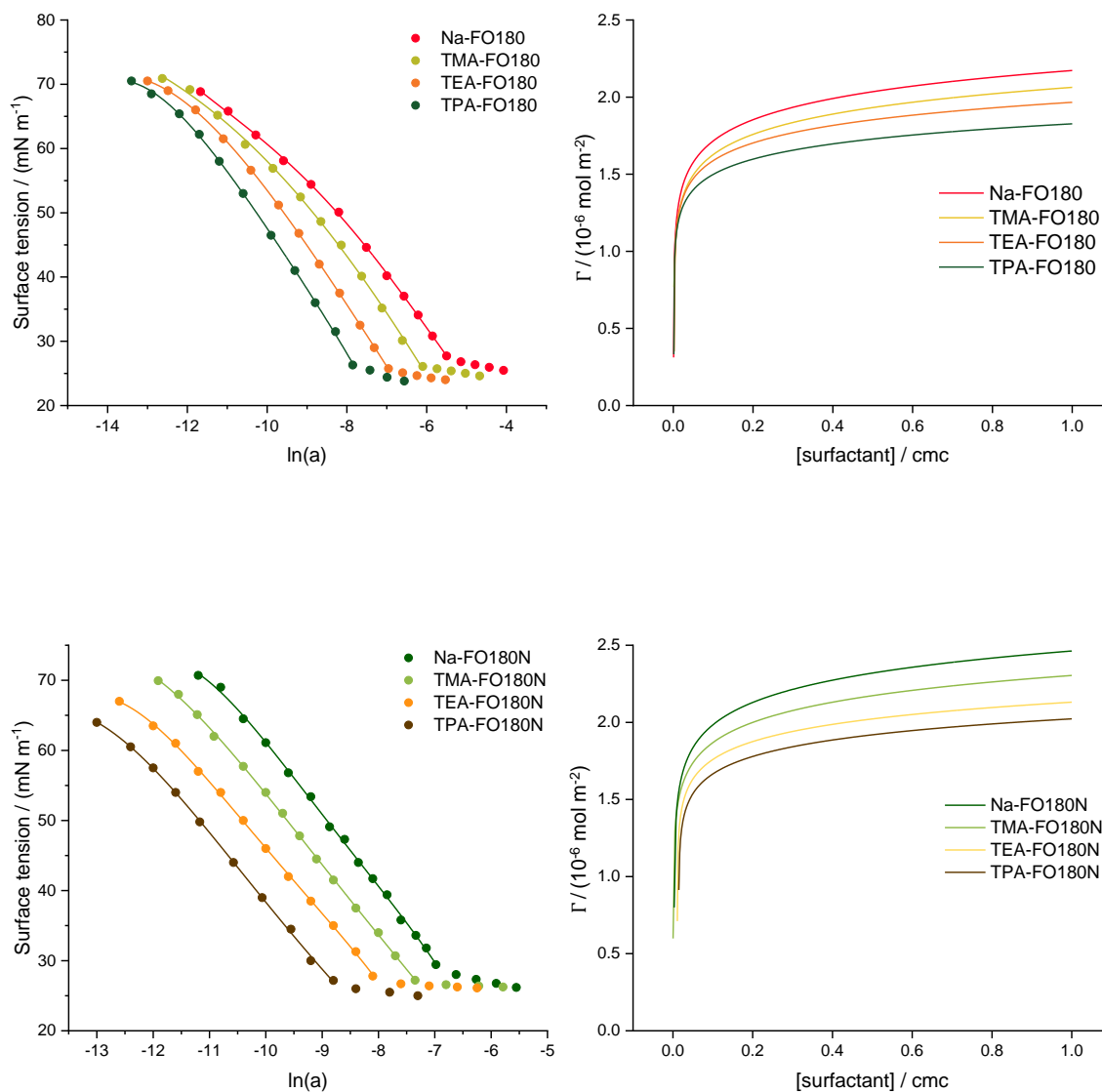


Figure 6.5: γ - $\ln(a)$ plots shown on the left for the FO180 and FO180N surfactant series at 25 °C (EDTA ratios noted in the text). Lines offset by $\pm 0.5 \ln(a)$ to improve clarity. Polynomial lines fitted to pre-cmc data are shown. Corresponding Γ vs reduced concentration (conc/cmc) adsorption isotherms for each surfactant shown on the right. Tensiometric parameters are listed in Table 6.1.

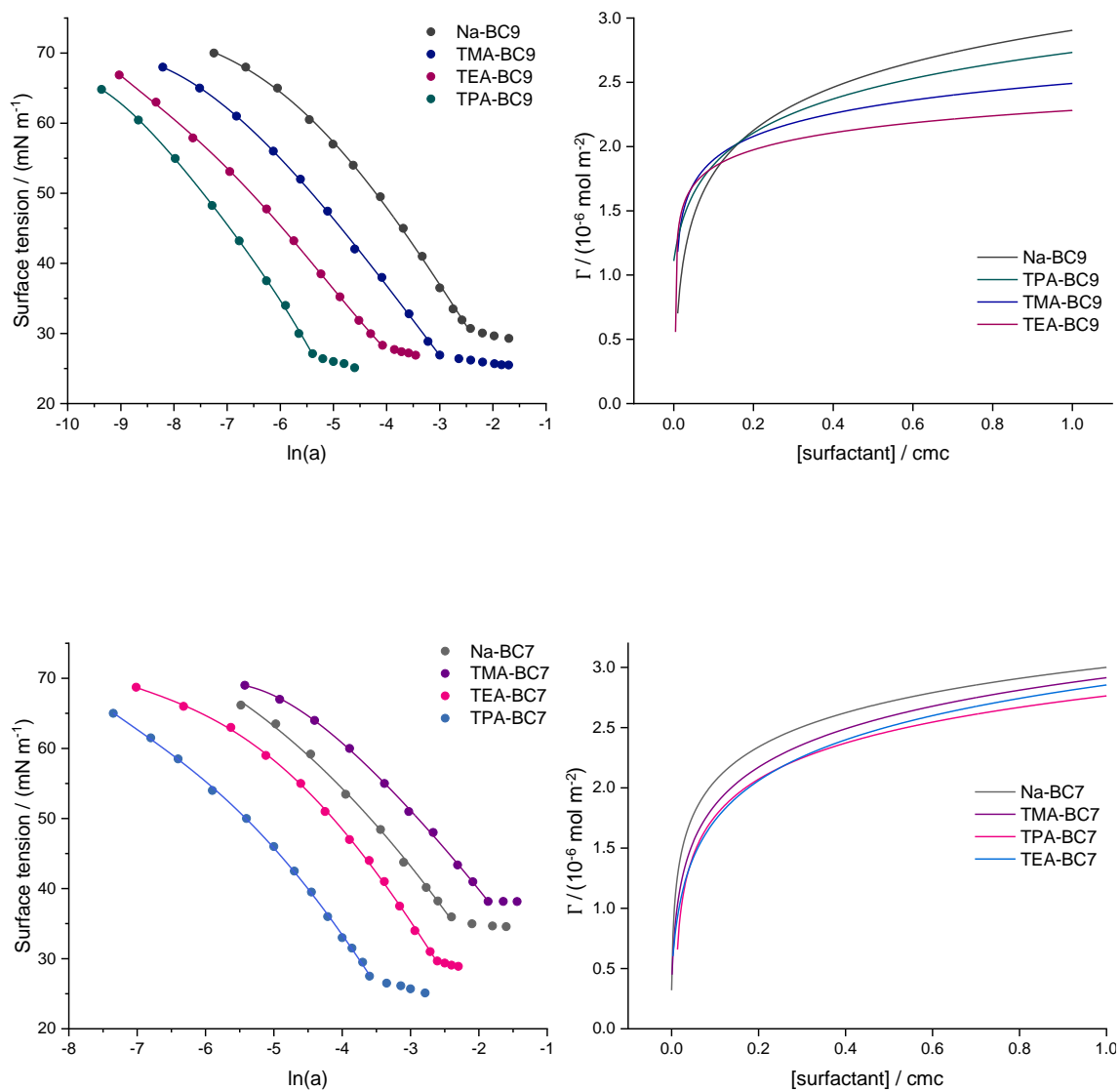


Figure 6.6: γ - $\ln(a)$ plots shown on the left for the BC9 and BC7 surfactant series at 25 °C (EDTA ratios noted in the text). Lines offset by $\pm 1 \ln(a)$ to improve clarity. Polynomial lines fitted to pre-cmc data are shown. Corresponding Γ vs reduced concentration (conc/cmc) adsorption isotherms for each surfactant shown on the right. Tensiometric parameters are listed in Table 6.1.

6.2.1 Critical micelle concentration

Previous studies with surfactants bearing TAA⁺ counterions suggest a greater negative free energy of micellisation upon increasing counterion size (ref. [8]). The work presented here agrees with this, where the cmc decreases in the order: Na⁺ > TMA⁺ > TEA⁺ > TPA⁺ for each surfactant series. This trend is highlighted in Figure 6.7. For ionic surfactants, as the hydration radius of the counterion decreases so should the degree of dissociation, which overall promotes micellisation. However, this effect is weak, and for organic counterions this can be overshadowed by hydrophobic interactions. Bonilha et al. showed that the binding strength of the TAA⁺ ion is dominated by their hydrophobicity, independent of the spatial distribution of the alkyl groups attached to nitrogen (ref. [9]). Furthermore, the binding affinities were considerably lower than expected, given the total chain hydrophobicity. Hence, it

Surfactant	cmc (mM)	γ_{cmc} (mN m ⁻¹) ± 0.2	A_{cmc} (Å ²) ± 2
Na-FO180	2.63 ± 0.03	27.2	92
TMA-FO180	1.50 ± 0.03	26.1	104
TEA-FO180	1.03 ± 0.03	25.7	110
TPA-FO180	0.891 ± 0.03	26.3	134
Na-FO180N	1.08 ± 0.03	27.5	69
TMA-FO180N	0.623 ± 0.03	27.8	82
TEA-FO180N	0.586 ± 0.03	26.9	102
TPA-FO180N	0.382 ± 0.03	26.8	110
Na-BC9	50.5 ± 0.3	30.8	56
TMA-BC9	40.3 ± 0.3	26.7	82
TEA-BC9	32.5 ± 0.3	28.1	92
TPA-BC9	9.91 ± 0.03	26.0	72
Na-BC7	408 ± 3	34.9	56
TMA-BC7	157 ± 3	38.1	65
TEA-BC7	67.4 ± 0.3	29.9	70
TPA-BC7	12.7 ± 0.3	26.9	69

Table 6.1: Surface properties derived from γ -ln(a) plots for the FO180, FO180N, BC9 and BC7 surfactant series.

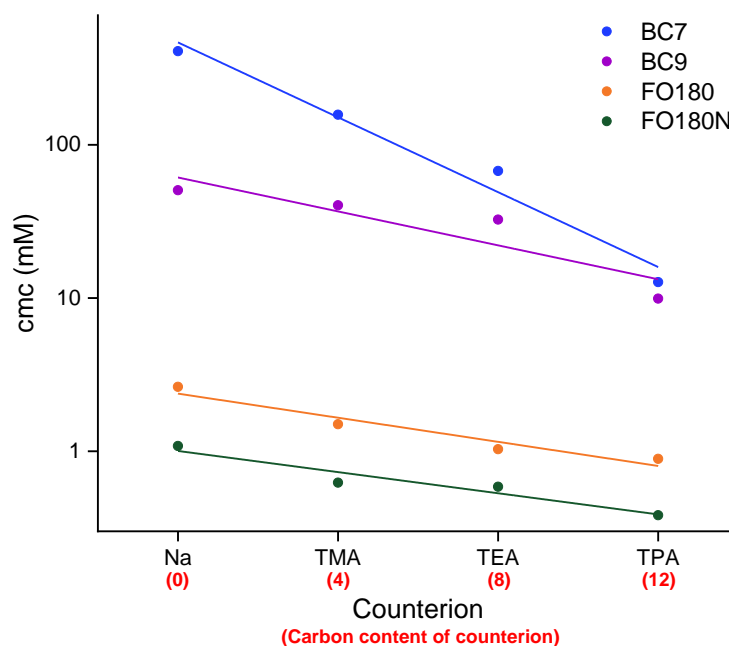


Figure 6.7: Variation in the critical micelle concentration for each single-chain surfactant series as the counterion is varied. Linear fits highlight the decreasing cmc with increasing counterion size.

would be expected that the decrease in cmc with increasing TAA⁺ counterion size will not be substantial, as is observed here. From the linear fits shown in Figure 6.7, the smaller the surfactant tail, the greater the decrease in cmc with increasing counterion size. This would be expected, as FO180/FO180N are C18 chains and therefore intrinsically hydrophobic. BC7 and BC9 being C7 and C9 chains respectively, could experience a greater increase in hydrophobicity with increasing counterion size. Furthermore, because the difference in cmc is smaller from Na-FO180 to TPA-FO180, compared to for example Na-BC9 to TPA-BC9, this highlights that for the more hydrophobic tails not all carbons are thermodynamically equivalent. For these systems, methylene groups added to the TAA⁺ counterion exhibit a weaker influence on the cmc; similar observations have been reported before for di-chain anionic surfactants (ref. [6]). It should also be highlighted that TPA-FO180/FO180N are at the limit of solubility. As TBA (tetrabutylammonium) equivalents were synthesised, but found to be insoluble in aqueous systems at room temperature.

6.2.2 Surface tension

From the γ_{cmc} values shown in Table 6.1, the surface activity is clearly altered as the counterion is changed. This is more pronounced for the smaller surfactant tails with BC7 showing a decrease of $\sim 10 \text{ mN m}^{-1}$ as the counterion is changed from Na^+ to TPA^+ , whereas for FO180 the difference is $\sim 1 \text{ mN m}^{-1}$. This can be explained by the relative hydrophobicity of the surfactant anion. Na-BC9 and Na-BC7 possess 9 and 7 carbons respectively in the molecular structure and are thus weakly hydrophobic, with $\text{cmc}'\text{s} = 50.5$ and 408 mM respectively. Therefore, such surfactants would perhaps expect to be insufficiently hydrophobic to strongly associate at the air-water interface producing a dense surface coverage. This is reflected in their γ_{cmc} values, 30.8 and 34.9 mN m^{-1} for Na-BC9 and Na-BC7 respectively. As the size of the counterion increases, the surfactant molecule will begin to possess sufficient hydrophobicity to promote dense surface coverages and hence higher surface activity. For both the BC9 and BC7 single-chain surfactant series, the lowest γ_{cmc} is generated by the TPA form of the surfactant. This highlights that for all surfactant molecules, to generate low γ_{cmc} a sufficient hydrophobicity is required to promote dense surface coverages. For single-chain surfactants with a small surfactant tail ($< \text{C}10$), a sodium counterion is likely to produce an ineffective surfactant. However, increasing hydrophobicity through large organic counterions is a suitable method to greatly improve surface activity.

The BC7 and BC9 single-chain surfactant series introduced here possess surfactant tails which have been introduced in the previous chapter as di-chain surfactants di-BC₉SS and HS3 (BC7). It is of interest to compare the properties of these surfactant anions when in single-chain and di-chain surfactant form. In Section 5.3.1, surface tension values for alcohol precursors were provided. Table 6.2 provides similar data but for alcohol precursors of surfactants that feature in this chapter. As single-chain surfactants, the lowest surface energies generated are 26.0 and 26.9 mN m^{-1} for TPA-BC9 and TPA-BC7 respectively. In comparison, the di-chain surfactants di-BC₉SS and HS3 generate $\gamma_{\text{cmc}} = 24.5$ and 29.7 mN m^{-1} respectively. Interestingly the anion of BC9 generates lower γ_{cmc} as a di-chain surfactant, but BC7 as a single-chain surfactant. This is perhaps due to the enhanced flexibility of BC9 over BC7, possessing two further CH_2 groups along the tail. Therefore, when present as

di-chain surfactants with two tails closely neighbouring each other, BC9 will be able to more readily adopt conformations generating high surface densities. BC7 with its short, bulky tail structure struggles to mimic pure alkane densities at the surface as a di-chain surfactant (HS3 $\gamma_{\text{cmc}} = 29.7 \text{ mN m}^{-1}$). As a single-chain surfactant there is more conformational freedom between neighbouring tails by not being bound to the same head group, which you would expect to be more suitable for a short, bulky tail structure. As a single-chain surfactant, BC7 lacks sufficient hydrophobicity to promote adequate adsorption, which can be addressed by a bulky organic head group. From the surface tension values of the parent alcohols provided in Table 6.2, it is clear that TPA-BC7 is close to the limit of achievable performance, achieving $\gamma_{\text{cmc}} = 26.9 \text{ mN m}^{-1}$, compared to the parent alcohol 2,4-Dimethyl-3-pentanol generating $\gamma = 24.9 \text{ mN m}^{-1}$.

Surface properties for select members of the FO180 and FO180N surfactant series have been presented previously (ref. [19]). The cmc values shown in Table 6.1 compare well with the literature values however, γ_{cmc} and A_{cmc} values do not, with noticeably higher γ_{cmc} values being quoted in Table 6.1. The synthetic procedure outlined in ref. [19] does not involve glacial acetic acid and therefore does not eliminate common contaminants when reacting with chlorosulfonic acid, evident by respective ^1H NMR of equivalent surfactants. Comparing γ for the alcohol precursors in Table 6.2 of FO180 and FO180N, to the lowest γ_{cmc} generated by these single-chain surfactants (TEA-FO180 & TPA-FO180N) an interesting observation can be made. The surface tension of these particular single-chain surfactants is below that of the parent alcohols. This suggests that the surfactant is more effective than the alcohol at generating the surface density of a pure alkane. This observation has knowingly, never been made before for anionic HC surfactants. From the surface properties

Alcohol	γ (mN m^{-1}) ± 0.1
2,4-Dimethyl-3-pentanol (HS3/BC7)	24.9
2,6-Dimethyl-4-heptanol (di-BC ₉ SS/BC9)	23.1
FO180	25.8
FO180N	27.8

Table 6.2: Surface tension for select alcohols which are precursors for surfactants synthesised in this chapter. All measurements made at 25 °C.

shown in Table 6.1, as the head group is varied from $\text{Na}^+ \rightarrow \text{TPA}^+$, for both the FO180 and FO180N surfactant series, the variation in γ_{cmc} is small. FO180 generates lower surface energies than all FO180N equivalents, likely due to the greater number of low surface energy CH_3 groups.²⁰ TEA-FO180 generates $\gamma_{\text{cmc}} = 25.7 \text{ mN m}^{-1}$, which is approaching surface energies of super-effective hydrocarbon surfactants ($< 25 \text{ mN m}^{-1}$). This is very low for a single-chain hydrocarbon surfactant. Due to the hydrophobic nature of FO180/FO180N tails, being C18 chains, surfactant molecules will strongly adsorb to the air-water interface. This is highlighted by the small variation in γ_{cmc} as counterion size is increased. Therefore, the variation in γ_{cmc} is due to a variation in packing efficiency brought on by a change in the head group. An interesting question arises; “Is it possible to identify a particular head group which more suitably accommodates a particular tail, improving packing efficiency?” This cannot be confidently assessed from γ_{cmc} alone.

6.2.3 Area occupied at the air-water interface

The area per molecule, or A_{cmc} , represents the average area that a surfactant molecule occupies at the air-water interface. It therefore provides a measure into how surfactant molecules are packing at the surface, highlighting structure-property relationships of surface tension. For all surfactants shown in Table 6.1, the area per molecule increases as the counterion is varied from Na^+ to TAA^+ . This is what would be expected, given the increased size of the head group. Similar trends have been found previously for several other TAA^+ hydrocarbon surfactant series (refs. [6, 19, 21]). Figure 6.8 shows the variation in γ_{cmc} and corresponding A_{cmc} with changing counterion for each surfactant series. The lowest γ_{cmc} generated by each surfactant series is highlighted by a dashed circle, as is the corresponding area per molecule. From evaluating the data shown in Figure 6.8, there appears to be an interesting observation relating γ_{cmc} and A_{cmc} for the most effective surfactants. Namely, the area per molecule shows an unexpected decrease for the counterion that generates the lowest surface tension. A smaller value for A_{cmc} suggests a more tightly packed surface film. This therefore suggests that for a particular tail, a certain TAA^+ counterion helps to further accommodate efficient packing between surfactant molecules. A similar trend was found for AOT bearing the same TAA^+

counterions, with the most effective surfactant TPA-AOT showing a lower than expected A_{cmc} given the trend from $\text{Na}^+ \rightarrow \text{TEA}^+$ (ref. [6]). Interestingly for all surfactant series studied, including AOT, the lowest surface energies are generated by the TPA form of the surfactant, except FO180 where this is true for TEA. Previous studies have suggested that for larger TAA⁺ counterions (TPA⁺ and TBA⁺), a single alkyl chain may penetrate into micelles (ref. [8]). Also, a study of TMADS concluded a penetration of part of the TMA⁺ ions at the air-water interface.²² Perhaps penetration of the counterion helps to generate densities which mimic a pure alkane surface. Small-angle neutron scattering (SANS) studies of the bulk aggregates formed could allow observations of this effect.

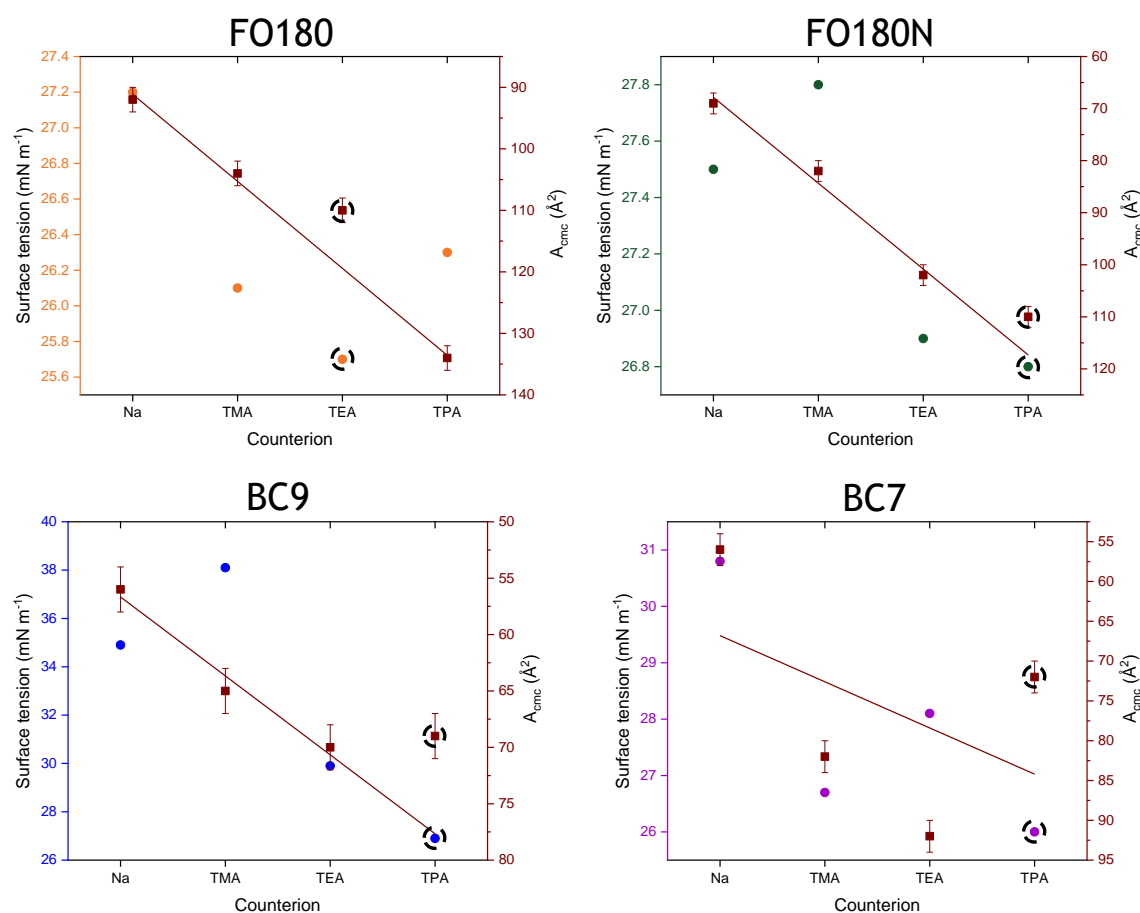


Figure 6.8: The surface tension at the cmc, as well as corresponding area per molecule (A_{cmc}) for each single-chain surfactant. Lines represent linear fits applied to A_{cmc} data. Lowest surface tension and corresponding area per molecule highlighted by a dashed circle for each surfactant series.

6.3 Small-angle neutron scattering

Small-angle neutron scattering (SANS) data were collected as consistent fractions above the cmc for all single-chain surfactants except the BC7 series. Scattering profiles for the FO180 and FO180N series are well described by a lamellar form factor with bilayer thickness D , and a distribution of thicknesses σ . The lowest concentration of Na-FO180 showed the formation of cylindrical aggregates with a cylinder radius C_r , and cylinder length C_l . The BC9 family produced scattering profiles which are consistent with charged spherical micelles, described by a spherical form factor with sphere radius R_{sphere} , polydispersity σ , multiplied by a Hayter-Penfold structure factor with charge z . The BC7 series could not be studied by SANS, due to weak scattering from small aggregates.

Scattering profiles for the FO180 and FO180N series are shown in Figures 6.9 and 6.10 respectively, where the lines represent fits to a lamellar form factor. The SANS parameters obtained from the fitted functions are included in Tables 6.3 and 6.4 for FO180 and FO180N respectively. Select members of the FO180/FO180N surfactant series presented here have been studied by SANS previously (ref. [19]) Aggregates of Na-FO180, TPA-FO180 and Na-FO180N were shown to form lamellar aggregates, which is consistent with the scattering profiles presented here. However, there was no change in the aggregate structure from cylinder to lamellar as observed here. The SANS parameters shown in Tables 6.3 and 6.4 agree well with that found previously in the literature. As the concentration is increased, for both surfactant series the lamellar bilayer thickness increases, although only subtly. Furthermore, as the counterion size is increased, the bilayer thickness appears to increase but again, only subtly. When comparing SANS parameters for the Na and TPA form of FO180/FO180N, the bilayer thickness shows a slight increase. This suggests ion association in these systems. However, if there was penetration of the TAA⁺ alkyl chain into the micelles, a larger increase in bilayer thickness would be expected. Previous SANS studies of TAA⁺ surfactants showed no penetration into the micelle for DS (dodecylsulfate) or AOT equivalents (ref. [6]). Studies of TAA⁺-AOT showed rich structural variation, forming a variety of different aggregate shapes with changing counterion. That is not what is observed here, with a lamellar structure dominating the aggregates formed. This highlights the greater effect of the surfac-

tant anion over the cation for these systems. Where overall, the organic head groups have little to no effect on the aggregates formed in both shape and size. This is perhaps due to the greater carbon number of the anion over even the largest cation, which will hence therefore dominate packing driven by the hydrophobic effect.

Scattering profiles for the BC9 series are shown in Figure 6.11, corresponding model fit parameters are included in Table 6.5. All surfactants in the BC9 surfactant series are well described by a spherical form factor with sphere radius R_{sphere} , and polydispersity σ . Na-BC9 through to TEA-BC9 show a mid-Q peak which is characteristic of charged micelles. The scattering profiles for these particular surfactants were multiplied by a Hayter-Penfold structure factor with charge z . Interestingly TPA-BC9 was more adequately described as uncharged spherical micelles. This suggests the larger TPA organic counterion helps to reduce repulsive interactions between micelles. From the radii shown in Table 6.5, there is a clear increase as the counterion is changed from Na^+ and TPA^+ . This suggests there is ion association between the cation and anion in TPA-BC9. Therefore, perhaps the long alkyl chains present on TPA help to overcome repulsion between neighbouring micelles. For the other members of this surfactant series, the sphere radius shows a subtle increase with increasing cation size, similar to the FO180/N series. The charge follows an expected increase as the concentration of surfactant in solution is increased.

It is apparent from the SANS data that the TAA^+ counterions have only a secondary effect on packing within the bulk. For the systems studied here, both the shape and size of the aggregates show no drastic effects when sodium is replaced. For all surfactant series studied, the greatest structural effects were seen when changing from Na^+ to TPA^+ . This would suggest that the TPA ions bind more strongly to the surfactant anion, consequently having a greater effect on surfactant molecules packing in the bulk. This agrees well with the work of Bonilha et al. (ref. [9]), which highlighted that the binding strength of alkylammonium ions is dominated by their hydrophobicity. As highlighted in the previous section, the most effective surfactant from each series presented here possesses a TPA counterion (except TEA-FO180). SANS studies suggest that this ion binds most strongly to the anion. Therefore, perhaps the increased molecular volume of the TAA^+ counterion is not responsible for enhanced surface packing, and it is the increased counterion binding strength.

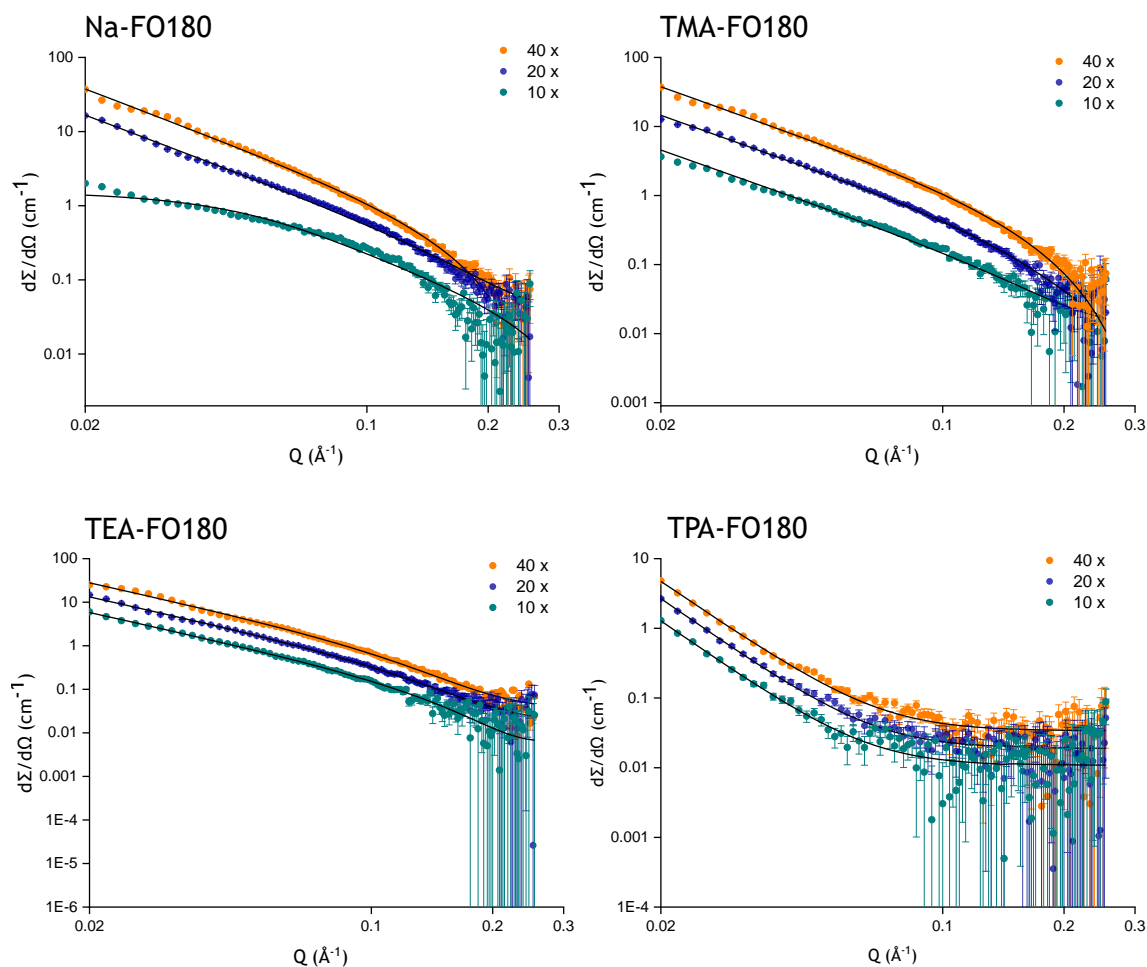


Figure 6.9: SANS profiles for Na-FO180, TMA-FO180, TEA-FO180 and TPA-FO180 in D_2O over a range of concentrations which are consistent multiples of the cmc. Measurements were made at 25 °C. The lines are fitted functions for scattering laws as described in the text. Data for all surfactants are from LOQ, ISIS.

Table 6.3: SANS model fit parameters to the Lamellar and Cylinder Structure models for the FO180 hedgehog surfactant series in D_2O . Parameters: bilayer thickness - D , polydispersity - σ , cylinder radius - C_r , cylinder length - C_l .

Parameter	Na-FO180			TMA-FO180			TEA-FO180			TPA-FO180		
	40x	20x	10x	40x	20x	10x	40x	20x	10x	40x	20x	10x
Conc x cmc	40x	20x	10x	40x	20x	10x	40x	20x	10x	40x	20x	10x
D (Å) \pm 0.1	19.3	17.6	-	20.2	19.9	19.3	21.8	20.6	22.8	24.3	21.3	22.8
σ	-	-	-	-	-	-	0.44	0.44	0.10	0.68	0.59	0.70
C_r (Å) \pm 0.1	-	-	16.1	-	-	-	-	-	-	-	-	-
C_l (Å) \pm 0.1	-	-	7.07	-	-	-	-	-	-	-	-	-

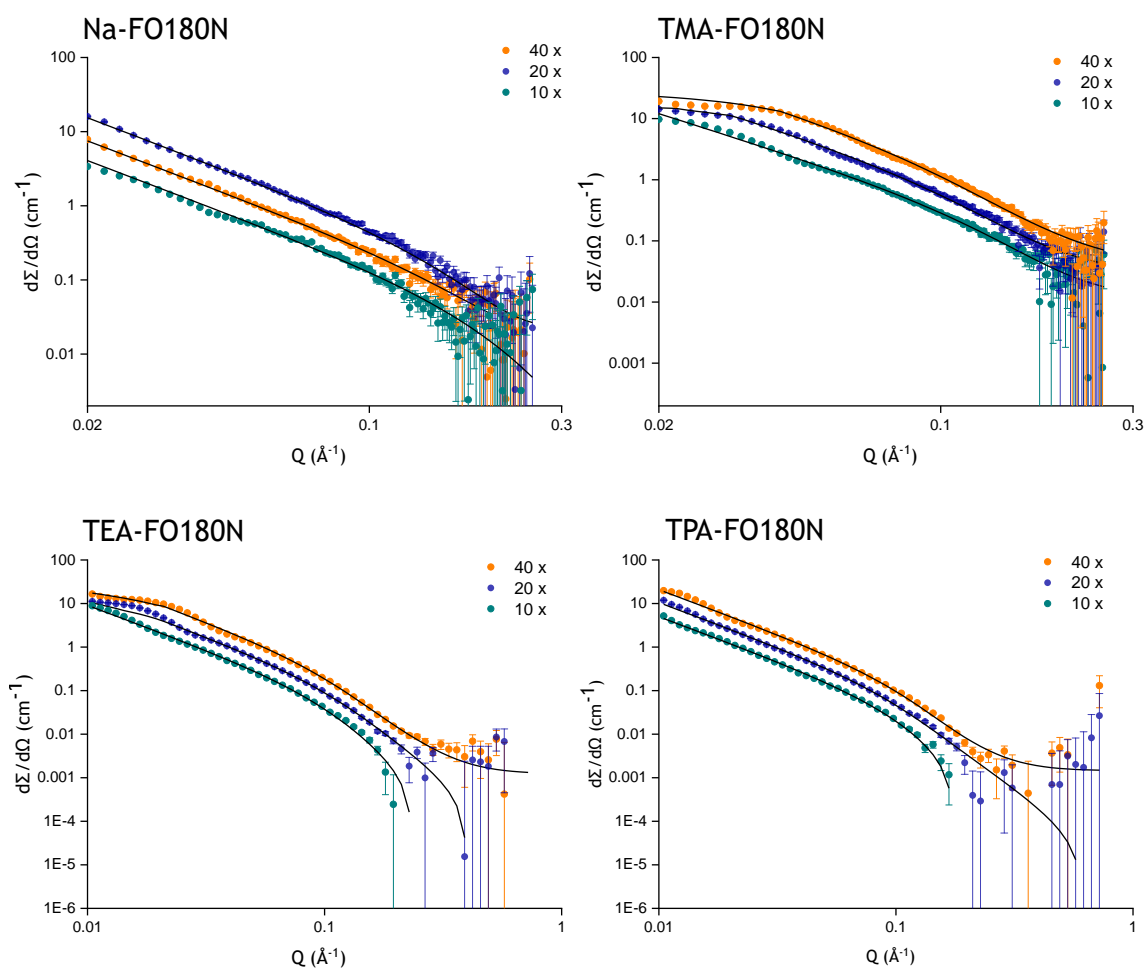


Figure 6.10: SANS model fit parameters for Na-FO180N, TMA-FO180N, TEA-FO180N and TPA-FO180N in D_2O over a range of concentrations which are consistent multiples of the cmc. Measurements were made at 25 °C. The lines are fitted functions for scattering laws as described in the text. Data for Na-FO180N and TMA-FO180N are from LOQ, ISIS. Data for TEA-FO180N and TPA-FO180N are from SANS 2D, ISIS.

Table 6.4: SANS model fit parameters for the Lamellar Structure model for the FO180N hedgehog surfactant series in D_2O . Parameters: bilayer thickness - D , polydispersity - σ .

Parameter	Na-FO180N			TMA-FO180N			TEA-FO180N			TPA-FO180N		
	40x	20x	10x	40x	20x	10x	40x	20x	10x	40x	20x	10x
Conc x cmc	40x	20x	10x	40x	20x	10x	40x	20x	10x	40x	20x	10x
D (Å) \pm 0.1	21.1	19.3	17.0	19.8	21.4	20.5	20.3	19.2	24.0	22.9	21.3	19.2
σ	-	-	-	0.81	0.63	0.47	0.71	0.71	0.52	0.57	0.71	0.81

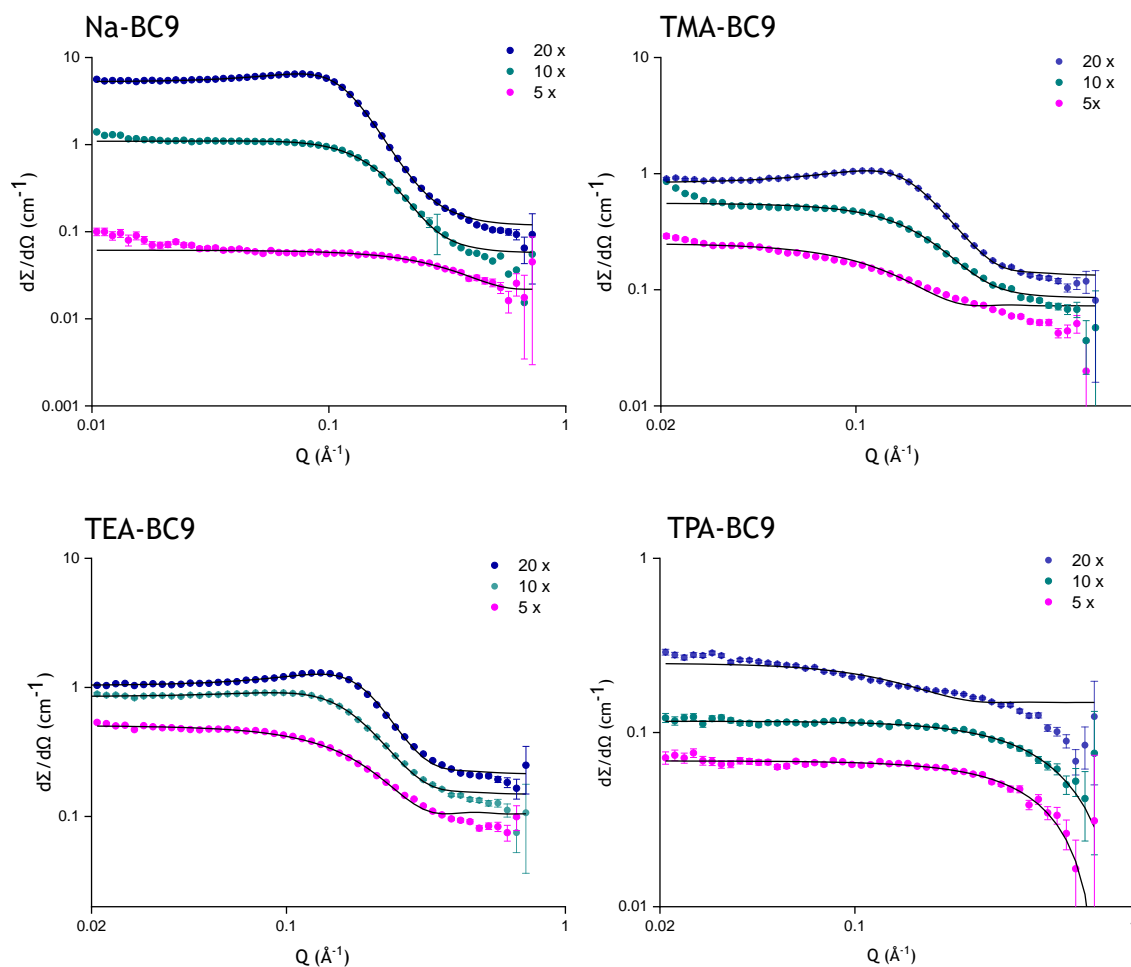


Figure 6.11: SANS profiles for Na-BC9, TMA-BC9, TEA-BC9 and TPA-BC9 in D_2O over a range of concentrations which are consistent multiples of the cmc. Measurements were made at 25 °C. The lines are fitted functions for scattering laws as described in the text. Data for TEA-BC9 is from LOQ, ISIS. Data for Na-BC9, TMA-BC9 and TPA-BC9 are from SANS 2D, ISIS.

Table 6.5: SANS model fit parameters for the Spherical Structure model for the BC9 hedgehog surfactant series in D_2O . Parameters: sphere radius - R_{sphere} , polydispersity - σ .

Parameter	Na-BC9			TMA-BC9			TEA-BC9			TPA-BC9		
	20x	10x	5x	20x	10x	5x	20x	10x	5x	20x	10x	5x
Conc x cmc	20x	10x	5x	20x	10x	5x	20x	10x	5x	20x	10x	5x
R_{sphere} (Å) \pm 0.1	10.9	8.06	6.61	10.8	7.33	7.01	10.5	10.7	9.48	13.9	12.5	10.3
σ	0.53	0.57	-	0.22	0.49	0.48	-	-	-	-	-	-
z	14	12	10	10	6	5	11	8	6	-	-	-

6.4 The tetrapropylammonium head group

The equilibrium surface tension, γ_{cmc} , area per molecule, A_{cmc} , and cmc have been evaluated for sixteen single-chain anionic HC surfactants. The surface coverage, Φ_{cmc} , is not equipped to account for a variable area per molecule dependent on the head group and therefore was not evaluated for these surfactants. From these data, for a particular tail is it possible to predict a TAA⁺ head group which will further improve packing efficiency and generate lower γ_{cmc} ? The only other HC surfactant to be studied by tensiometry with a variety of TAA⁺ counterions is AOT (ref. [6]). The surface tension generated by the TAA⁺-AOT analogues, along with the single-chain surfactants introduced in this chapter are shown in Figure 6.12. An average surface tension generated for each TAA⁺ counterion has also been included, highlighted on the figure. Interestingly, the lowest surface tensions are generated for the TPA analogue for a wide variety of structures. It should be highlighted that the same decreasing average is also seen if surface tension data for the BC7 series is ignored. Because such a wide variety of tail structures and sizes, single and di-chain, all generate lower surface energies when equipped with a TPA head group, this suggests that it is not the size of the head group that helps to promote efficient surface packing. But instead the TPA head group is simply a suitable head group for all HC surfactants to generate low γ_{cmc} . This is suggested to be due to strong counterion ion binding which helps to promote adsorption, thus increasing surface activity. Furthermore, the long alkyl chains were shown to reduce repulsion between neighbouring micelles of TPA-BC9. Therefore, it could be expected that the long alkyl chains present on TPA⁺ help to screen polar interactions between neighbouring head groups at the air water interface, generating a surface monolayer dominated by low surface energy non-polar interactions. Other smaller TAA⁺ cations will show a greater degree of dissociation and hence remove such benefits which help to generate low γ_{cmc} . The TPA head group is identified as a promising alternative to the sodium counterion which is commonly observed for anionic surfactants. The performance of conventionally ineffective HC surfactants can be drastically improved, for example, a TPA-tri-chain equivalent of di-C6SS (6 carbon linear chain) can generate $\gamma_{\text{cmc}} = 25.4 \text{ mN m}^{-1}$.²³ Providing an alternative approach to generate low surface energies with hydrocarbon surfactants.

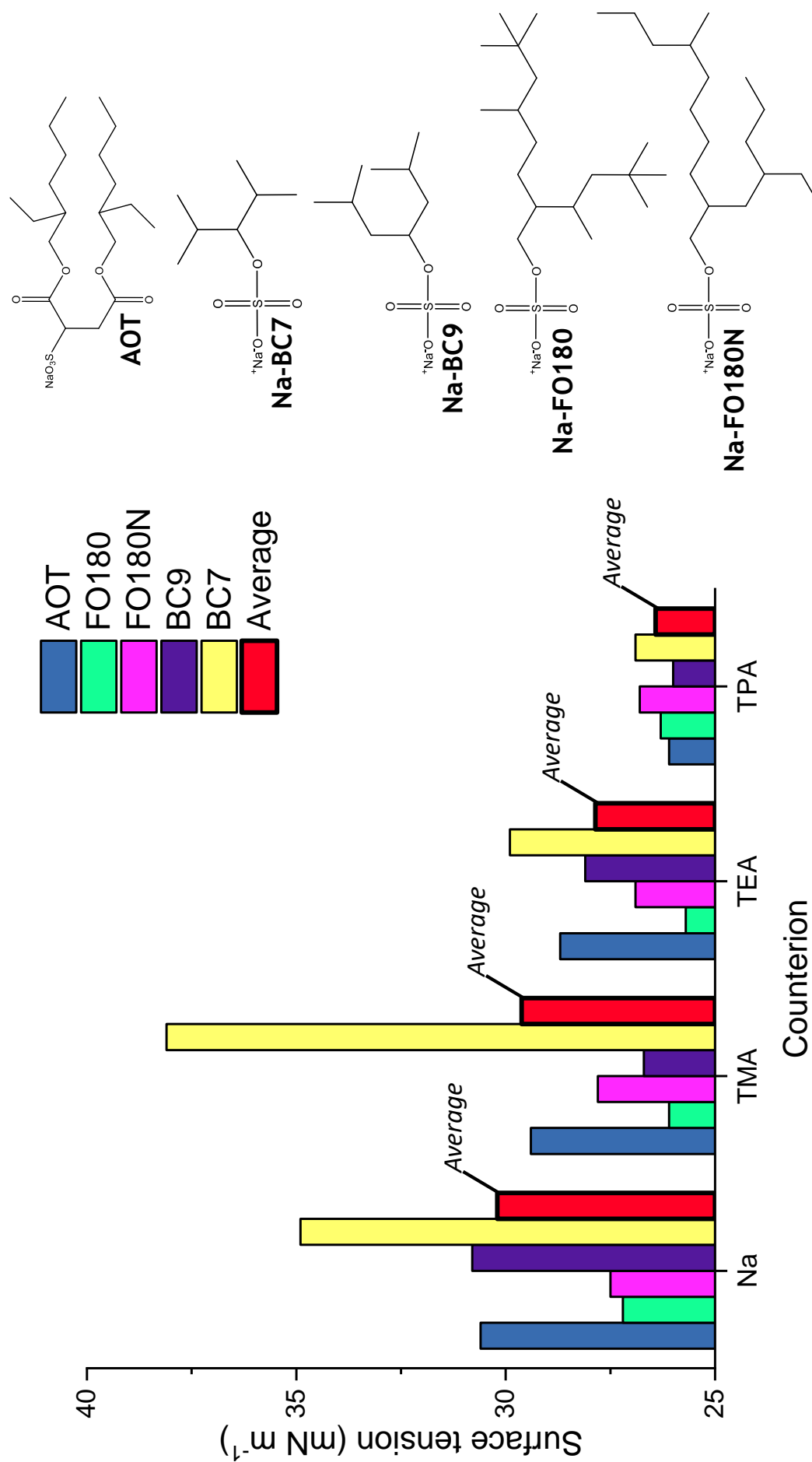


Figure 6.12: Equilibrium surface tension data for five single-chain surfactant families with the same variety of TAA⁺ counterions. An average surface tension has been taken for each counterion, highlighted on the figure.

6.5 Conclusions

The ability to improve the equilibrium surface tension by changing the surfactant counterion has been highlighted. Here, conventional monovalent metal ions are replaced by organic tetraalkylammonium (TAA) counterions. Previous studies have highlighted the potential of TAA counterions which as lead to unique classes of surfactants (ref. [15]), and greater control over certain surface properties (ref. [21]). Never before has the surface tension been evaluated for such a wide array of TAA-HC surfactants.

By keeping the surfactant tail constant and varying the head group, structure-property relationships have been identified which are dependent on the head group alone. With this approach, the tetrapropylammonium (TPA) counterion has shown to be an effective replacement to the sodium counterion commonly seen for anionic HC surfactants. This is because lower surface energies are generated with a TPA counterion, almost seemingly independent of the tail structure. This has been highlighted to be due to 1) the greater binding strength of the TPA head group increasing surfactant surface activity (ref. [9]) and 2) the long alkyl chains help to reduce polar interactions between neighbouring head groups. Although the TPA head group is not unknown in surfactant science (refs. [4, 8]), its enhanced ability to reduce surface tension has gone largely unnoticed. Hence, this study promotes the special properties that the TPA head group can offer to improve the effectiveness of HC surfactants. Providing a useful insight to fine tune the properties of an already effective surfactant, establishing a new generation of highly-effective hydrocarbon surfactants.

References

- [1] Berr, S. S.; Jones, R. R. *J. Phys. Chem.* **1989**, *93*, 2555–2558.
- [2] Chen, S.-H. *Annu. Rev. Phys. Chem.* **1986**, *37*, 351–399.
- [3] Clint, J. H. *Surfactant aggregation*; Springer Science & Business Media, 2012.
- [4] Attwood, D.; Florence, A. *Surfactant system*; 1983.
- [5] Rosen, M. J.; Kunjappu, J. T. *Surfactants and interfacial phenomena*; John Wiley & Sons, 2012.
- [6] Brown, P.; Butts, C.; Dyer, R.; Eastoe, J.; Grillo, I.; Guittard, F.; Rogers, S.; Heenan, R. *Langmuir* **2011**, *27*, 4563–4571.
- [7] Lu, J. R.; Marrocco, A.; Su, T. J.; Thomas, R. K.; Penfold, J. *J. Colloid Interface Sci.* **1993**, *158*, 303–316.
- [8] Benrraou, M.; Bales, B. L.; Zana, R. *J. Phys. Chem. B* **2003**, *107*, 13432–13440.
- [9] Bonilha, J. B.; Georgetto, R. M. Z.; Abuin, E.; Lissi, E.; Quina, F. *J. Colloid Interface Sci.* **1990**, *135*, 238–245.
- [10] Firestone, M. A.; Dzielawa, J. A.; Zapol, P.; Curtiss, L. A.; Seifert, S.; Dietz, M. L. *Langmuir* **2002**, *18*, 7258–7260.
- [11] Bowers, J.; Butts, C. P.; Martin, P. J.; Vergara-Gutierrez, M. C.; Heenan, R. K. *Langmuir* **2004**, *20*, 2191–2198.
- [12] Wang, C.; Yan, P.; Xing, H.; Jin, C.; Xiao, J.-X. *J. Chem. Eng. Data* **2010**, *55*, 1994–1999.

- [13] Bales, B. L.; Benrraou, M.; Tiguida, K.; Zana, R. *J. Phys. Chem. B* **2005**, *109*, 7987–7997.
- [14] Tan, J.; Feng, S. *J. Chem. Eng. Data* **2014**, *59*, 1830–1834.
- [15] Brown, P.; Butts, C. P.; Eastoe, J.; Grillo, I.; James, C.; Khan, A. *J. Colloid Interface Sci.* **2013**, *395*, 185–189.
- [16] Almgren, M.; Swarup, S. *J. Phys. Chem.* **1983**, *87*, 876–881.
- [17] Moore, W. J. *Physical Chemistry*; Longman, 1972; Vol. 1.
- [18] Aue, D. H.; Webb, H. M.; Bowers, M. T. *J. Am. Chem. Soc.* **1976**, *98*, 318–329.
- [19] Alexander, S.; Smith, G. N.; James, C.; Rogers, S. E.; Guittard, F.; Saganaka, M.; Eastoe, J. *Langmuir* **2014**, *30*, 3413–3421.
- [20] Zisman, W. A. *Adv. Chem. Ser.* **1964**, *43*, 1–51.
- [21] Pottage, M. J.; Greaves, T. L.; Garvey, C. J.; Tabor, R. F. *J. Colloid Interface Sci.* **2016**, *475*, 72–81.
- [22] Su, T.; Lu, J.; Thomas, R.; Penfold, J. *J. Phys. Chem. B* **1997**, *101*, 937–943.
- [23] Robinson, R.; Stokes, R. *Physical Chemistry*; Butterworths [1965, reprinted 1970] London, 1970.

Chapter 7

Mixed Surfactant Systems

7.1 Introduction

When humans first added copper to tin and made what became known as bronze, the potential of mixing was identified. Since then, humans have not stopped experimenting by mixing different components. Mixing different surfactants together was a natural step to develop our understanding of colloidal chemistry and indeed, mixed surfactant systems now account for nearly all practical applications of surfactants. But practically, what great advantages do mixed systems possess over single component systems?

1. Due to impurities in starting materials and therefore the variability in reaction products, it is less expensive to produce a mixture of surfactants than an isomerically pure surfactant.
2. Mixed surfactant systems often provide better performance because they exploit synergistic behaviour between different surfactants, or they provide qualitatively different types of performance in a single formulation (e.g. cleaning plus fabric softening).

Because of their superior performance, mixtures of surfactants have been a topic of great interest in recent years.^{1,2} Many different surfactant mixtures have been studied, the most extensive being fluorocarbon-hydrocarbon (FC-HC) mixtures which include anionic-anionic,³ anionic-cationic,⁴ anionic-nonionic,⁵ cationic-cationic etc.⁶ Mixed systems formed from surfactants with the same hydrophobic group (FC-FC,

HC-HC) have also been studied, but far less extensively. The surface tension generated by binary surfactant systems is a well explored area,^{7,8} but to date there have been no published studies that investigate the effect on surface tension when mixing straight and branched chain HC surfactants. Here, a series of anionic-anionic hydrocarbon mixed systems are introduced which generate surface energies lower than either constituent surfactant, comparable with a typical alkane e.g. $\gamma_{\text{n-dodecane}} = 25.4 \text{ mN m}^{-1}$. Synergistic effects on surface tension have been shown previously for mixtures of different surfactants due to coulombic interactions i.e. ionic/non-ionic.⁹ Previous groups have studied anionic-anionic HC systems,¹⁰ although not reporting synergistic surface tension effects and therefore, this appears to be the first report which shows a synergistic reduction of γ when mixing hydrocarbon surfactants of like charge.

The critical micelle concentration (cmc), interaction parameter (β) and micellar composition (x_1) have been evaluated using Rubingh's regular solution theory which was introduced in Chapter 3. The interaction parameter β is a qualitative measure of the interaction between the different surfactant species. A positive value suggests an antagonistic interaction whereas a negative value suggests synergistic mixing. A value of zero indicates ideal mixing. For example, negative deviations from ideality have been observed for mixed cmc's of cationic-anionic systems, where head group interactions are capable of overcoming mutual phobicity of the hydrophobic chains in the mixed micelles.¹¹ When mixing surfactants with like charge, evidence of demixing has been observed and many of the systems discussed here show demixing according to RST. For FC-HC surfactant mixtures, this can often be explained due to the immisibility of surfactant hydrophobic groups in the core of the micelle. For mixtures with the same hydrophobic group (HC-HC), demixing is likely due to steric effects which restrict mixing based on geometries of the surfactants.

The general property of low aqueous surface tension introduced in Chapter 2 states that low surface energies are generated when surfactant molecules efficiently pack, generating dense surface layers. Previous studies have exploited electrostatic effects between different head groups to generate lower surface tensions (ref. [9]). However, when mixing surfactants together with the same head group, effects observed at the air-water interface are exclusively dependent on the surfactant tails.

Hence, this study directly shows how low surface energies can be generated by simply exploiting packing efficiency, to generate surface monolayers which more closely resemble a pure alkane. By making small systematic variations in the tail structure and measuring the change in surface tension, structure-property relationships of effective HC-HC systems have been identified. This will help guide the design of future super-effective HC-HC mixed systems. This work has provided an unexplored insight into generating low surface energies, improving our fundamental understanding of controlling surface tension and providing practical solutions to using HC surfactants industrially, for low surface energy applications.

7.1.1 Surfactants investigated

To investigate the relationships between molecular structure and surface tension for mixed surfactant systems, it is sensible to choose a systematic series of systems where the structures do not differ too greatly. This then allows a genuine insight into how minor changes in the structure affect surface tension and hence, highlights possible general structure-property relationships. The investigation is primarily concerned with studying the effects on surface tension when mixing branched and linear chain hydrocarbon surfactants. To do this, common linear di-chain surfactants di-C6SS, di-C7SS and di-C8SS were selected, and mixed with the novel hedgehog surfactants AOTA and AOTB introduced in Chapter 5. To extend this investigation, two branched surfactants HS3 and AOT, with total tail carbon numbers of 7 and 8 respectively were also mixed with AOTA and AOTB. Finally, the most successful mixed system, i.e. the one that generated the lowest surface energies, was mixed with TMS-hedgehogs AOTSiA and AOTSiB to see if the packing efficiency at the surface could be improved even further. Figure 7.1 shows all surfactant mixtures studied in this investigation. The cmc's and surface tensions generated by the individual surfactant components has been discussed in Chapter 5. All surfactants used in this investigation were shown to be pure, producing clean systems without the presence of surface-active impurities as detailed in Section 4.5.

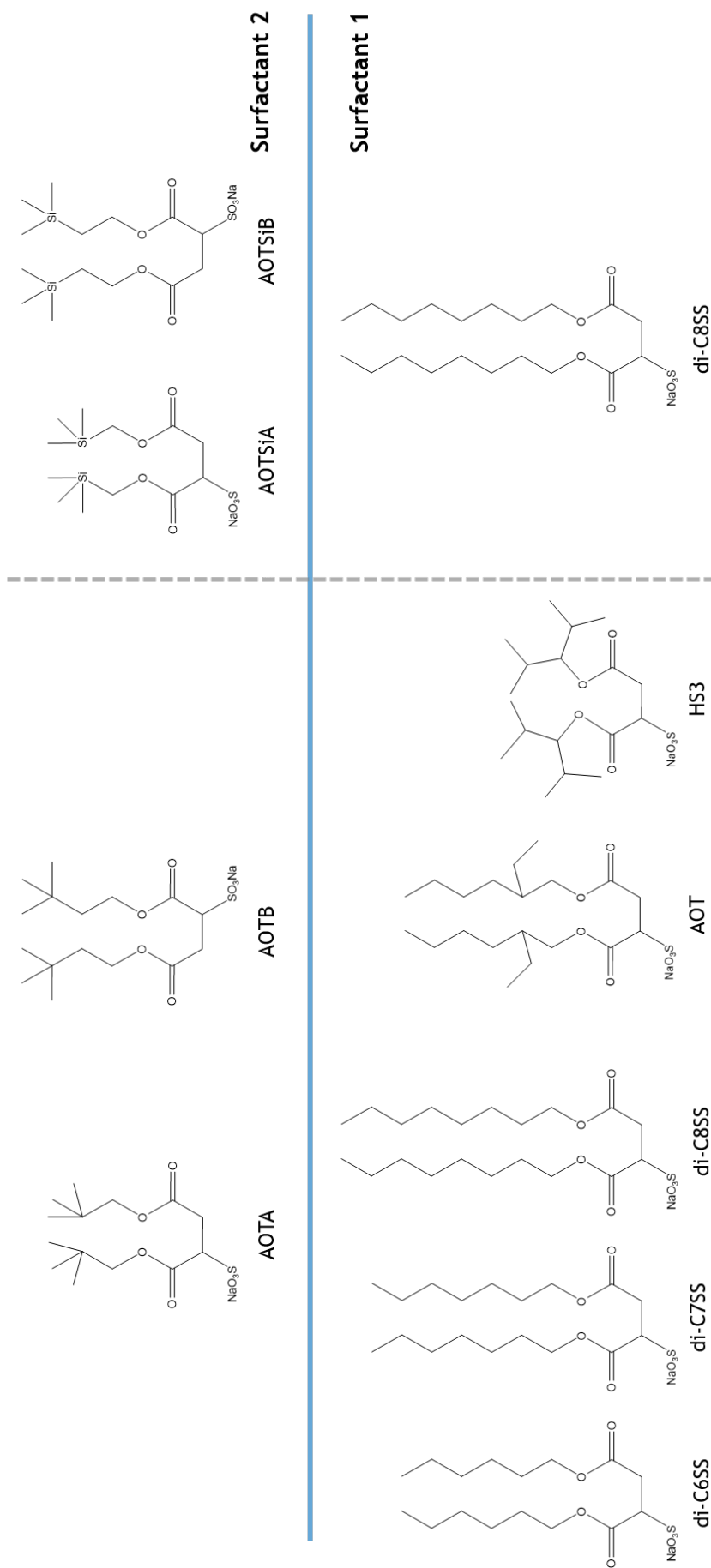


Figure 7.1: Mixed systems studied. Each structure from 'Surfactant 1' was mixed with both AOTA & AOTB, apart from di-C8SS which was also mixed with AOTSiA/SiB.

7.2 Determining cmc's of mixed systems

For a pure surfactant system at the cmc, the area per molecule, packing efficiency, and surface composition, are all dependent on one molecular structure. Therefore, relationships between surface tension and surfactant structure are often straightforward to identify. To study the effects of packing between surfactant molecules at the air-water interface for a binary surfactant system, the surface composition is no longer dependent on one surfactant. In order to identify relationships between surface tension and surfactant structure for a mixed system, it is important to measure the surface tension at a variety of surface compositions, which can be achieved by varying the molar ratios of each surfactant present in solution. For this investigation, the mole fractions selected for all systems were: 0.1:0.9, 0.25:0.75, 0.5:0.5, 0.75:0.25 and 0.9:0.1. For the linear-branched mixed systems (e.g. di-C6SS : AOTB) two further ratios were investigated - 0.01:0.99 and 0.99:0.01.

The critical micelle concentration depends on the extent to which a hydrophobic tail disrupts the isotropically arranged hydrogen bonding network of water. For a mixed system, this will be related to the amount of each surfactant present. Therefore, the cmc for each molar ratio must be determined separately. For the systems investigated here, only anionic surfactants are present and therefore, measuring the electrical conductivity of an aqueous solution over a suitable concentration range is an appropriate technique to determine the cmc. From these data, the critical micelle concentrations are identified as the concentration where the gradient noticeably decreases, which signifies the formation of micelles hence, reducing the ability for further surfactant molecules to carry charge through the solution. The experimental procedure for determining cmc's by conductivity was outlined in Section 4.6.1, and the data analysis has been thoroughly described in Section 5.2.2. Conductivity data and analysis is shown for select molar ratios of the di-C7SS:AOTB mixed system in Figure 7.2. For all other mixed systems, cmc analysis can be found in the Supporting Information.

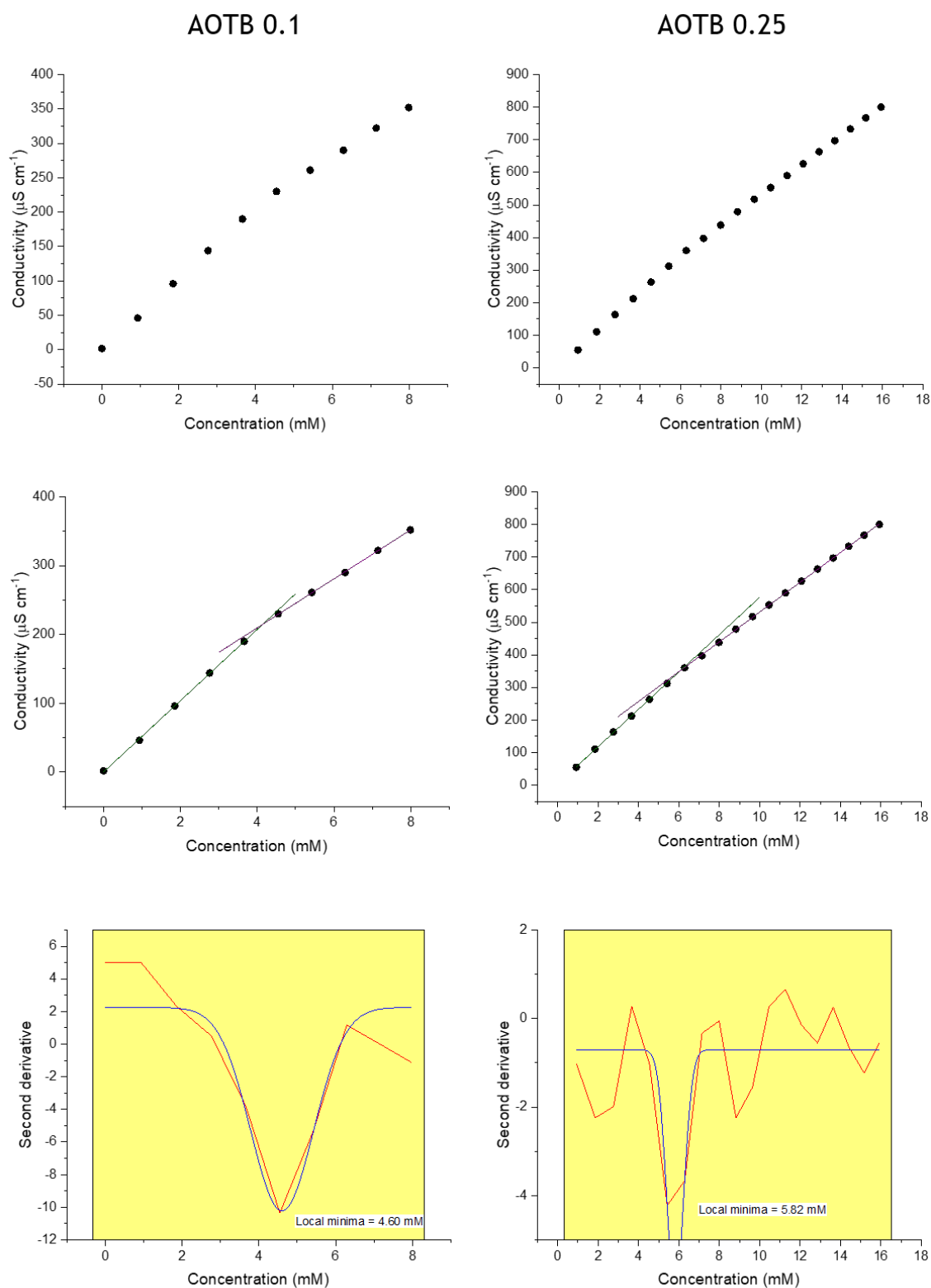


Figure 7.2: Conductivity data for di-C7SS:AOTB mixed system at molar ratios shown at the top of the figure. Gaussian distribution applied over double derivative of conductivity data to more accurately assign the break point.

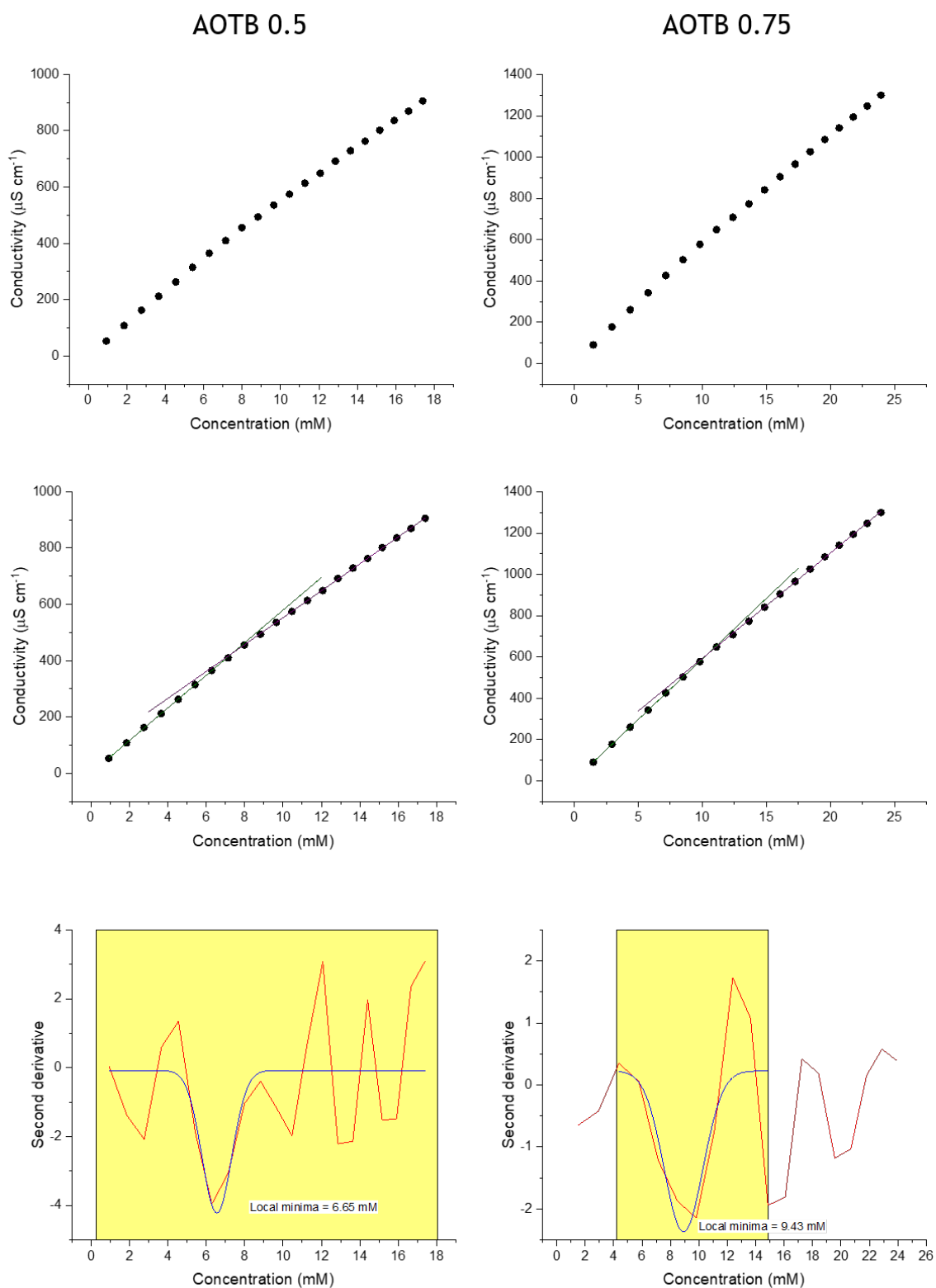


Figure 7.2a: Conductivity data for di-C7SS:AOTB mixed system at molar ratios shown at the top of the figure. Gaussian distribution applied over double derivative of conductivity data to more accurately assign the break point.

7.3 Analysis of cmc data using Regular Solution Theory

Theory

With cmc values for a mixed system and each pure surfactant, it is possible to model surfactant mixtures according to regular solution theory and determine the interaction parameter β , as well as estimating the micellar composition x^1 (see Section 3.2.2). This data is shown in Tables 7.1-7.3 for all mixed systems.

The critical micelle concentration C_{id}^* estimates the ideal cmc, that is, the cmc of a mixed system if it exhibits ideal behaviour. The values of C_{id}^* are a qualitative indicator of the interaction taking place between the two anionic surfactants. For example, if the experimentally obtained cmc value is lower than that calculated assuming ideal mixing, a synergistic interaction is indicated. Figure 7.3 shows the variation of cmc with mole fraction of AOTB for the three linear mixtures, where experimentally determined cmc's are higher, indicating an antagonistic interaction. Also, small variations in structure clearly make a noticeable difference to packing between molecules within the micelle.

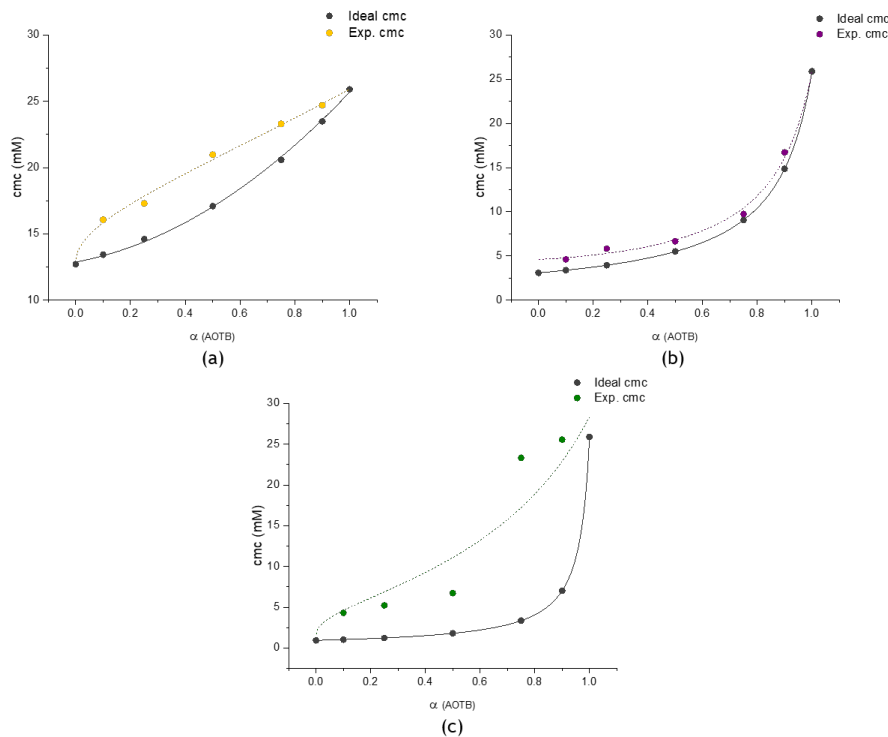


Figure 7.3: Variation of cmc (C^*) with mole fraction of AOTB (α) for three mixtures: a) di-C6SS + AOTB, b) di-C7SS + AOTB and c) di-C8SS + AOTB.

Interaction parameter - β

In order to describe the interaction taking place between the two surfactants in a quantitative manner, the interaction parameter β is used. The β values shown in Tables 7.1-7.3 are positive for nearly all mixed systems studied, with many values being > 10 . This shows strong antagonistic interactions between the two anionic surfactants. For a mixture of similarly charged surfactants, previous studies have identified behaviour close to that of an ideal mixture (ref. [11]). However, the mixtures were formed from two anionic surfactants that share similar structures and therefore, steric constraints between the two surfactants will be minimal. For the systems studied here, the structures involved are sterically very different. From examining the data in Tables 7.1-7.3 more closely, for nearly all systems, the magnitude of β decreases as the molar ratio of AOTA or AOTB increases. In fact, for the highest molar ratios of AOTA/B, the β parameter decreases close to 0, or even becomes negative. Showing that the interaction between the two surfactants becomes less antagonistic, or even synergistic. Therefore, it is clear that at low molar ratios (< 0.5), the presence of AOTA/AOTB hinders the formation of micelles. The linear di-chain surfactants possess long alkyl chains with a good degree of flexibility that will allow close packing between surfactant molecules, reflected in the area per molecules e.g. di-C6SS $A_{\text{cmc}} = 62 \text{ \AA}^2$, di-C8SS $A_{\text{cmc}} = 55 \text{ \AA}^2$.¹² When mixed with AOTA/AOTB or AOTSiA/SiB, the bulky volume of the chain tips will reduce the degree of freedom and hence packing efficiency between the long alkyl chains in the micelle. Therefore, a higher concentration will be required in order to overcome the electrostatic repulsive forces between the charged head groups. As the molar ratio of AOTA/B increases (> 0.75) we begin to see a decrease in β . Perhaps as the micelle becomes more heavily composed of AOTA/B, the space between surfactant molecules in the micelle can be efficiently filled by the flexible long alkyl chains of the other di-chain component. This would increase the van der Waals interactions within the micelle creating a more hydrophobic core. Interestingly, the mixed systems HS3 : AOTA / AOTB show synergistic micelle formation, with β being < 0 for most molar ratios. Although the chemical structures of HS3 and AOTA/B differ, they share similar area per molecules (HS3 $A_{\text{cmc}} = 79 \text{ \AA}^2$, AOTA/B $A_{\text{cmc}} = 79/75 \text{ \AA}^2$ respectively) and therefore, it could be expected that when packing together

they sterically accommodate each other, increasing the van der Waals interactions between tails and thus the free energy change of micellisation.

Micellar mole fraction - x_1

With a knowledge of calculated β parameter values and using equation 3.29 in Section 3.2.2, the micellar mole fractions of the mixed systems (x_1) can be estimated (values shown in Tables 7.1-7.3). It is clear that the values of x_1 deviate depending on the bulk mole fraction value (α), and the hydrophobic chain length of surfactant 1 participating within the mixed micelle (see Figure 7.1). From analysing the data shown in Tables 7.1-7.3, all systems which mix antagonistically show very low values of x_1 for low mole ratios of AOTA/B (i.e. rich in surfactant 1). This is likely due to the large difference in cmc of each pure component. For example, di-C7SS and AOTA possess cmc's = 3.07 mM and 89.6 mM respectively, when mixed at a 50:50 ratio, mixed micelles are formed at a concentration of 7.43 mM. This value of C^* is $\sim 2.5x$ the cmc of pure di-C7SS, and $0.08x$ the cmc of pure AOTA. Therefore, at this concentration, perhaps the majority of AOTA molecules are involved in the surface monolayer, with only a small proportion being involved in the mixed micelle.

As the value of α increases, and the value of x_1 increases, it is interesting to note that the two values never become equal i.e., the composition of the mixed micelle is always shifted towards the component being surfactant 1. Again, this could be due to the values of C^* nearly always being above the cmc of pure surfactant 1, but below that of pure surfactant 2. Hence the onset of micelle formation will be brought on by surfactant 1. For certain systems such as di-C8SS:AOTSiA/AOTSiB, the values of x_1 predicted by RST suggest a minimal incorporation of surfactant 2 into the mixed micelle, even at high values of α . This seems unlikely, given the values of C^* are not similar to pure di-C8SS, which one would expect if the mixed micelles were composed purely of di-C8SS. This is perhaps more a manifestation of the limitations of RST, which assumes that the molecules in the mixed system are of comparable volume i.e., share similar structures, which is not true of these systems. However, the values predicted by RST in Tables 7.1-7.3 still give an insight about the interactions between surfactant molecules in the micelle. Which is important to help fully characterise the structure-performance relationships of mixed systems.

Table 7.1: Mole fraction of AOTA or AOTB in bulk (α), in mixed micelles (x_1), experimental mixed cmc (C^*), ideal value of mixed cmc (C_{id}^*) and interaction parameter (β) for the di-C6SS and di-C7SS : AOTA / AOTB mixed systems.

α	C_{id}^*	C^*	β	x_1
di-C6SS : AOTA				
0	12.70	-	-	-
0.10	13.92	16.73	13.40	3.0×10^{-8}
0.25	16.22	18.31	14.40	2.85×10^{-8}
0.50	22.31	22.63	0.14	0.113
0.75	35.72	35.94	0.03	0.298
0.90	55.89	45.83	-0.80	0.544
1	89.60	-	-	-
di-C6SS : AOTB				
0	12.70	-	-	-
0.10	13.42	16.07	14.60	2.95×10^{-8}
0.25	14.59	17.29	15.50	2.95×10^{-8}
0.50	17.08	20.97	1.12	0.196
0.75	20.58	23.30	0.55	0.624
0.90	23.48	24.70	0.39	0.851
1	25.90	-	-	-
di-C7SS : AOTA				
0	3.07	-	-	-
0.10	3.40	6.04	12.30	2.98×10^{-8}
0.25	4.05	6.30	13.30	2.86×10^{-8}
0.50	5.94	7.43	14.20	2.82×10^{-8}
0.75	11.14	17.75	15.40	2.93×10^{-8}
0.90	23.46	23.95	0.12	0.224
1	89.60	-	-	-
di-C7SS : AOTB				
0	3.07	-	-	-
0.10	3.37	4.60	13.30	2.98×10^{-8}
0.25	3.94	5.82	14.50	2.98×10^{-8}
0.50	5.49	6.65	15.30	2.91×10^{-8}
0.75	9.06	9.73	0.39	0.223
0.90	14.85	16.71	0.47	0.521
1	25.90	-	-	-

Table 7.2: Mole fraction of AOTA or AOTB in bulk (α), in mixed micelles (x_1), experimental mixed cmc (C^*), ideal value of mixed cmc (C_{id}^*) and interaction parameter (β) for the di-C8SS : AOTA/AOTB and AOTSiA/AOTSiB mixed systems.

α	C_{id}^*	C^*	β	x_1
di-C8SS : AOTA				
0	0.93	-	-	-
0.10	1.03	2.93	11.61	2.97×10^{-8}
0.10	1.03	7.48	12.54	2.99×10^{-8}
0.25	1.24	1.65	11.95	2.97×10^{-8}
0.25	1.24	6.66	13.34	2.99×10^{-8}
0.50	1.84	3.51	13.40	2.97×10^{-8}
0.75	3.61	13.95	15.18	2.98×10^{-8}
0.90	8.51	5.40	-3.05	0.273
1	89.60	-	-	-
di-C8SS : AOTB				
0	0.93	-	-	-
0.10	1.03	4.31	13.23	2.99×10^{-8}
0.25	1.23	5.23	14.34	2.99×10^{-8}
0.50	1.80	6.74	15.29	2.98×10^{-8}
0.75	3.36	23.32	17.12	2.48×10^{-8}
0.90	7.03	25.57	17.21	2.98×10^{-8}
1	25.90	-	-	-
di-C8SS : AOTSiA				
0	0.93	-	-	-
0.10	1.03	2.66	11.78	2.99×10^{-8}
0.25	1.23	5.66	13.45	2.99×10^{-8}
0.50	1.84	6.92	14.35	2.98×10^{-8}
0.75	3.57	12.51	15.53	2.48×10^{-8}
0.90	8.28	11.82	15.47	2.99×10^{-8}
1	68.10	-	-	-
di-C8SS : AOTSiB				
0	0.93	-	-	-
0.10	1.03	1.47	12.65	2.97×10^{-8}
0.25	1.22	1.85	13.79	2.98×10^{-8}
0.50	1.76	3.83	15.21	2.99×10^{-8}
0.75	3.16	11.69	16.73	2.99×10^{-8}
0.90	6.09	11.91	16.93	2.99×10^{-8}
1	15.90	-	-	-

Table 7.3: Mole fraction of AOTA or AOTB in bulk (α), in mixed micelles (x_1), experimental mixed cmc (C^*), ideal value of mixed cmc (C_{id}^*) and interaction parameter (β) for the HS3 : AOTA/AOTB and AOT : AOTA/AOTB mixed systems.

α	C_{id}^*	C^*	β	x_1
HS3 : AOTA				
0	33.60	-	-	-
0.10	35.81	34.62	-0.68	0.0697
0.25	39.79	33.62	1.26	0.0285
0.50	48.84	36.31	-1.37	0.357
0.75	63.25	68.14	0.30	0.535
0.90	76.78	62.57	-1.04	0.693
1	89.60	-	-	-
HS3 : AOTB				
0	33.60	-	-	-
0.10	32.60	25.21	-1.68	0.250
0.25	31.26	24.93	-1.02	0.364
0.50	29.24	25.44	-0.57	0.551
0.75	27.47	31.44	1.06	0.901
0.90	26.51	19.49	-2.35	0.768
1	25.90	-	-	-
AOT : AOTA				
0	2.60	-	-	-
0.10	2.88	6.39	12.39	2.97×10^{-8}
0.25	3.43	6.74	13.36	2.96×10^{-8}
0.50	5.05	6.87	14.07	2.97×10^{-8}
0.75	9.57	18.46	15.46	2.98×10^{-8}
0.90	20.62	16.09	-1.29	0.303
1	89.60	-	-	-
AOT : AOTB				
0	2.60	-	-	-
0.10	2.86	7.16	13.74	2.98×10^{-8}
0.25	3.35	7.13	14.65	2.99×10^{-8}
0.50	4.73	7.12	15.34	2.99×10^{-8}
0.75	7.99	10.15	2.57	2.99×10^{-8}
0.90	13.66	14.93	0.36	0.0256
1	25.90	-	-	-

7.4 Linear-branched mixed systems

With cmc 's estimated, the surface tension generated at each mole fraction was determined using a K100 tensiometer following the experimental procedure outlined in Section 4.6.2. For all systems studied, the surface tension was recorded at 1.1x the cmc to ensure a fully saturated surfactant monolayer. First, the synergistic effects of mixing straight and branched chain surfactants are discussed.

7.4.1 Surface tension results

Table 7.4 shows the surface tension generated at each mole fraction for the di-C6SS, di-C7SS and di-C8SS systems mixed with AOTA/B.

Table 7.4: Mixed cmc 's (C^*) and surface tension values (γ_{cmc}) at mole fractions of AOTA / AOTB (α), for the di-C6SS, di-C7SS and di-C8SS mixed systems.

α	C^*	γ_{cmc} (mN m ⁻¹) ± 0.1	C^*	γ_{cmc} (mN m ⁻¹) ± 0.1
	di-C6SS : AOTA		di-C6SS : AOTB	
0	12.7	29.0	12.7	29.0
0.10	16.7	28.5	16.1	26.7
0.25	18.3	28.3	17.3	28.3
0.50	22.6	27.9	21.0	27.9
0.75	35.9	26.4	23.3	27.3
0.90	45.8	28.7	24.7	28.7
1	89.6	30.2	25.9	26.7
	di-C7SS : AOTA		di-C7SS : AOTB	
0	3.04	30.2	3.04	30.2
0.10	6.04	27.3	4.60	28.0
0.25	6.30	27.9	5.82	27.5
0.50	7.43	26.2	6.65	27.0
0.75	17.8	25.4	9.73	26.7
0.90	24.0	25.2	16.7	26.9
1	89.6	30.2	25.9	26.7
	di-C8SS : AOTA		di-C8SS : AOTB	
0	0.93	30.4	0.93	30.4
0.10	2.93	24.4	4.31	25.6
0.25	1.65	24.8	5.23	26.2
0.50	3.51	25.1	6.74	26.8
0.75	14.0	24.5	23.3	25.1
0.90	5.40	25.0	25.6	25.6
1	89.6	30.2	25.9	26.7

To help examine and compare the surface energies generated by each mixed system to that of the pure surfactants, the data from Table 7.4 can be visualised more easily by being plotted as a column figure, see Figure 7.4. The surface tension generated at a particular mole fraction is represented by column height, and the dashed lines represent γ_{cmc} of the pure surfactants. From Figure 7.4 it is clear that many of the mixed systems generate lower surface energies than either of the constituent surfactants. Interestingly, for all three linear surfactants, when mixed with AOTA a lower surface tension is formed at every mole fraction studied. For AOTB, a lower surface energy is formed only when mixed with di-C8SS. Furthermore, when comparing the three linear surfactants, di-C8SS forms mixtures that can most effectively reduce the surface tension of water, with some mixtures capable of reducing the surface tension 6 mN m^{-1} lower than the most effective pure surfactant component. The di-C8SS:AOTA system at a 25:75 molar ratio generates $\gamma_{\text{cmc}} = 25.1 \text{ mN m}^{-1}$, comparable to pure alkanes e.g. $\gamma_{\text{n-dodecane}} = 25.4 \text{ mN m}^{-1}$. This is a remarkable reduction in surface tension. Given that both surfactants are anionic and share the same polar head group, the synergistic effect that is clearly observed at the air-water interface cannot be due to a coulombic interaction between the two surfactants. It must be due to a synergistic interaction between the surfactant tails, i.e. an improved packing efficiency generating a surface that more closely resembles a pure alkane.

When comparing AOTA and AOTB within a single system, at essentially all mole fractions the AOTB systems generate higher surface tensions. This is interesting as AOTB is a noticeably more effective pure surfactant than AOTA ($\gamma_{\text{AOTA}} = 30.2 \text{ mN m}^{-1}$ and $\gamma_{\text{AOTB}} = 26.7 \text{ mN m}^{-1}$). Therefore, clearly the addition of a single CH_2 group present within the tail of AOTB has an adverse effect on packing within the mixed monolayer. Given that AOTA and AOTB share the same chain-tip structure, for the linear-branched mixed systems studied here, the slightly smaller volume of AOTA seems critical to help generate very low surface energies.

From the information presented in Figure 7.4, the synergistic effect of mixing these particular linear and branched surfactants is clear. However, the reasons as to why are not. To explain these results, further experiments are necessary to highlight the underlying structure-property relationships that make these super-effective systems successful.

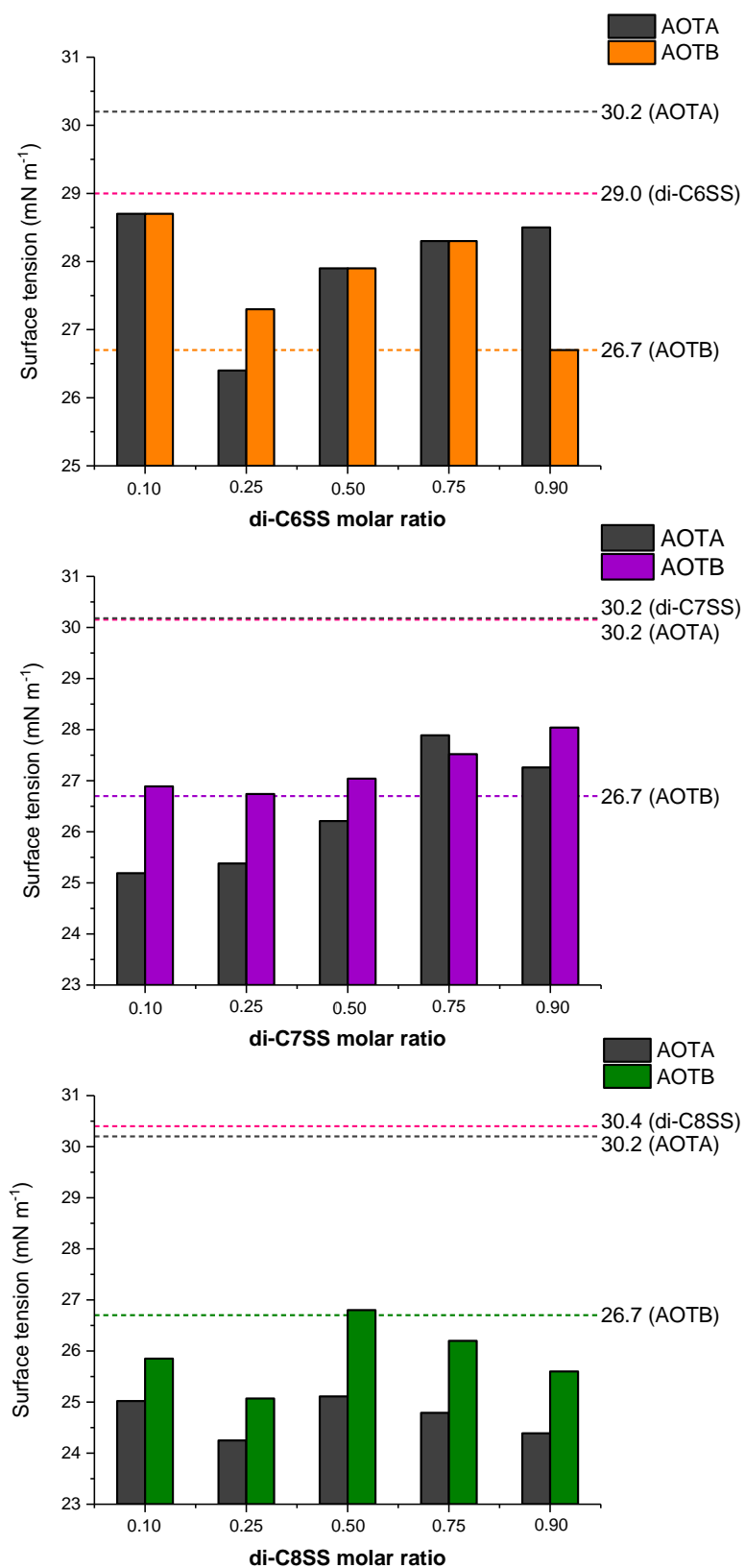


Figure 7.4: Surface tension at each mole fraction where column height represents the surface tension generated, and the dashed lines represent γ_{cmc} of the pure surfactants.

7.4.2 Effect of chain length

When linear surfactants di-C6SS, di-C7SS and di-C8SS are mixed with the branched hedgehog AOTA, the only variation in structure between the systems is an additional CH_2 group present on the linear tail. To more easily compare how the surface tension changes with increasing linear chain length, Figure 7.5 shows surface tension data for these systems (from Table 7.4) plotted as a column figure. It is clear that at each mole fraction, the surface tension decreases with increasing chain length. Hence, when mixed with AOTA a longer linear chain forms mixed systems that more effectively mimics the density of a pure alkane, thus generating a lower surface free energy. This is perhaps a surprising relationship as the longer the linear chain, the more the surface becomes populated by higher surface energy $-\text{CH}_2$ groups.¹³

To further investigate this relationship, AOTA was mixed with sodium dodecylsulfate (SDS). The common linear anionic surfactant SDS is a heavily investigated, understood, and widely available twelve carbon long single-chain surfactant. There have been several studies investigating the surface tension of SDS mixed with cationic surfactants,^{14,15} but far fewer with anionic surfactants,¹⁶ and to date none with branched anionic HC surfactants. Although it is a single-chain surfactant,

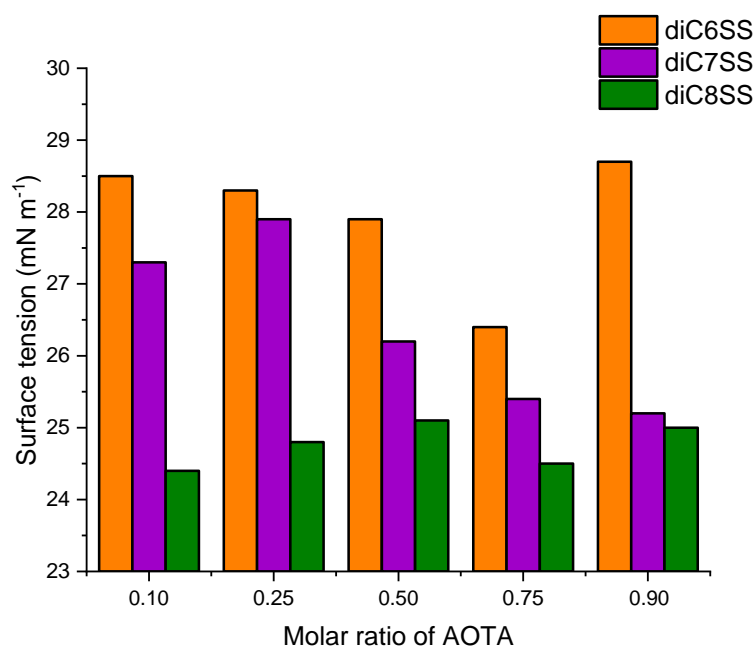


Figure 7.5: Surface tension at each mole fraction of AOTA for the di-C6SS, di-C7SS and di-C8SS mixed systems.

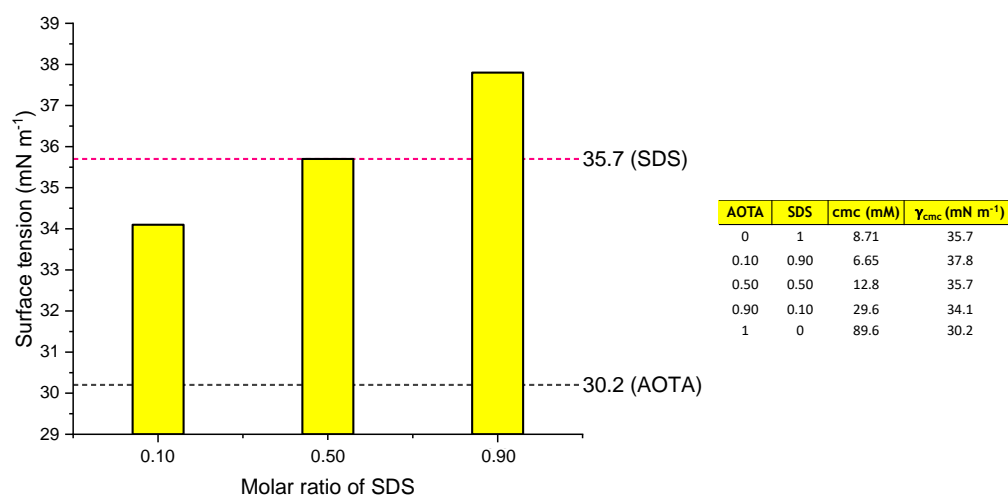


Figure 7.6: Surface tension at varying mole fractions of SDS mixed with AOTA, dashed line represents γ_{cmc} of pure SDS and AOTA.

and thus not directly comparable to the di-chain linear surfactants, it does provide an insight into mixing longer linear alkyl chains with AOTA. SDS was mixed with AOTA at 0.1, 0.5 and 0.9 mole fractions. The critical micelle concentration at each mole fraction was determined (see Supporting Info.), and the surface tension measured, see Figure 7.6. None of the systems presented in Figure 7.6 form lower surface tensions than either of the constituent surfactants. The mixed system with a mole fraction of 0.1 SDS does form a lower surface tension than SDS itself, however, this is possibly just due to the bulk phase being heavily composed of AOTA which has $\gamma_{cmc} = 30.2 \text{ mN m}^{-1}$. From these results, it is clear that AOTA will not generate low surface energies when simply mixed with another anionic surfactant possessing a long linear alkyl chain. This also suggests that both surfactants mixed should possess the same number of tails, i.e. both single-chains, di-chains etc.

A longer linear chain may generate low surface energies when mixed with AOTA because it is more effective at reducing polar interactions between the two head groups by keeping them further apart. If this was true, comparatively higher surface energies would be expected when mixed with AOTB, as the two head groups would be brought closer together. From Figure 7.4, this is exactly what is seen for the vast majority of systems.

7.4.3 Importance of the linear component

If one examines γ between mole fractions for the various systems presented in Figure 7.4, there appears to be no trend highlighting which of the two surfactant components dominate the low surface energies generated. To further explain why some of the mixed systems introduced here are so highly effective, in particular di-C8SS : AOTA, it is important to understand mixing within the monolayer to help explain the synergistic effect observed. One way this can be investigated is to study the surface properties of mixtures formed from compositions heavily weighted to each surfactant component. Surface energies generated can then be compared to surface properties of the pure components, where the degree of variation will identify the surfactant with the greatest influence. The surface tension of each linear-branched mixed system was measured at mole fractions of 0.01/0.99 AOTA and 0.01 AOTB. The conductivity of each system was first determined (see Supporting Info.). The cmc's and surface tensions generated for each mixed system are shown in Table 7.5.

Figure 7.7 shows a visual representation of the surface tension data from Table 7.5 for 0.01 mole fractions of AOTA and AOTB. Interestingly, when the linear di-chain surfactant is in excess, only a tiny proportion of AOTA/B is required to reduce γ below what di-C6SS, di-C7SS or di-C8SS can generate. The *tert*-butyl chain-tip

Table 7.5: Mixed cmc's (C^*) and surface tension values (γ_{cmc}) at mole fractions of AOTA / AOTB (α), for the di-C6SS, di-C7SS and di-C8SS mixed systems.

α	C^*	γ_{cmc} (mN m^{-1}) ± 0.1	C^*	γ_{cmc} (mN m^{-1}) ± 0.1
	di-C6SS : AOTA		di-C6SS : AOTB	
0	12.7	29.0	12.7	29.0
0.01	12.9	28.9	13.7	28.4
0.99	69.9	28.4	-	-
1	89.6	30.2	25.9	26.7
	di-C7SS : AOTA		di-C7SS : AOTB	
0	3.04	30.2	3.04	30.2
0.01	4.56	28.2	4.58	29.6
0.99	68.2	26.6	-	-
1	89.6	30.2	25.9	26.7
	di-C8SS : AOTA		di-C8SS : AOTB	
0	0.93	30.4	0.93	30.4
0.01	1.71	29.6	1.93	28.1
0.99	65.8	25.7	-	-
1	89.6	30.2	25.9	26.7

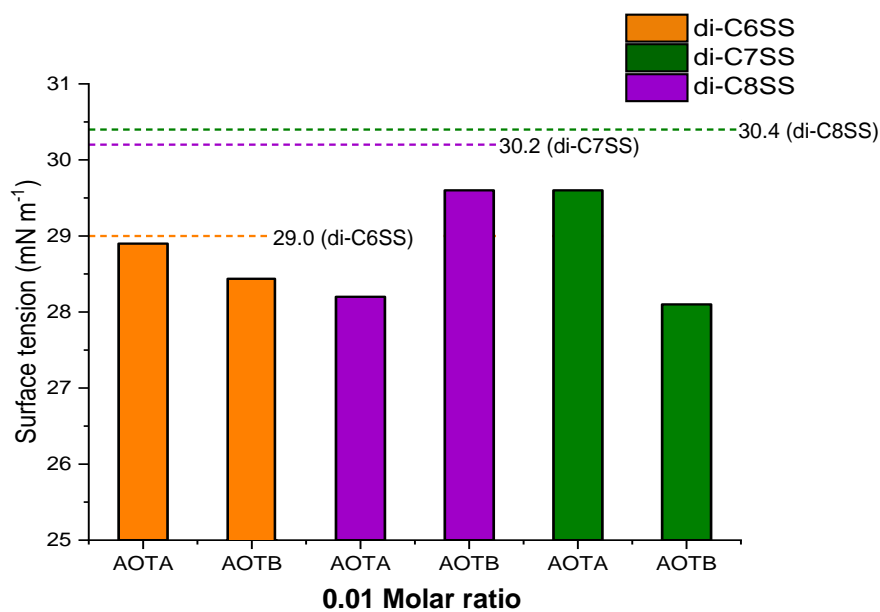


Figure 7.7: Surface tension at 0.01 mole fractions of AOTA or AOTB mixed with C6SS, C7SS or C8SS. Dashed line represents γ_{cmc} of the pure linear di-chain surfactants.

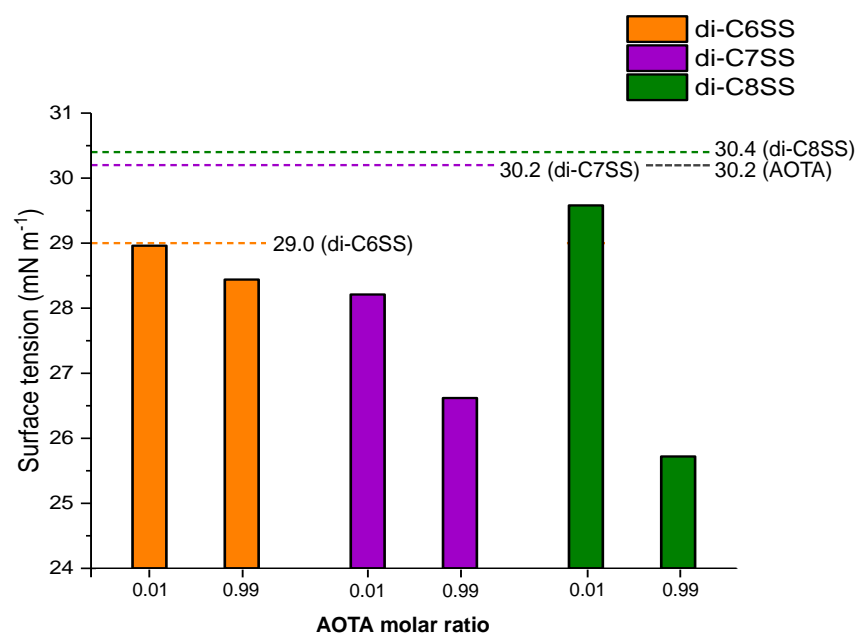


Figure 7.8: Surface tension at 0.01 and 0.99 mole fractions of AOTA mixed with either C6SS, C7SS or C8SS. Dashed line represents γ_{cmc} of pure AOTA and each linear di-chain surfactant.

structure of AOTA/B appears to be very effective at space-filling the monolayer with low surface energy CH_3 groups, having a strong influence on the system. However, to quantitatively compare the influence of each surfactant within these binary mixed systems, surface properties must be compared to systems where AOTA/B is the component in excess.

Figure 7.8 compares surface tension data for linear-branched systems at mole fractions of 0.01 and 0.99 AOTA. For each mixed system investigated, a lower γ is formed at the higher mole fraction of AOTA, as shown in Figure 7.8. Given that for pure AOTA $\gamma_{\text{cmc}} = 30.2 \text{ mN m}^{-1}$, the surface tensions generated at the cmc's of these 0.99 AOTA mixtures are substantially lower. The di-C8SS : AOTA system with 1 % di-C8SS generates a surface tension 5 mN m^{-1} lower than pure AOTA. Comparatively, when the system involves 1 % AOTA a surface tension is generated only 1 mN m^{-1} lower (than pure AOTA). The same trend is seen for the other linear-branched mixed systems. Therefore, this suggests that the linear surfactant more effectively fills the space between AOTA molecules, generating a surface which closely resembles a pure alkane, rather than the opposite being true. Simply put, linear chains seem to be more effective at filling the space between bulky highly branched chains, rather than the other way round. However, for this to be true, the highly branched surfactant should itself generate an efficiently filled monolayer (i.e. a high Φ_{cmc}). This way, there will not be an unachievable amount of space to be filled by the linear surfactant which will possess a $-\text{CH}_3$ chain tip and $-\text{CH}_2-$ chain body with volumes of 54 and 27 \AA^3 respectively.¹⁷ AOTA and AOTB both meet this criteria, achieving $\Phi_{\text{cmc}} = 0.87$ and 0.82 respectively.

7.4.4 Packing efficiency at the surface

In Chapter 5, one way to reduce γ which was introduced was to increase the molecular volume of the surfactant chain-tips. Subsequently, this leads to a more efficiently filled area per molecule for the surfactant (i.e. a high Φ_{cmc}), generating a lower surface free energy. The results presented in this chapter have shown how low surface energies can also be generated by mixing short highly branched surfactants with long linear surfactants. Provided the linear surfactant is of sufficient length to effectively reduce polar interactions between the head groups, and the branched surfactant can generate an efficiently packed monolayer. To further investigate the subtleties of surfactant packing in binary mixed systems, the linear di-chain surfactant di-C8SS was mixed with AOTSiA and AOTSiB. The surface properties of the TMS-hedgehogs AOTSiA/SiB have already been discussed in Section 5.4. The linear di-chain surfactant di-C8SS was selected as it generates the lowest surface energies when mixed with AOTA/B. The experimentally determined cmc's of the di-C8SS : AOTSiA/SiB systems were first introduced in Table 7.2, and the micellar properties predicted by RST in Section 7.3. Therefore, only the surface properties of these systems will be discussed here.

Table 7.6 provides experimentally determined cmc's and surface tensions generated for the di-C8SS : AOTSiA/SiB mixed systems. This data is visually represented in Figure 7.9. The surface energies generated by the di-C8SS : AOTSiA system are lower than γ_{cmc} for each pure component at every mole fraction studied. However, for AOTSiB, mixed systems are formed which generate γ_{cmc} higher than γ_{cmc} of the most effective component, for every mole fraction. This is not the same trend

Table 7.6: Mixed cmc's (C^*) and surface tension values (γ_{cmc}) at mole fractions of AOTSiA / AOTSiB (α), for the di-C8SS mixed systems.

α	C^*	γ_{cmc} (mN m ⁻¹) ± 0.1	C^*	γ_{cmc} (mN m ⁻¹) ± 0.1
	di-C8SS : AOTSiA		di-C8SS : AOTSiB	
0	0.93	29.0	0.93	29.0
0.10	2.66	25.9	1.47	25.5
0.25	5.66	25.8	1.85	25.3
0.50	6.92	25.5	3.83	25.4
0.75	12.5	25.6	11.7	25.9
0.90	11.8	26.0	11.9	26.2
1	68.1	27.0	15.9	24.3

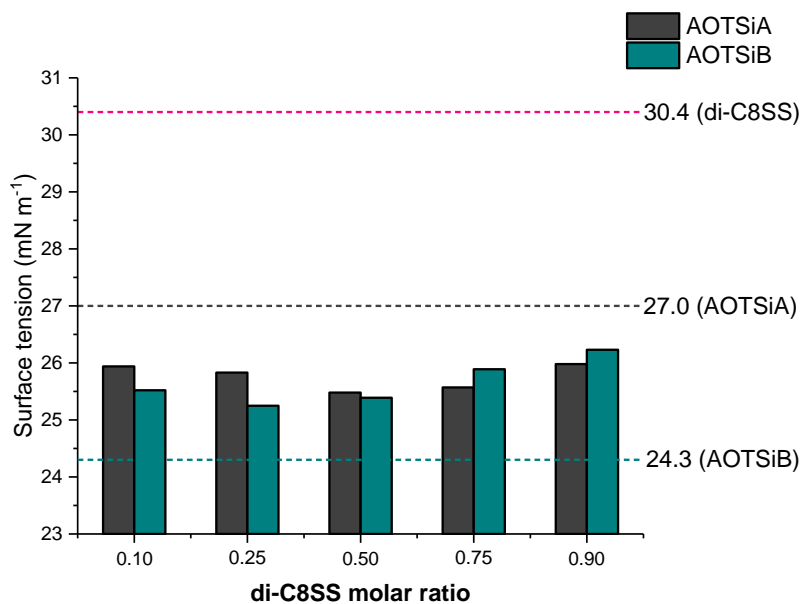


Figure 7.9: Surface tension at each mole fraction where column height represents the surface tension generated, and the dashed lines represent γ_{cmc} of each pure surfactant.

that was seen for di-C8SS : AOTA/B, where every mixture generated lower surface energies than its constituent components. Furthermore, the values of γ_{cmc} are lower for di-C8SS : AOTA than di-C8SS : AOTSiA. Given that for AOTA $\gamma_{\text{cmc}} = 30.2 \text{ mN m}^{-1}$ and for AOTSiA $\gamma_{\text{cmc}} = 27.0 \text{ mN m}^{-1}$, this is perhaps not what one would expect. Clearly when mixing AOTSiA with di-C8SS, the slight increase in molecular volume of the chain tip has adverse effects on packing within the mixed monolayer. Highlighting the sensitive relationship between molecular structure and surface tension for binary anionic systems.

As suggested in Section 7.4.2, for the systems studied here, a longer linear chain is more effective because it reduces polar interactions between the two head groups. Therefore, we might expect di-C8SS : AOTSiB to not generate surface energies substantially lower than di-C8SS : AOTB, which is indeed the case. However, given the success of di-C8SS : AOTA, and the relatively lower γ_{cmc} of AOTSiA, it is plausible for di-C8SS : AOTSiA to generate even lower surface energies, which is not what is observed. This might be explained following the arguments laid out in the previous section, i.e. the lowest surface energies generated by these mixed systems are a product of the branched surfactants packing efficiently, and the small

amount of space present in the monolayer being filled by the linear surfactant. But what if the branched surfactant already packs too efficiently?

The packing efficiency, Φ_{cmc} , of a surfactant is calculated from V_{cal} divided by V_{meas} (see Section 2.7). Where V_{cal} is the molecular volume of the surfactant tail based on the summation of the individual fragments, and V_{meas} is the largest volume the tail could occupy, based on its area per molecule (A_{cmc}) and tail length (τ). V_{free} is the amount of space left, calculated from $V_{\text{meas}} - V_{\text{cal}}$. From a knowledge of experimentally determined values of A_{cmc} and Φ_{cmc} for AOTA/AOTSiA,¹⁸ V_{free} can be calculated. A depiction of the volumes used to calculate Φ_{cmc} , as well as calculated values of V_{free} for AOTA and AOTSiA are shown in Figure 7.10. It is clear to see that AOTSiA is nearer limit of efficient packing, with a value of $V_{\text{free}} = 17 \text{ \AA}^3$ compared to 54 \AA^3 for AOTA. Therefore, when both are mixed with a di-chain linear surfactant, the volume of space within a monolayer of AOTSiA surfactant molecules will perhaps not be sufficiently large enough to easily accommodate the additional volume of the linear tail ($-\text{CH}_3 / -\text{CH}_2- = 54 / 27 \text{ \AA}^3$ respectively, ref. [17]). Interestingly, a monolayer of AOTA surfactant molecules has an estimated 54 \AA^3 volume of free space per surfactant molecule, which is the same as the volume of a $-\text{CH}_3$ group. Perhaps this is further reason why AOTA forms such low surface energies when mixed with linear counterparts.

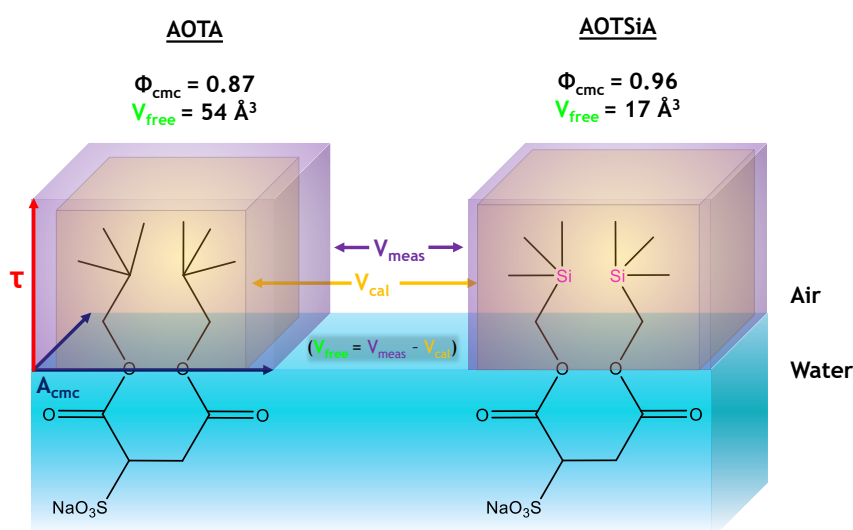


Figure 7.10: A representation of the volumes V_{cal} and V_{meas} which are used to calculate Φ_{cmc} . Values of V_{free} calculated for AOTA and AOTSiA are also shown.

7.5 Branched-branched mixed systems

When mixing anionic hydrocarbon surfactants, one approach to form low surface energies is to mix linear and branched surfactants. Because, spaces present within the monolayer are filled, generating a denser surface layer than what the pure constituent surfactants can achieve, thus further reducing γ . However, as highlighted in Section 7.4, this is not true for all mixtures of branched-linear anionic hydrocarbon surfactants. The lowest surface energies were formed by mixtures that obeyed the following criteria:

- Both surfactants should possess the same number of tails, i.e. di-chain, single-chain etc.
- The tail of the linear component should be sufficiently long enough, and likewise the tail of the branched component short enough, to reduce polar interactions between head groups of each constituent surfactant.
- The branched surfactant should pack efficiently at the air-water interface (high Φ_{cmc}), to present a suitably small amount of free space that can be effectively filled by the linear surfactant.

To further explore the relationship between surface tension and packing efficiency for mixed hydrocarbon systems, as well as the generality of these criteria above, the hedgehog surfactants AOTA and AOTB were individually mixed with two branched surfactants, HS3 and AOT. Aerosol-OT could be considered the di-chain equivalent of SDS, being a readily available, heavily explored and widely understood surfactant.¹⁹⁻²¹ Previous studies have explored structure-property relationships of mixed systems involving AOT,²² but there have been very few which involve AOT with other anionic hydrocarbon surfactants. AOT was also selected because it has a tail which is 6 carbons long, see Figure 7.1, and thus provides a branched comparison to di-C6SS. HS3 is a hedgehog surfactant that was introduced in Chapter 5. It was selected for this study due to its highly saturated, compact tail, which provides many low surface energy $-\text{CH}_3$ groups, in a similar fashion to AOTA and AOTB.

7.5.1 Surface tension results

With cmc 's estimated, the surface tension generated at each mole fraction was determined using a K100 tensiometer following the experimental procedure outlined in Section 4.6.2. For all systems studied, the surface tension was recorded at 1.1x the cmc to ensure a fully saturated surfactant monolayer. These data are recorded in Table 7.7, and the surface tension data visually represented in Figure 7.11. From examining Figure 7.11, there is a noticeable effect on γ_{cmc} when the linear component is replaced by a branched surfactant.

For AOT, there are some similarities to the mixed systems formed with its linear equivalent di-C6SS. Both systems generate lower surface energies than either constituent surfactant when AOTA is involved, but not AOTB. Interestingly, AOT : AOTA generates lower surface energies than di-C6SS : AOTA at all mole fractions studied. The lowest surface energies generated by AOT : AOTA are a remarkable 5 mN m^{-1} lower than either pure surfactant, similar to the super-effective di-C8SS : AOTA system. Therefore, the slightly branched nature of AOT is clearly beneficial. From Figure 7.11, the lowest surface energies are formed at the higher mole fractions of AOTA/B. This is similar to what was seen with the linear systems, and therefore,

Table 7.7: Mixed cmc 's (C^*) and surface tension values (γ_{cmc}) at mole fractions of AOTA / AOTB (α), for the HS3 and AOT mixed systems.

α	C^*	$\gamma_{cmc} \text{ (mN m}^{-1}\text{)}$ ± 0.1	C^*	$\gamma_{cmc} \text{ (mN m}^{-1}\text{)}$ ± 0.1
	HS3 : AOTA		HS3 : AOTB	
0	33.6	29.7	33.6	29.7
0.10	35.8	32.4	32.6	29.7
0.25	39.8	30.6	31.3	28.5
0.50	48.8	31.1	29.2	27.8
0.75	63.2	28.8	27.5	27.5
0.90	76.8	28.8	26.5	31.8
1	89.6	30.2	25.9	26.7
	AOT : AOTA		AOT : AOTB	
0	2.60	30.4	2.60	30.4
0.10	6.39	28.0	2.86	28.4
0.25	6.74	27.5	3.35	27.6
0.50	6.87	26.4	4.73	27.5
0.75	18.5	25.5	7.99	27.2
0.90	16.1	25.6	13.7	26.7
1	89.6	30.2	25.9	26.7

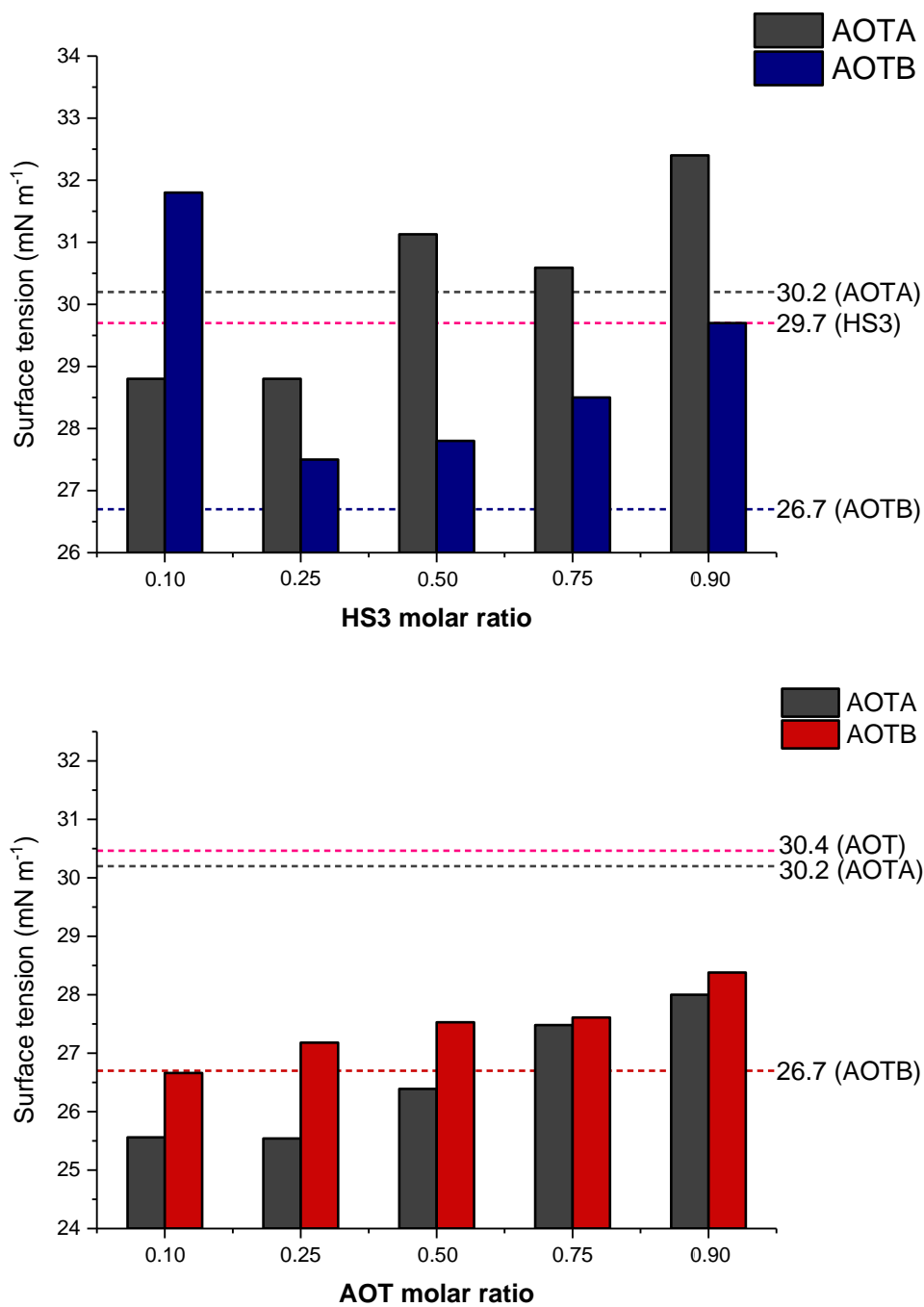


Figure 7.11: Surface tension at each mole fraction where column height represents the surface tension generated, and the dashed lines represent γ_{cmc} of the pure surfactants.

this also suggests that the lowest surface energies are formed when AOT effectively fills the space present in a monolayer of AOTA or AOTB. So why does AOTA mix more effectively with AOT than di-C6SS?

AOT does share a similar area per molecule with AOTA, 75 and 79 Å² respectively, compared to di-C6SS where $A_{\text{cmc}} = 62$ Å². Therefore perhaps AOTA and AOT can more easily pack together as they occupy geometrically similar areas. However, this is unlikely as di-C8SS $A_{\text{cmc}} = 55$ Å² which is not similar to AOTA's A_{cmc} , but when mixed clearly display synergistic packing. As was suggested in Section 7.4.2, when mixing with a longer linear chain, lower surface energies are generated due to the distance between head groups of each linear/branched surfactant being increased, reducing polar interactions within the monolayer. The branched ethyl group present on the tail of AOT sits close to the head group. Therefore, when mixing with AOTA perhaps this branched ethyl group acts to further shield the head groups of AOTA and AOT from each other. Which compared to a linear C6 chain will more effectively reduce polar interactions between the two.

When mixed with AOTA/B, HS3 shows signs of antagonistic mixing within the monolayer, generating surface energies higher than either constituent surfactant. This is true for all mixtures at all mole fractions except HS3 : AOTA at $\alpha = 0.1$ and 0.25. Interestingly, lower surface energies are generated when HS3 is mixed with AOTB, not AOTA like all other systems studied in this chapter.

One of the criteria outlined at the start of Section 7.5 was that when mixing anionic hydrocarbon surfactants, one component should possess a long alkyl tail to reduce polar interactions with the head group of the other component. HS3 does not meet this requirement, and similar to AOTA/B, possesses a tail with a bulky chain-tip presenting many $-\text{CH}_3$ groups. Therefore, because of their bulky nature, when mixed the tails will not be able to pack efficiently together to fill spaces present in the monolayer. Furthermore, because HS3, AOTA and AOTB are all small surfactants, when packing together neighbouring head groups will be close to each other, similar to a monolayer of each pure component. When mixing with AOTB, which has a longer tail than AOTA, one would expect lower surface energies due to an increased distance between head groups, which is seen in Figure 7.11.

7.6 Generating low surface energies

Throughout this chapter a variety of linear-branched / branched-branched hydrocarbon mixtures have been studied. All of the mixtures are composed from anionic surfactants, which has allowed a closer look at only the synergistic effects between differing surfactant tails. Synergistic effects between the head groups can be disregarded as they are all sulfosuccinate surfactants with sodium counterions, and therefore, the synergistic surface properties observed are due to interactions between tails. This section aims to consolidate the general structure-property relationships which have been identified, and can thus guide future designs when selecting anionic hydrocarbon surfactants to mix and achieve very low surface energies.

1. *Surfactants should possess the same number of tails.*

That is, they should both be di-chain or single-chain surfactants. This was shown to allow surfactants to pack much more efficiently at the surface to generate low surface energies.

2. *The effective chain length of each surfactant should be different.*

To generate dense surface layers and hence low surface energies, polar interactions between head groups of different surfactants must be reduced. This can be achieved by mixing long and short chain surfactants. Or similarly, branching the long tail to shield polar interactions between head groups

3. *The branched surfactant should pack efficiently at the surface.*

The lowest surface energies were generated by mixing short highly branched, and long linear surfactants. The branched surfactants were shown to give high values of Φ_{cmc} , leaving a small amount of space which appropriately accommodates the volume of the linear tail chain-tip. However, this relationship was also shown to be sensitive and for the small branched surfactant, the free volume of space per surfactant molecule should be evaluated first, to identify possible synergistic mixing within the monolayer.

7.7 Conclusions

Over sixty mixtures of anionic hydrocarbon surfactants have been studied, where branched and linear tails have been combined to enhance packing within the surfactant monolayer at the air-water interface. Many mixtures generate lower surface tensions than either constituent component, with some generating γ_{cmc} as low as 24 mN m^{-1} . These very low surface energies are comparable with certain pure liquid alkanes, $\gamma_{\text{n-dodecane}} = 25.4 \text{ mN m}^{-1}$. By making small systematic variations in the molecular structure of the surfactant tail, it has been possible to identify structure-property relationships for these effective binary systems. Furthermore, by keeping the head group of each surfactant the same (sulfosuccinate), the structure-property relationships identified are dependent on the surfactant tail. Hence, this provides a genuine insight into the relationship between packing efficiency and surface tension. Although other studies have investigated mixing hydrocarbon surfactants (ref. [10]), none have explored mixing branched and straight tail surfactants, or produced such low surface energies from mixed hydrocarbon surfactant systems. The low surface energies generated by these binary mixtures has been attributed to efficient space-filling within the mixed monolayer (ref. [23]), whilst also effectively reducing polar interactions between head groups. However, this relationship is shown to be sensitive, as minor changes in the tail structure can greatly increase the surface tensions generated. The most effective systems follow a simple set of criteria, namely: 1) surfactants possess the same number of tails 2) the effective chain length of each surfactant is noticeably different and 3) the branched surfactant can pack efficiently at the surface. Previous studies have highlighted synergistic surface tension effects due to coulombic interactions (ref. [9]). Overall, the results presented here highlight a novel approach to generating low surface energies, which is to improve packing efficiency at the surface by mixing appropriately selected surfactants. This guides new ways of employing hydrocarbon surfactants in practical applications that require low surface energies, reducing the use of more conventional, but environmentally hazardous fluorocarbon surfactants.

References

- [1] Holland, P. M.; Rubingh, D. N. *Mixed surfactant systems: an overview*; ACS Publications, 1992.
- [2] Christian, S. D.; Scamehorn, J. F. *Solubilization in surfactant aggregates*; CRC Press, 1995; Vol. 55.
- [3] Asakawa, T.; Johten, K.; Miyagishi, S.; Nishida, M. *Langmuir* **1988**, *4*, 136–140.
- [4] Guo-Xi, Z.; Bu-Yao, Z. *Colloid. Polym. Sci.* **1983**, *261*, 89–91.
- [5] Tamori, K.; Esumi, K.; Meguro, K. *J. Colloid Interface Sci.* **1991**, *142*, 236–243.
- [6] Smith, I.; Ottewill, R. *Surface Active Agents*; 1979; pp 77–87.
- [7] Danov, K.; Kralchevska, S.; Kralchevsky, P.; Ananthapadmanabhan, K.; Lips, A. *Langmuir* **2004**, *20*, 5445–5453.
- [8] Sharma, K. S.; Rodgers, C.; Palepu, R. M.; Rakshit, A. *J. Colloid Interface Sci.* **2003**, *268*, 482–488.
- [9] Bera, A.; Ojha, K.; Mandal, A. *J. Surfactants Deterg.* **2013**, *16*, 621–630.
- [10] Shinoda, K. *J. Phys. Chem.* **1954**, *58*, 541–544.
- [11] Vora, S.; George, A.; Desai, H.; Bahadur, P. *J. Surfactants Deterg.* **1999**, *2*, 213–221.
- [12] Nave, S.; Eastoe, J.; Penfold, J. *Langmuir* **2000**, *16*, 8733–8740.
- [13] Zisman, W. A. *Adv. Chem. Ser.* **1964**, *43*, 1–51.

- [14] Yan, Y.; Huang, J.; Li, Z.; Han, F.; Ma, J. *Langmuir* **2003**, *19*, 972–974.
- [15] Zhang, R.; Zhang, L.; Somasundaran, P. *J. Colloid Interface Sci.* **2004**, *278*, 453–460.
- [16] Rana, D.; Neale, G.; Hornof, V. *Colloid. Polym. Sci.* **2002**, *280*, 775–778.
- [17] Krafft, M. P.; Riess, J. G. *Chem. Rev.* **2009**, *109*, 1714–1792.
- [18] Czajka, A.; Hill, C.; Peach, J.; Pegg, J. C.; Grillo, I.; Guittard, F.; Rogers, S. E.; Sagisaka, M.; Eastoe, J. *Phys. Chem. Chem. Phys.* **2017**, *19*, 23869–23877.
- [19] Nave, S.; Eastoe, J.; Heenan, R. K.; Steytler, D.; Grillo, I. *Langmuir* **2000**, *16*, 8741–8748.
- [20] Nave, S.; Eastoe, J.; Heenan, R. K.; Steytler, D.; Grillo, I. *Langmuir* **2002**, *18*, 1505–1510.
- [21] Nave, S.; Paul, A.; Eastoe, J.; Pitt, A. R.; Heenan, R. K. *Langmuir* **2005**, *21*, 10021–10027.
- [22] Ali, H. E.-S. *J. Surfactants Deterg.* **2007**, *10*, 117–124.
- [23] Czajka, A.; Hazell, G.; Eastoe, J. *Langmuir* **2015**, *31*, 8205–8217.

PROJECT CONCLUSIONS

The structure-property relationships of hydrocarbon surfactants have been explored through single-chain sulfonates and di-chain sulfosuccinates. Relationships between structure and performance have been examined through surface and bulk techniques, including tensiometry and small-angle neutron scattering (SANS). Here, the properties of effective hydrocarbon surfactants have been outlined by studying systematic series, where small variations in structure have allowed greater insight into the underlying structure-property relationships of hydrocarbon surfactants.

The first, and perhaps most significant issue to address is the purity of each surfactant studied. As all surfactants investigated in this research were synthesised and not purchased (except AOT and SDS), it was critical to establish, and maintain a high purity for all systems. Rigorous cleaning procedures, further surface experiments (EDTA), and various purification methods were found to be necessary to establish a high purity.¹ Previous work has highlighted the importance of removing excess salts to measure and study accurate adsorption isotherms.² Once the desired surfactant purity was confirmed, it is equally imperative that the surface properties of the surfactant are determined accurately from a standard procedure that allows an impartial comparison to other surfactants and literature. Therefore, important considerations when determining accurate surface properties for novel ionic surfactants were first outlined.

To develop the surface performance of hydrocarbon surfactants, relationships between structure and surface tension must be developed beyond our current understanding.³ Which fundamentally, improves our understanding of controlling surface tension. By evaluating the surface coverage, Φ_{cmc} , of the most effective fluorocarbon, hydrocarbon and silicone surfactants, the first general structure-property relationship of low aqueous surface tension has been identified.⁴ Namely, for all surfactants, low aqueous surface tensions are generated through efficient surface packing which helps to generate dense surface coverages. Therefore, to improve the performance of hydrocarbon surfactants, the surfactant structure must be developed to generate surface densities which effectively mimic a pure alkane.

Branching the tail is an effective approach to reduce the surface energies generated by hydrocarbon surfactants due to an increase in the number of low surface energy CH_3 groups.⁵ This idea has been further reinforced by the introduction of highly branched hydrocarbon surfactants termed *hedgehog* surfactants, achieving surface energies $\sim 25 \text{ mN m}^{-1}$, down from $\sim 30 \text{ mN m}^{-1}$ generated by conventional linear hydrocarbon surfactants.⁶ A series of hedgehog surfactants were introduced where the $\text{CH}_3 : \text{CH}_2$ ratio was systematically increased. As the ratio was increased, lower surface energies were generated parallel to an increase in the surface coverage, Φ_{cmc} . This highlighted the importance of the *tert*-butyl group to generate low surface tensions, possessing the highest methyl content of any alkyl moiety. A novel series of surfactants were introduced where carbon in the *tert*-butyl group was replaced with silicon. This was shown to be an effective method to increase the surface coverage, leading to the lowest surface tensions currently generated by hydrocarbon surfactants (AOTSiC $\gamma_{\text{cmc}} = 22.8 \text{ mN m}^{-1}$). By comparing surface properties for several novel series of hydrocarbon surfactant introduced with previous literature, it was possible to identify structural characteristics shared by all effective hydrocarbon surfactants. This was shown to be dependent on a) the alkyl chain length of the surfactant tail, b) the degree of branching at the chain-tip and c) the degree of branching away from the chain tip. Based on these properties, a new index to assess potential performance and help guide the design of super-effective surfactant tails has been introduced, H_γ .

With the properties of an effective hydrocarbon tail outlined through H_γ , attempts were made to improve surfactant effectiveness by controlling the identity of the head group. Utilising tetraalkylammonium (TAA) counterions, the lowest surface energies have been reported for single-chain surfactants, some being below that of their respective parent alcohol. However, the head group was shown to have only minor effects on aggregation within the bulk through SANS.⁷ By comparing a range of different tails with the same variety of head groups, the tetrapropylammonium counterion was shown to be an effective replacement to generate lower surface energies than the common sodium counterion. This is thought to be due to weaker polar interactions between neighbouring head groups.⁸

With the structural characteristics of effective hydrocarbon surfactants estab-

lished, final developments were focused on more practical applications of hydrocarbon surfactants, i.e. mixed systems. Forming binary systems was shown to be an effective method to improve surface coverage and generate very low surface energies $< 25 \text{ mN m}^{-1}$, approaching that of certain pure alkanes ($\gamma_{\text{n-dodecane}} = 25.4 \text{ mN m}^{-1}$). Linear surfactants can effectively fill the ‘spaces’ present within a monolayer of branched surfactant molecule, with many linear-branched systems generating lower surface energies than either constituent surfactant. By forming mixed systems from a large variety of structures, it was possible to identify structure-property relationships of effective systems helping guide the design of future possible combinations: 1) surfactants should possess the same number of tails, 2) the effective chain length of each surfactant should be different, and 3) the branched surfactant should pack efficiently at the surface.

This research highlights the subtle nature of generating surface energies close to the limit of achievable performance with hydrocarbon surfactants. Furthermore, it consolidates structure-property relationships at the air-water interface to highlight structural characteristics of effective hydrocarbon surfactants. Now, a guide has been established to design effective hydrocarbon surfactants, where the lowest surface energies for single-chain, di-chain and mixed surfactants systems have been achieved through the principles outlined. The future for hydrocarbon surfactants as alternatives to fluorosurfactants looks strong with the hydrocarbon guide to constructing, surfactants at the design limit.

References

- [1] Eastoe, J. et al. *Langmuir* **2000**, *16*, 4511-4518.
- [2] An, S.; Lu, J.; Thomas, R.; Penfold, J. *Langmuir* **1996**, *12*, 2446-2453.
- [3] Nave, S.; Eastoe, J.; Penfold, J. *Langmuir* **2000**, *16*, 8733-8740.
- [4] Czajka, A.; Hazell, G.; Eastoe, J. *Langmuir* **2015**, *31*, 8205-8217.
- [5] Sagisaka, M. et al. *Langmuir* **2014**, *30*, 6057-6063.
- [6] Alexander, S. et al. *Langmuir* **2014**, *30*, 3413-3421.
- [7] Bonilha, J. B. et al. *J. Colloid Interface Sci.* **1990**, *135*, 238-245.
- [8] Brown, P. et al. *J. Colloid Interface Sci.* **2013**, *395*, 185-189.

FUTURE OUTLOOK

There are various avenues that can be explored to continue and extend the work presented here, which would both complement and enhance the results which have been gained so far.

1. *Thermodynamic studies*

To gain a deeper insight into relationships between structure and performance, future work should consider studying the associated free energy changes (i.e. micellisation) for hydrocarbon surfactants presented in this work. The di-chain series (i.e. HS/TMS) are suitable candidates because: 1) the free energy changes would be associated with systematic structural changes, and 2) there is also great variation in γ_{cmc} with each systematic structural change.

2. *Tertiary alcohol surfactants*

The main principles of effective hydrocarbon surfactants outlined in this work are all dependent on surfactants synthesised from primary and secondary alcohols. To synthesise hydrocarbon surfactants from tertiary alcohols would not only likely generate the lowest surface energies achieved to date, it would provide the final link to bind all current structure-property relationships.

3. *Reflectometry of mixed surfactants systems*

The mixed systems chapter introduced many successful combinations of linear-branched hydrocarbon surfactants. Although it is a struggle to deuterate branched surfactants, linear surfactants can be deuterated with relative ease. Studying the surface compositions of these systems by reflectometry would provide unmatched insight into structure-packing relationships within the monolayer. Further explaining the extraordinary properties observed.

4. *Lower surface energies*

A few suggestions are outlined here to generate potentially even lower surface energies, which are perhaps more suitable as masters project: mixing anionic-cationic linear-branched surfactants, TPA head group with super-effective surfactants.

- *This page intentionally left blank* -

SUPPORTING INFORMATION



TABLE OF CONTENTS

8.1 NMR and EA analysis

8.1.1	AOTA	218
8.1.2	AOTB	219
8.1.3	AOTSiA	220
8.1.4	AOTSiB	221
8.1.5	AOTSiC	223
8.1.6	HS1	224
8.1.7	HS2	225
8.1.8	HS3	226
8.1.9	di-C6SS	227
8.1.10	di-C7SS	228
8.1.11	di-C8SS	229
8.1.12	Na-FO180	230
8.1.13	TMA-FO180	231
8.1.14	TEA-FO180	232
8.1.15	TPA-FO180	233
8.1.16	Na-FO180N	234
8.1.17	TMA-FO180N	235
8.1.18	TEA-FO180N	236
8.1.19	TPA-FO180N	237
8.1.20	Na-BC9	238
8.1.21	TMA-BC9	239
8.1.22	TEA-BC9	240
8.1.23	TPA-BC9	241
8.1.24	Na-BC7	242
8.1.25	TMA-BC7	243
8.1.26	TEA-BC7	244
8.1.27	TPA-BC7	245
8.1.27	SDS	246
8.1.28	AOT	247

8.2 Conductivity data and cmc analysis - Mixed systems

8.2.1	di-C6SS : AOTA / AOTB	248
8.2.2	di-C7SS : AOTA / AOTB	256
8.2.3	di-C8SS : AOTA / AOTB	264
8.2.4	di-C8SS : AOTSiA / AOTSiB	272
8.2.5	HS3 : AOTA / AOTB	278
8.2.6	AOT : AOTA / AOTB	284
8.2.7	SDS : AOTA / AOTB	290

8.3 Conductivity data and cmc analysis - Surfactants

8.3.1	SDS	292
8.3.2	AOT	293
8.3.3	di-C6SS	294
8.3.4	di-C7SS	295
8.3.5	di-C8SS	296

8.4 BASIC code - Mixed systems 297

8.4 Techniques - Wilhelmy plate 299

8.1 NMR and EA analysis

The following pages provide the NMR and EA analysis for all surfactants synthesised in this thesis. Peak assignments and integrations are provided, where good agreement is found between experimentally and theoretically determined values.

8.1.1 AOTA

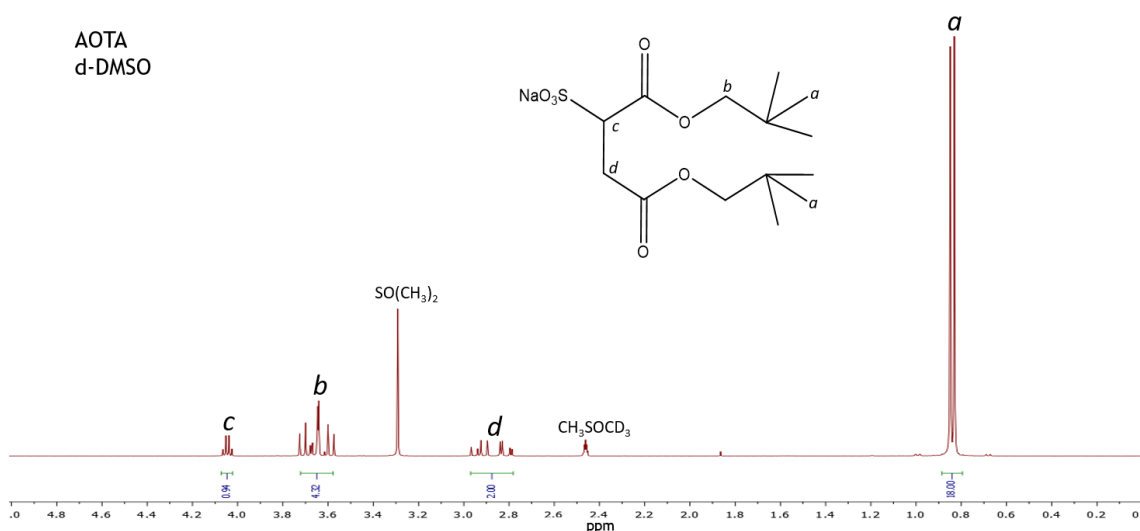


Table 8.1: Data from ¹H NMR spectrum of AOTA with corresponding elemental analysis shown below where experimentally obtained values are shown in blue.

Chemical Shift (ppm)	Molecular fragment	Integration	Identified proton
AOTA			
0.80 - 0.87	-CH ₂ -C(CH ₃) ₃	18.00	a
2.78 - 2.97	-CO-CH ₂ -	2.00	d
3.58 - 3.72	NaO ₃ S-CH-	4.32	b
4.02 - 4.07	-O-CH ₂ -	0.94	c

Theoretical - Experimental		
C	H	S
46.66 - 46.76	6.99 - 7.19	8.90 - 8.78

8.1.2 AOTB

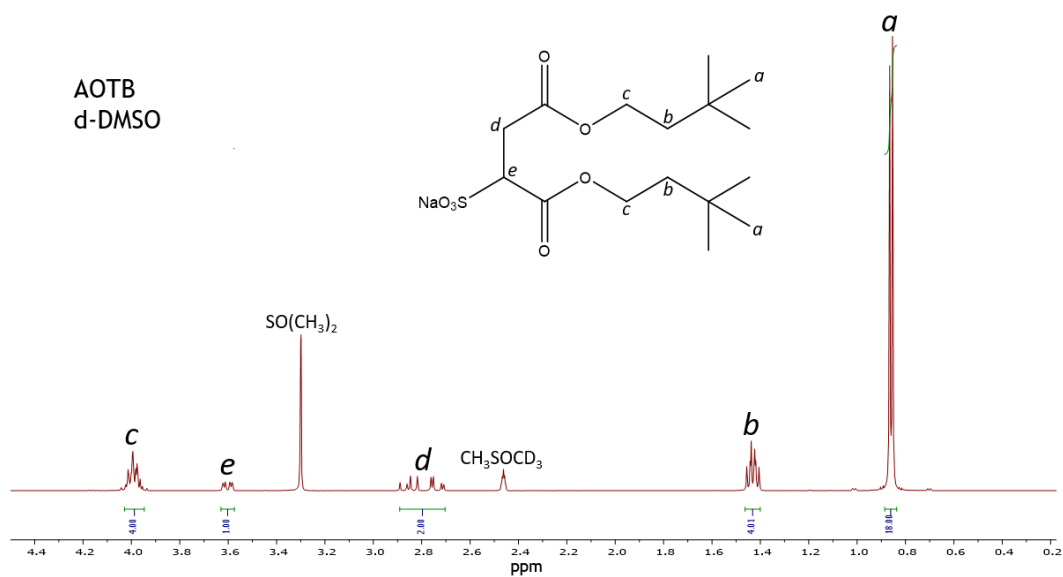


Table 8.2: Data from ¹H NMR spectrum of AOTB with corresponding elemental analysis shown below where experimentally obtained values are shown in blue.

Chemical Shift (ppm)	Molecular fragment	Integration	Identified proton
AOTB			
0.84 - 0.89	-CH ₂ -C(CH ₃) ₃	18.00	a
1.40 - 1.46	-CH ₂ -CH ₂ -	4.01	b
2.70 - 2.89	-CO-CH ₂ -	2.00	d
3.57 - 3.63	NaO ₃ S-CH-	1.00	e
3.95 - 4.03	-O-CH ₂ -	4.00	c

Theoretical - Experimental		
C	H	S
49.40 - 49.89	7.47 - 7.34	8.24 - 8.17

8.1.3 AOTSiA

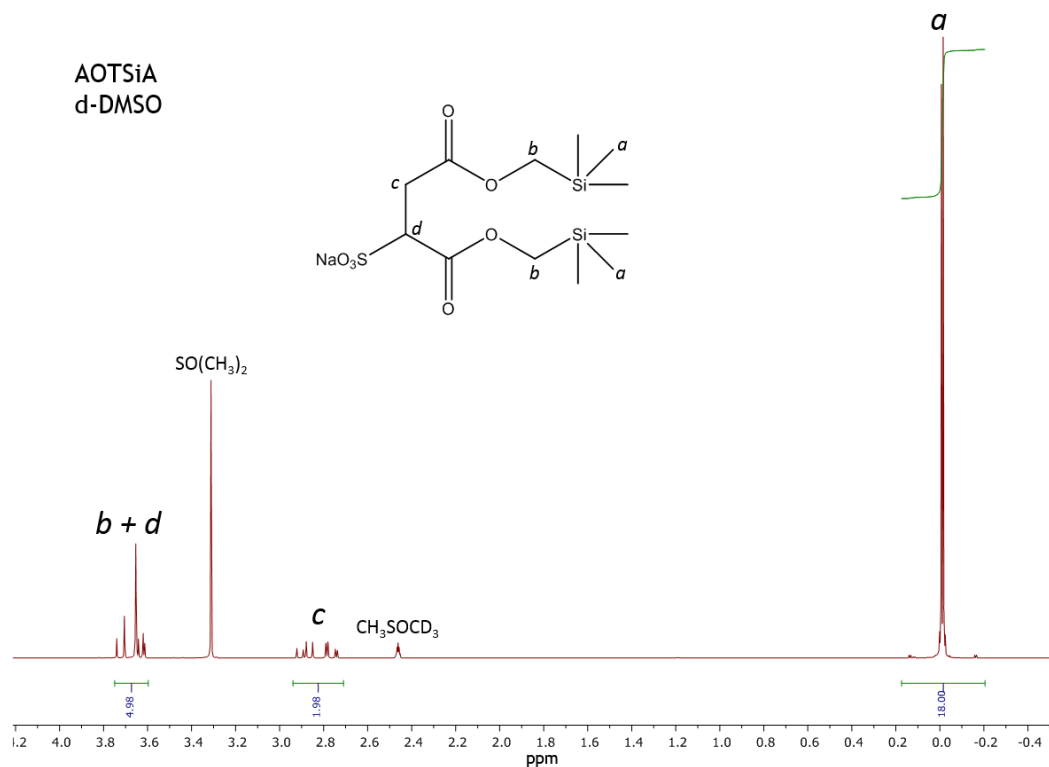


Table 8.3: Data from ¹H NMR spectrum of AOTSiA with corresponding elemental analysis shown below where experimentally obtained values are shown in blue.

Chemical Shift (ppm)	Molecular fragment	Integration	Identified proton									
AOTSiA												
-0.21 - 0.17	-CH ₂ -(SiCH ₃) ₃	18.00	a									
2.71 - 2.94	-CO-CH ₂ -	1.98	c									
3.60 - 3.75	-O-CH ₂ - NaO ₃ S-CH-	4.98	b + d									
<table border="1"> <thead> <tr> <th colspan="3">Theoretical - Experimental</th> </tr> <tr> <th>C</th> <th>H</th> <th>S</th> </tr> </thead> <tbody> <tr> <td>36.72 - 36.98</td> <td>6.42 - 6.48</td> <td>8.17 - 8.01</td> </tr> </tbody> </table>				Theoretical - Experimental			C	H	S	36.72 - 36.98	6.42 - 6.48	8.17 - 8.01
Theoretical - Experimental												
C	H	S										
36.72 - 36.98	6.42 - 6.48	8.17 - 8.01										

8.1.4 AOTSiB

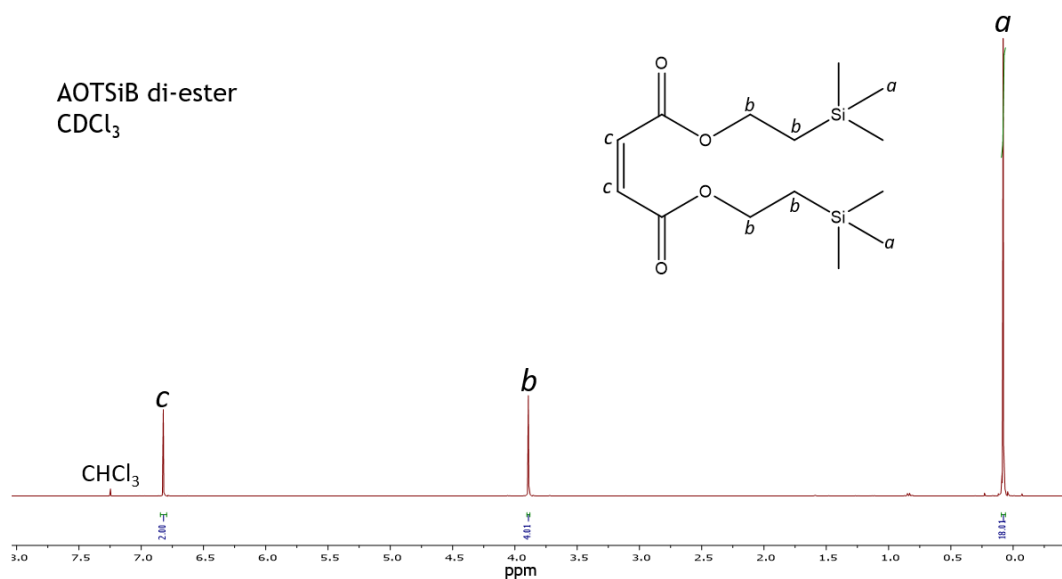


Table 8.4: Data from ¹H NMR spectrum of AOTSiB di-ester with corresponding elemental analysis shown below where experimentally obtained values are shown in blue.

Chemical Shift (ppm)	Molecular fragment	Integration	Identified proton
AOTSiB			
0.061 - 0.094	-CH ₂ -Si(CH ₃) ₃	18.01	a
3.88 - 3.90	-O-C ₂ H ₄ -	4.01	b
6.80 - 6.85	-CO-CH ₂ -CO-	2.00	c

Theoretical - Experimental	
C	H
53.07 - 54.04	8.85 - 8.77

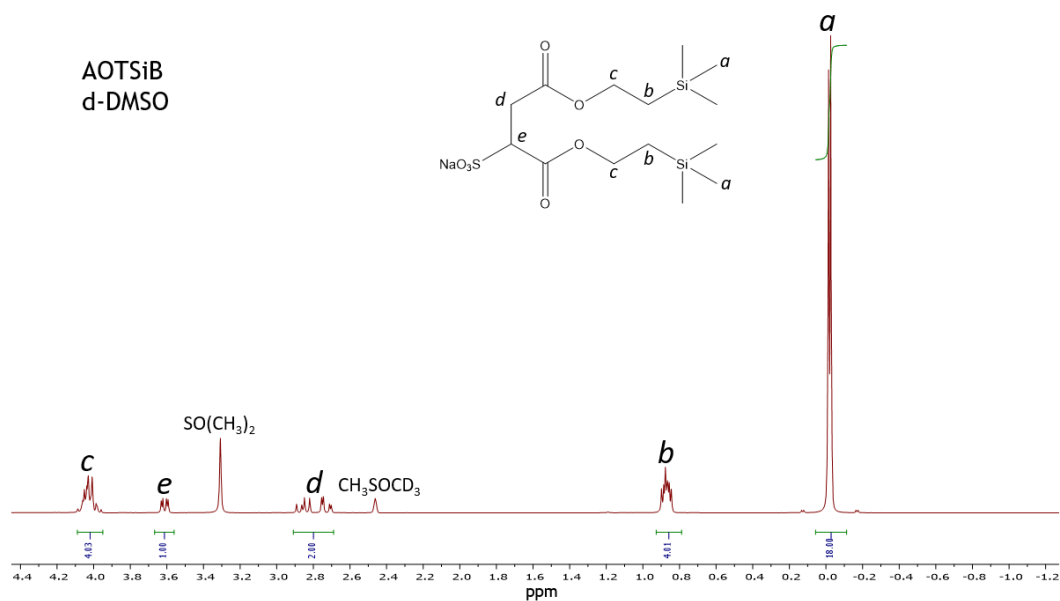


Table 8.5: Data from ^1H NMR spectrum of AOTSiB with corresponding elemental analysis shown below where experimentally obtained values are shown in blue.

Chemical Shift (ppm)	Molecular fragment	Integration	Identified proton
AOTSiB			
-0.11 - 0.057	$-\text{CH}_2-\text{Si}(\text{CH}_3)_3$	18.00	a
0.79 - 0.93	$-\text{CH}_2-\text{CH}_2-$	4.01	b
2.69 - 2.91	$-\text{CO}-\text{CH}_2-$	2.00	d
3.56 - 3.67	$\text{NaO}_3\text{S}-\text{CH}-$	1.00	e
3.95 - 4.09	$-\text{O}-\text{CH}_2-$	4.03	c

Theoretical - Experimental		
C	H	S
39.98 - 40.12	6.98 - 6.98	7.62 - 7.48

8.1.5 AOTSiC

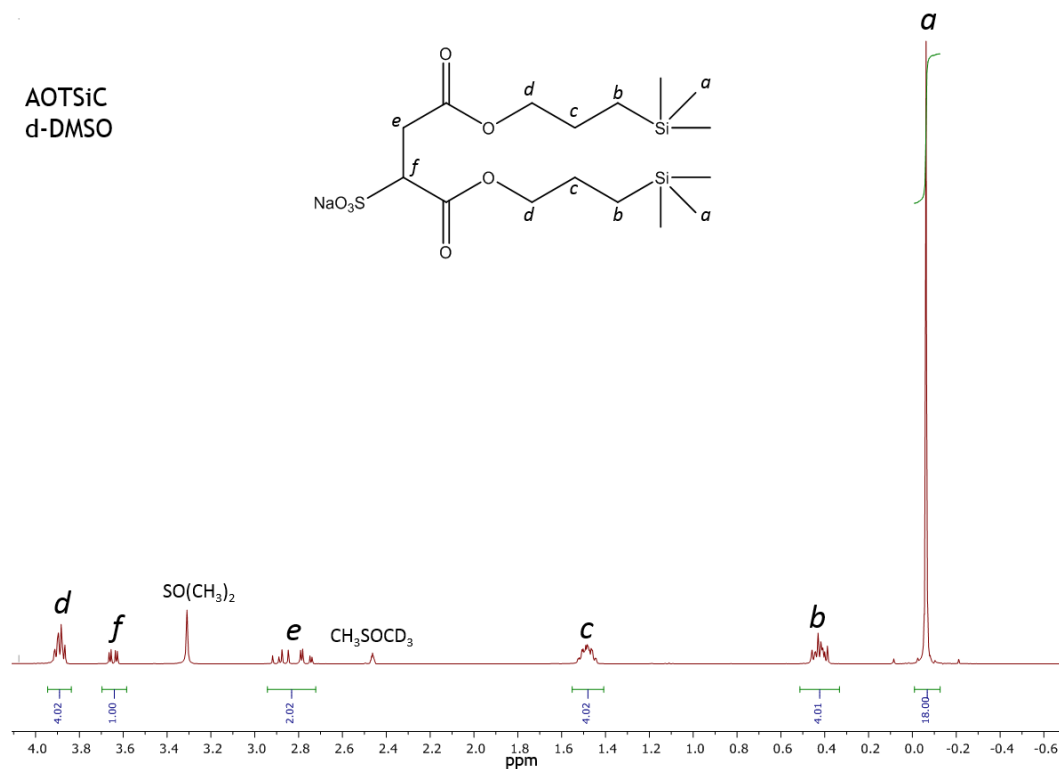


Table 8.6: Data from ^1H NMR spectrum of AOTSiC with corresponding elemental analysis shown below where experimentally obtained values are shown in blue.

Chemical Shift (ppm)	Molecular fragment	Integration	Identified proton
AOTSiC			
-0.13 - -0.010	$-\text{CH}_2-\text{Si}(\text{CH}_3)_3$	18.00	a
0.33 - 0.51	$-\text{CH}_2-\text{Si}(\text{CH}_3)_3$	4.01	b
1.41 - 1.55	$-\text{O}-\text{CH}_2-\text{CH}_2-$	4.02	c
2.72 - 2.94	$-\text{CO}-\text{CH}_2-$	2.02	e
3.59 - 3.70	$\text{NaO}_3\text{S}-\text{CH}-$	1.00	f
3.84 - 3.95	$-\text{O}-\text{CH}_2-$	4.03	d

Theoretical - Experimental		
C	H	S
42.83 - 42.88	7.41 - 7.48	7.15 - 7.07

8.1.6 HS1

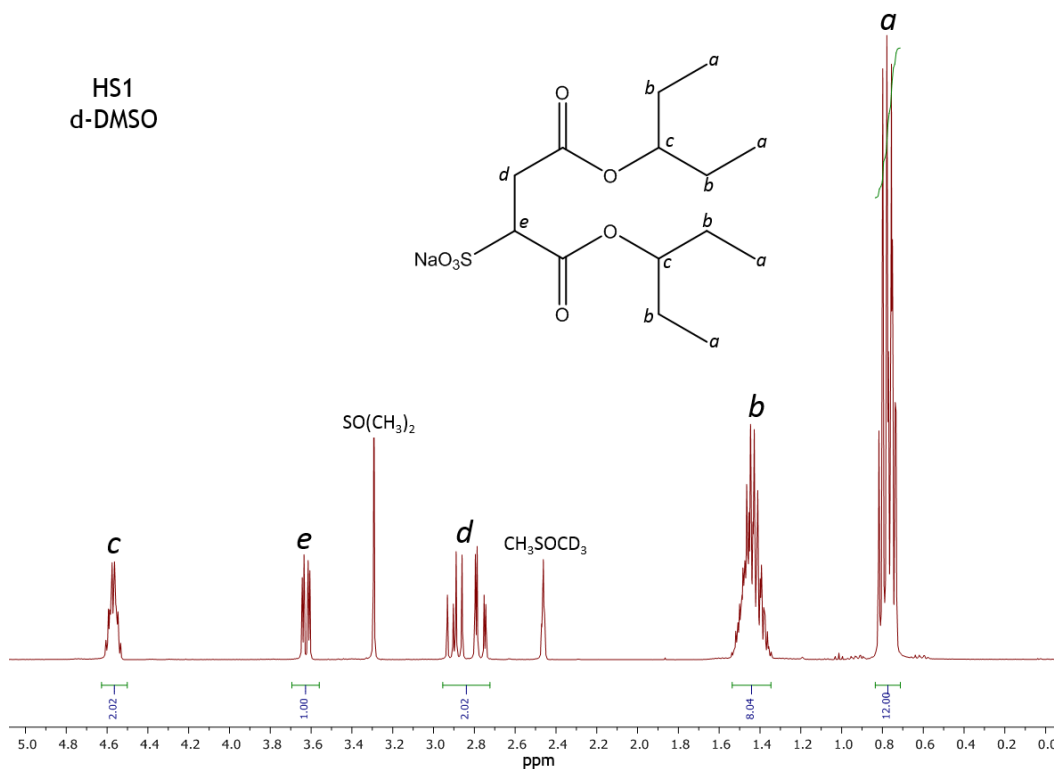


Table 8.7: Data from ^1H NMR spectrum of HS1 with corresponding elemental analysis shown below where experimentally obtained values are shown in blue.

Chemical Shift (ppm)	Molecular fragment	Integration	Identified proton
HS1			
0.71 - 0.84	$-\text{CH}_2-\text{CH}_3$	12.00	a
1.35 - 1.54	$-\text{CH}-\text{CH}_2-\text{CH}_3$	8.04	b
2.73 - 2.96	$-\text{CO}-\text{CH}_2-$	2.02	d
3.56 - 3.69	$\text{NaO}_3\text{S}-\text{CH}-$	1.00	e
4.50 - 4.63	$-\text{O}-\text{CH}-(\text{CH}_2)_2$	2.02	c

Theoretical - Experimental		
C	H	S
46.66 - 46.74	6.99 - 7.00	8.90 - 8.47

8.1.7 HS2

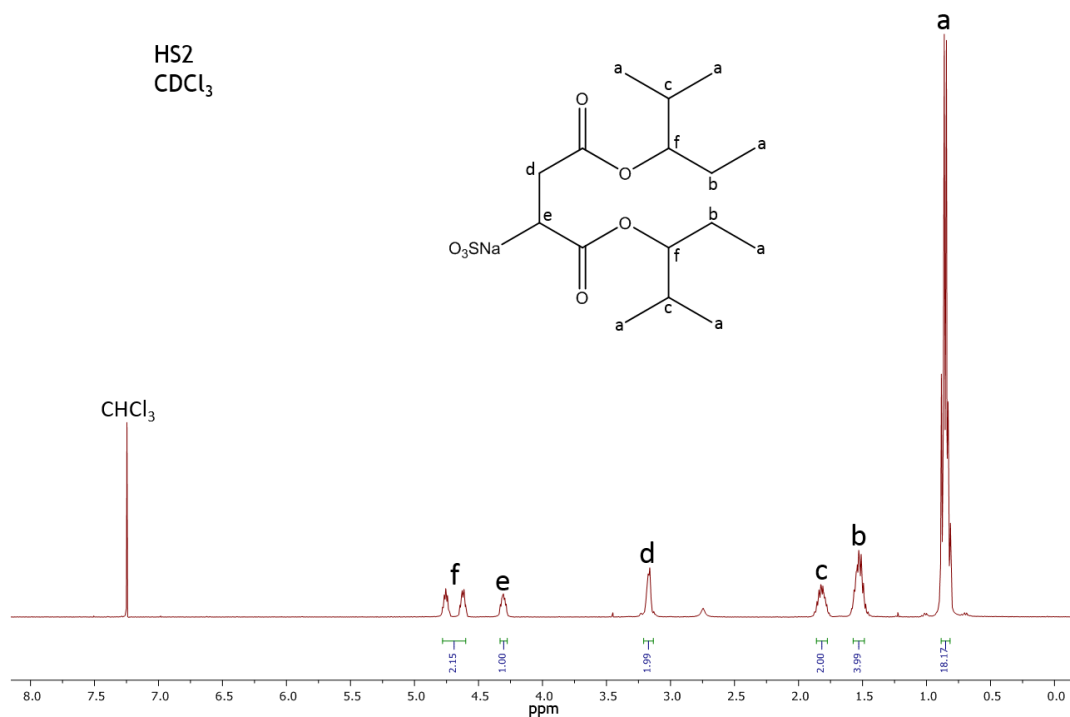


Table 8.8: Data from ¹H NMR spectrum of HS2 with corresponding elemental analysis shown below where experimentally obtained values are shown in blue.

Chemical Shift (ppm)	Molecular fragment	Integration	Identified proton
HS2			
0.82 - 0.89	-CH ₂ -CH ₃ -CH-(CH ₃) ₂	18.17	a
1.49 - 1.57	-CH-CH ₂ -CH ₃	3.99	b
1.78 - 1.86	-CH-CH-(CH ₃) ₂	2.00	c
3.13 - 3.21	-CO-CH ₂ -	1.99	d
4.28 - 4.33	NaO ₃ S-CH-	1.00	e
4.60 - 4.78	-O-CH-	2.15	f

Theoretical - Experimental		
C	H	S
49.47 - 49.24	7.53 - 7.59	8.25 - 8.17

8.1.8 HS3

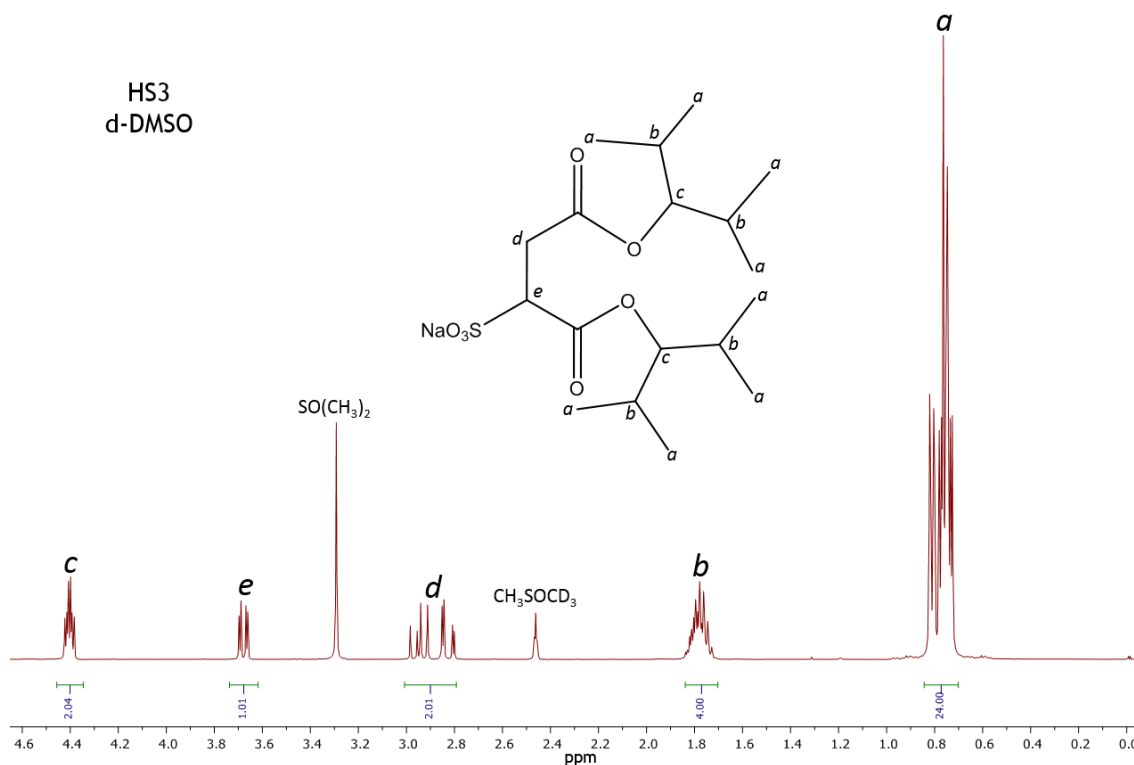


Table 8.9: Data from ¹H NMR spectrum of HS3 with corresponding elemental analysis shown below where experimentally obtained values are shown in blue.

Chemical Shift (ppm)	Molecular fragment	Integration	Identified proton
HS3			
0.70 - 0.84	-CH-(CH ₃) ₂	24.00	a
1.70 - 1.84	-CH-CH-(CH ₃) ₂	4.00	b
2.79 - 3.01	-CO-CH ₂ -	2.01	d
3.62 - 3.74	NaO ₃ S-CH-	1.01	e
4.35 - 4.46	-O-CH-	2.04	c

Theoretical - Experimental		
C	H	S
51.91 - 51.41	7.99 - 7.81	7.70 - 7.55

8.1.9 di-C6SS

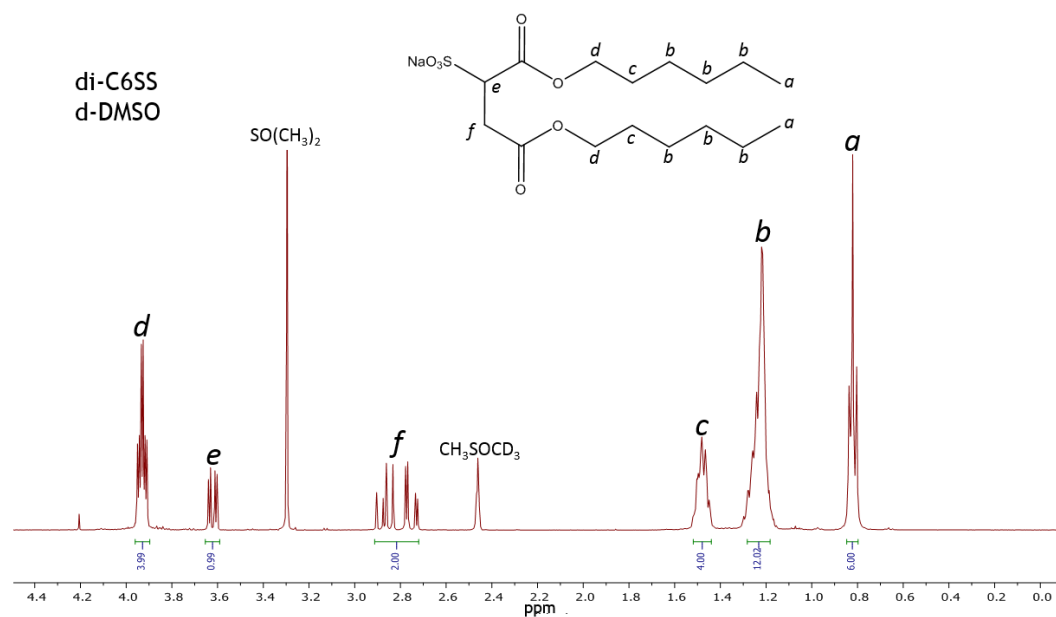


Table 8.10: Data from ^1H NMR spectrum of di-C6SS with corresponding elemental analysis shown below where experimentally obtained values are shown in blue.

Chemical Shift (ppm)	Molecular fragment	Integration	Identified proton
di-C6SS			
0.80 - 0.85	$-\text{CH}_2-\text{CH}_3$	6.00	a
1.18 - 1.28	$-\text{CH}_2-\text{C}_3\text{H}_6-$	12.02	b
1.45 - 1.52	$-\text{O}-\text{CH}_2-\text{CH}_2-$	4.00	c
2.72 - 2.91	$-\text{CO}-\text{CH}_2-$	2.00	f
3.59 - 3.65	$\text{NaO}_3\text{S}-\text{CH}-$	0.99	e
3.90 - 3.96	$-\text{O}-\text{CH}_2-$	3.99	d

Theoretical - Experimental		
C	H	S
49.47 - 49.26	7.53 - 7.32	8.25 - 7.94

8.1.10 di-C7SS

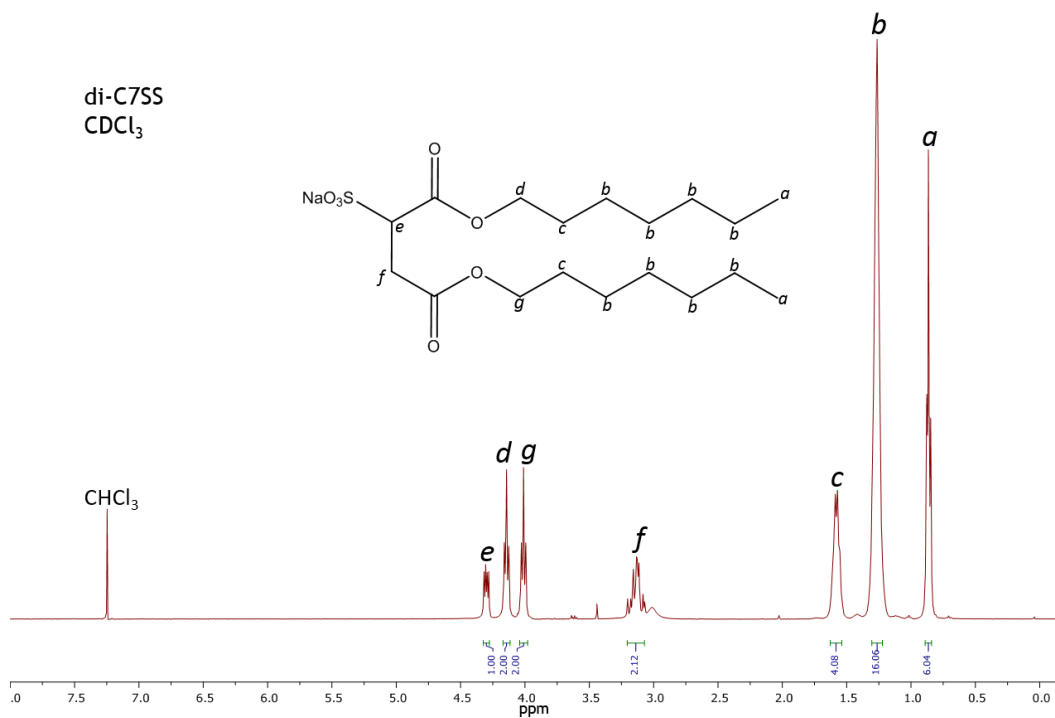


Table 8.11: Data from ¹H NMR spectrum of di-C7SS with corresponding elemental analysis shown below where experimentally obtained values are shown in blue.

Chemical Shift (ppm)	Molecular fragment	Integration	Identified proton
di-C7SS			
0.84 - 0.89	-CH ₂ -CH ₃	6.04	a
1.22 - 1.31	-CH ₂ -C ₄ H ₈ -	16.06	b
1.54 - 1.63	-O-CH ₂ -CH ₂ -	4.08	c
3.07 - 3.21	-CO-CH ₂ -	2.12	f
3.98 - 4.04	-O-CH ₂ -	2.00	g
4.12 - 4.17	-O-CH ₂ -	2.00	d
4.28 - 4.32	NaO ₃ S-CH-	1.00	e

Theoretical - Experimental		
C	H	S
51.91 - 51.72	7.99 - 7.82	7.70 - 7.68

8.1.11 di-C8SS

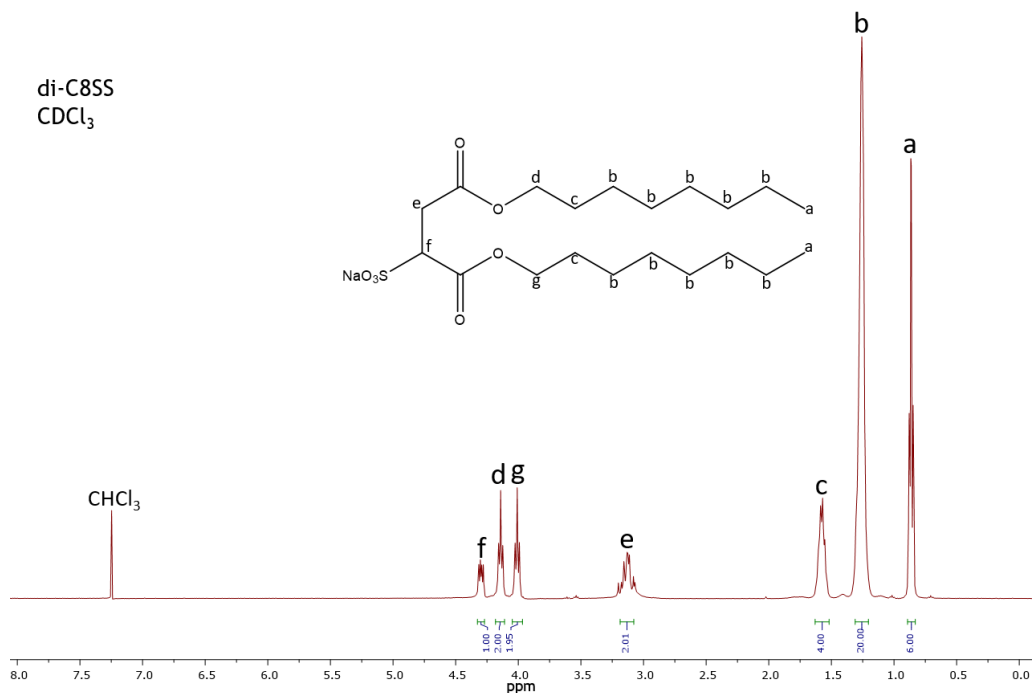


Table 8.12: Data from ¹H NMR spectrum of di-C8SS with corresponding elemental analysis shown below where experimentally obtained values are shown in blue.

Chemical Shift (ppm)	Molecular fragment	Integration	Identified proton
di-C8SS			
0.83 - 0.89	-CH ₂ -CH ₃	6.00	a
1.20 - 1.31	-CH ₂ -C ₄ H ₈ -	20.00	b
1.52 - 1.63	-O-CH ₂ -CH ₂ -	4.00	c
3.08 - 3.19	-CO-CH ₂ -	2.01	e
3.97 - 4.05	-O-CH ₂ -	1.95	g
4.11 - 4.18	-O-CH ₂ -	2.00	d
4.27 - 4.33	NaO ₃ S-CH-	1.00	f

Theoretical - Experimental		
C	H	S
54.04 - 54.21	8.39 - 8.53	7.21 - 7.33

8.1.12 Na-FO180

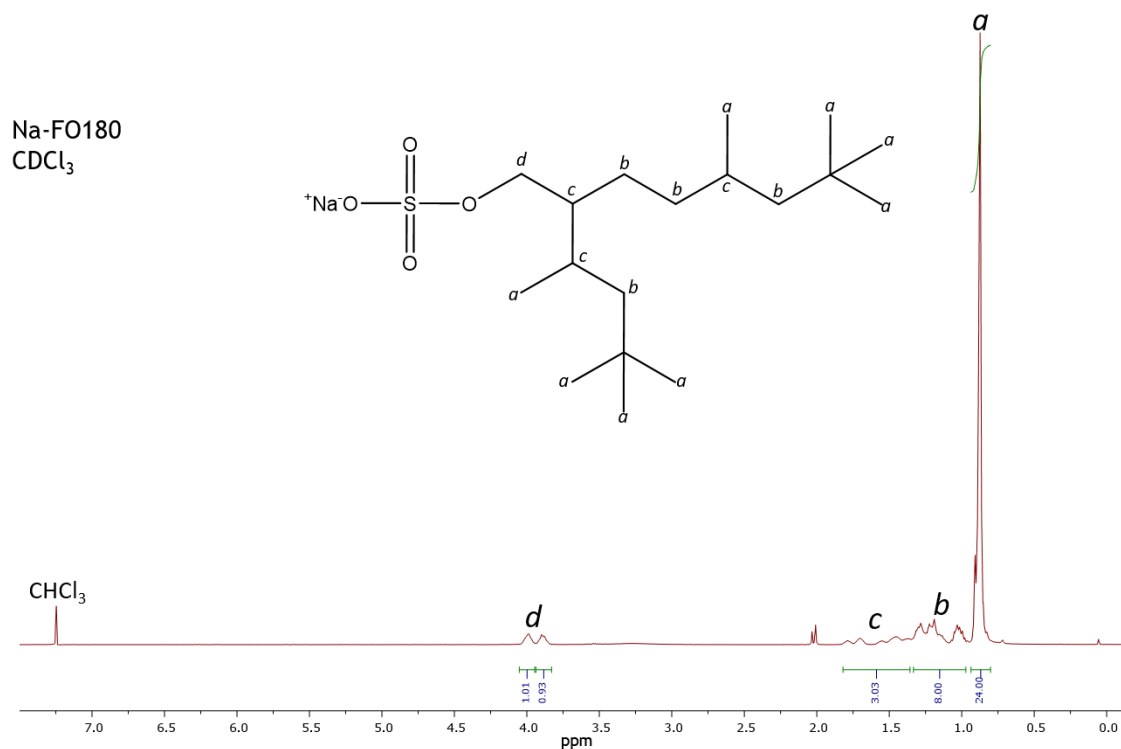


Table 8.13: Data from ¹H NMR spectrum of Na-FO180 with corresponding elemental analysis shown below where experimentally obtained values are shown in blue.

Chemical Shift (ppm)	Molecular fragment	Integration	Identified proton
Na-FO180			
0.80 - 0.94	-CH ₂ -C(CH ₃) ₃ -CH-CH ₃	24.00	a
0.97 - 1.33	-CH-CH ₂ -	8.00	b
1.36 - 1.82	-CH ₃ -CH-	3.03	c
3.83 - 4.05	-O-CH ₂ -	1.94	d

Theoretical - Experimental		
C	H	S
58.03 - 58.35	10.01 - 10.24	8.61 - 8.54

8.1.13 TMA-FO180

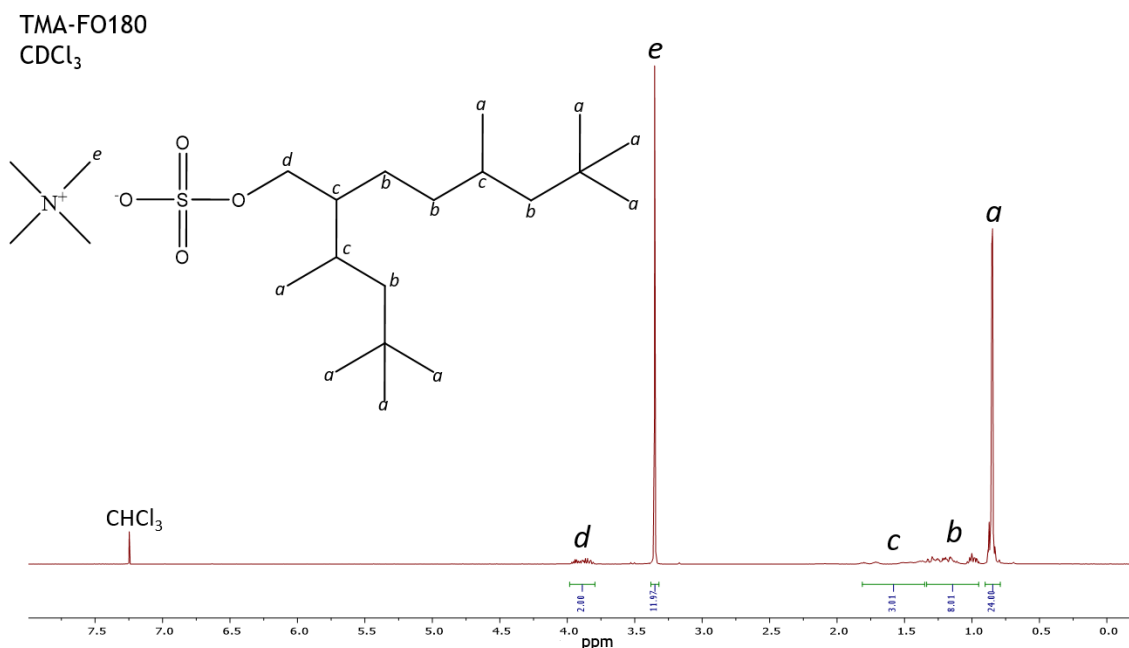


Table 8.14: Data from ¹H NMR spectrum of TMA-FO180 with corresponding elemental analysis shown below where experimentally obtained values are shown in blue.

Chemical Shift (ppm)	Molecular fragment	Integration	Identified proton
TMA-FO180			
0.79 - 0.90	-CH ₂ -C(CH ₃) ₃ -CH-CH ₃	24.00	a
0.95 - 1.34	-CH-CH ₂ -	8.01	b
1.35 - 1.81	-CH ₃ -CH-	3.01	c
3.32 - 3.38	N-CH ₃	11.97	e
3.79 - 3.98	-O-CH ₂ -	1.94	d

Theoretical - Experimental			
C	H	S	N
62.37 - 62.07	11.66 - 11.49	7.57 - 7.42	3.31 - 3.09

8.1.14 TEA-FO180

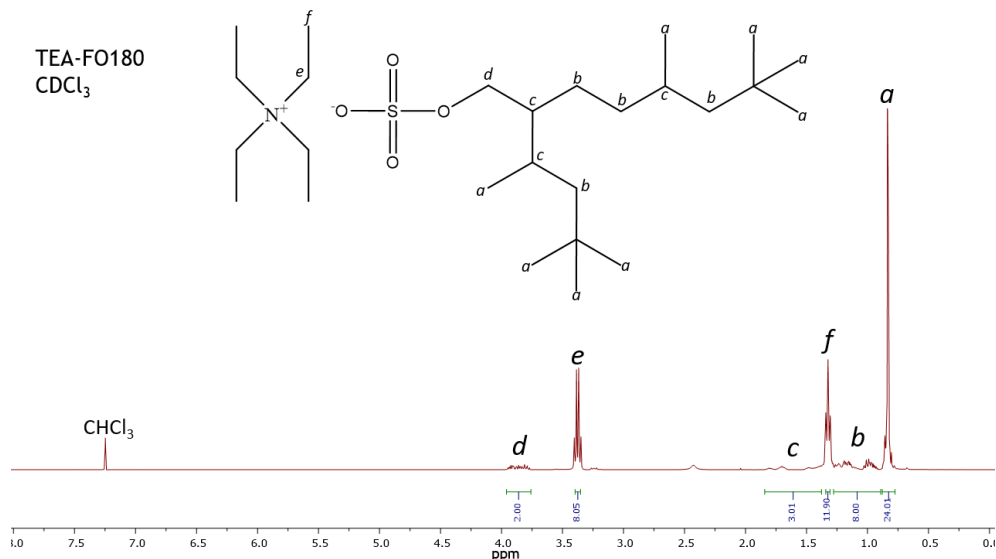


Table 8.15: Data from ^1H NMR spectrum of TEA-FO180 with corresponding elemental analysis shown below where experimentally obtained values are shown in blue.

Chemical Shift (ppm)	Molecular fragment	Integration	Identified proton
TEA-FO180			
0.77 - 0.88	$-\text{CH}_2-\text{C}(\text{CH}_3)_3$ $-\text{CH}-\text{CH}_3$	24.01	a
0.89 - 1.28	$-\text{CH}-\text{CH}_2-$	8.00	b
1.31 - 1.34	$\text{N}-\text{CH}_2-\text{CH}_3$	11.90	f
1.38 - 1.84	$-\text{CH}_3-\text{CH}-$	3.01	c
3.35 - 3.40	$\text{N}-\text{CH}_2-\text{CH}_3$	8.05	e
3.76 - 3.96	$-\text{O}-\text{CH}_2-$	2.00	d

Theoretical - Experimental			
C	H	S	N
65.09 - 64.92	11.97 - 12.05	6.68 - 6.46	2.92 - 3.05

8.1.15 TPA-FO180

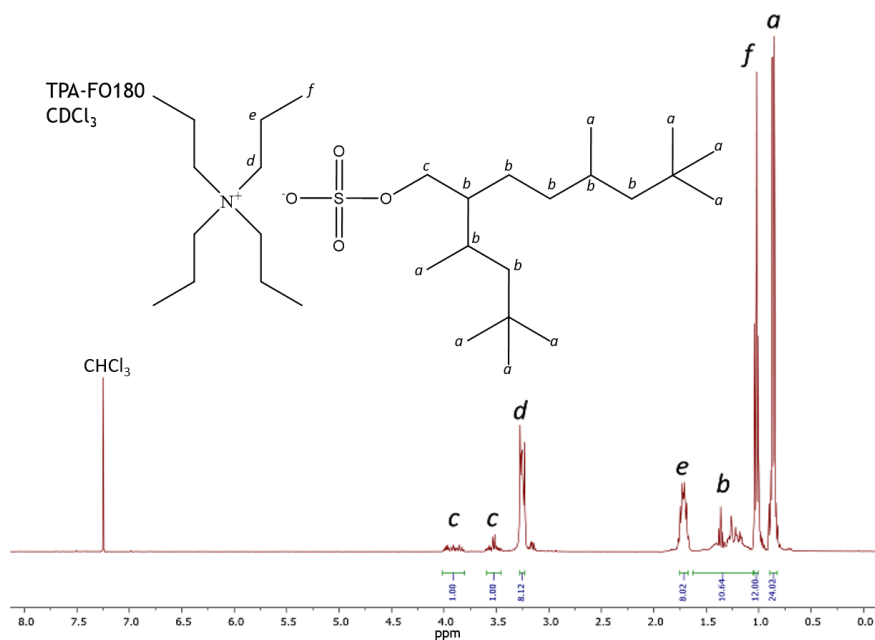


Table 8.16: Data from ^1H NMR spectrum of TPA-FO180 with corresponding elemental analysis shown below where experimentally obtained values are shown in blue.

Chemical Shift (ppm)	Molecular fragment	Integration	Identified proton
TPA-FO180			
0.81 - 0.90	$-\text{CH}_2-\text{C}(\text{CH}_3)_3$ $-\text{CH}-\text{CH}_3$	24.02	a
1.01 - 3.05	$\text{N}-\text{CH}_2-\text{CH}_2-\text{CH}_3$	12.00	f
1.06 - 1.67	$-\text{CH}-\text{CH}_2-$ $-\text{CH}_3-\text{CH}-$	10.64	b
1.67 - 1.76	$\text{N}-\text{CH}_2-\text{CH}_2-\text{CH}_3$	8.02	e
3.23 - 3.27	$\text{N}-\text{CH}_2-\text{CH}_2-\text{CH}_3$	8.12	d
3.45-3.61, 3.80-4.01	$-\text{O}-\text{CH}_2-$	2.00	c
Theoretical - Experimental			
C	H	S	N
67.24 - 67.52	12.23 - 12.41	5.98 - 5.68	2.61 - 2.66

8.1.16 Na-FO180N

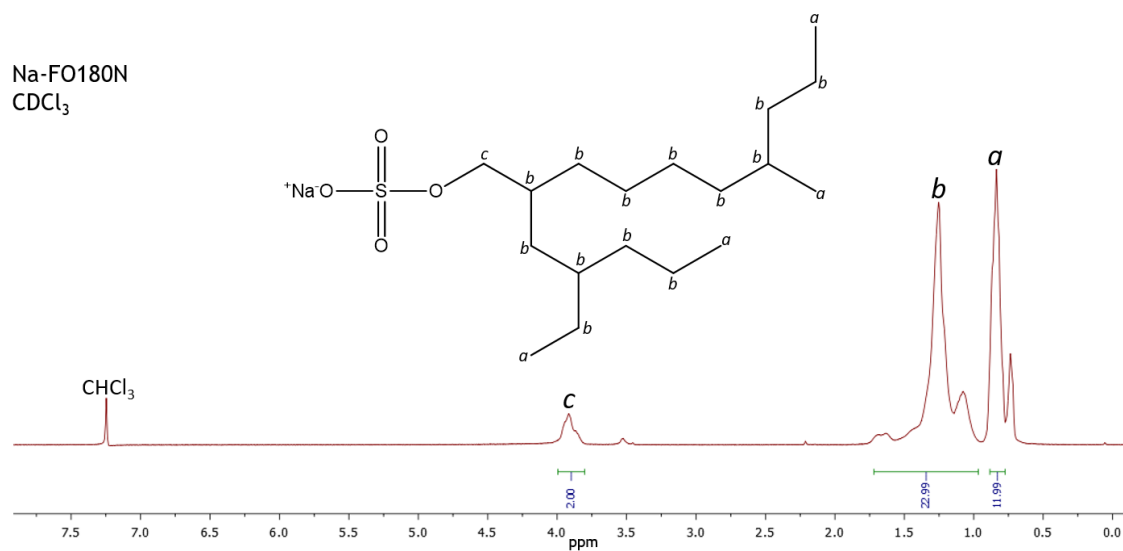


Table 8.17: Data from ¹H NMR spectrum of Na-FO180N with corresponding elemental analysis shown below where experimentally obtained values are shown in blue.

Chemical Shift (ppm)	Molecular fragment	Integration	Identified proton
Na-FO180N			
0.76 - 0.88	-CH ₂ -CH ₃	11.99	a
0.96 - 1.80	-CH ₃ -CH ₂ - -CH ₂ -CH ₂ - -CH ₂ -CH-	22.99	b
3.87 - 3.96	-O-CH ₂ -	2.00	c

Theoretical - Experimental		
C	H	S
58.03 - 58.13	10.01 - 10.14	8.61 - 8.54

8.1.17 TMA-FO180N

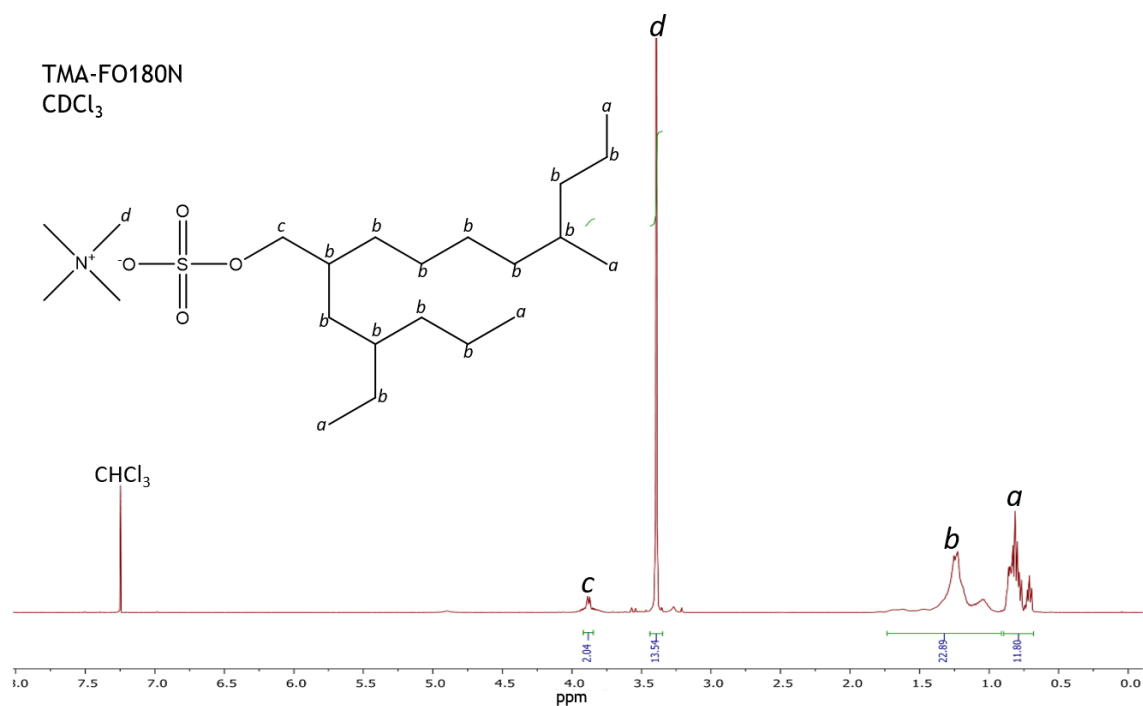


Table 8.18: Data from ¹H NMR spectrum of TMA-FO180N with corresponding elemental analysis shown below where experimentally obtained values are shown in blue.

Chemical Shift (ppm)	Molecular fragment	Integration	Identified proton
TMA-FO180N			
0.68 - 0.90	-CH ₂ -CH ₃	11.80	a
0.91 - 1.73	-CH ₃ -CH ₂ - -CH ₂ -CH ₂ - -CH ₂ -CH-	22.89	b
3.35 - 3.44	N-CH ₃	13.54	d
3.83 - 3.90	-O-CH ₂ -	2.04	c

Theoretical - Experimental			
C	H	S	N
62.37 - 62.31	11.66 - 11.89	7.57 - 7.21	3.31 - 3.08

8.1.18 TEA-FO180N

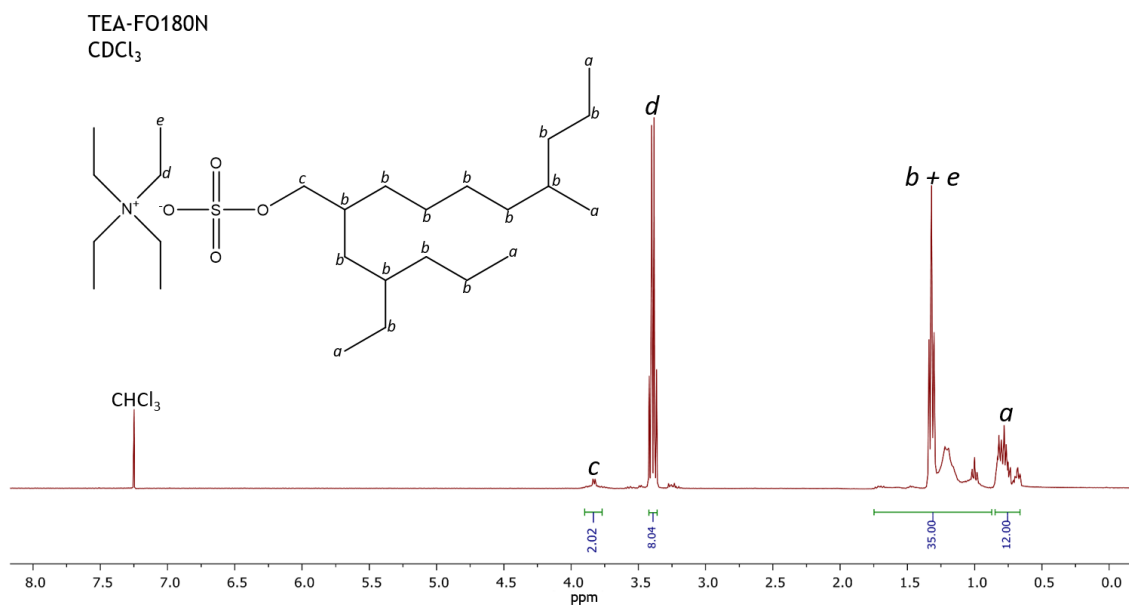


Table 8.19: Data from ¹H NMR spectrum of TEA-FO180N with corresponding elemental analysis shown below where experimentally obtained values are shown in blue.

Chemical Shift (ppm)	Molecular fragment	Integration	Identified proton
TEA-FO180N			
0.66 - 0.85	-CH ₂ -CH ₃	12.00	a
0.87 - 1.75	-CH ₃ -CH ₂ - -CH ₂ -CH ₂ - -CH ₂ -CH- N-CH ₂ -CH ₃	35.00	b + e
3.36 - 3.42	N-CH ₂ -CH ₃	8.04	d
3.76 - 3.87	-O-CH ₂ -	2.02	c

Theoretical - Experimental			
C	H	S	N
65.09 - 64.95	11.97 - 11.72	6.68 - 6.39	2.92 - 2.94

8.1.19 TPA-FO180N

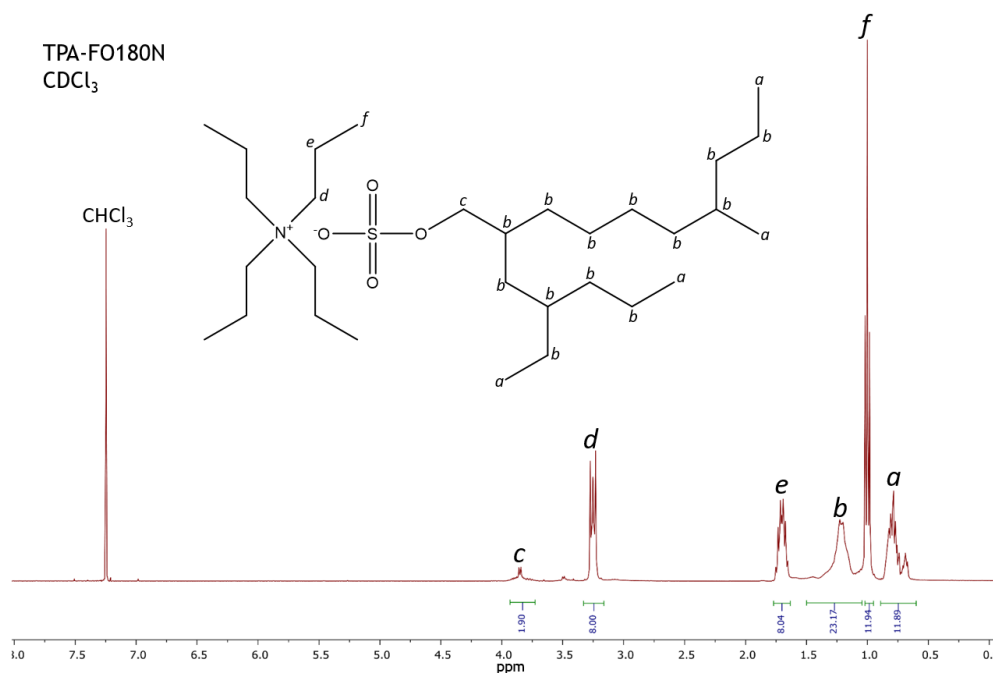


Table 8.20: Data from ¹H NMR spectrum of TPA-FO180N with corresponding elemental analysis shown below where experimentally obtained values are shown in blue.

Chemical Shift (ppm)	Molecular fragment	Integration	Identified proton
TPA-FO180N			
0.61 - 0.89	-CH ₂ -CH ₃	11.89	a
0.94 - 1.03	N-CH ₂ -CH ₂ -CH ₃	11.94	f
1.06 - 1.50	-CH ₃ -CH ₂ - -CH ₂ -CH ₂ - -CH ₂ -CH-	23.17	b
1.63 - 1.77	N-CH ₂ -CH ₂ -CH ₃	8.04	e
3.16 - 3.34	N-CH ₂ -CH ₂ -CH ₃	8.00	d
3.73 - 3.94	-O-CH ₂ -	1.90	c

Theoretical - Experimental			
C	H	S	N
67.24 - 67.22	12.23 - 12.36	5.98 - 6.69	2.61 - 2.36

8.1.20 Na-BC9

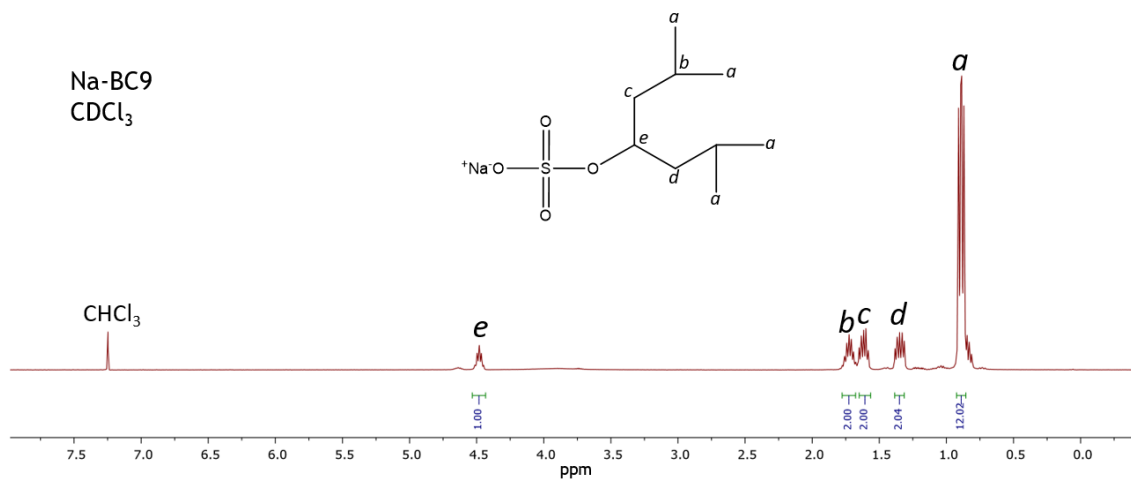


Table 8.21: Data from ¹H NMR spectrum of Na-BC9 with corresponding elemental analysis shown below where experimentally obtained values are shown in blue.

Chemical Shift (ppm)	Molecular fragment	Integration	Identified proton
Na-BC9			
0.83 - 0.94	-CH-(CH ₃) ₂	12.02	a
1.30 - 1.39	-CH-CH ₂ CH ₂ -	2.04	d
1.55 - 1.65	-CH-CH ₂ CH ₂ -	2.00	c
1.69 - 1.78	-CH-(CH ₃) ₂	2.00	b
4.45 - 4.53	-O-CH-(CH ₂) ₂ -	1.00	e

Theoretical - Experimental		
C	H	S
43.89 - 43.74	7.78 - 7.82	13.02 - 12.75

8.1.21 TMA-BC9

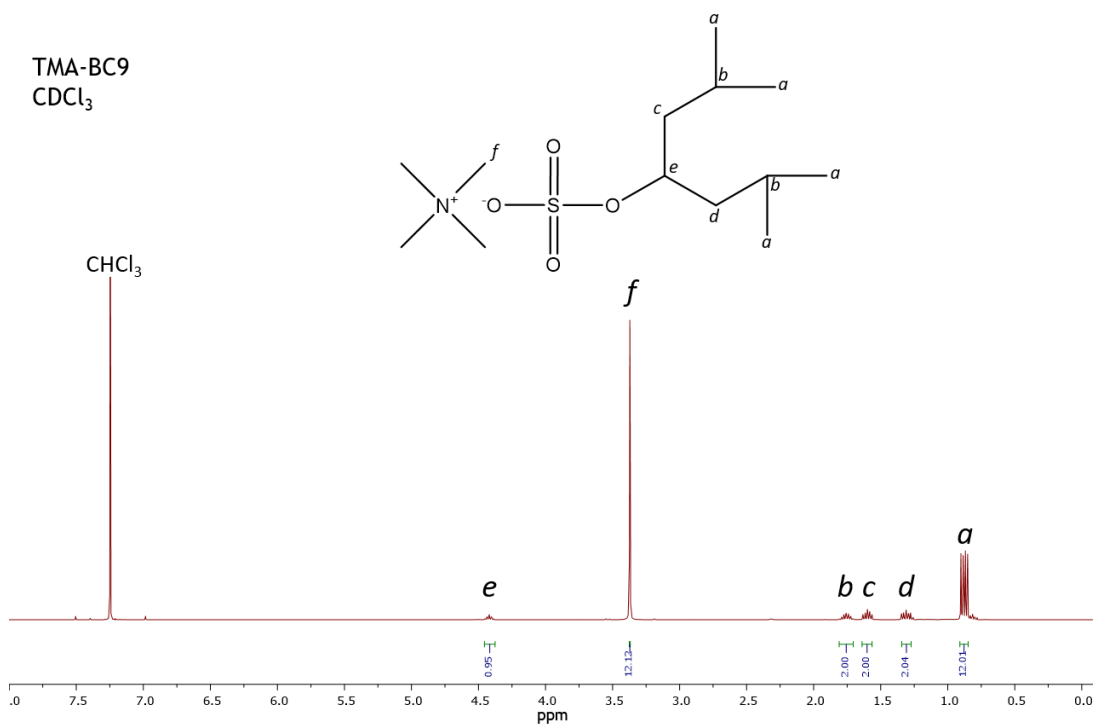


Table 8.22: Data from ¹H NMR spectrum of TMA-BC9 with corresponding elemental analysis shown below where experimentally obtained values are shown in blue.

Chemical Shift (ppm)	Molecular fragment	Integration	Identified proton
TMA-BC9			
0.85 - 0.91	-CH-(CH ₃) ₂	12.01	a
1.27 - 1.34	-CH-CH ₂ CH ₂ -	2.04	d
1.56 - 1.64	-CH-CH ₂ CH ₂ -	2.00	c
1.71 - 1.81	-CH-(CH ₃) ₂	2.00	b
3.37 - 3.38	N-CH ₃	12.13	f
4.38 - 4.46	-O-CH-(CH ₂) ₂ -	0.95	e

Theoretical - Experimental			
C	H	S	N
52.49 - 52.36	10.51 - 10.66	10.78 - 10.24	4.71 - 4.98

8.1.22 TEA-BC9

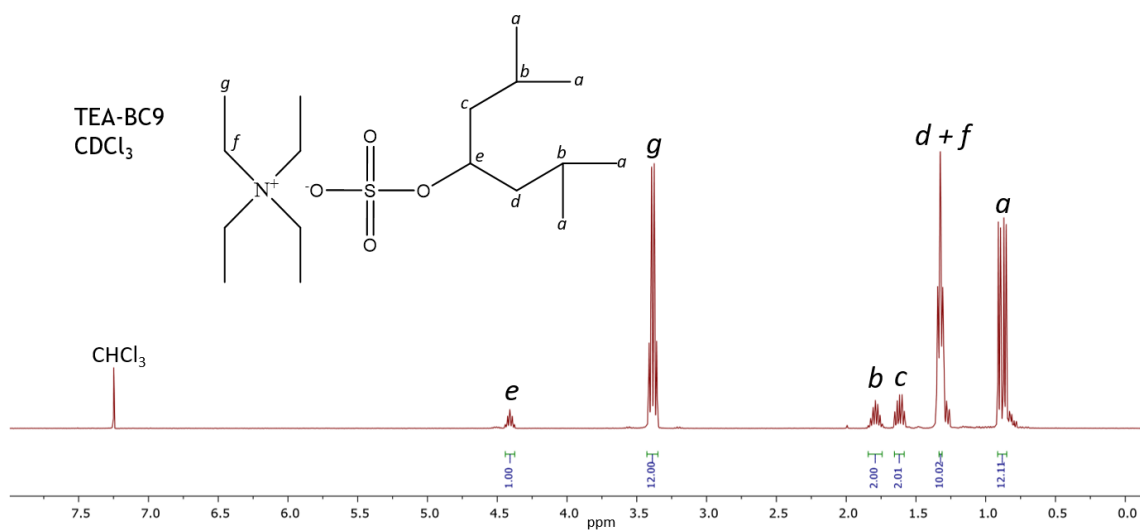


Table 8.23: Data from ^1H NMR spectrum of TEA-BC9 with corresponding elemental analysis shown below where experimentally obtained values are shown in blue.

Chemical Shift (ppm)	Molecular fragment	Integration	Identified proton
TEA-BC9			
0.85 - 0.93	$-\text{CH}-(\text{CH}_3)_2$	12.11	a
1.30 - 1.35	$-\text{CH}-\text{CH}_2\text{CH}_2-$ $\text{N}-\text{CH}_2\text{CH}_3$	10.02	d + f
1.58 - 1.67	$-\text{CH}-\text{CH}_2\text{CH}_2-$	2.01	c
1.74 - 1.84	$-\text{CH}-(\text{CH}_3)_2$	2.00	b
3.35 - 3.43	$\text{N}-\text{CH}_2\text{CH}_3$	12.00	g
4.37 - 4.45	$-\text{O}-\text{CH}-(\text{CH}_2)_2-$	1.00	e

Theoretical - Experimental			
C	H	S	N
57.75 - 57.69	11.12 - 11.26	9.07 - 9.33	3.96 - 4.24

8.1.23 TPA-BC9

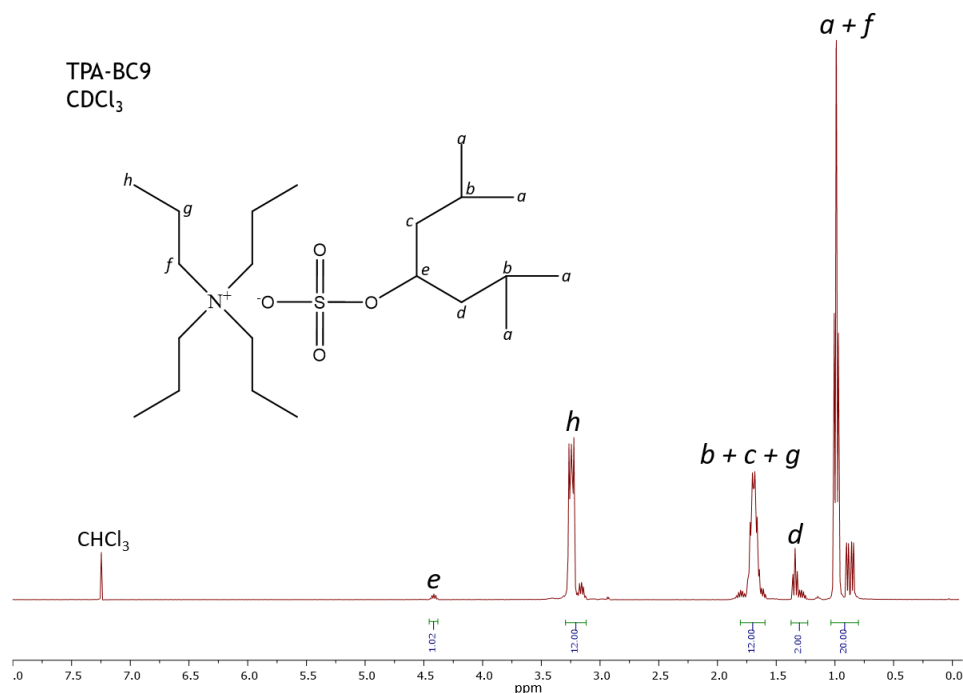


Table 8.24: Data from ¹H NMR spectrum of TPA-BC9 with corresponding elemental analysis shown below where experimentally obtained values are shown in blue.

Chemical Shift (ppm)	Molecular fragment	Integration	Identified proton
TPA-BC9			
0.80 - 1.03	-CH-(CH ₃) ₂ N-CH ₂ CH ₂ CH ₃	20.00	a + f
1.24 - 1.38	-CH-CH ₂ CH ₂ -	10.02	d
1.60 - 1.81	-CH-(CH ₃) ₂ -CH-CH ₂ CH ₂ - N-CH ₂ CH ₂ CH ₃	12.00	b + c + g
3.12 - 3.29	N-CH ₂ CH ₂ CH ₃	12.00	h
4.38 - 4.45	-O-CH-(CH ₂) ₂ -	1.02	e

Theoretical - Experimental			
C	H	S	N
61.57 - 61.41	11.56 - 11.62	7.83 - 8.09	3.42 - 3.15

8.1.24 Na-BC7

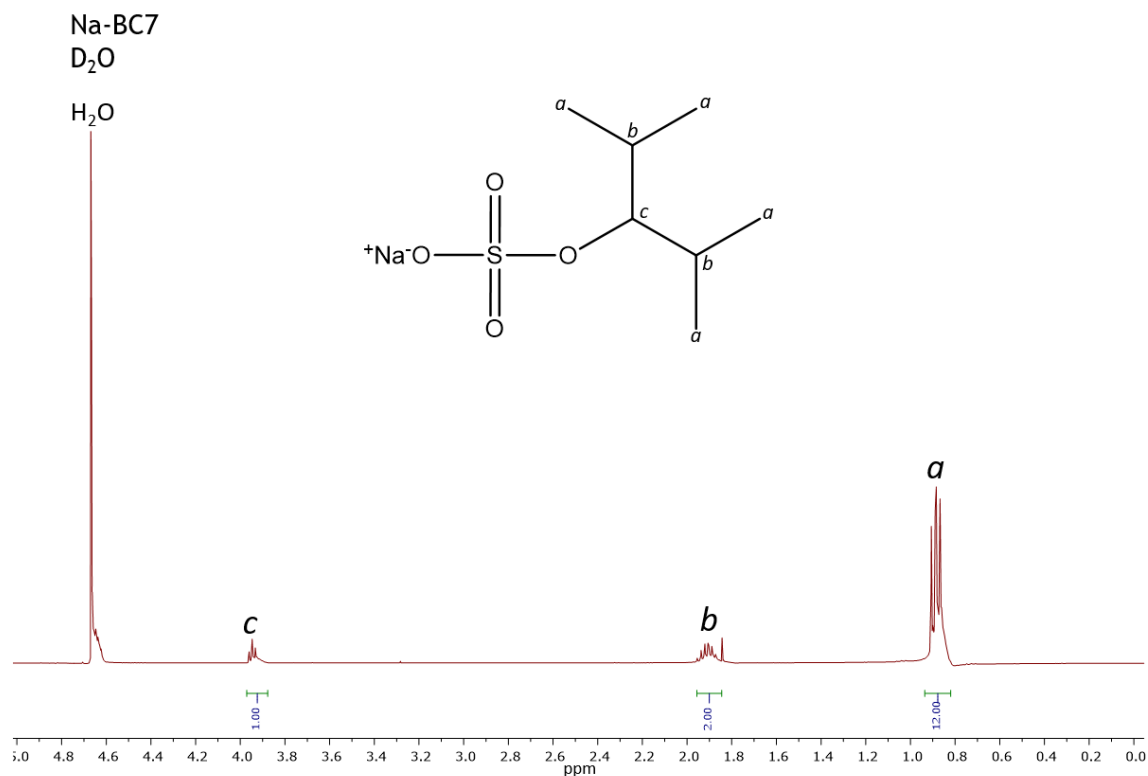


Table 8.25: Data from ¹H NMR spectrum of Na-BC7 with corresponding elemental analysis shown below where experimentally obtained values are shown in blue.

Chemical Shift (ppm)	Molecular fragment	Integration	Identified proton
Na-BC7			
0.85 - 0.94	-CH-(CH ₃) ₂	12.00	a
1.84 - 1.96	-CH-(CH ₃) ₂	2.00	b
3.87 - 3.97	-O-CH-(CH) ₂ -	1.00	c

Theoretical - Experimental		
C	H	S
38.52 - 38.71	6.93 - 7.05	14.69 - 14.66

8.1.25 TMA-BC7

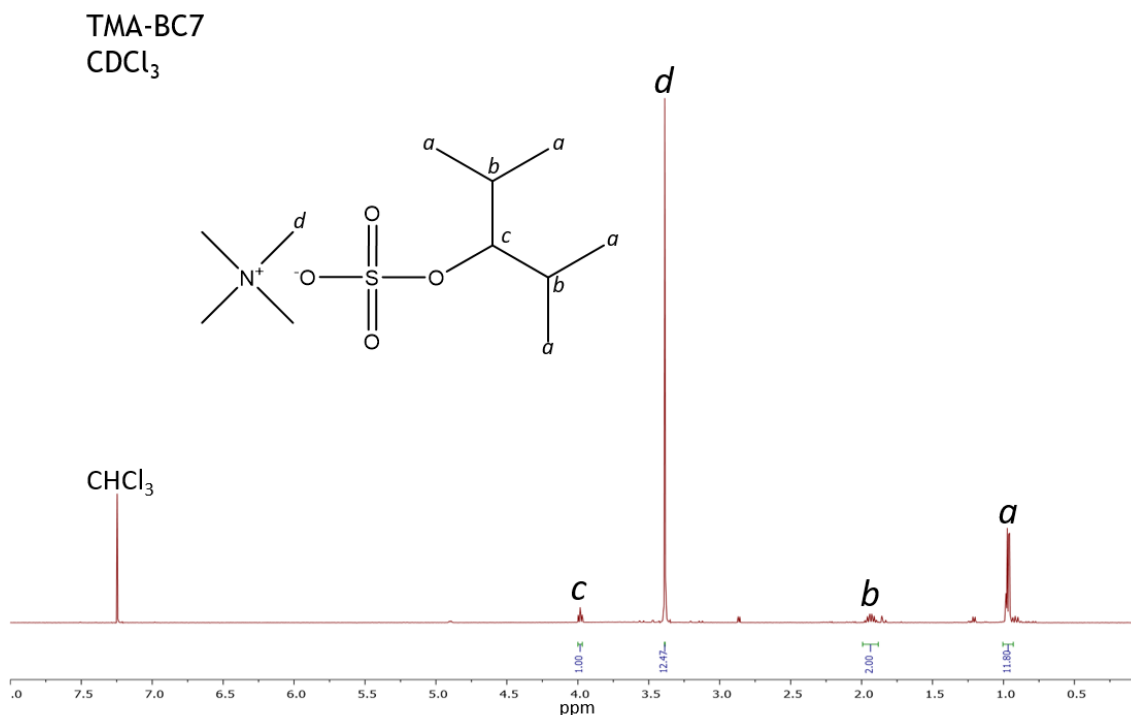


Table 8.26: Data from ¹H NMR spectrum of TMA-BC7 with corresponding elemental analysis shown below where experimentally obtained values are shown in blue.

Chemical Shift (ppm)	Molecular fragment	Integration	Identified proton
TMA-BC7			
0.93 - 1.00	-CH-(CH ₃) ₂	11.80	a
1.88 - 1.99	-CH-(CH ₃) ₂	2.00	b
3.38 - 3.39	N-CH ₃	12.47	d
3.97 - 4.00	-O-CH-(CH) ₂ -	1.00	c

C	Theoretical - Experimental		
	H	S	N
49.04 - 49.28	10.10 - 10.00	11.90 - 11.52	5.20 - 4.95

8.1.26 TEA-BC7

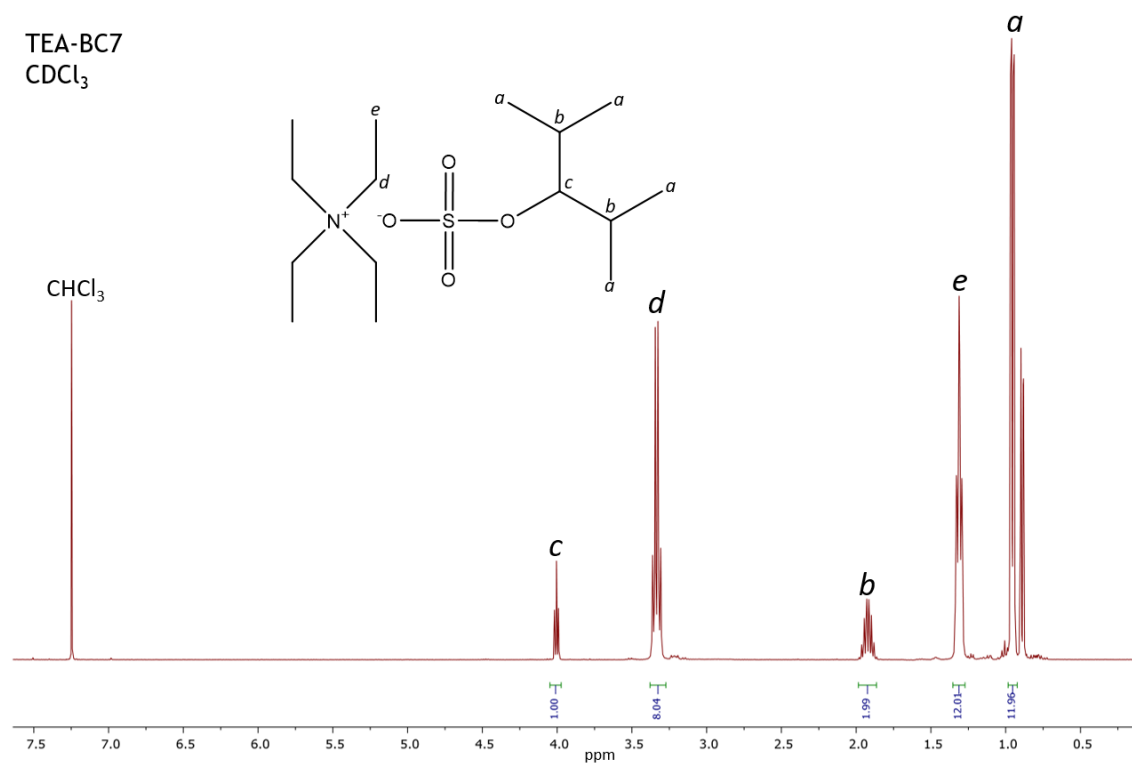


Table 8.27: Data from ¹H NMR spectrum of TEA-BC7 with corresponding elemental analysis shown below where experimentally obtained values are shown in blue.

Chemical Shift (ppm)	Molecular fragment	Integration	Identified proton
TEA-BC7			
0.92 - 0.98	-CH-(CH ₃) ₂	11.96	a
1.27 - 1.35	N-CH ₂ CH ₃	12.01	e
1.86 - 1.99	-CH-(CH ₃) ₂	1.99	b
3.27 - 3.38	N-CH ₂ CH ₃	8.04	d
3.97 - 4.05	-O-CH-(CH) ₂ -	1.00	c

Theoretical - Experimental			
C	H	S	N
55.35 - 55.29	10.84 - 10.99	9.85 - 9.97	4.30 - 4.28

8.1.27 TPA-BC7

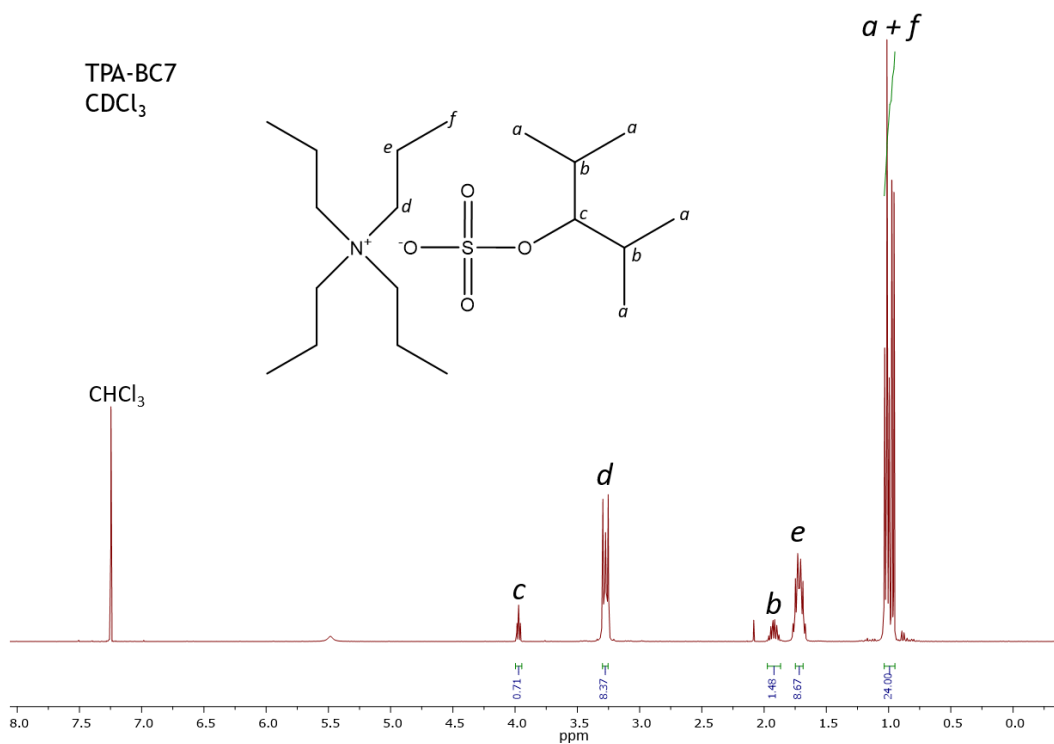


Table 8.28: Data from ¹H NMR spectrum of TPA-BC7 with corresponding elemental analysis shown below where experimentally obtained values are shown in blue.

Chemical Shift (ppm)	Molecular fragment	Integration	Identified proton
TPA-BC7			
0.95 - 1.04	-CH-(CH ₃) ₂ N-CH ₂ CH ₂ CH ₃	24.00	a + f
1.69 - 1.75	N-CH ₂ CH ₂ CH ₃	8.67	e
1.87 - 1.97	-CH-(CH ₃) ₂	1.48	b
3.25 - 3.30	N-CH ₂ CH ₂ CH ₃	8.37	d
3.95 - 4.00	-O-CH-(CH) ₂ -	0.71	c

Theoretical - Experimental			
C	H	S	N
59.80 - 59.67	11.36 - 11.02	8.40 - 7.81	3.67 - 3.92

8.1.28 SDS

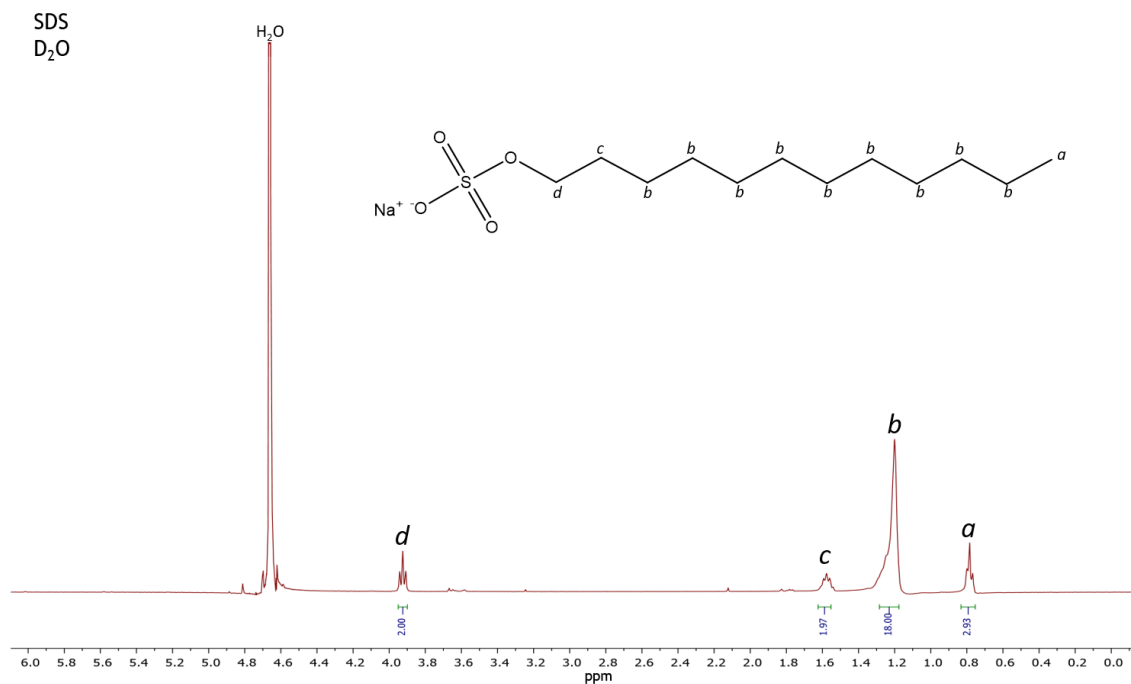


Table 8.29: Data from ¹H NMR spectrum of SDS with corresponding elemental analysis shown below where experimentally obtained values are shown in blue.

Chemical Shift (ppm)	Molecular fragment	Integration	Identified proton
SDS			
0.85 - 0.94	-CH ₂ -CH ₃	2.93	a
1.84 - 1.96	-(CH ₂) ₉ -	18.00	b
3.87 - 3.97	-O-CH ₂ -CH ₂ -	1.97	c
3.87 - 3.97	-O-CH ₂ -CH ₂ -	2.00	d

Theoretical - Experimental		
C	H	S
54.31 - 52.28	9.50 - 9.69	12.08 - 11.56

8.1.29 AOT

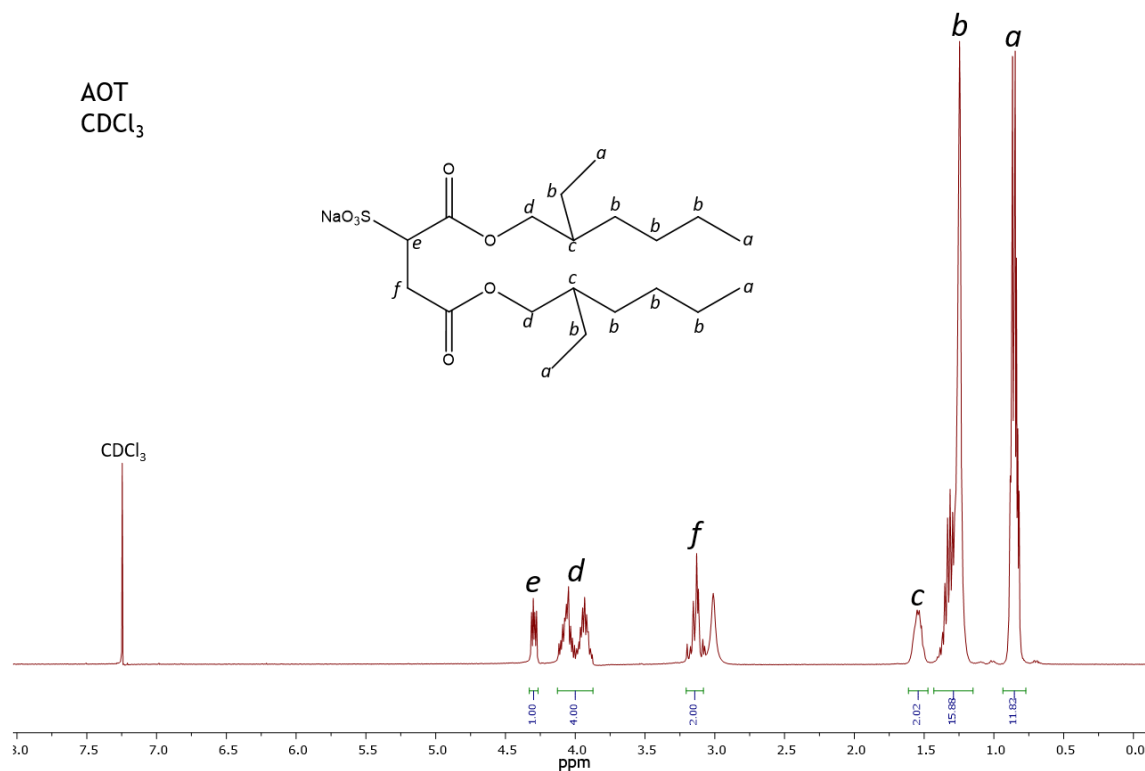


Table 8.30: Data from ¹H NMR spectrum of AOT with corresponding elemental analysis shown below where experimentally obtained values are shown in blue.

Chemical Shift (ppm)	Molecular fragment	Integration	Identified proton
AOT			
0.78 - 0.94	-CH ₂ -CH ₃	11.82	a
1.15 - 1.43	CH ₃ -(CH ₂) ₃ - CH ₃ -CH ₂ -CH-	15.88	b
1.47 - 1.65	CH ₃ -CH ₂ -CH-	2.02	c
3.09 - 3.21	-O-CH ₂ -	4.00	d
3.88 - 4.13	NaO ₃ S-CH-	1.00	e
4.27 - 4.33	-CO-CH ₂ -	2.00	f

Theoretical - Experimental		
C	H	S
54.31 - 52.28	9.50 - 9.69	12.08 - 11.56

8.2 Conductivity data and cmc analysis - Mixed systems

The following pages provide the conductivity data and analysis that was used to determine the cmc of each mixed surfactant system discussed in this thesis. The experimental procedure is described in Section 4.6.1 (all measurements were made at 295 K).

8.2.1 di-C6SS : AOTA / AOTB

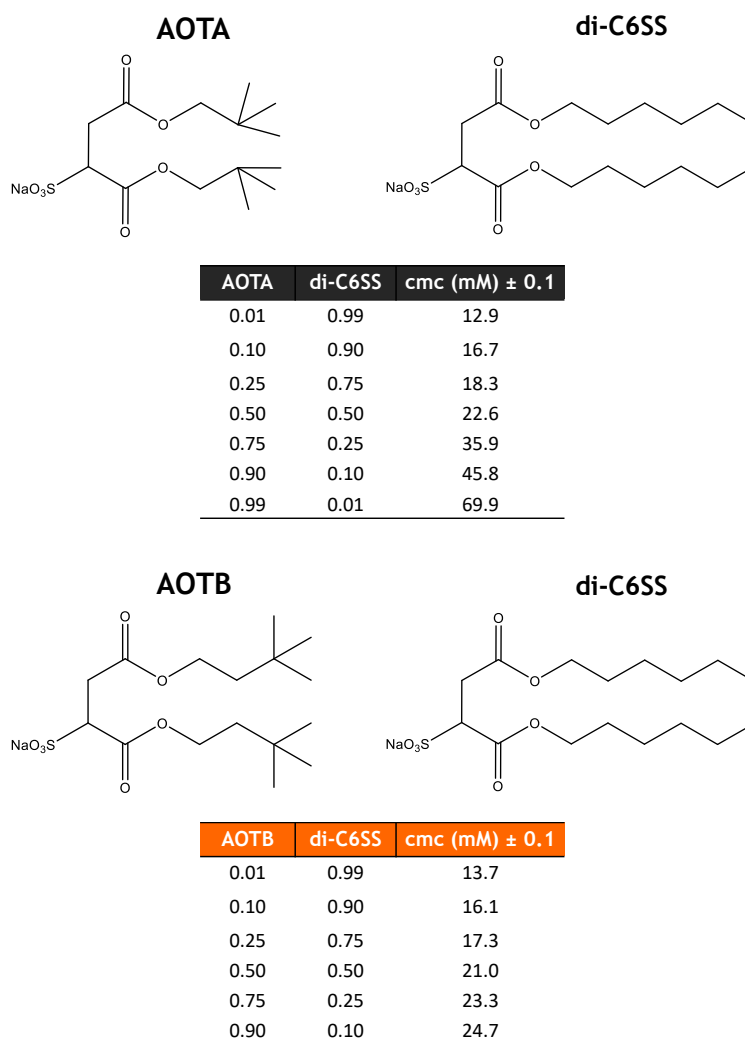


Figure 8.1a: Summary of the cmc values for di-C6SS : AOTA / AOTB mixed surfactant systems at varying molar ratios.

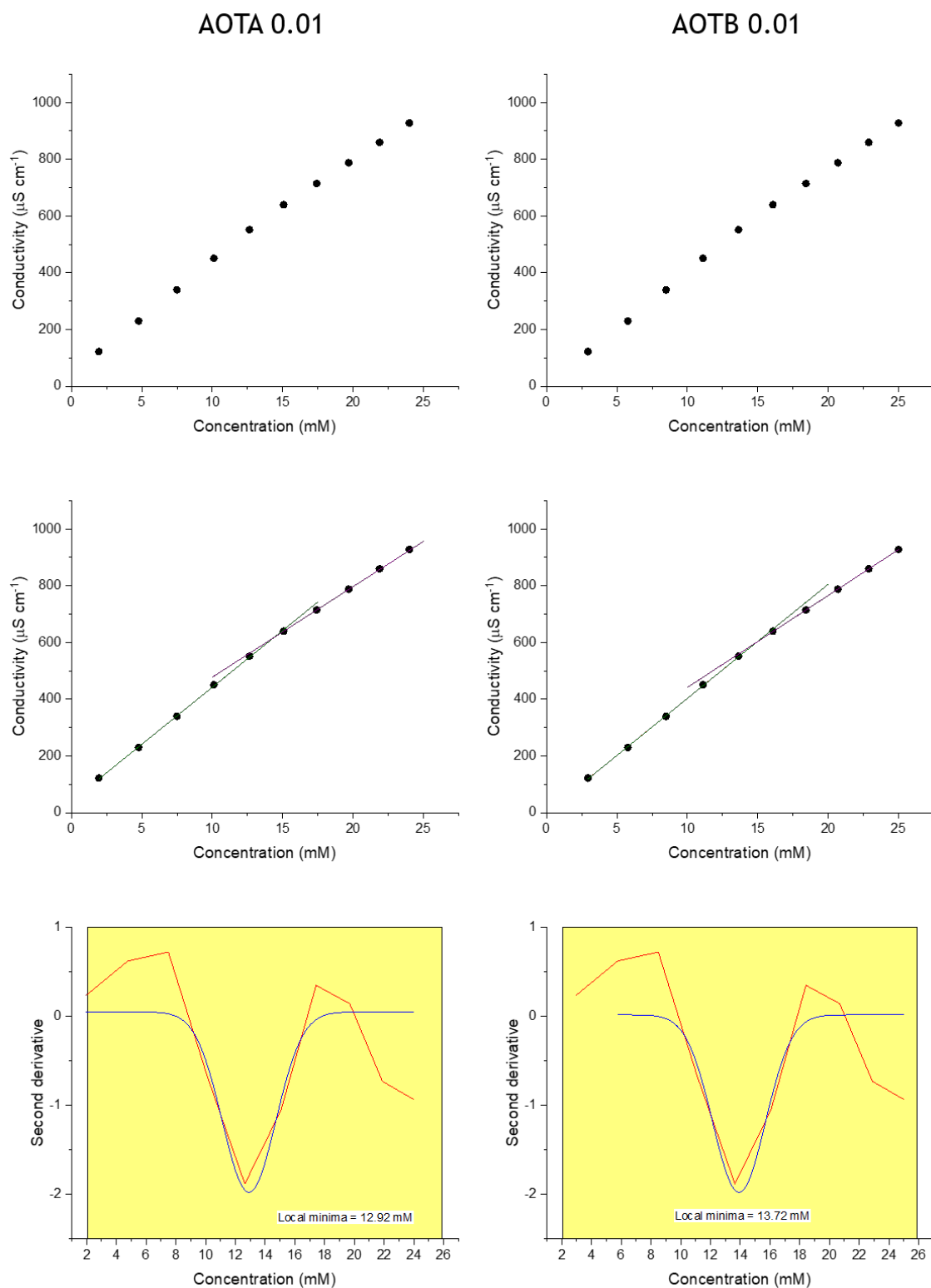


Figure 8.1b: Conductivity data used to determined cmcs of di-C6SS mixed system at a molar ratio of 0.01 X, where X is either AOTA / AOTB.

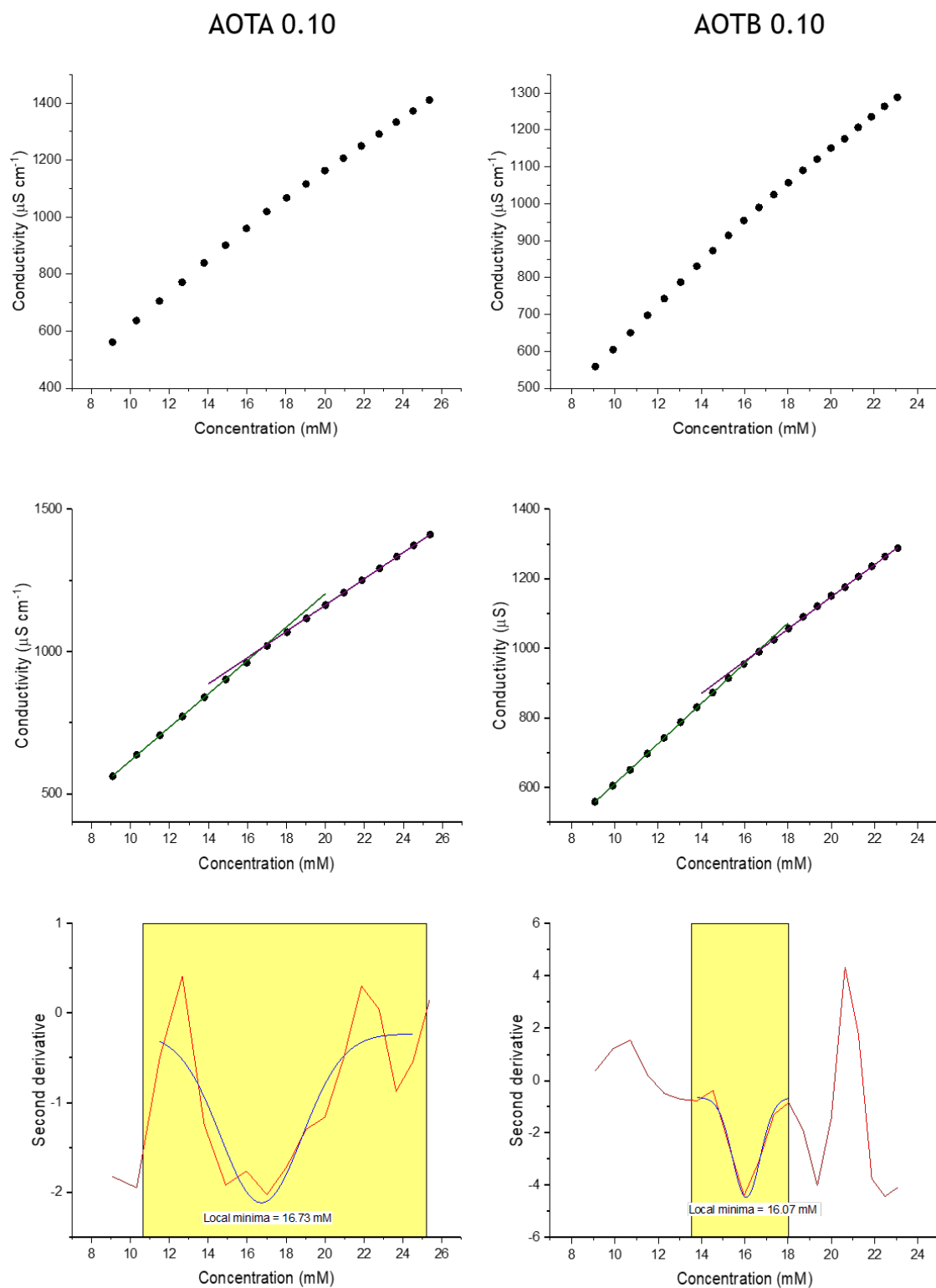


Figure 8.1c: Conductivity data used to determined cmcs of di-C6SS mixed system at a molar ratio of 0.1 X, where X is either AOTA / AOTB.

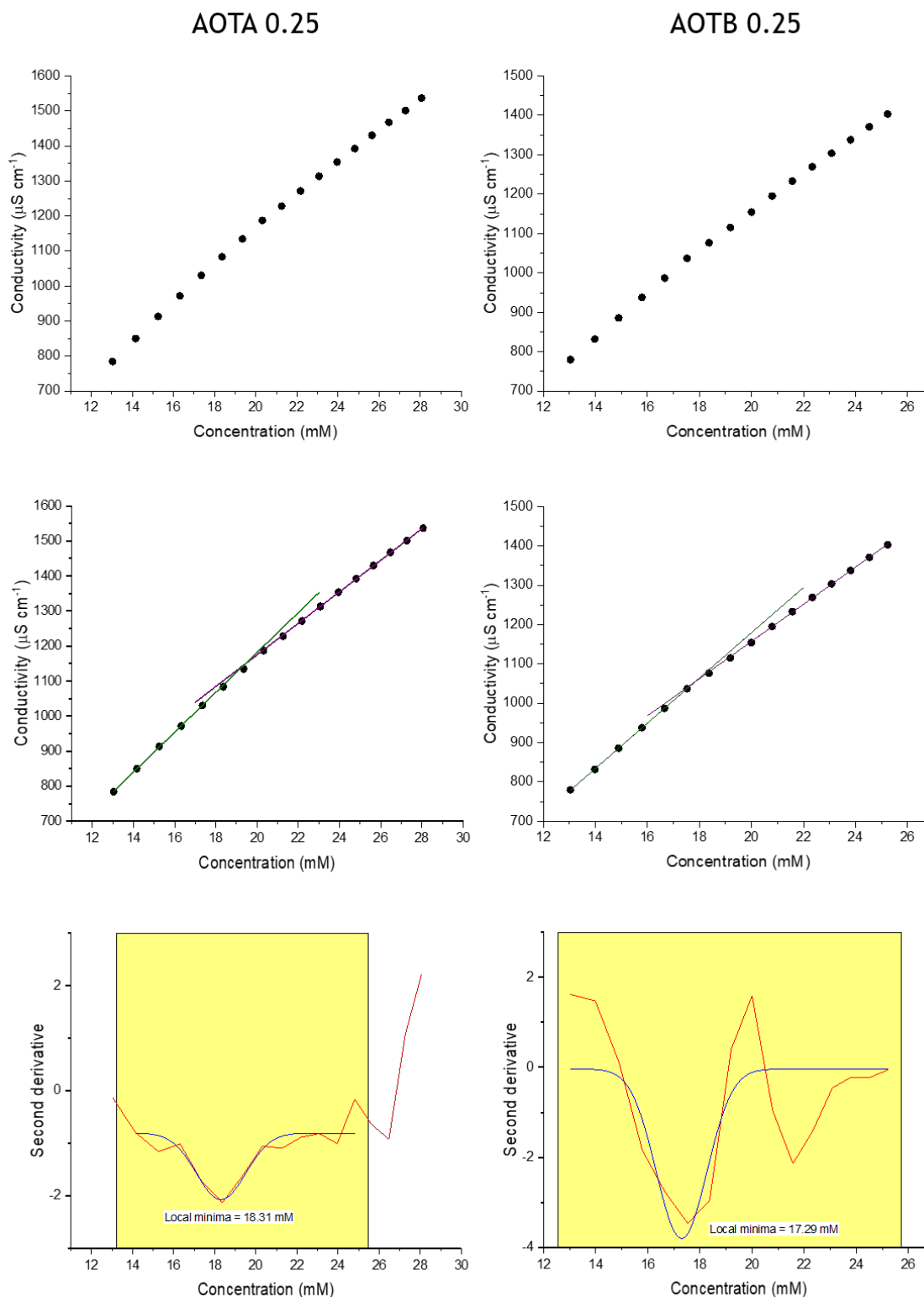


Figure 8.1d: Conductivity data used to determined cmcs of di-C6SS mixed system at a molar ratio of 0.25 X, where X is either AOTA / AOTB.

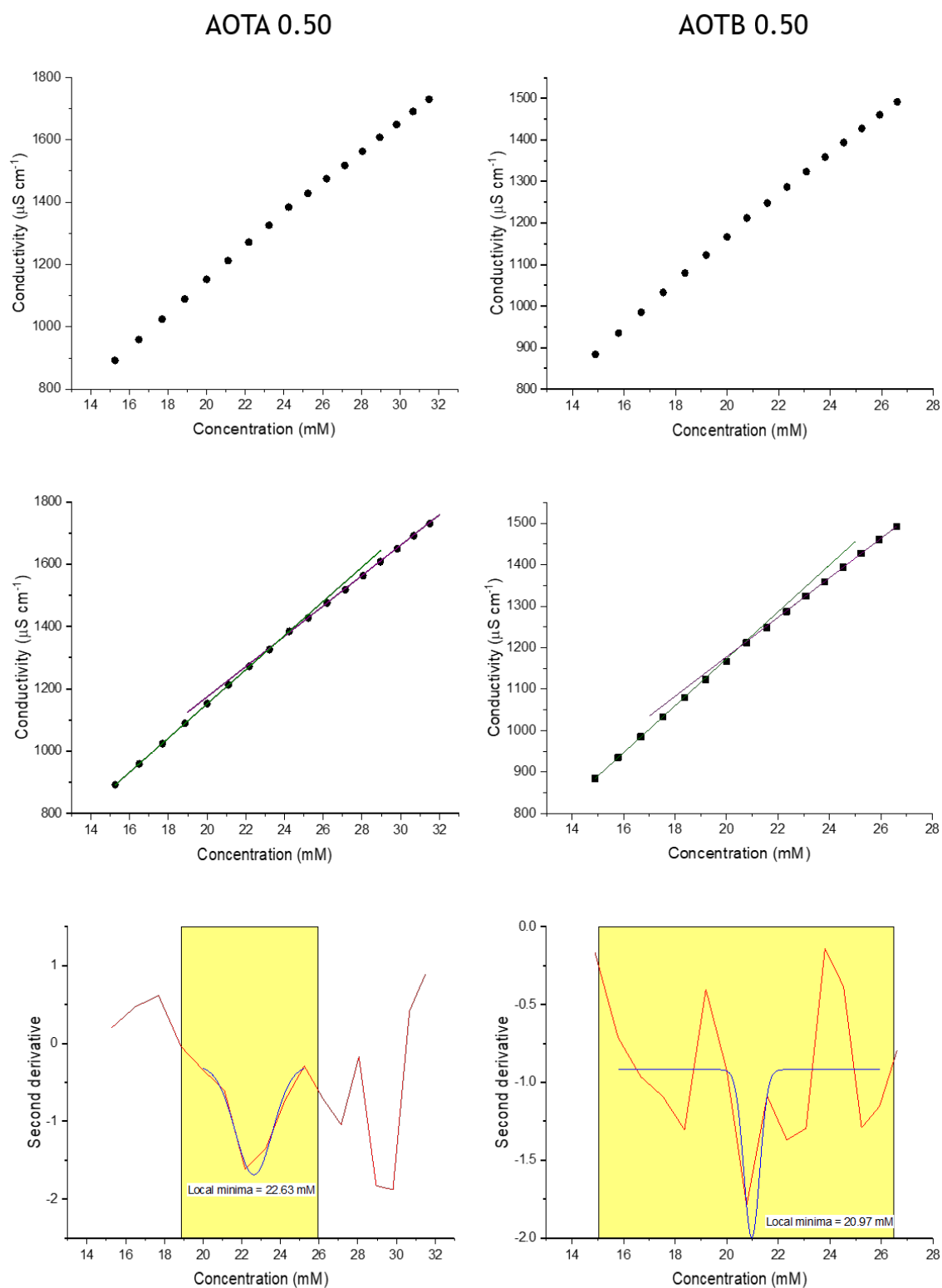


Figure 8.1e: Conductivity data used to determined cmcs of di-C6SS mixed system at a molar ratio of 0.5 X, where X is either AOTA / AOTB.

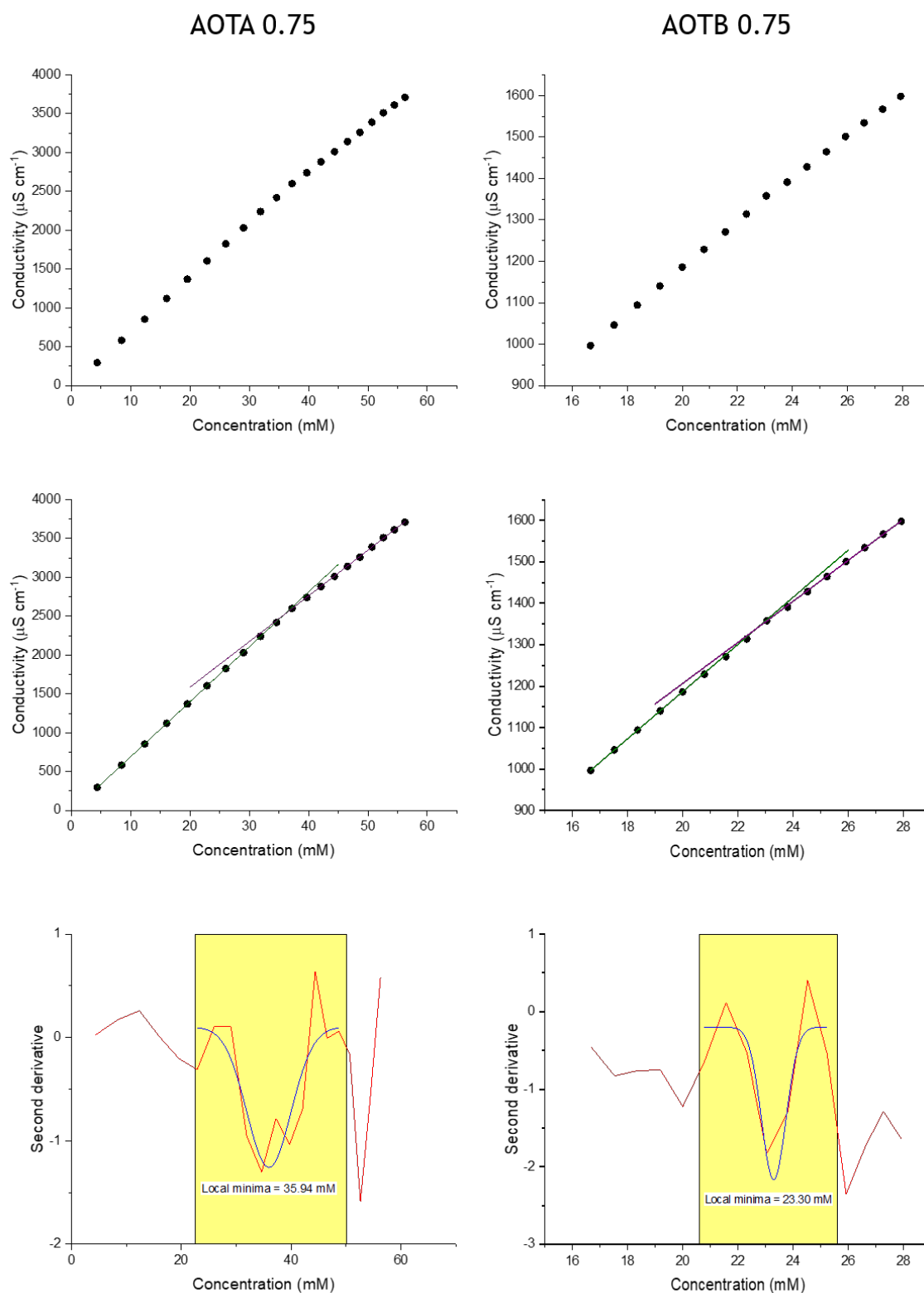


Figure 8.1f: Conductivity data used to determined cmcs of di-C6SS mixed system at a molar ratio of 0.75 X, where X is either AOTA / AOTB.

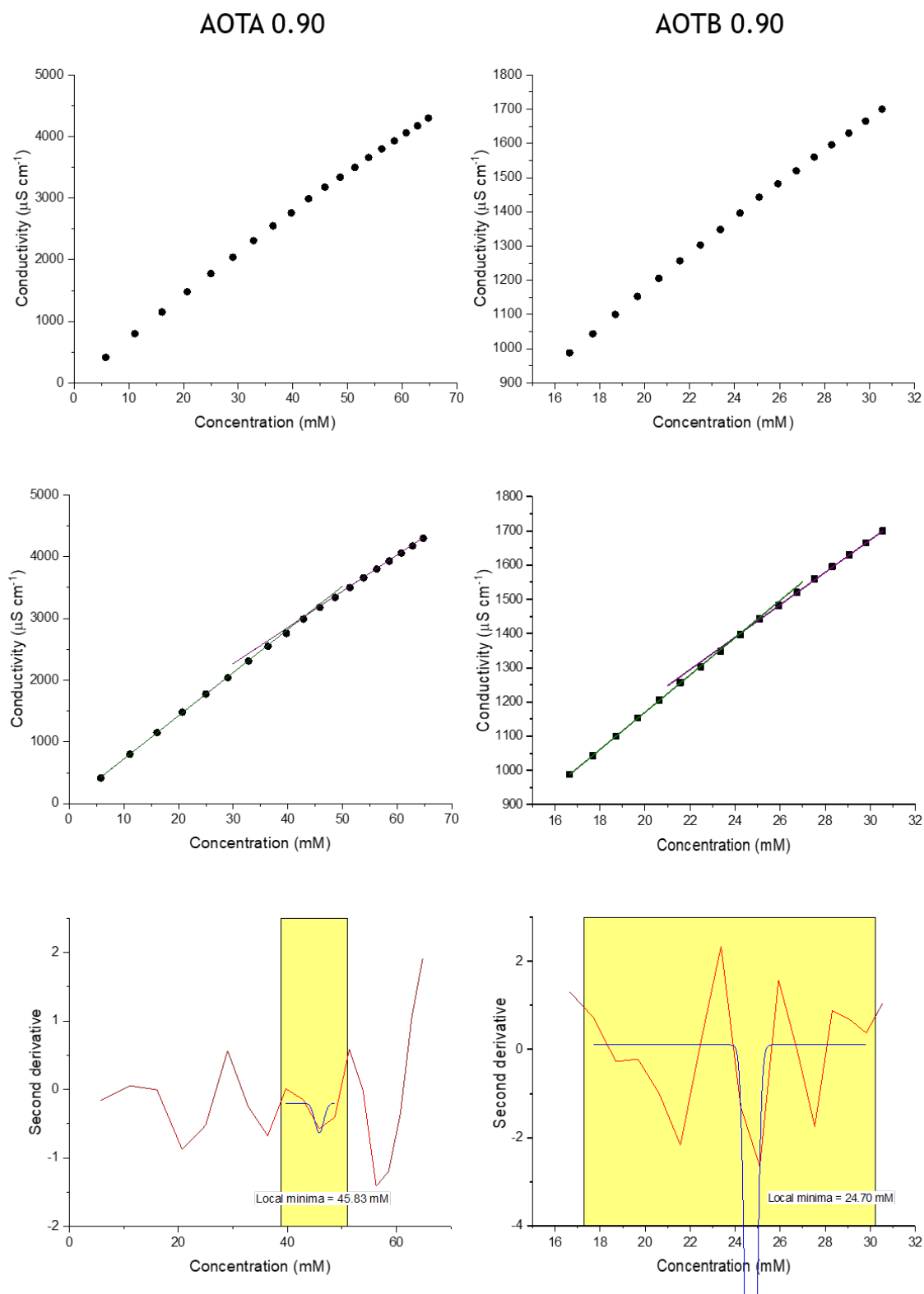


Figure 8.1g: Conductivity data used to determined cmcs of di-C6SS mixed system at a molar ratio of 0.9 X, where X is either AOTA / AOTB.

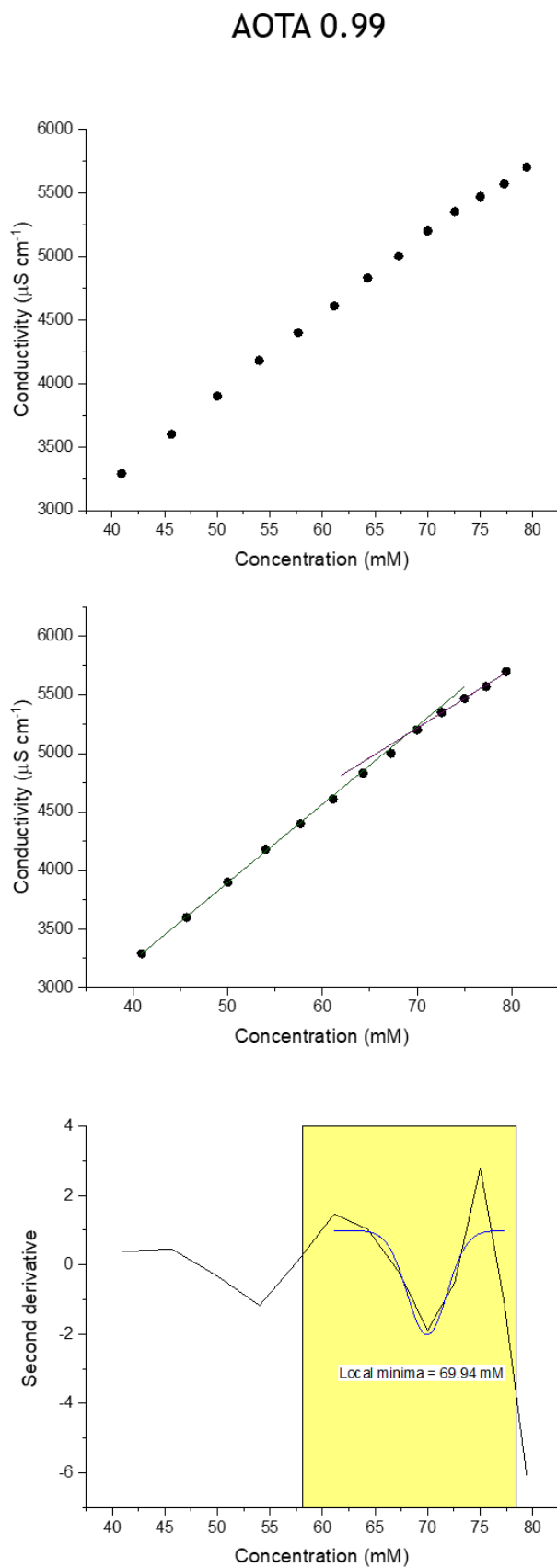
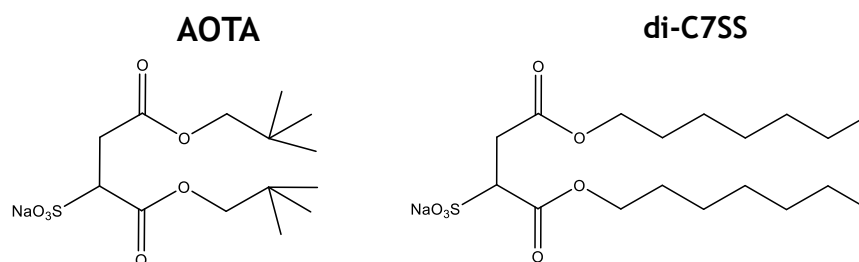
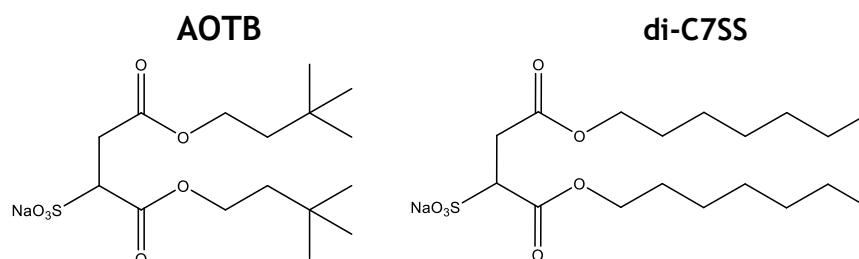


Figure 8.1h: Conductivity data used to determine the cmc of di-C6SS mixed system at a molar ratio of 0.99 AOTA.

8.2.2 di-C7SS : AOTA / AOTB



AOTA	di-C7SS	cmc (mM) \pm 0.1
0.01	0.99	4.56
0.10	0.90	6.04
0.25	0.75	6.30
0.50	0.50	7.43
0.75	0.25	17.8
0.90	0.10	24.0
0.99	0.01	68.2



AOTB	di-C7SS	cmc (mM) \pm 0.1
0.01	0.99	4.58
0.10	0.90	4.60
0.25	0.75	5.82
0.50	0.50	6.65
0.75	0.25	9.73
0.90	0.10	16.7

Figure 8.2a: Summary of the cmc values for di-C7SS : AOTA / AOTB mixed surfactant systems at varying molar ratios.

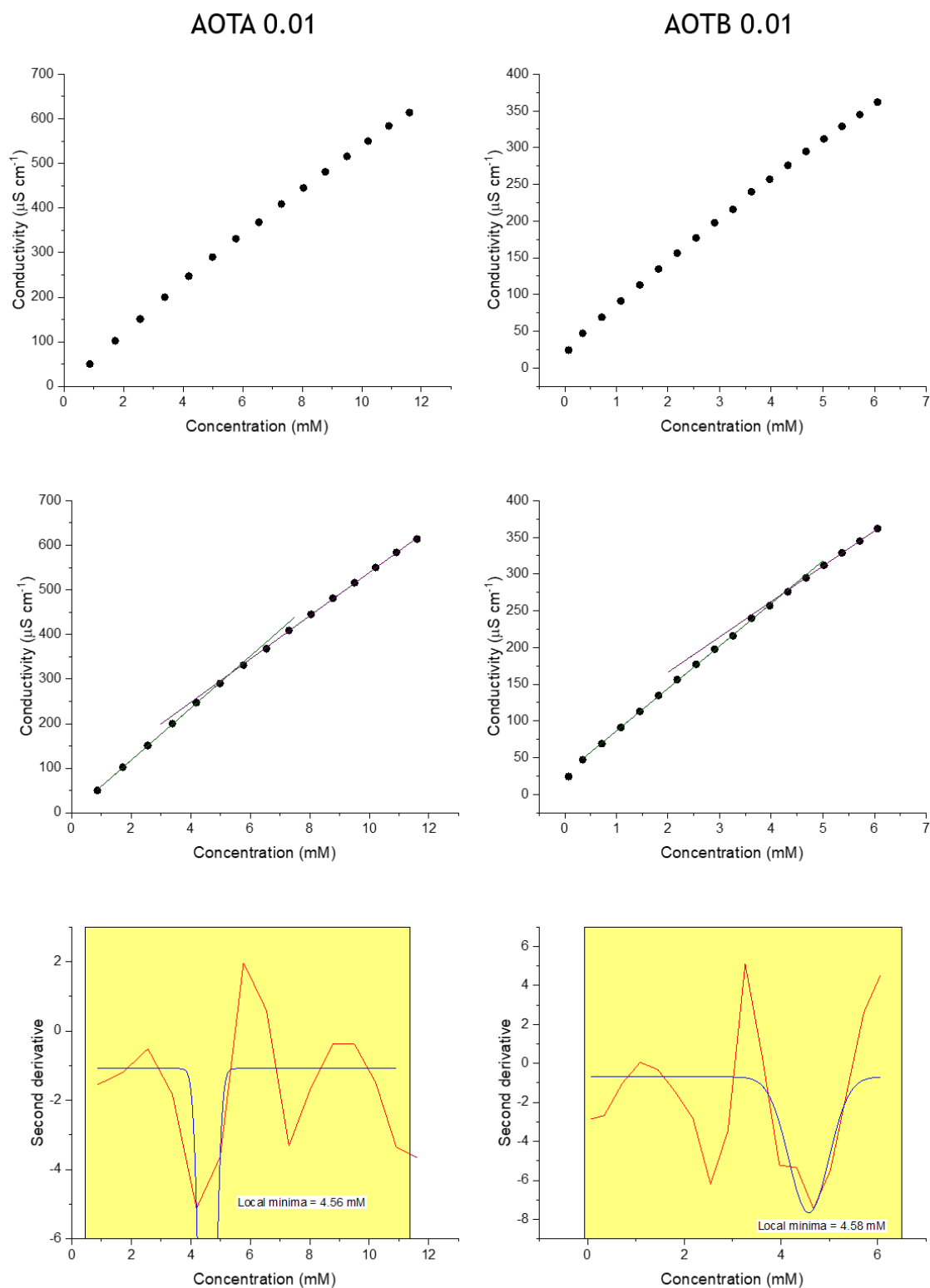


Figure 8.2b: Conductivity data used to determined cmcs of di-C7SS mixed system at a molar ratio of 0.01 X, where X is either AOTA / AOTB.

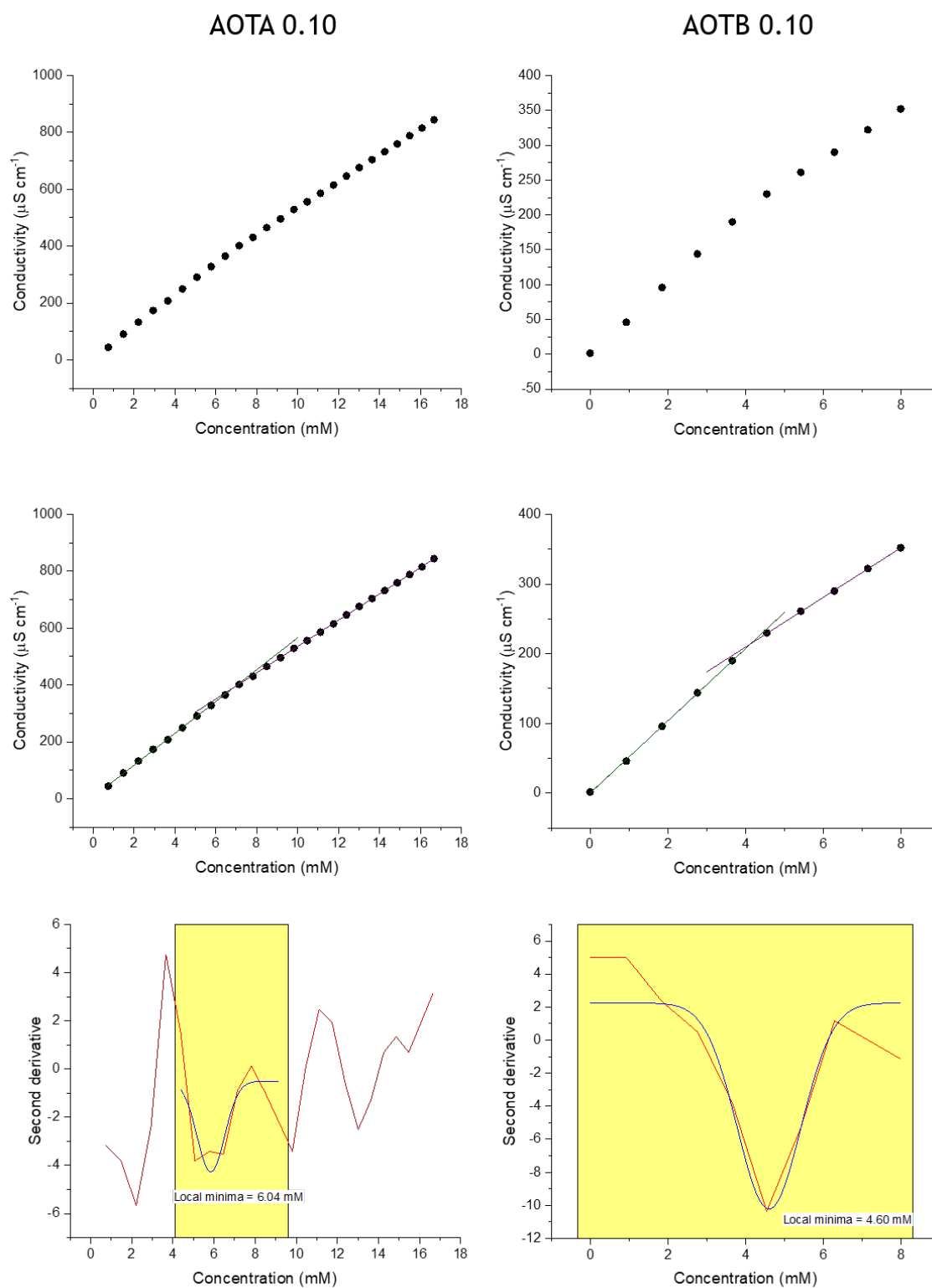


Figure 8.2c: Conductivity data used to determined cmcs of di-C7SS mixed system at a molar ratio of 0.1 X, where X is either AOTA / AOTB.

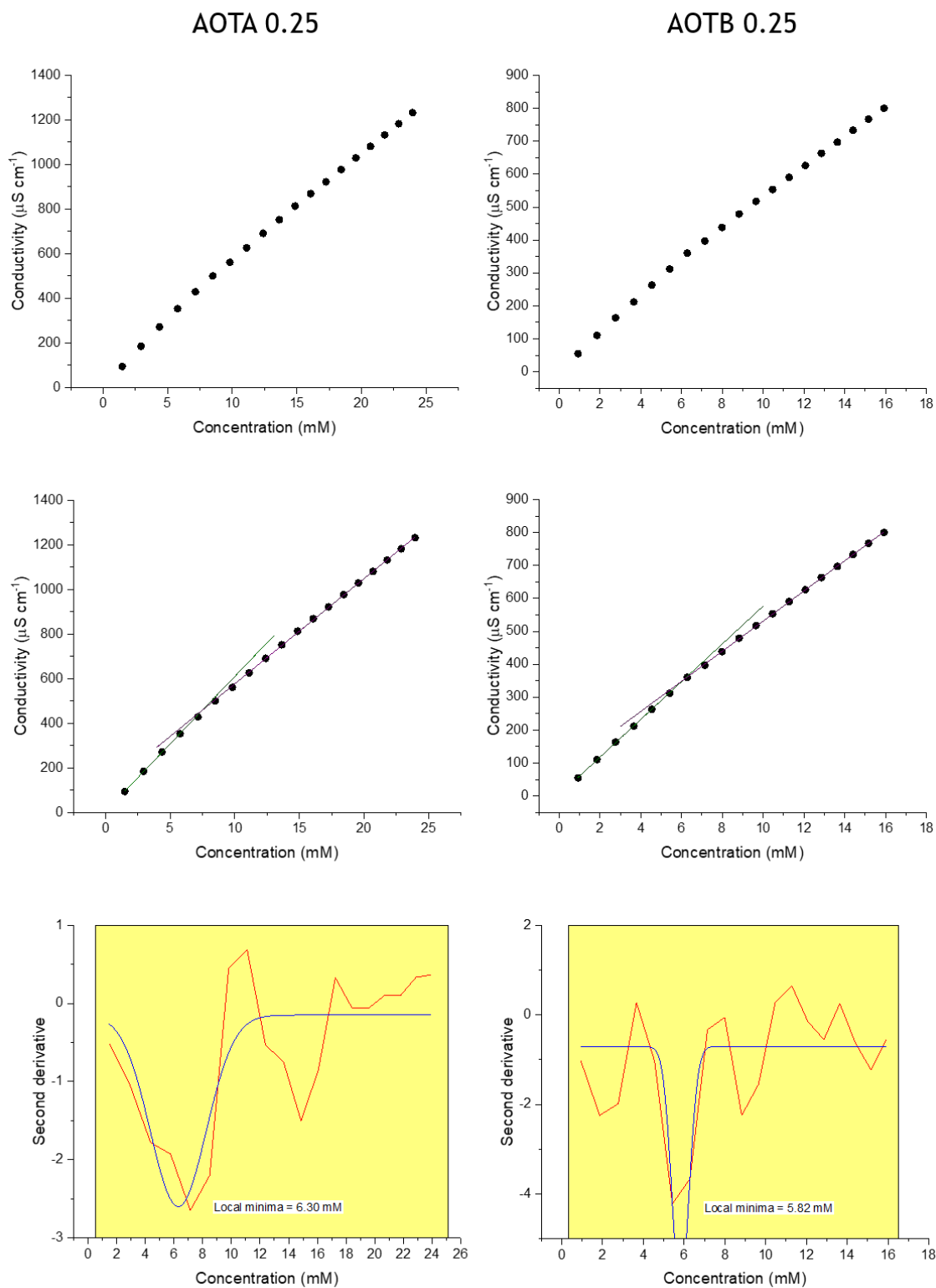


Figure 8.2d: Conductivity data used to determined cmcs of di-C7SS mixed system at a molar ratio of 0.25 X, where X is either AOTA / AOTB.

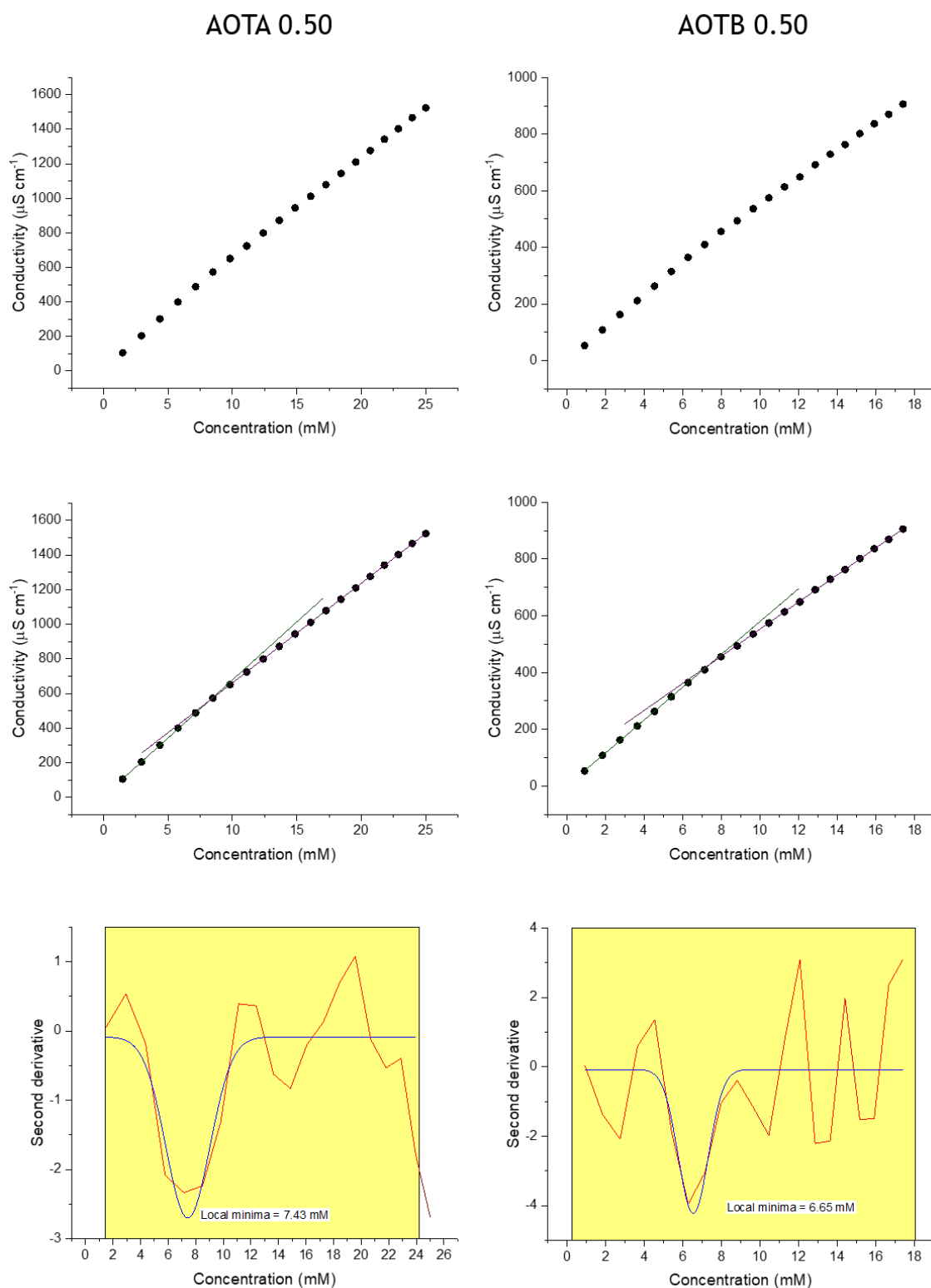


Figure 8.2e: Conductivity data used to determined cmcs of di-C7SS mixed system at a molar ratio of 0.5 X, where X is either AOTA / AOTB.

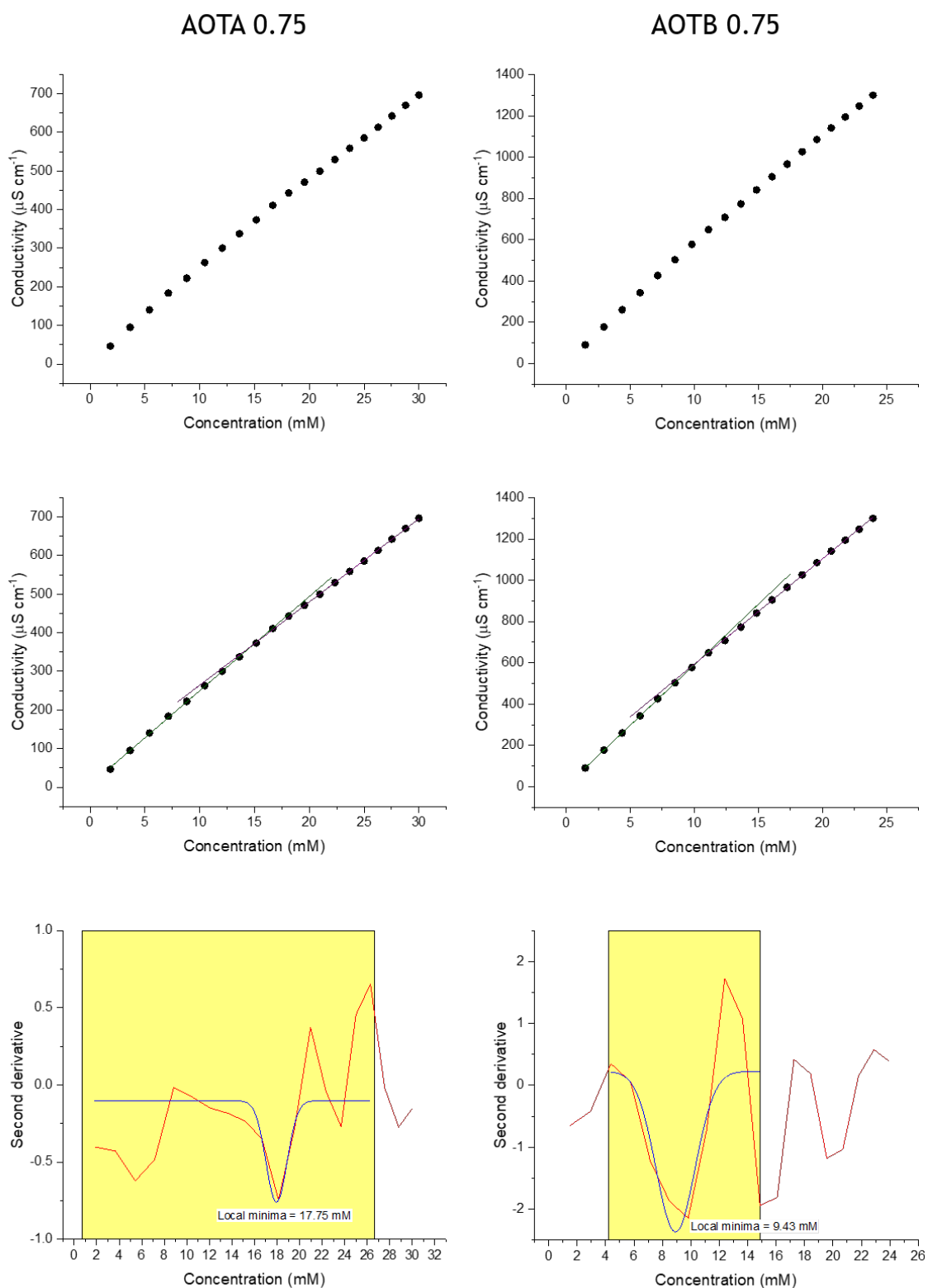


Figure 8.2f: Conductivity data used to determined cmcs of di-C7SS mixed system at a molar ratio of 0.75 X, where X is either AOTA / AOTB.

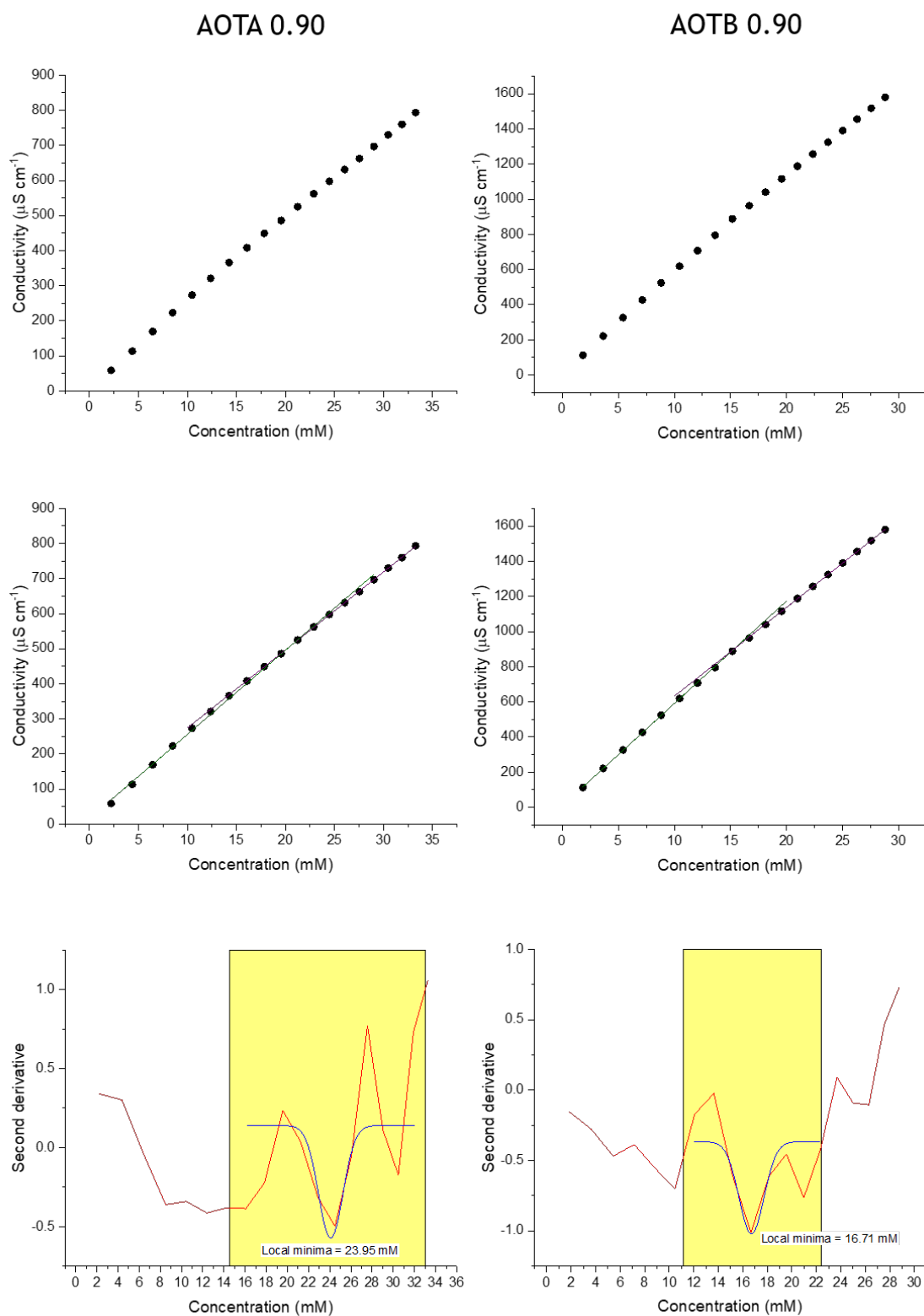


Figure 8.2g: Conductivity data used to determined cmcs of di-C7SS mixed system at a molar ratio of 0.9 X, where X is either AOTA / AOTB.

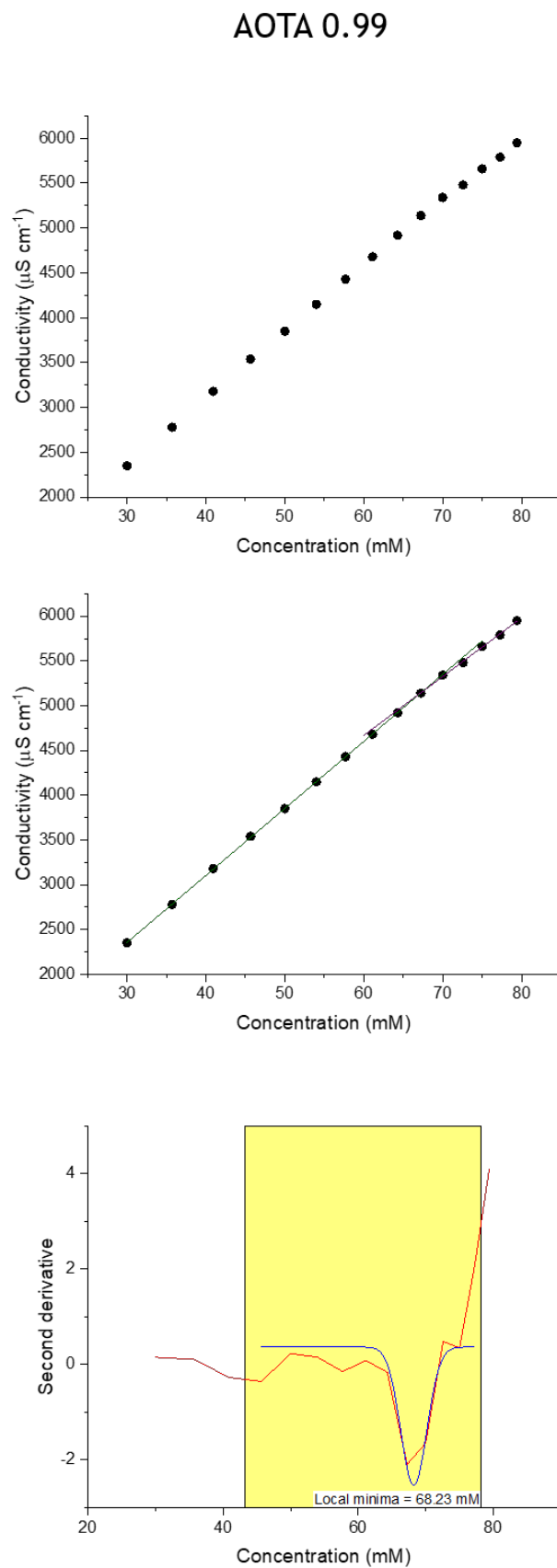


Figure 8.2h: Conductivity data used to determined cmc of di-C7SS mixed system at a molar ratio of 0.99 AOTA.

8.2.3 di-C8SS : AOTA / AOTB

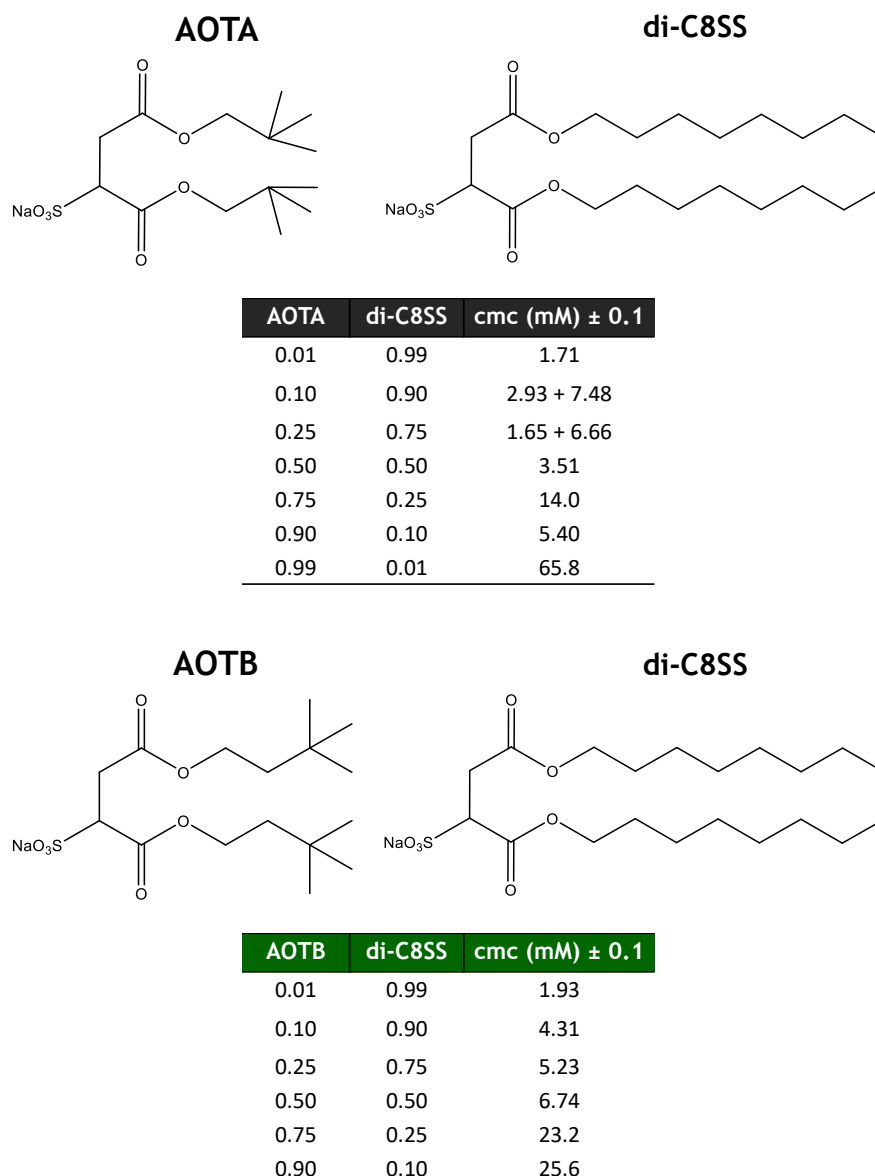


Figure 8.3a: Summary of the cmc values for di-C8SS : AOTA / AOTB mixed surfactant systems at varying molar ratios.

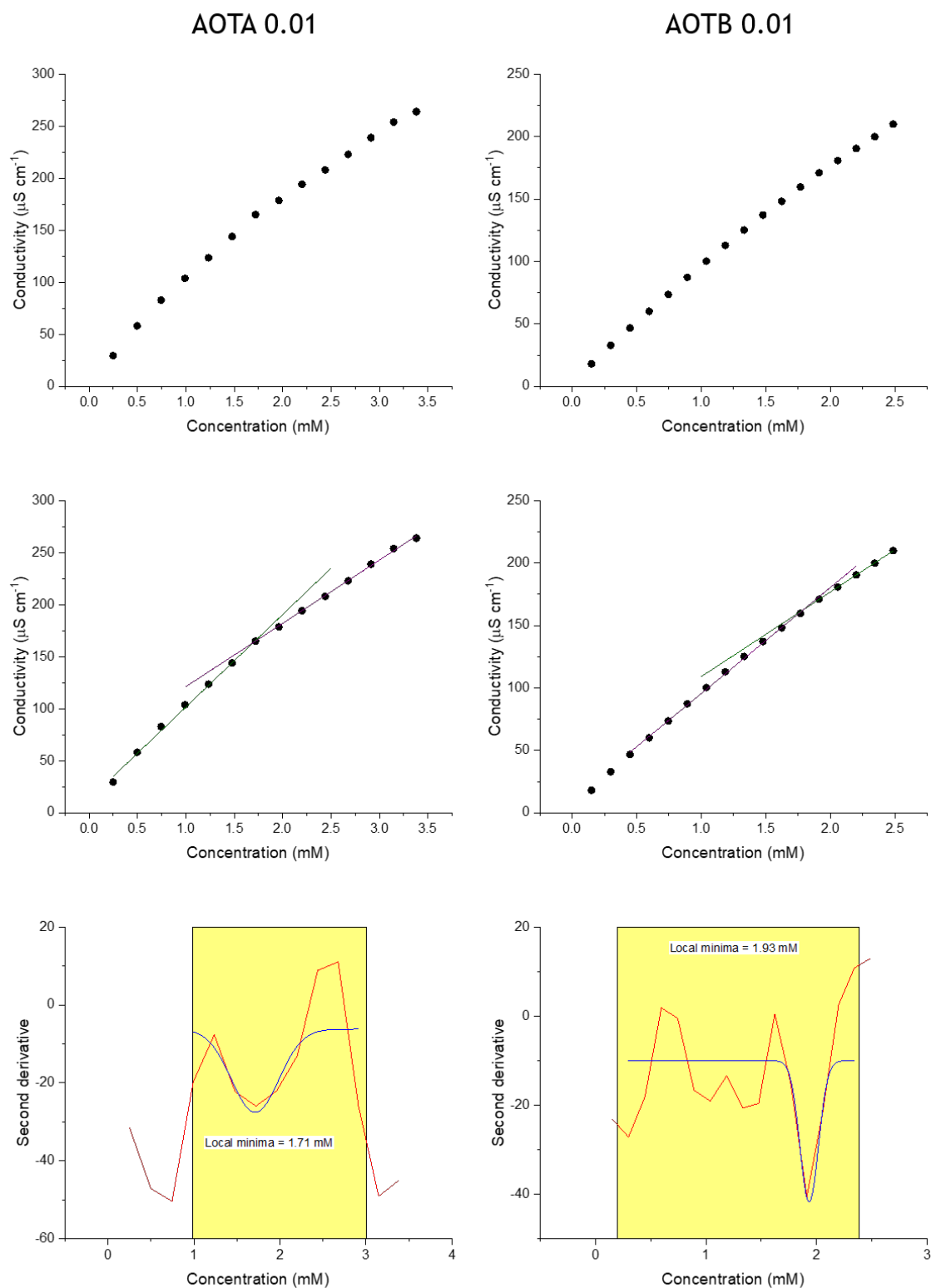


Figure 8.3b: Conductivity data used to determined cmcs of di-C8SS mixed system at a molar ratio of 0.01 X, where X is either AOTA / AOTB.

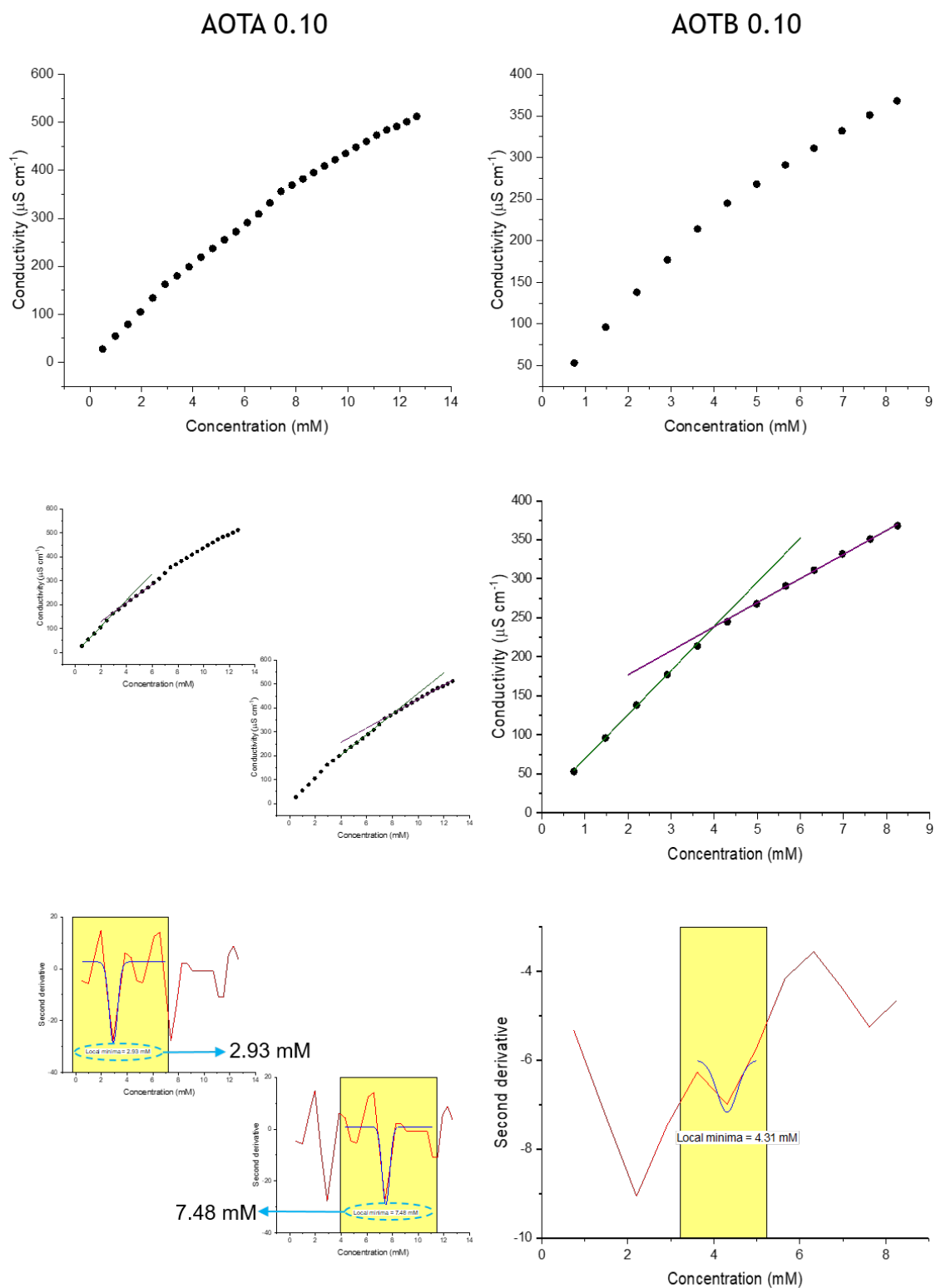


Figure 8.3c: Conductivity data used to determined cmcs of di-C8SS mixed system at a molar ratio of 0.1 X, where X is either AOTA / AOTB.

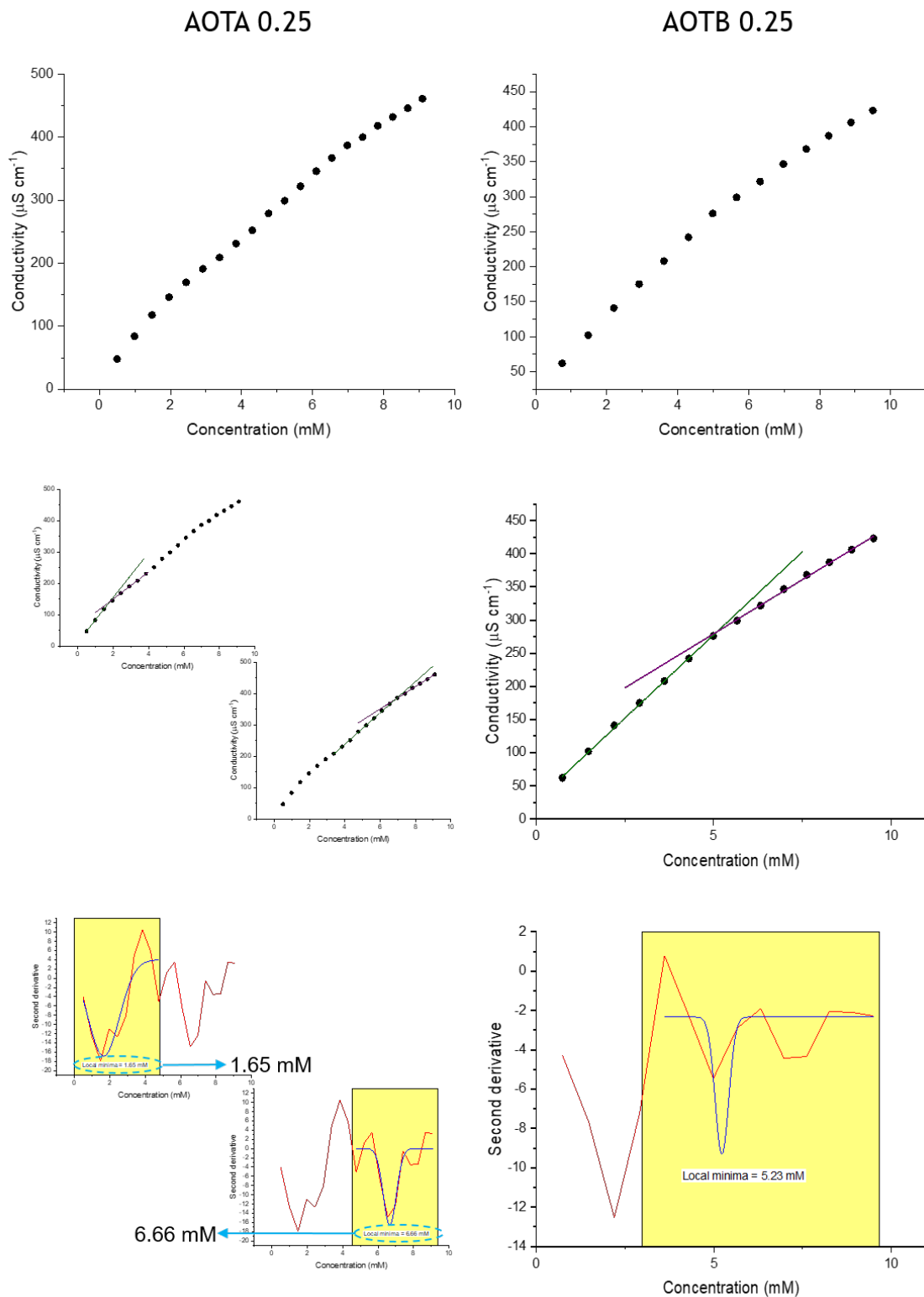


Figure 8.3d: Conductivity data used to determined cmcs of di-C8SS mixed system at a molar ratio of 0.25 X, where X is either AOTA / AOTB.

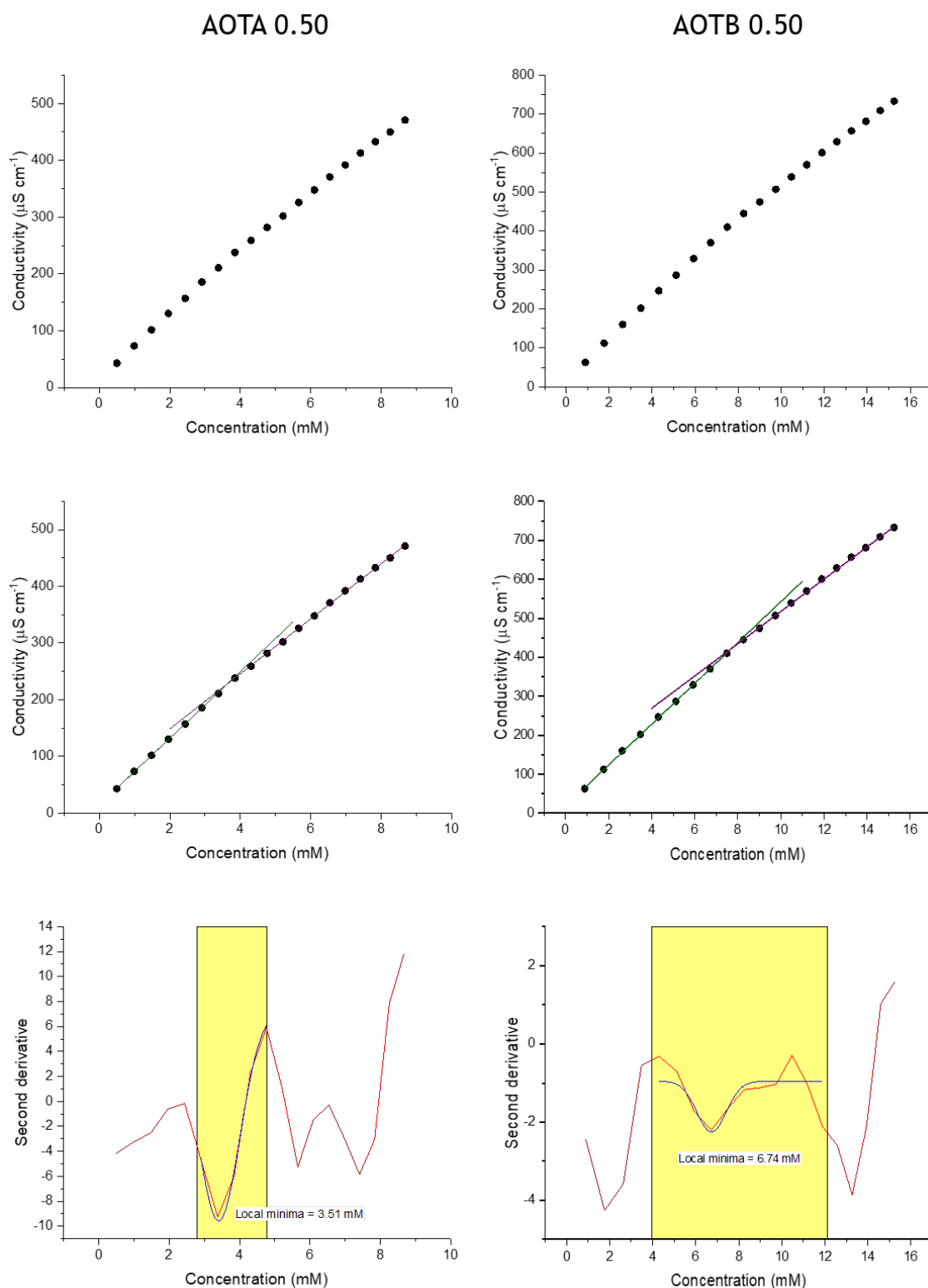


Figure 8.3e: Conductivity data used to determined cmcs of di-C8SS mixed system at a molar ratio of 0.5 X, where X is either AOTA / AOTB.

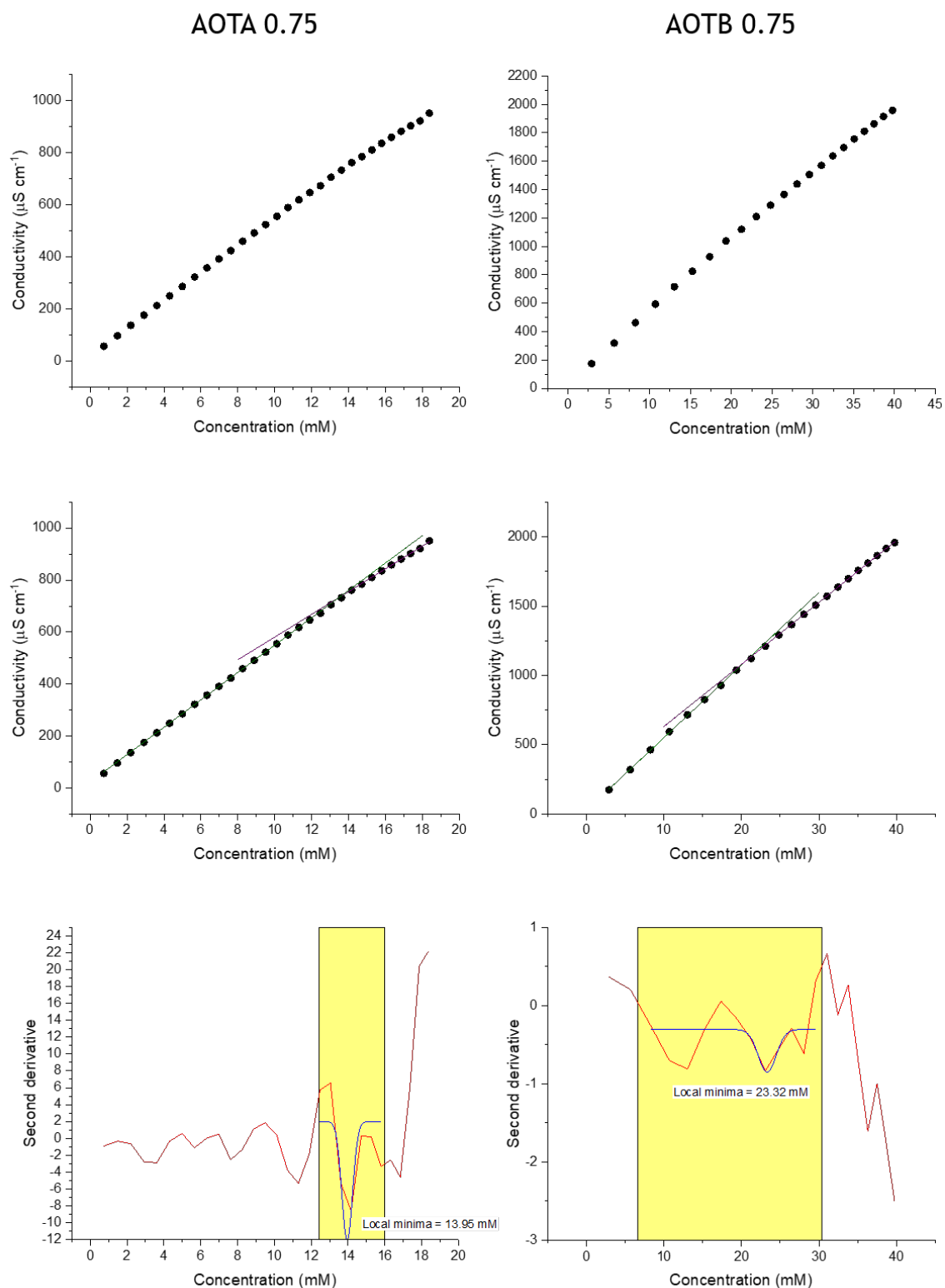


Figure 8.3f: Conductivity data used to determined cmcs of di-C8SS mixed system at a molar ratio of 0.75 X, where X is either AOTA / AOTB.

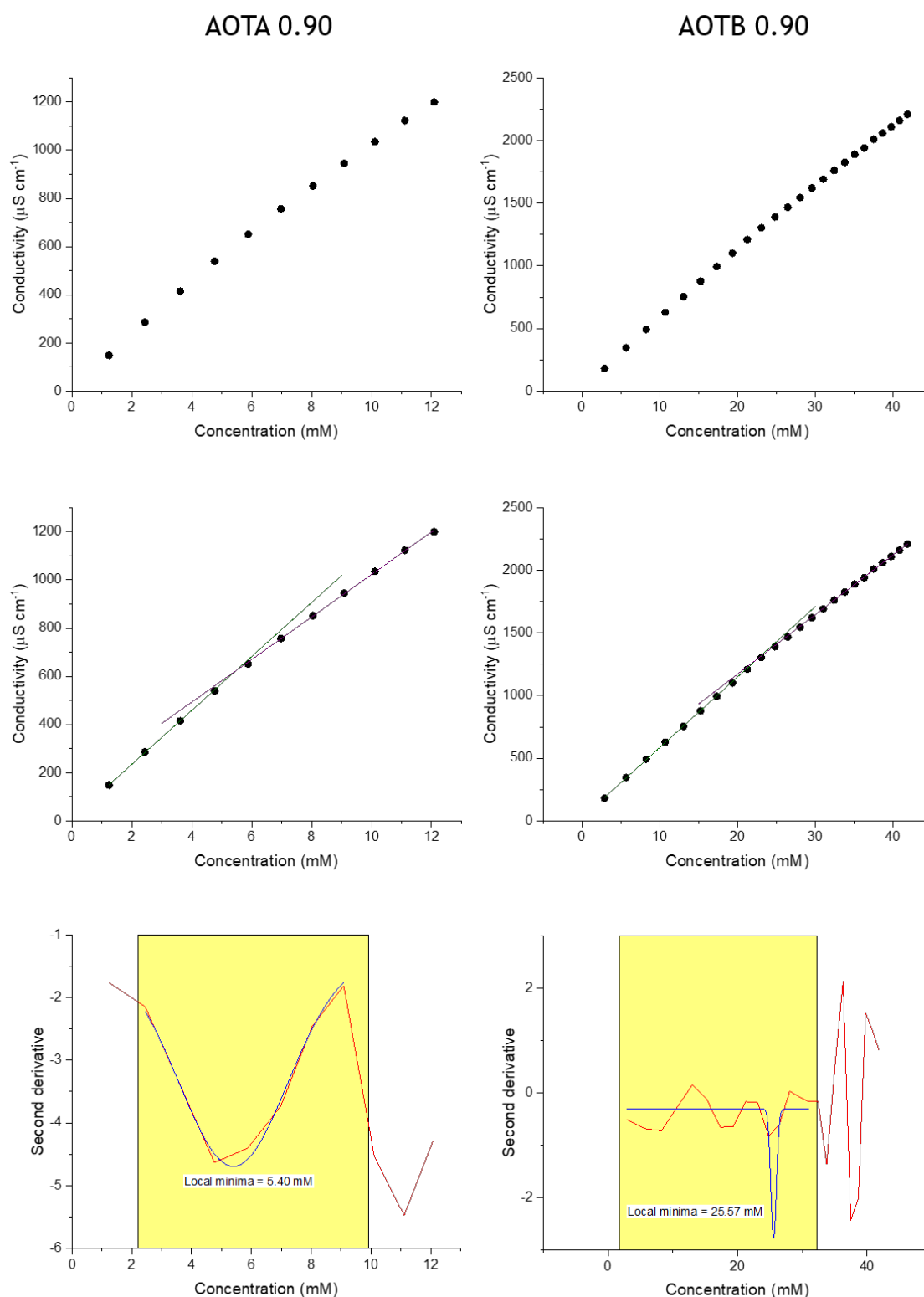


Figure 8.3g: Conductivity data used to determined cmcs of di-C₈SS mixed system at a molar ratio of 0.9 X, where X is either AOTA / AOTB.

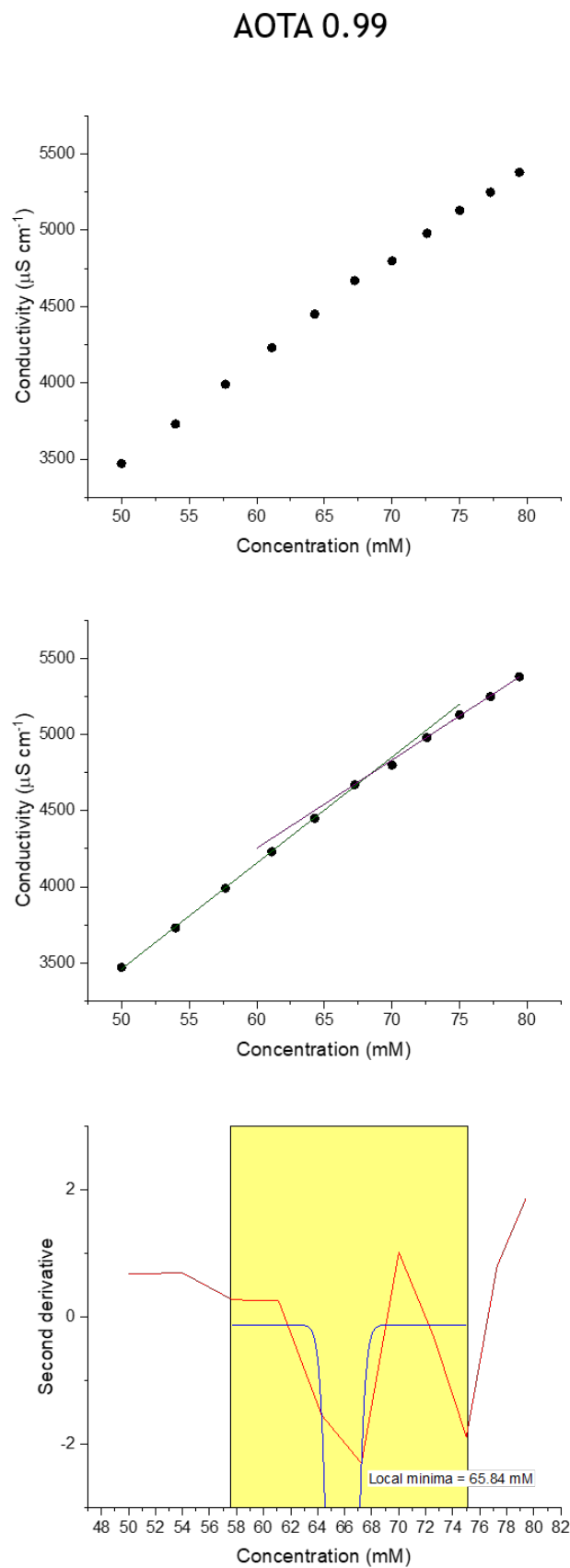
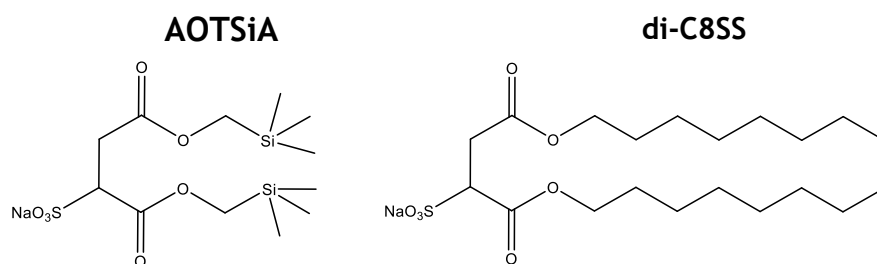
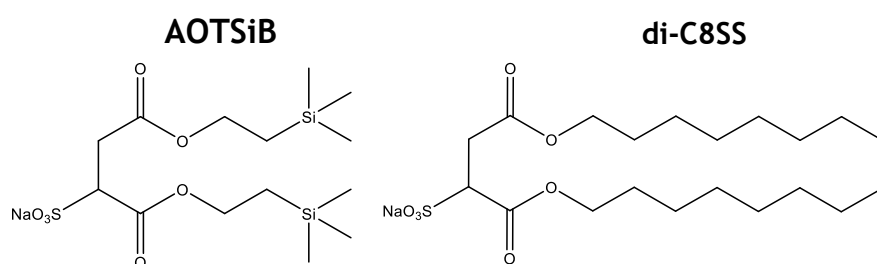


Figure 8.3h: Conductivity data used to determined cmc of di-C8SS mixed system at a molar ratio of 0.99 AOTA.

8.2.4 di-C8SS : AOTSiA / AOTSiB



AOTSiA	di-C8SS	cmc (mM) \pm 0.1
0.10	0.90	2.66
0.25	0.75	5.66
0.50	0.50	6.92
0.75	0.25	12.5
0.90	0.10	11.8



AOTSiB	di-C8SS	cmc (mM) \pm 0.1
0.10	0.90	1.47
0.25	0.75	1.85
0.50	0.50	3.83
0.75	0.25	11.7
0.90	0.10	11.9

Figure 8.4a: Summary of the cmc values for di-C8SS : AOTSiA / AOTSiB mixed surfactant systems at varying molar ratios.

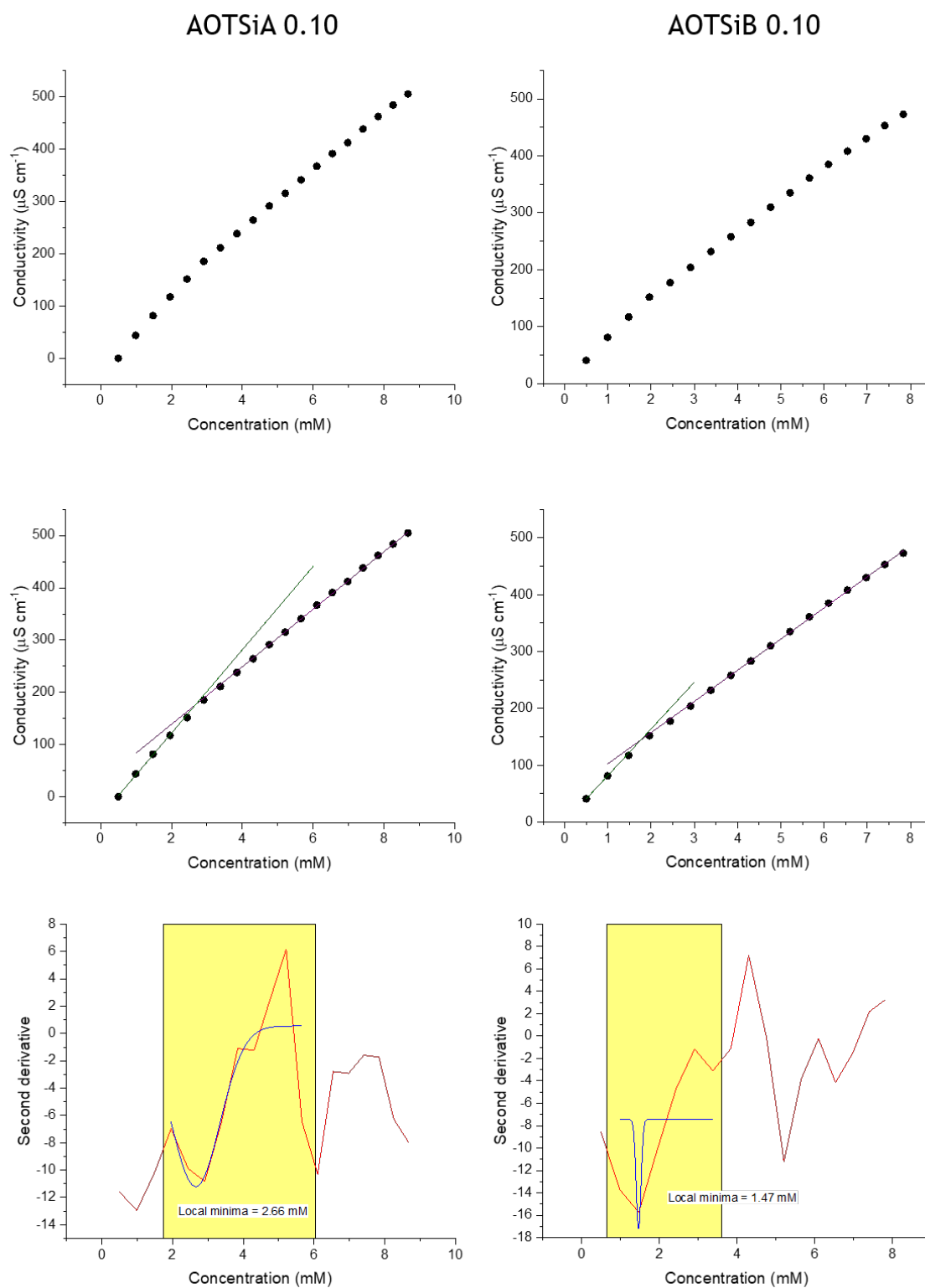


Figure 8.4b: Conductivity data used to determine cmcs of di-C8SS mixed system at a molar ratio of 0.1 X, where X is either AOTSiA / AOTSiB.

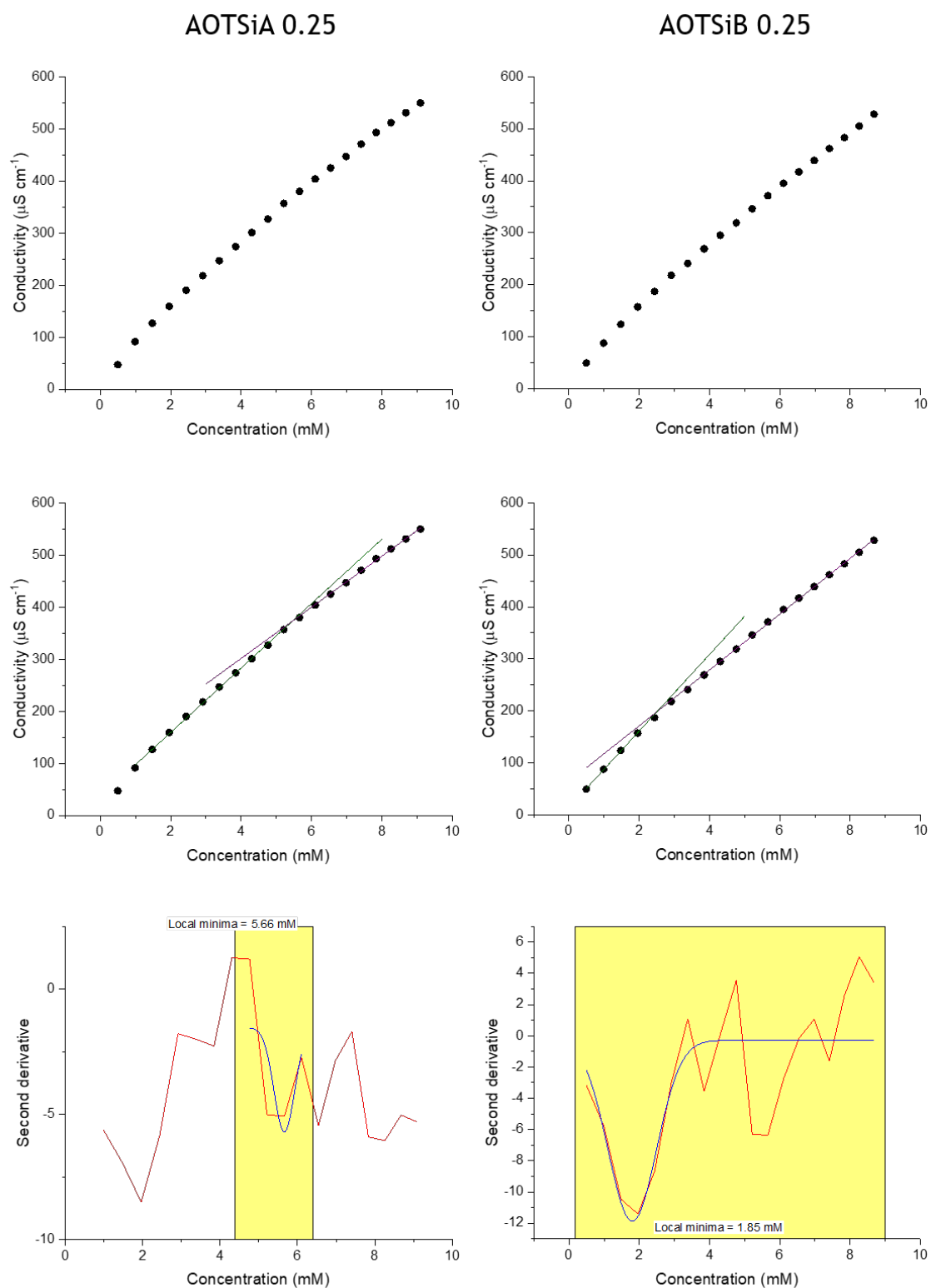


Figure 8.4c: Conductivity data used to determined cmcs of di-C8SS mixed system at a molar ratio of 0.25 X, where X is either AOTSiA / AOTSiB.

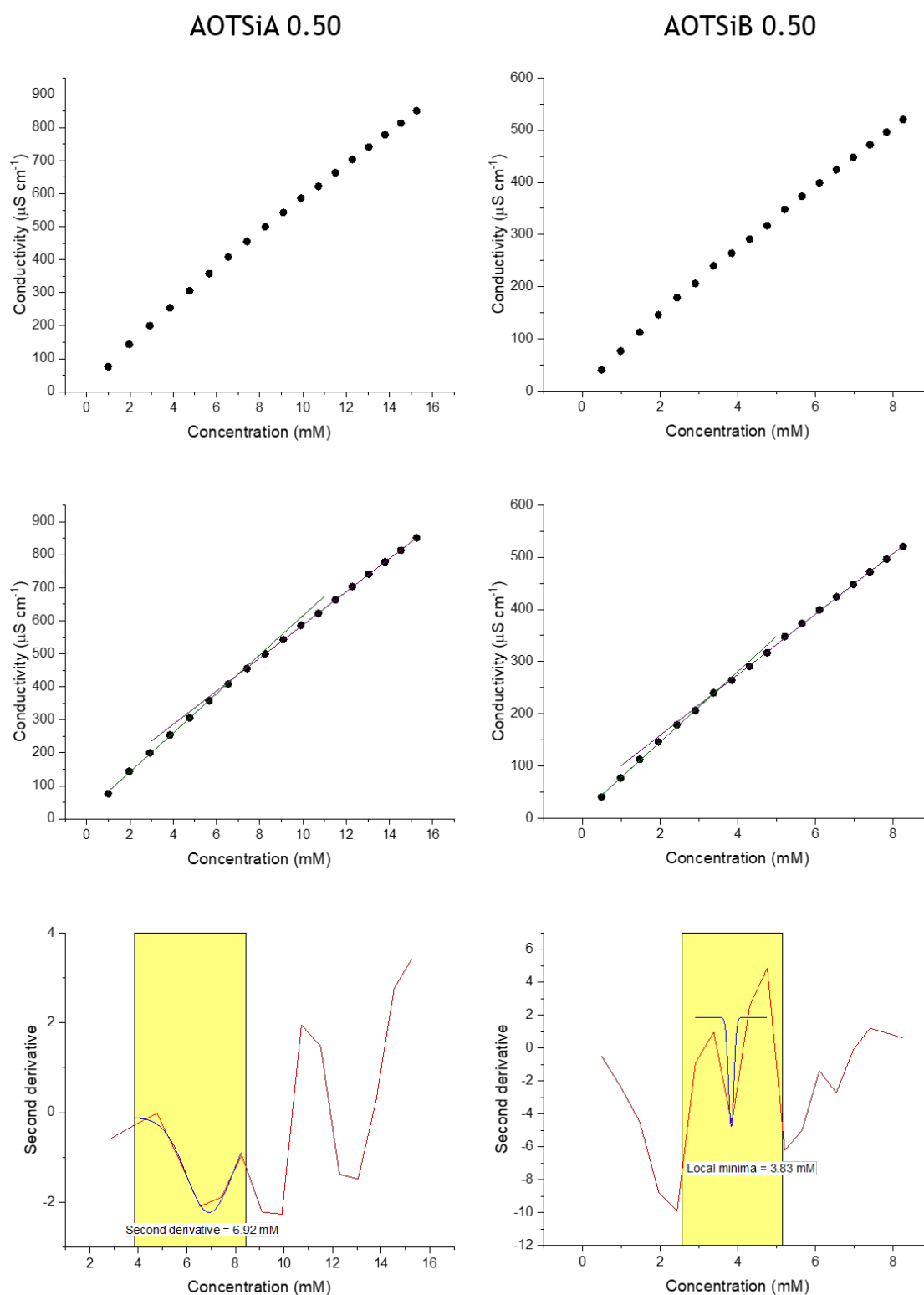


Figure 8.4d: Conductivity data used to determined cmcs of di-C8SS mixed system at a molar ratio of 0.5 X, where X is either AOTSiA / AOTSiB.

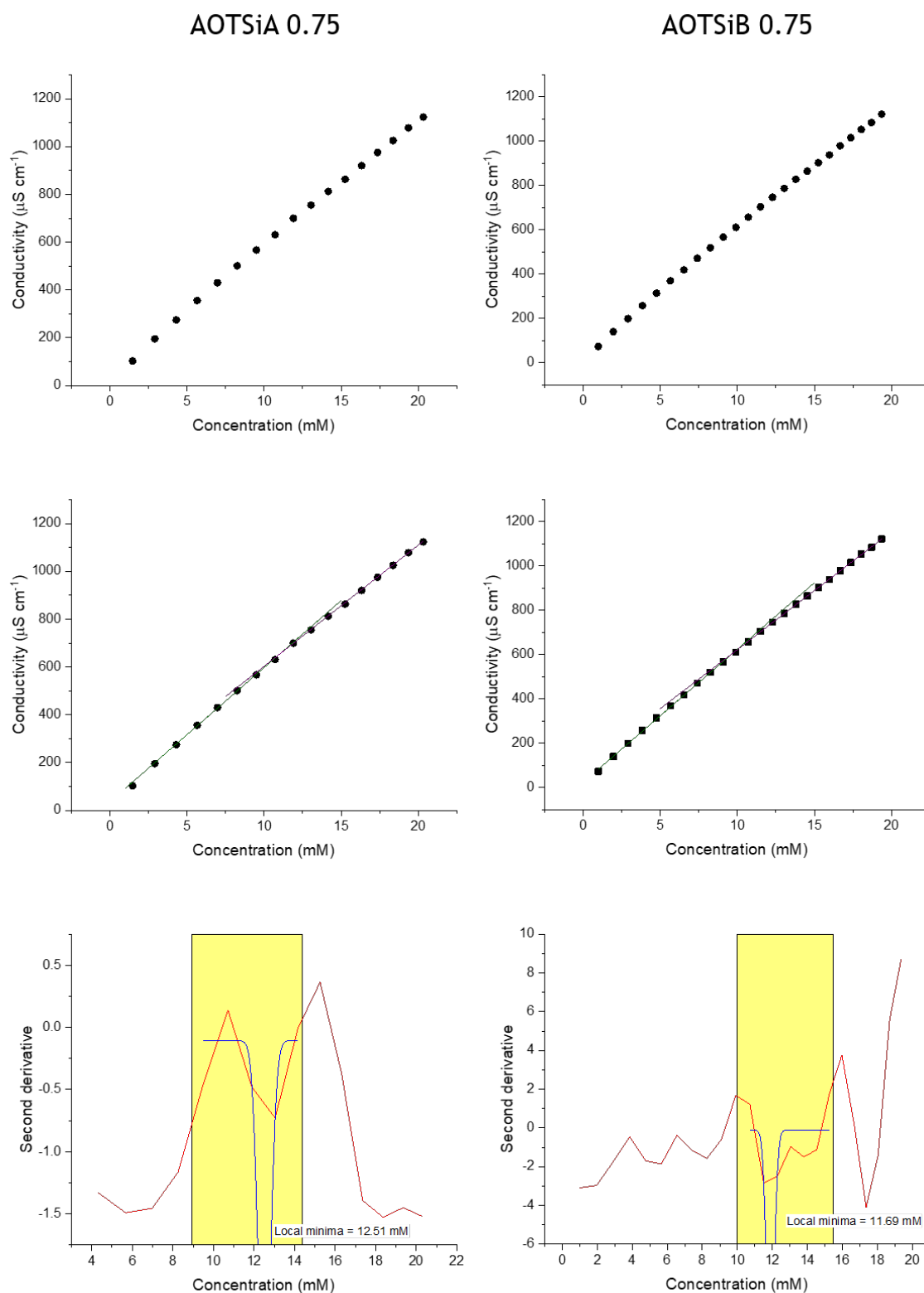


Figure 8.4e: Conductivity data used to determined cmcs of di-C8SS mixed system at a molar ratio of 0.75 X, where X is either AOTSiA / AOTSiB.

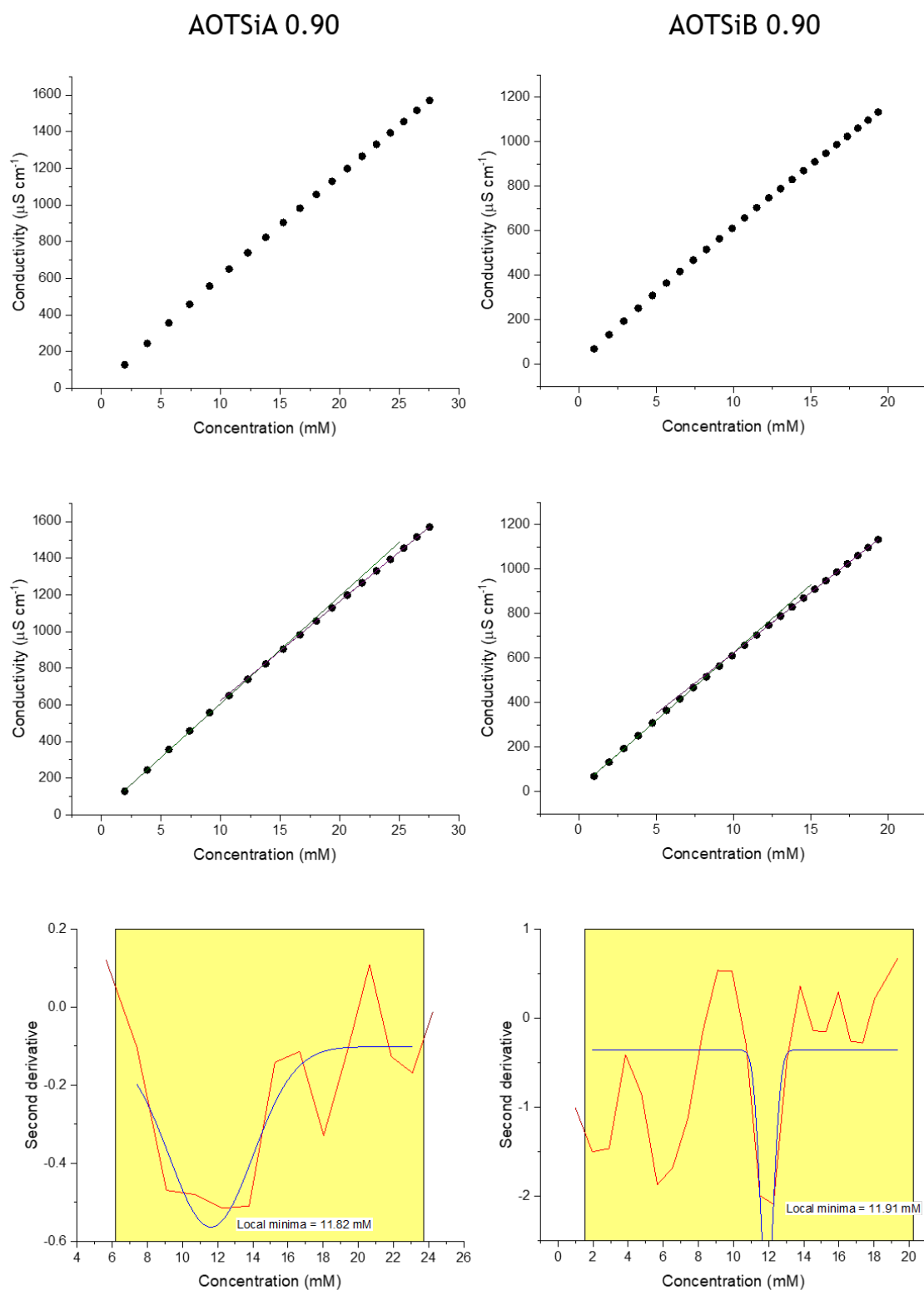


Figure 8.4f: Conductivity data used to determined cmcs of di-C8SS mixed system at a molar ratio of 0.9 X, where X is either AOTSiA / AOTSiB.

8.2.5 HS3 : AOTA / AOTB

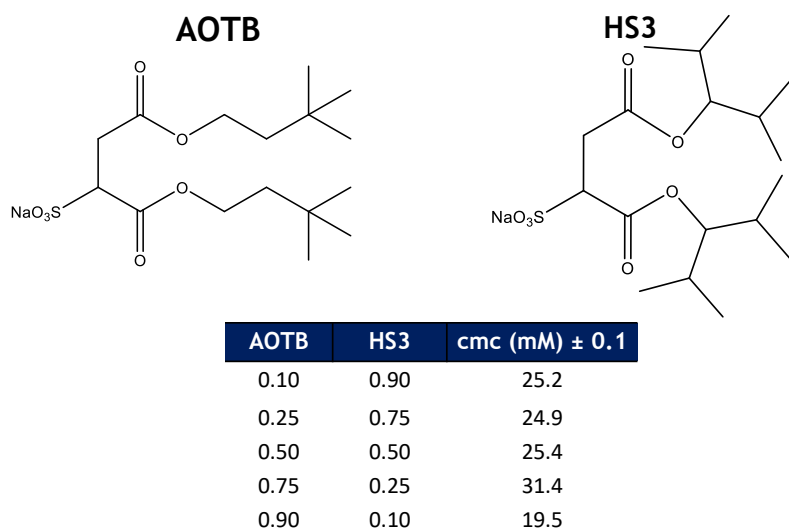
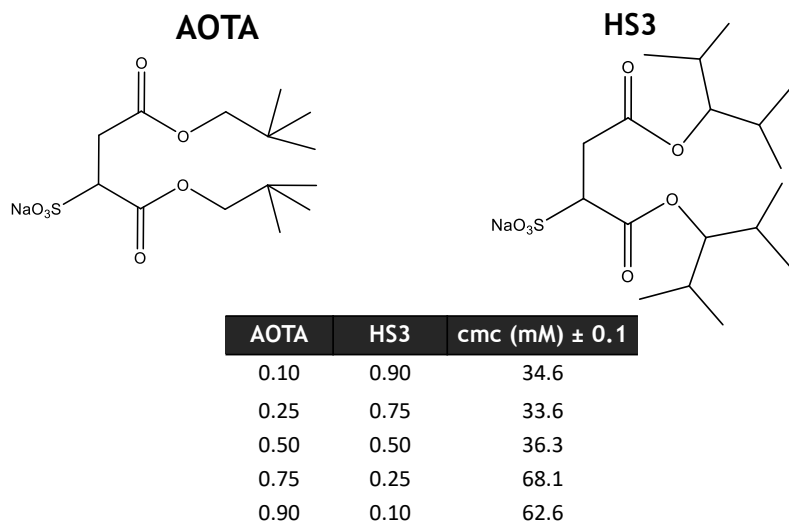


Figure 8.5a: Summary of the cmc values for HS3 : AOTA / AOTB mixed surfactant systems at varying molar ratios.

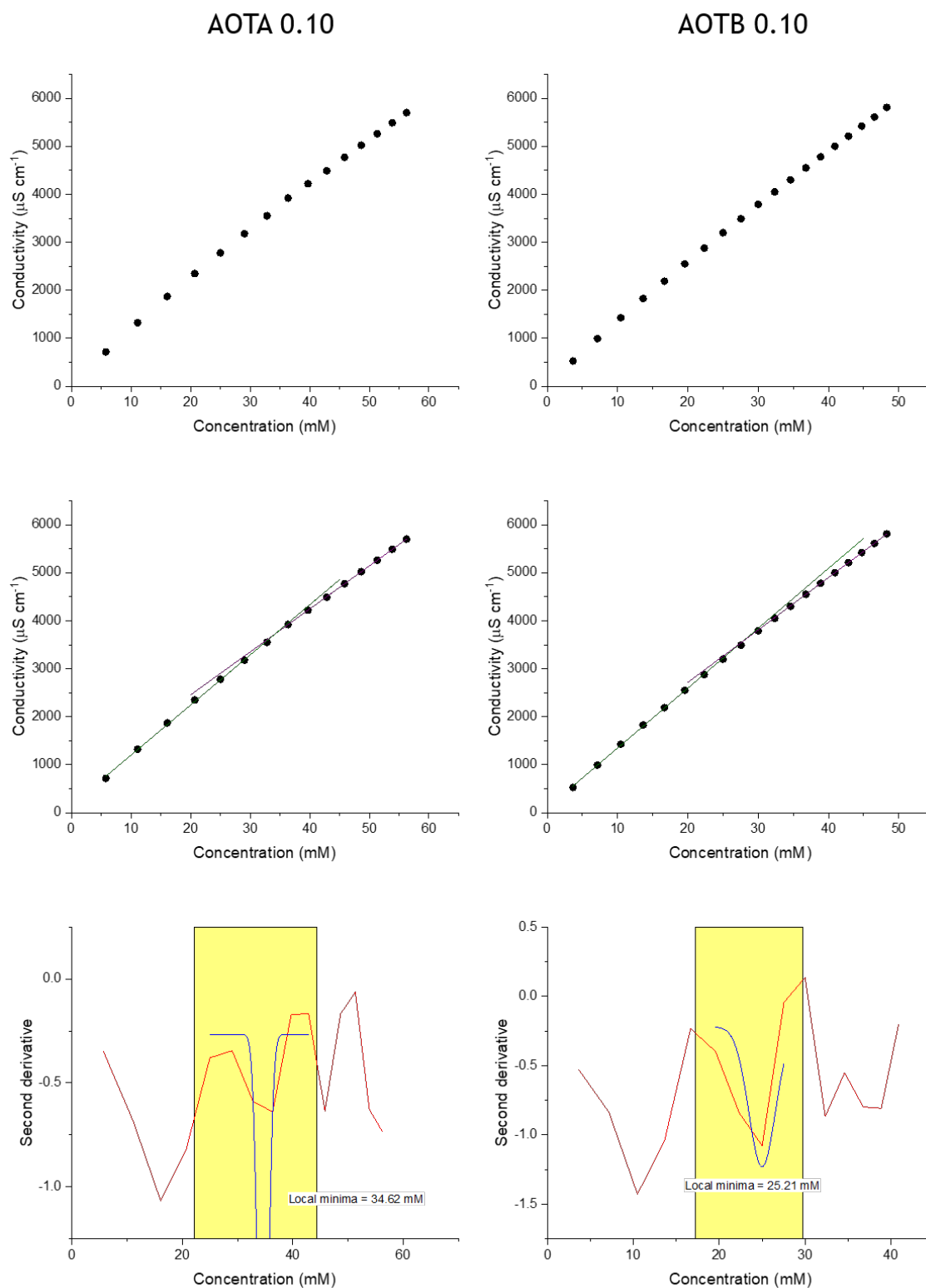


Figure 8.5b: Conductivity data used to determined cmcs of HS3 mixed system at a molar ratio of 0.1 X, where X is either AOTA / AOTB.

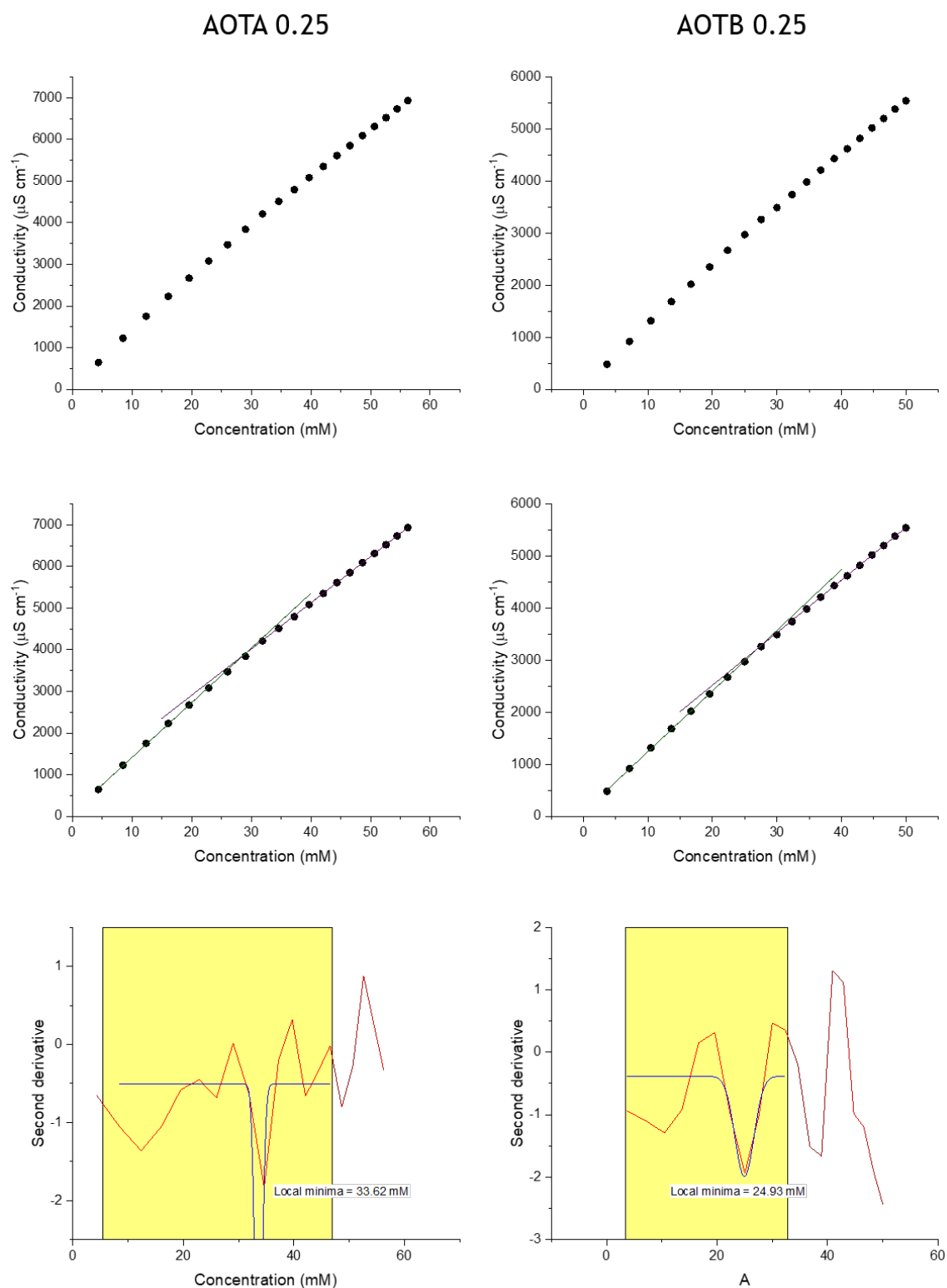


Figure 8.5c: Conductivity data used to determined cmcs of HS3 mixed system at a molar ratio of 0.25 X, where X is either AOTA / AOTB.

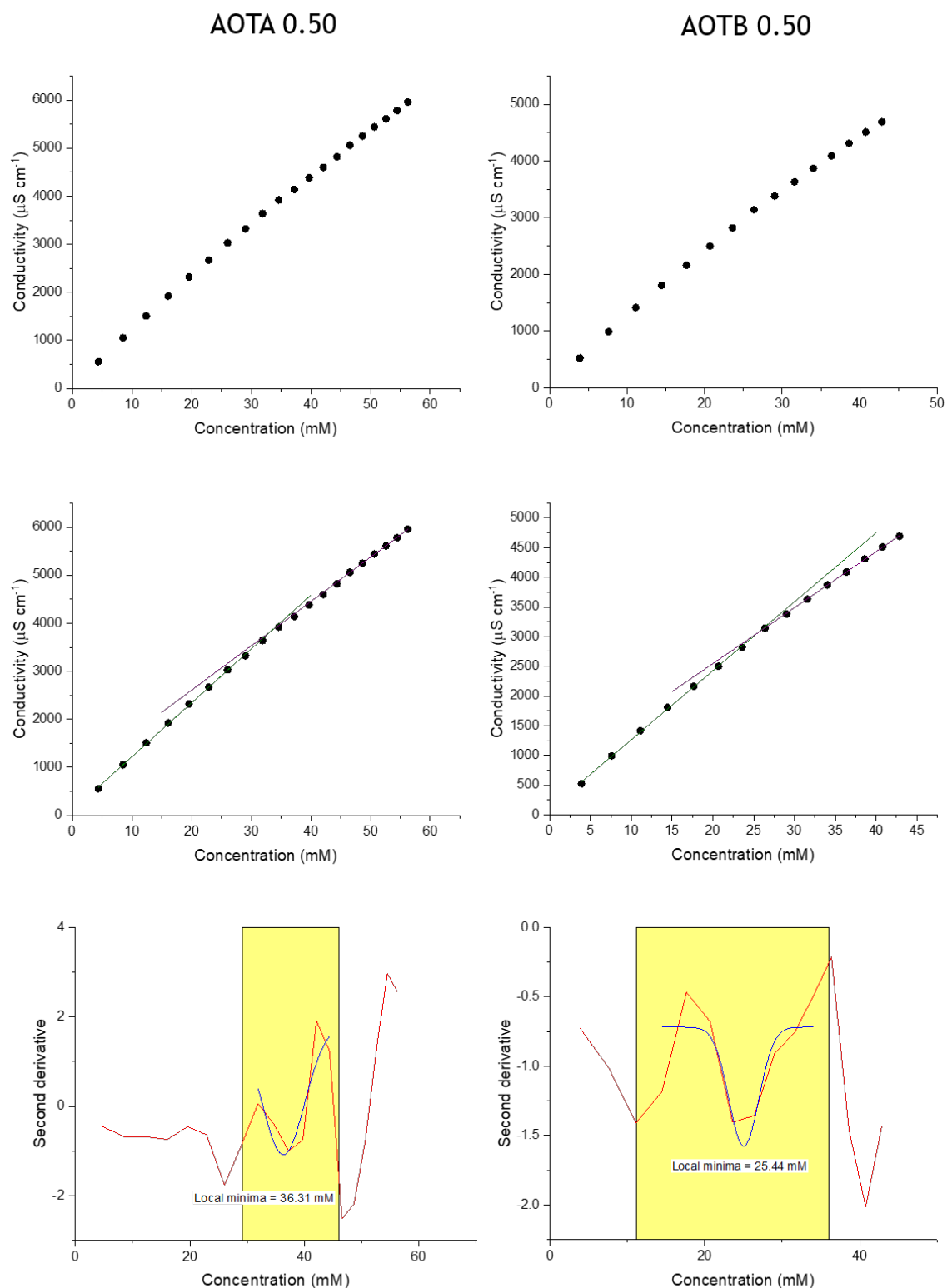


Figure 8.5d: Conductivity data used to determine cmcs of HS3 mixed system at a molar ratio of 0.5 X, where X is either AOTA / AOTB.

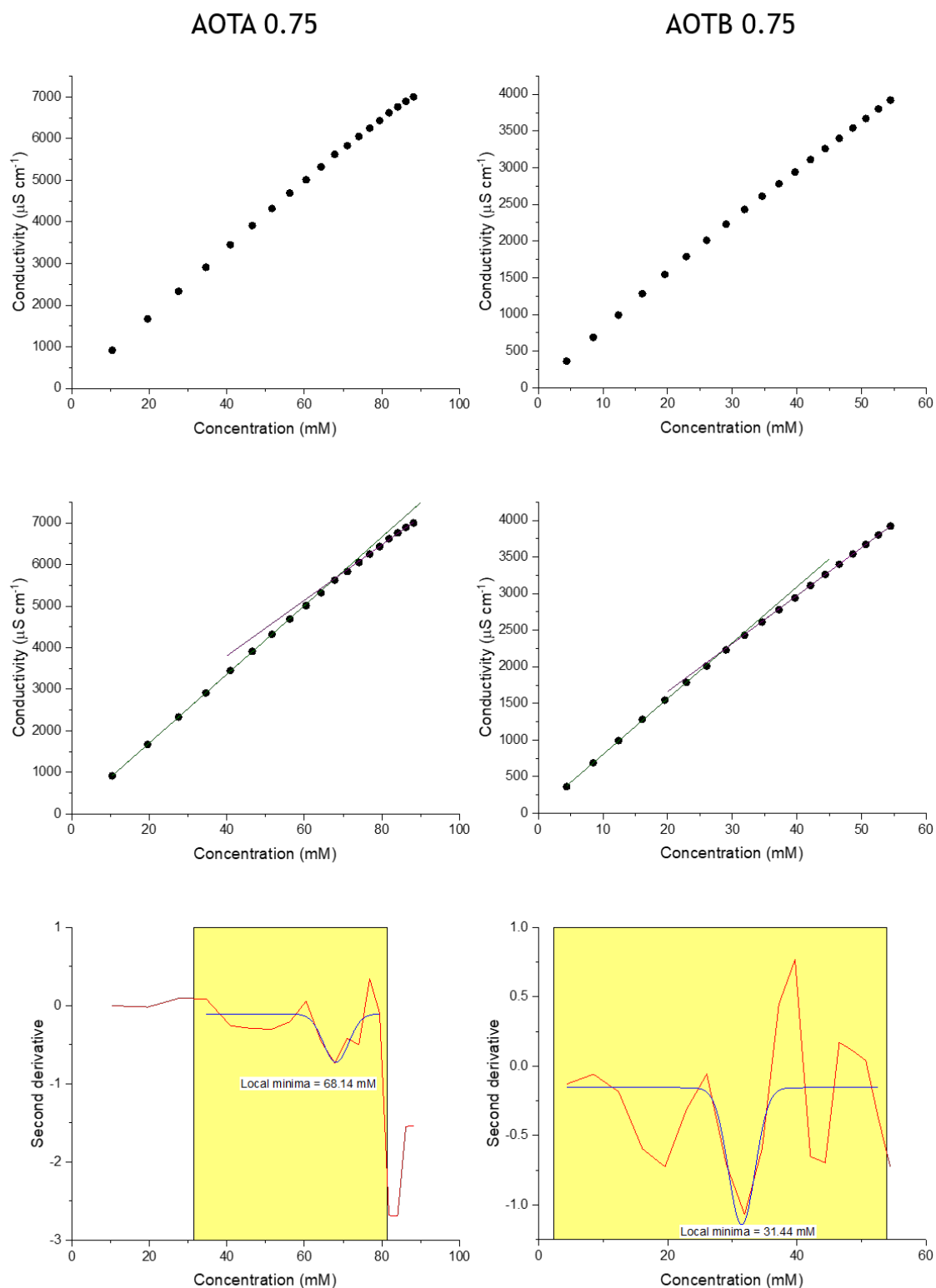


Figure 8.5e: Conductivity data used to determined cmcs of HS3 mixed system at a molar ratio of 0.75 X, where X is either AOTA / AOTB.

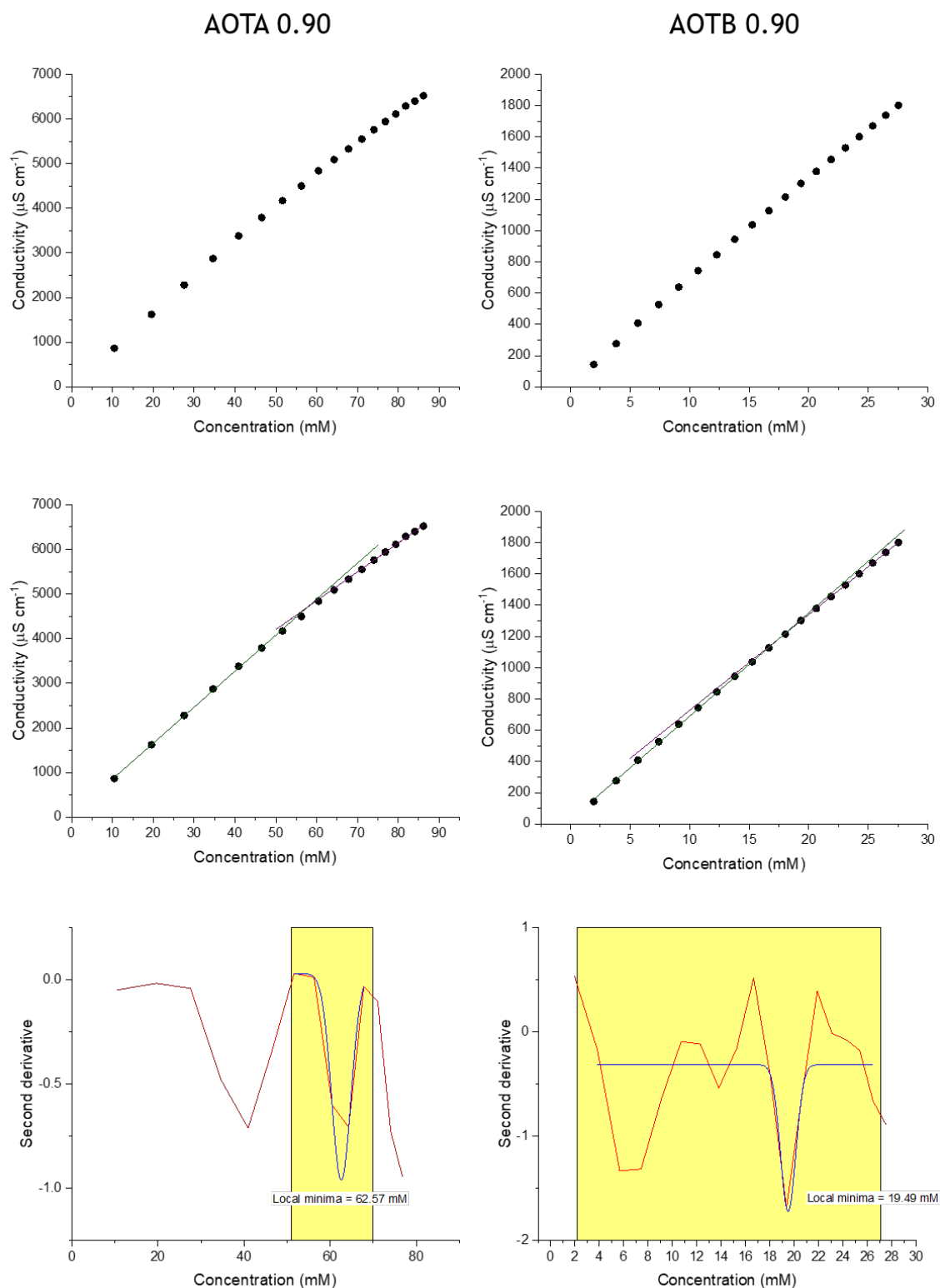


Figure 8.5f: Conductivity data used to determined cmcs of HS3 mixed system at a molar ratio of 0.9 X, where X is either AOTA / AOTB.

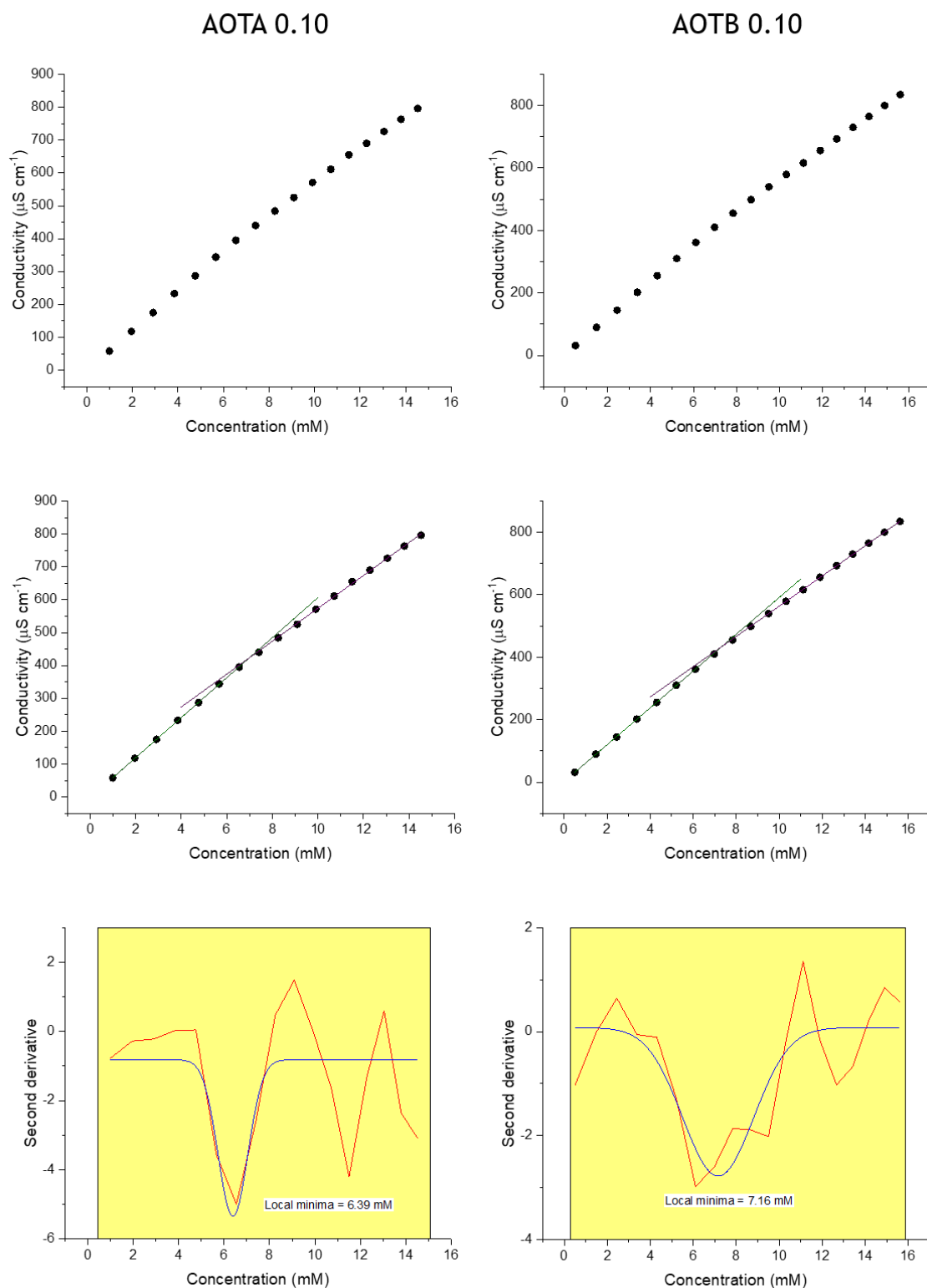


Figure 8.6b: Conductivity data used to determined cmcs of AOT mixed system at a molar ratio of 0.1 X, where X is either AOTA / AOTB.

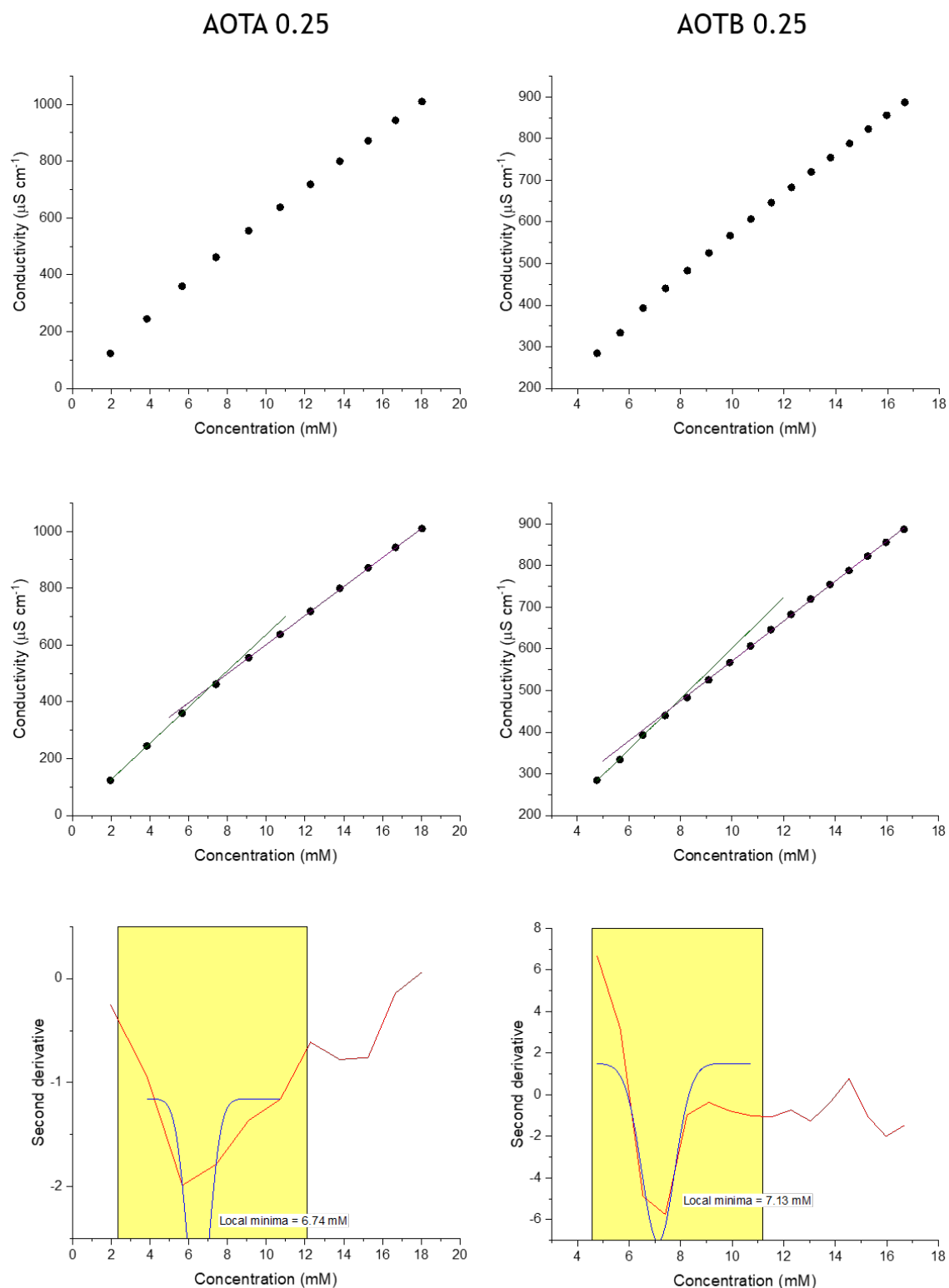


Figure 8.6c: Conductivity data used to determined cmcs of AOT mixed system at a molar ratio of 0.25 X, where X is either AOTA / AOTB.

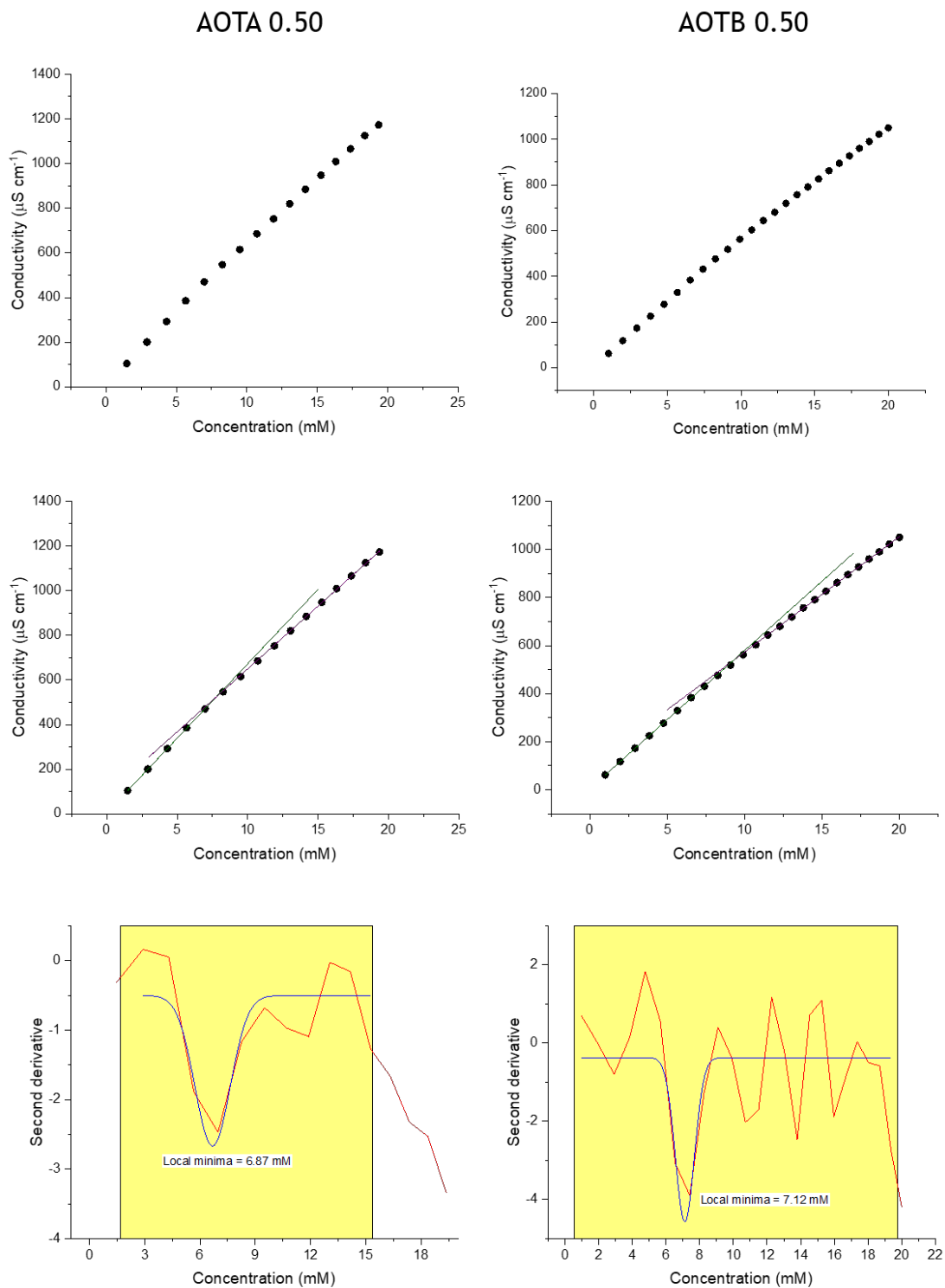


Figure 8.6d: Conductivity data used to determined cmcs of AOT mixed system at a molar ratio of 0.5 X, where X is either AOTA / AOTB.

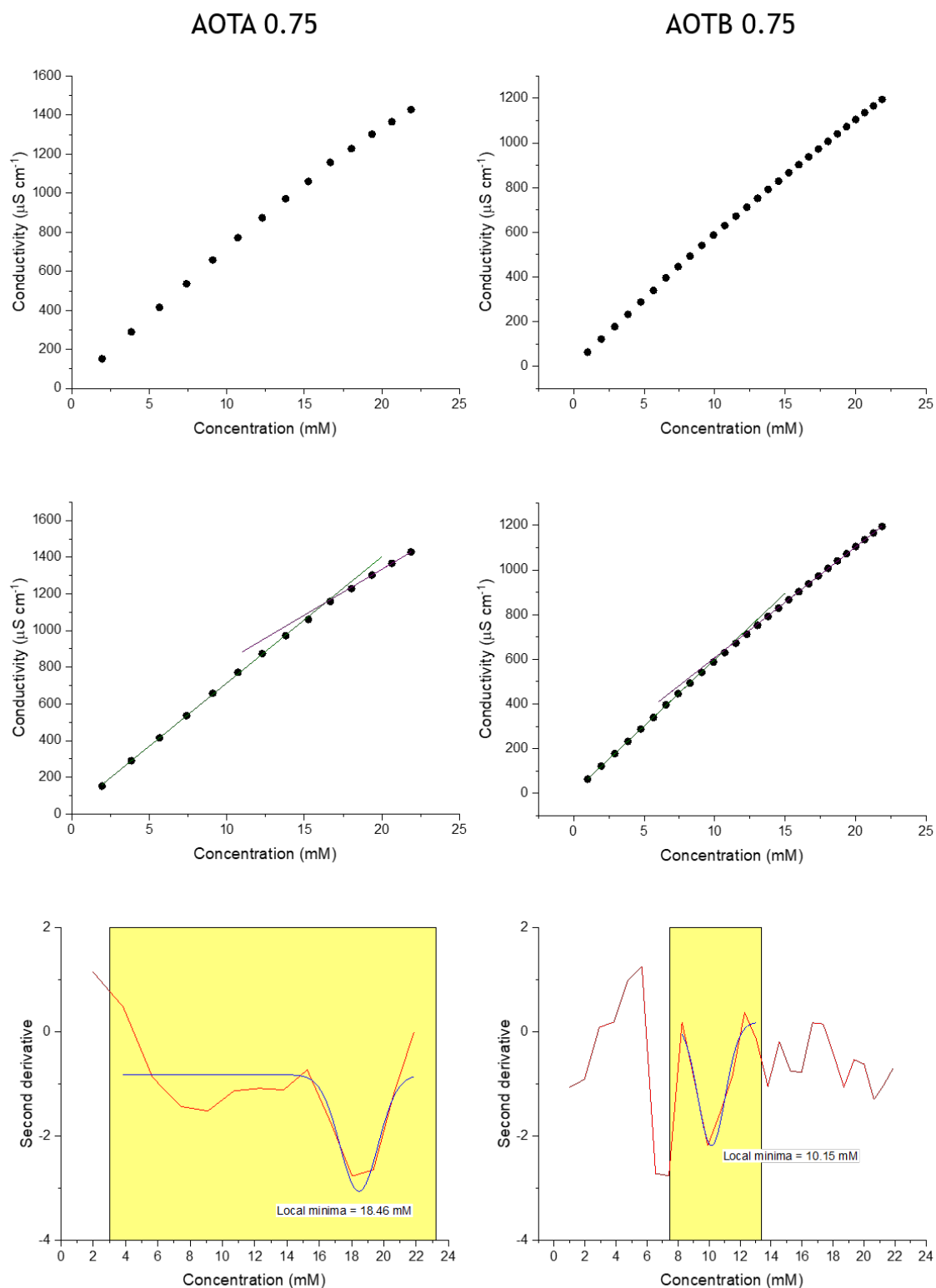


Figure 8.6e: Conductivity data used to determined cmcs of AOT mixed system at a molar ratio of 0.75 X, where X is either AOTA / AOTB.

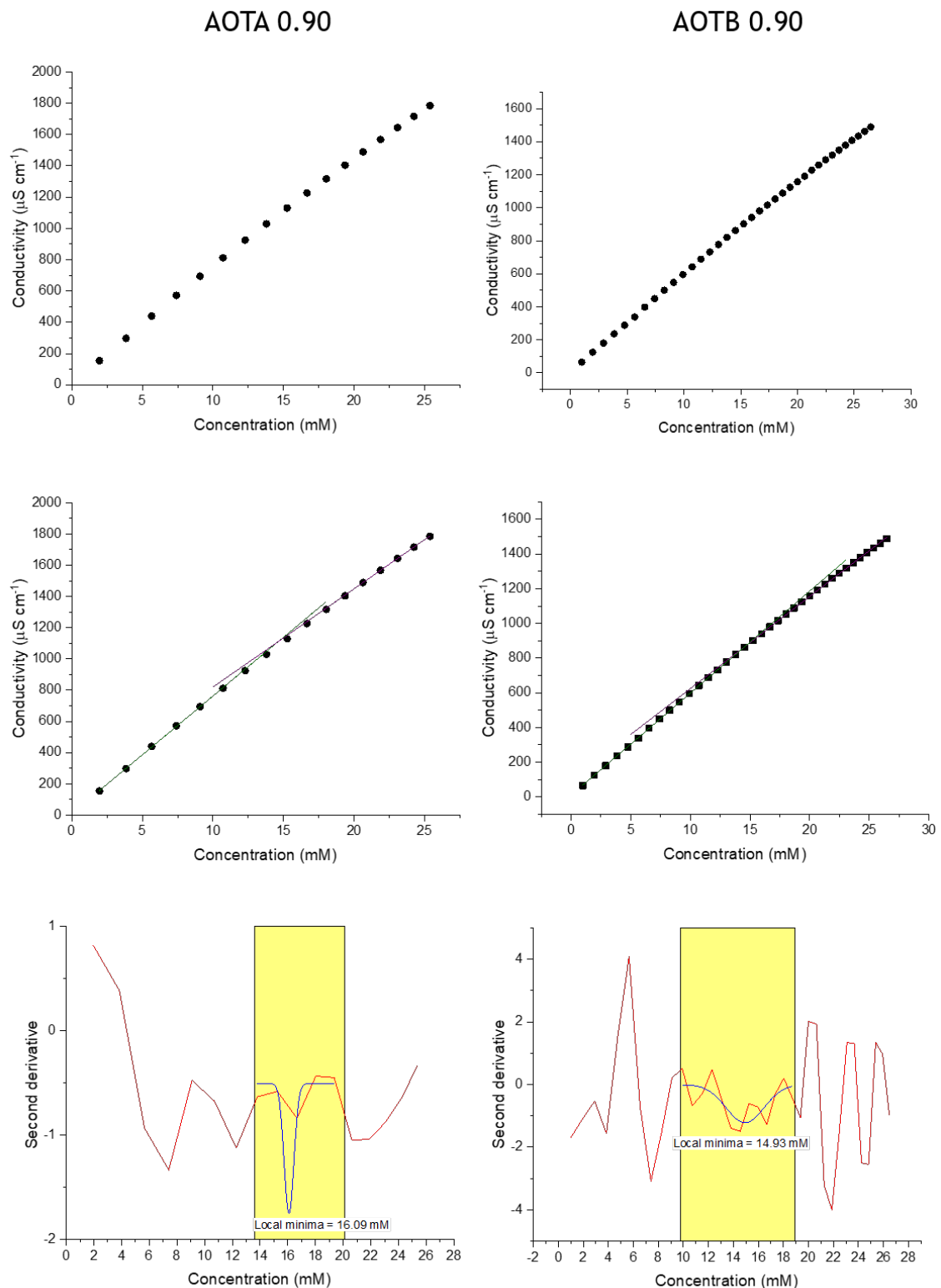
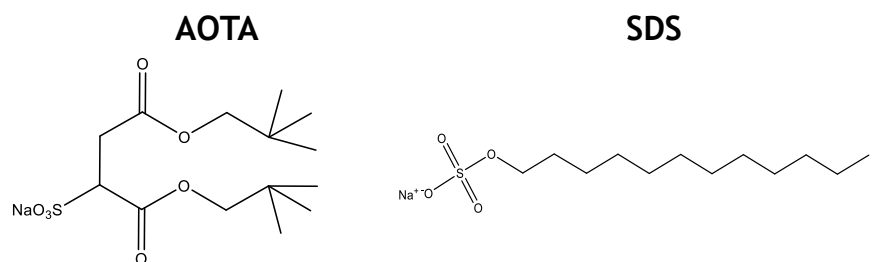


Figure 8.6f: Conductivity data used to determined cmcs of AOT mixed system at a molar ratio of 0.9 X, where X is either AOTA / AOTB.

8.2.7 SDS : AOTA



AOTA	SDS	cmc (mM) \pm 0.1
0.1	0.9	6.65
0.5	0.5	12.8
0.9	0.1	29.6

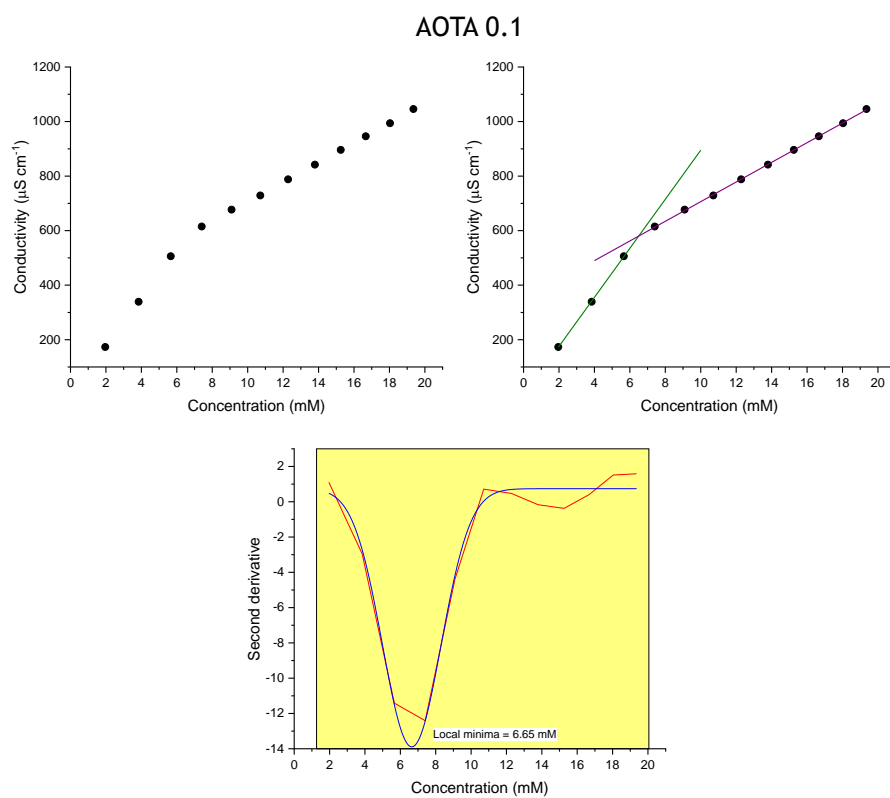


Figure 8.7a: Summary of the cmc values for SDS : AOTA mixed surfactant systems at varying molar ratios.

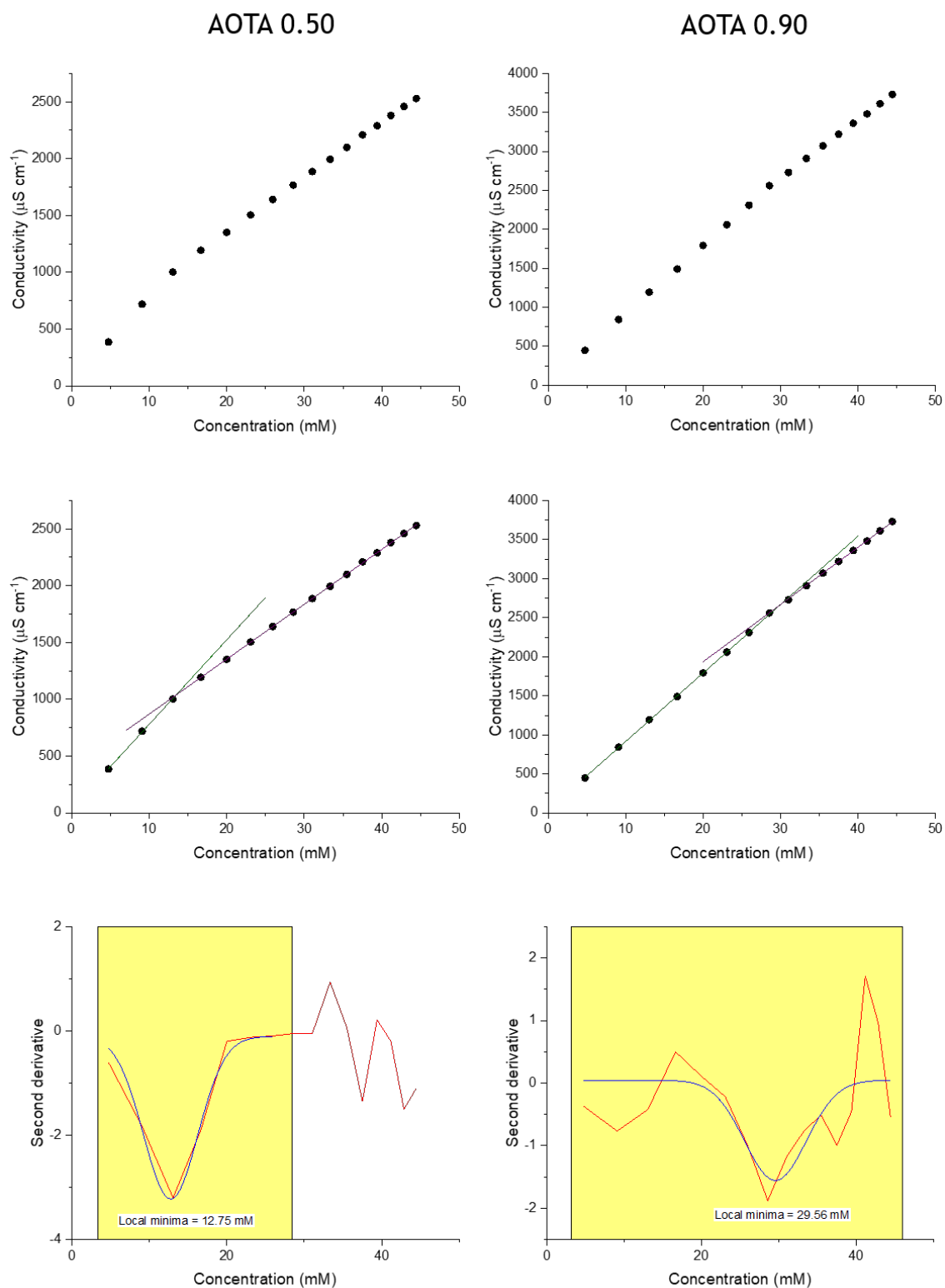


Figure 8.7b: Conductivity data used to determined cmcs of SDS mixed system at a molar ratio of 0.5 & 0.9 X, where X is AOTA.

8.3 Conductivity data and cmc analysis - Surfactants

The following pages provide the conductivity data and analysis that was used to determine the cmc of various surfactants discussed in this thesis. The experimental procedure is described in Section 4.6.1 (all measurements were made at 295 K).

8.3.1 SDS

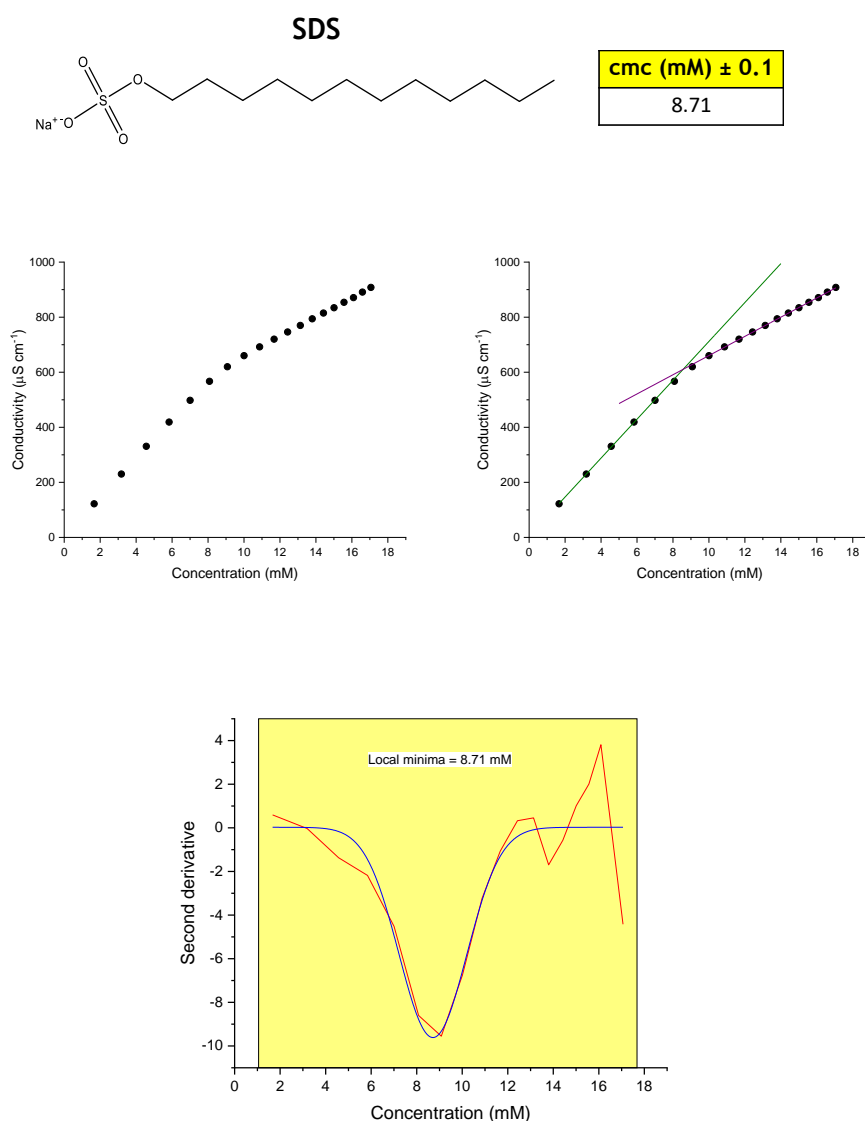


Figure 8.8: Conductivity data and analysis used to determine the cmc of SDS.

8.3.2 AOT

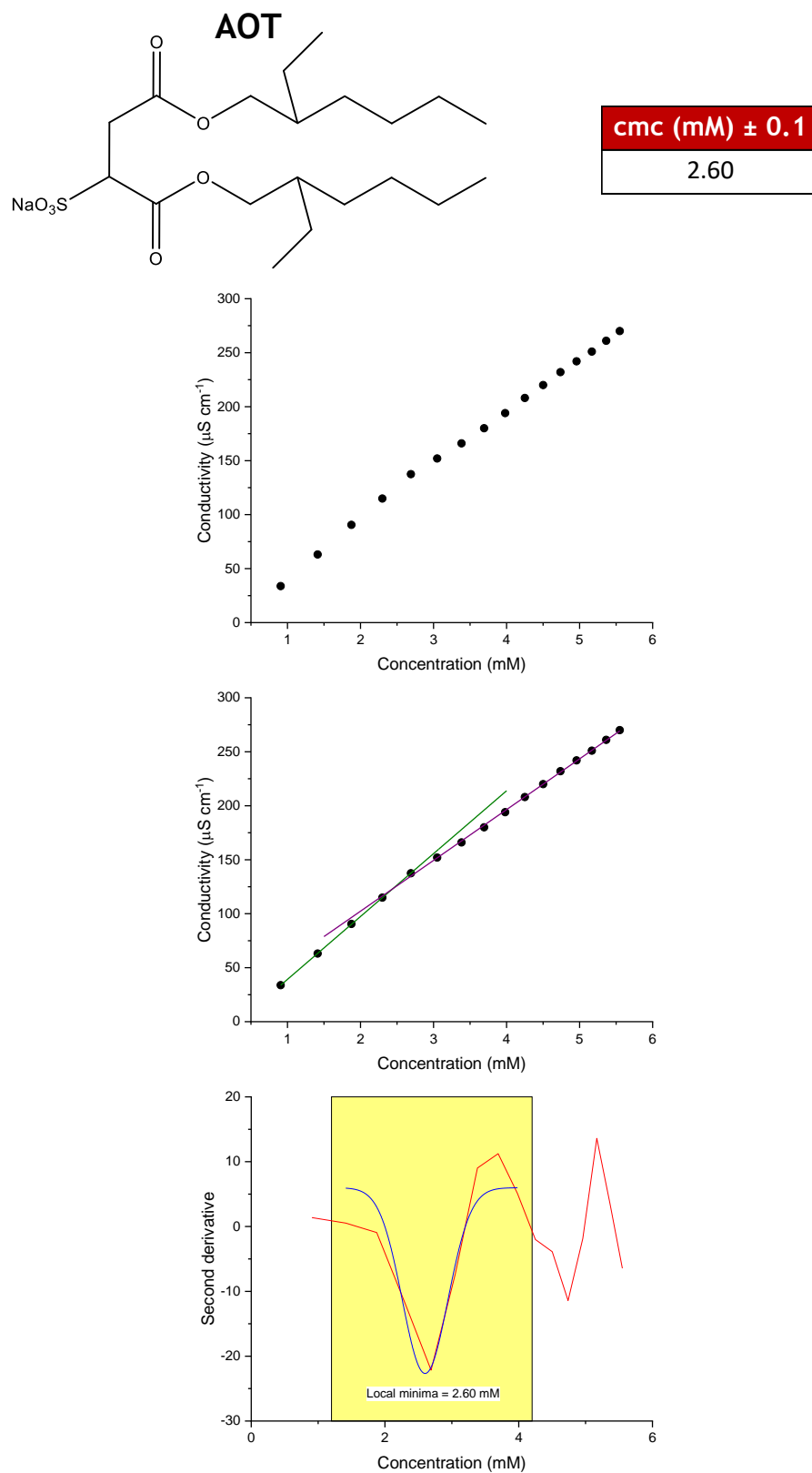


Figure 8.9: Conductivity data and analysis used to determine the cmc of AOT.

8.3.3 di-C6SS

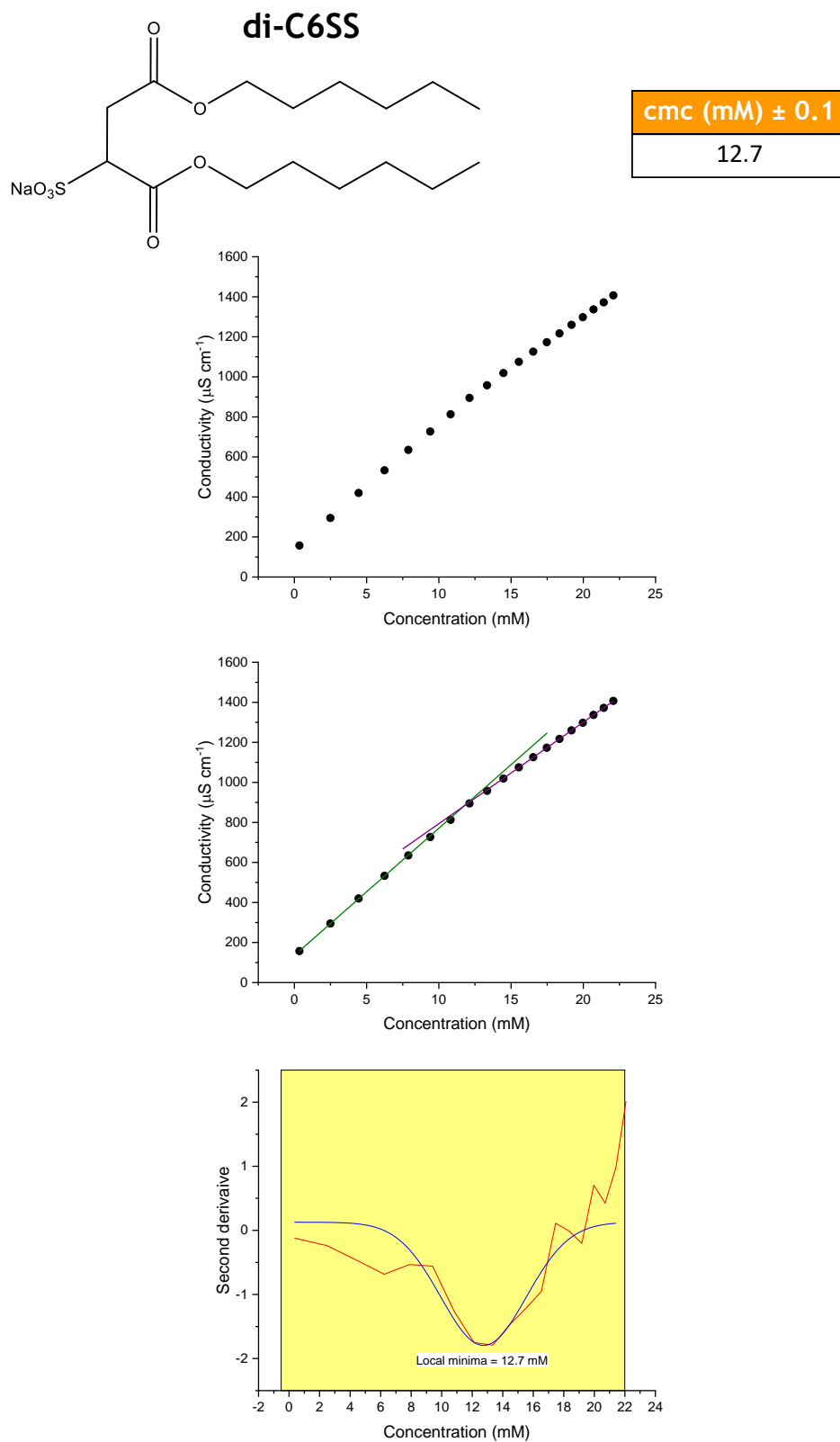


Figure 8.10: Conductivity data and analysis used to determine the cmc of di-C6SS.

8.3.4 di-C7SS

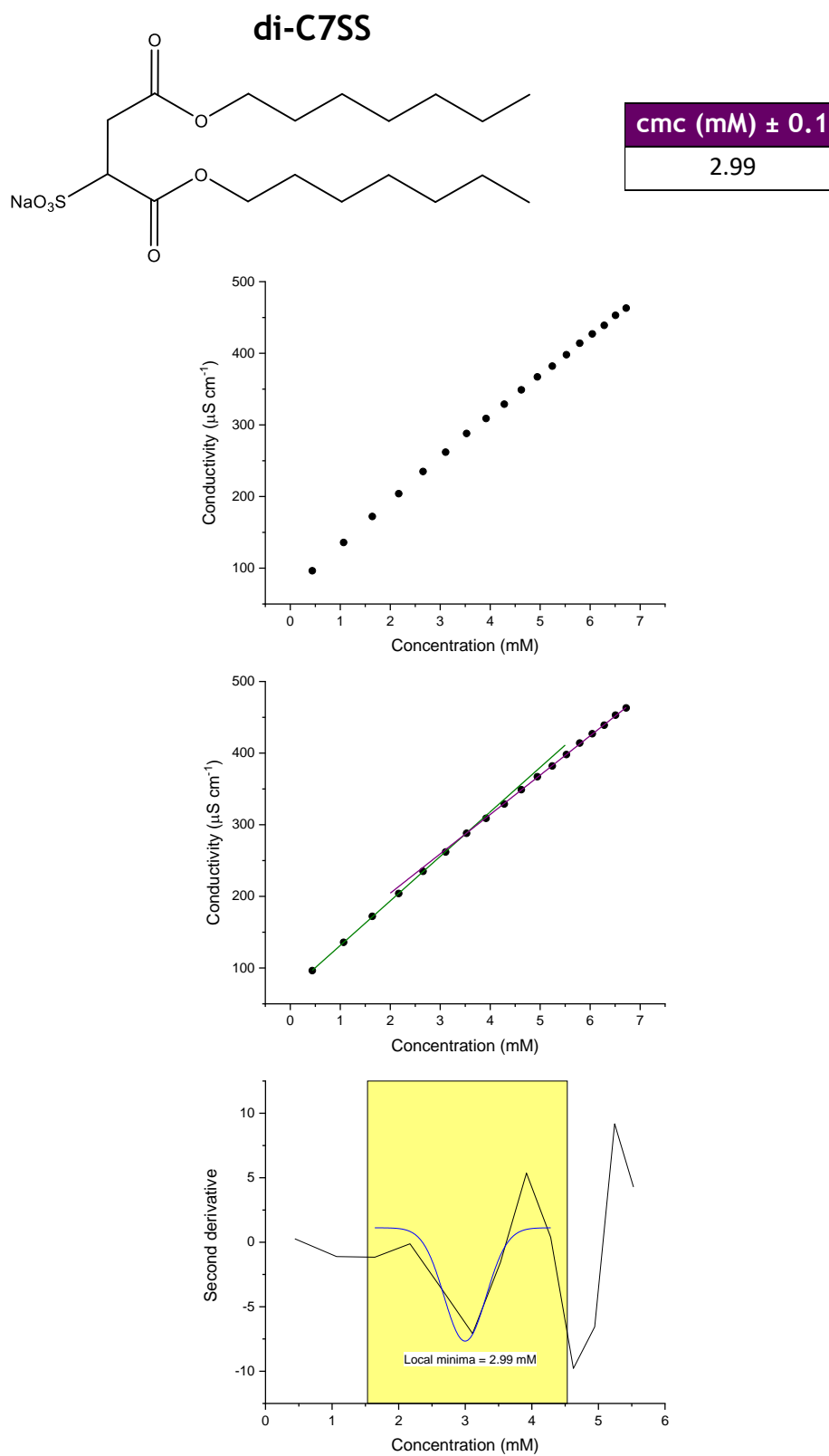


Figure 8.11: Conductivity data and analysis used to determine the cmc of di-C7SS.

8.3.5 di-C8SS

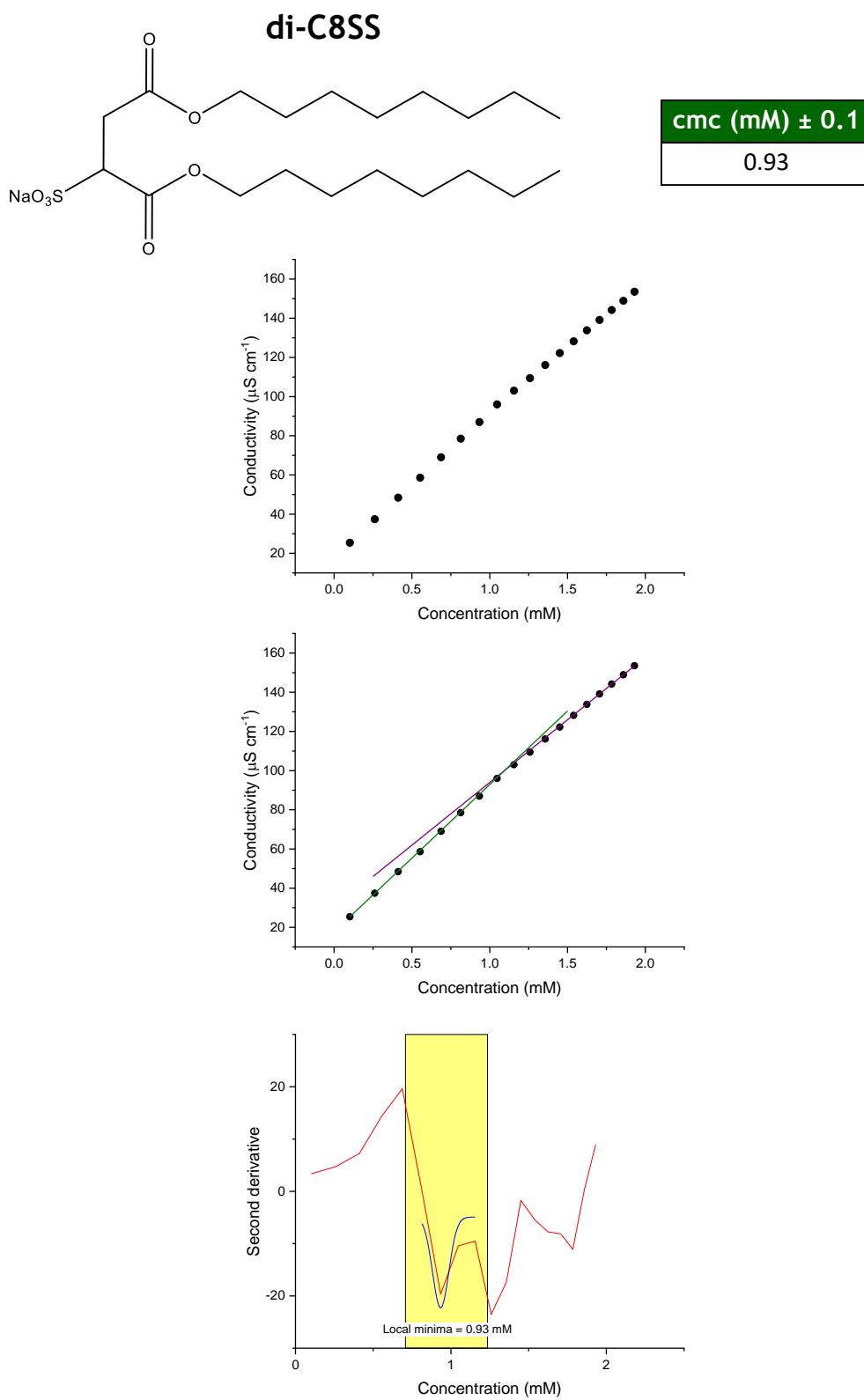


Figure 8.12: Conductivity data and analysis used to determine the cmc of di-C8SS.

8.4 BASIC code - Mixed systems

In Section 3.2.2 a simplified account of Regular solution theory (RST) for mixed systems was provided. With knowledge of an experimentally determined mixed cmc, as well as the cmc for the pure surfactant components, it is possible to estimate the mixed cmc if behaving ideally, C_{id}^* , and to calculate the deviation from ideality, i.e. the interaction parameter β . Both C_{id}^* and β can be calculated from iterative solutions of Equations 3.29 and 3.30. There are several feasible approaches to doing this. Here, a simple program was made using BASIC, where the various parameters (cmc of pure components, cmc of mixture etc.) can be typed in and the iterative solution found. Below all details are provided to aid future scientists that themselves may wish to adopt a similar approach.

Program - JustBASIC v1.01 (downloaded from www.justbasic.com)

Code -Interaction parameter, β

```

REM - CALCULATE MICELLAR BETA FROM BINARY MIXED CMC
input "Input A1, CMC1, CMC2, CMCM "; A1, CMC1, CMC2, CMCM
A2 = 1 - A1: G1 = CMCM * A1/CMC1: G2 = CMCM * A2/CMC2
X1 = 0: X2 = 1
FOR I = 1 TO 25
  XM1 = 0.5 * (X1 + X2): XM2 = 1 - XM1
  F1 = XM1*XM1 * LOG(G1/XM1): F2 = XM2*XM2 * LOG(G2/XM2)
  F = F1 - F2
  IF F > 0 THEN X1 = XM1 ELSE IF F < 0 THEN X2 = XM1 ELSE GOTO 110
NEXT I
BETA = LOG (G1/XM1) / (XM2 * XM2): print "MICELLAR BETA = "; BETA

```

A1 = mole fraction of surfactant one

CMC1 = cmc of surfactant one

CMC2 = cmc of surfactant two

CMCM = cmc of surfactant mixture

Code -Ideal mixed cmc, C_{id}^* (i.e. set $\beta = 0$)

```
REM - CALCULATE IDEAL BINARY MIXED CMC
```

```
input "Input BETA, A1, CMC1, CMC2 "; BETA, A1, CMC1, CMC2
```

```
A2 = 1 - A1: X1 = 0: X2 = 1: G = A1*CMC2 / (A2*CMC1)
```

```
FOR I = 1 TO 25
```

```
XM1 = 0.5 * (X1 + X2): XM2 = 1 - XM1
```

```
F1 = EXP(BETA*XM2*XM2): F2 = EXP(BETA*XM1*XM1)
```

```
F = G * F2*XM2 / (F1*XM1)
```

```
IF F > 1 THEN X1 = XM1 ELSE IF F < 1 THEN X2 = XM1 ELSE GOTO 100
```

```
NEXT I
```

```
CMCM = 1/(A1/(F1*CMC1)+A2/(F2*CMC2)): print "MIXED CMC = "; CMCM
```

8.5 Techniques - Wilhelmy plate

The Wilhelmy plate method is a surface technique for measuring either the surface tension of a liquid, the interfacial tension between two liquids, or the contact angle between a liquid and solid. In this research the Wilhelmy plate method has been used to measure the surface tension of various surfactant solutions and therefore, this section will focus on measuring the equilibrium (static) surface tension.

As well as the Wilhelmy plate, the other, and more common method to measure surface tension is using a Du Noüy ring tensiometer. What advantages does the Wilhelmy plate offer over the Du Noüy ring? When measuring the surface tension with a Du Noüy ring tensiometer, the ring is pulled through the surface during the measurement. Whereas with the Wilhelmy plate, the plate is not moved during the measurement and instead the surface tension is inferred from a meniscus formed on the plates perimeter. The plate is not in motion and thus, the entire surface is in equilibrium. However, using the ring technique causes a non-equilibrium state in the liquid as the ring is pulled through the surface. Because of this, only the Wilhelmy plate can allow accurate determination of surface kinetics, and also does not require correction factors to calculate surface tensions.

In a typical experiment to measure the equilibrium surface tension, the plate is lowered to the liquid surface, a meniscus is formed, and then the plate is raised so that the bottom edge of the plate lies on the plane of the surface, see Figure 8.13.

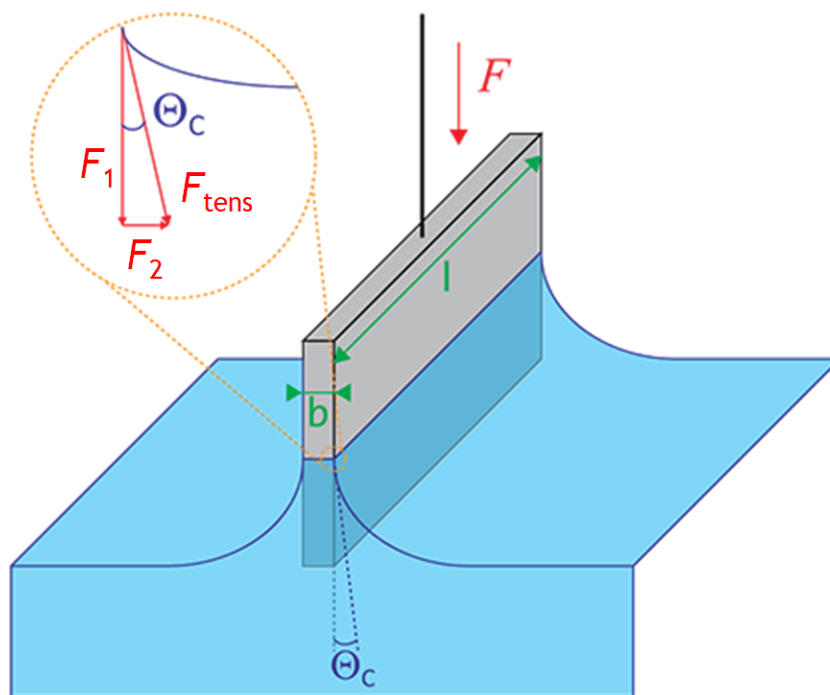


Figure 8.13: Illustration of the Wilhelmy plate method (from www.dataphysics.de).

At the three-phase contact line, highlighted on the figure, a tension force F_{tens} acts tangentially to the liquid surface. This force can be split into its parallel (F_2) and perpendicular (F_1) components:

$$F_1 = F_{\text{tens}} \cos \theta_c \quad (8.1)$$

$$F_2 = F_{\text{tens}} \sin \theta_c \quad (8.2)$$

The tensiometric balance only experiences the perpendicular part of the tension force (F_1), which matches the gravitational force F_G of the formed meniscus. With the surface tension (γ) of a liquid defined as the force per unit length, it is possible to obtain the Wilhelmy equation:

$$\gamma = \frac{F_{\text{tens}}}{L} = \frac{F_1}{L \cos \theta_c} = \frac{F_G}{L \cos \theta_c} \quad (8.3)$$

where L equals the wetted length (i.e. $L = 2b + 2l$), and θ is the contact angle between the liquid phase and the plate. In practice, the contact angle is rarely measured and instead, complete wetting is assumed so $\theta = 0$ and the equation simplifies (i.e. $\cos 0 = 1$). Hence, by knowledge of the plate dimensions and measured gravitational force, the surface tension can be determined. The plate is made from a iridium-platinum material which helps to ensure complete wetting. Furthermore, common practice is to clean the plate under the blue flame of a Bunsen burner between measurements and therefore, the material should be both inert and heat resistant.

